DROPLET-GAS INTERACTION IN AN ATMOSPHERE POLLUTED BY AMMONIA AND SULPHUR DIOXIDE

A thesis submitted for the degree of
Doctor of Philosophy in the Faculty of Engineering
of the University of London

by

Ishmael Emeka Iheozor-Ejiofor (M.Sc.)

Department of Chemical Engineering and Chemical Technology
Imperial College of Science and Technology

September 1985

IN MEMORY OF

RACHEL

MABEL

and

GAIUS

Dedicated to:-

Hector

Yvonne

Dante

Rommel

Ann-Mary

Achilleus

Zipporah

ABSTRACT

The removal from the atmosphere of anthropogenic SO_2 is by deposition and chemical transformation. Homogeneous gas phase oxidation in the absence of free radicals and sunlight has been shown to be unimportant. Heterogeneous oxidation in aqueous droplet is however important especially in the presence of iron and manganese ion catalysts. Ammonia is also known to enhance droplet phase oxidation but investigators are not unanimous on its mechanism. This study is a laboratory simulation of the droplet phase oxidation of SO_2 in the presence of NH_3 and manganous ion.

Sulphate salt solution droplets in contact with air, SO_2 and NH_3 in a flowing tubular reactor absorbed these gases and as a result of the SO_2 oxidation and the consequent increase in their sulphate loading, grew by he condensation of water from the vapour phase. Concurrently, the aerosols underwent droplet size change by coagulation. The changes in aerosol size and chemical composition were studied using both light scattering and chemical techniques.

In the first set of experiments, the growth characteristics of $(NH_4)_2SO_4$ aerosols were studied in the absence of the reacting gases. The effects of residence time, relative humidity and initial solute concentrations of the droplets on the evolution of droplet size distribution were used in demonstrating the mode of condensation and coagulation in aerosol droplets whose solute contents are time-invariant. In the second set, the droplet phase oxidation of SO_2 in the presence of known gas phase concentrations of SO_2 and NH_3 was studied by particle size analysis and chemical techniques.

The results showed that NH_3 substantially enhanced the oxidation of SO_2 but that in the presence of Mn^{2+}, oxidation was progressively depressed as NH_3 concentration increased. Using the results, contributions were made to the measurement of a rate constant. The chemical and physical backgrounds to the above observations are discussed.

Acknowledgements

I would like to express my appreciation to the Combustion Research Group under Professor F. J. Weinberg, F.R.S. in general and to Dr. H. J. Michels, Dr. A. R. Jones and other individual members of the group who rendered assistance in the way of suggestions and encouragement. My sincerest gratitude goes to Dr. M. D. Carabine, my supervisor for his advice and helpful suggestions and for the keen interest he had shown in my welfare.

My sincere thanks go to the college administration, in particular to Messrs B. K. Gooch, the Deputy Registrar and N. C. Wheatley, the Senior Assistant Registrar for their efforts in facilitating the transfer of funds from Nigeria for my maintenance. My appreciation is expressed to all the members of the departmental technical and support staff who assisted during the course of the work, in particular, Ian Drummond of the Analytical Services Laboratory and Colin Smith of the glass workshop.

My sincerest appreciation goes to my father and my wife for their patience and the personal sacrifices they made during the course of this work.

Finally, I have to thank Hilary Hughes for her accurate and prompt typing.

CONTENTS

Title Page			1
Dedications			2
Abstract			4
Acknowledgements			5
Contents			6
List of Tables			9
List of Illustrations			14
Chapter I:		INTRODUCTION	19
Chapter II:		BACKGROUND THEORY	23
	II.1	Ammonium Sulphate Precursors in the Troposphere	23
	II.1.1	Ammonia	23
	II.1.2	Sulphur Dioxide	24
	II.2	The Fate of Tropospheric Sulphur Dioxide	31
	II.3	Oxidation of Sulphur Dioxide	49
	II.3.1	Homogeneous oxidation	49
	II.3.2	Heterogeneous oxidation	51
	II.4	Aerosols	80
	II.4.1	Atmospheric Aerosols	80
	II.4.2	Nucleation	82
	II.4.3	Evaporation	89
	II.4.4	Coagulation	94
	II.4.5	Aerosol sampling	99
	II.4.6	Generation of Aerosols	100
	II.4.7	Particle Size Statistics	105
	II.4.8	Optical Properties of Aerosols	108
	II.4.9	Particle Size Analysis	114
Chapter III:		EXPERIMENTAL METHOD	119
	III.1	General Description	119
	III.1.1	The Air Supply System	119
	III.1.2	The Aerosol Generator	123
	III.1.3	The Light Scattering Unit	129
	III.2	Optimisation of the Equipment	137

III.3	Aerosol Droplet Size Analysis	152
III.3.1	Light Scattering Study of Ammonium Sulphate aerosols	152
III.3.2	Light Scattering Study of the Droplet-gas Interacting System	155
III.4	Aerosol Chemical analysis	157
III.4.1	Absorption of Sulphur Dioxide by Scrubbing Liquids	157
III.4.2	Separation of Sulphur Dioxide from Droplets	159
III.4.3	Sulphur Dioxide Analysis	167
III.4.4	Droplet Sampling Methods	173
III.4.5	Sulphate Analysis	177
Chapter IV:	RESULTS AND DISCUSSIONS	189
IV.1	Model Description	189
IV.2	Light scattering study of ammonium sulphate aerosols	191
IV.2.1	The Effect of Master Solution Concentration	191
IV.2.2	The Effect of Generator Flowrate	197
IV.2.3	The Effect of Relative Humidity	202
IV.2.4	The Effect of Residence Time	202
IV.3	Light Scattering study of gas-droplet interacting systems	213
IV.3.1	Size Analysis of Oxidation Product of sulphur dioxide in the absence of ammonia	213
IV.3.2	Sulphur Dioxide Oxidation in the Presence of NH_3	218
IV.3.3	Mn^{2+} ion catalysed oxidation of SO_2 in the presence of ammonia	235
IV.4	Sulphur Dioxide Oxidation Monitoring by Chemical Method	242
IV.4.1	Sulphate Concentration	242
IV.4.2	Aerosol liquid water concentration	242
IV.5	Reaction Rate and Rate Constants	246
IV.6	Application to Stack Plume	260
Chapter V:	CONCLUSIONS AND SUGGESTIONS FOR FURTHER RESEARCH	263
V.1	Behavior of ammonium sulphate solution aerosols	263

V.2	Sulphur dioxide oxidation - monitoring by means of light scattering	264
V.3	Monitoring by means of Chemical analysis	264
V.4	Recommendations and suggestions for further work	265

REFERENCES 267

APPENDIX:

A	Some thermodynamic constants used in the study	281
B	Plume dispersion parameters	283
C	Inversion of droplet size to sulphate concentration	285
D	Reaction Kinetics of the aerosol system	289
E	Computer programme POLY	295

List of Tables

Table II.1: Ammonia source in U.K. 26

Table II.2: Tropospheric burden of sulphur compounds 26

Table II.3: Global volcanic sulphur dioxide 30

Table II.4: Anthropogenic sources of atmospheric sulphur dioxide 30

Table II.5: The historical increase in sulphur dioxide emission 30

Table II.6: The historical production of SO_2 yielding products 30

Table II.7: Transformation and deposition rates of sulphur dioxide 38

Table II.8: Sulphur dioxide dry deposition 38

Table II.9: Comparison of dry and wet deposition using two models 46

Table II.10: The atmospheric sulphur budget over Western Europe 46

Table II.11: The pseudo first order rate constants for uncatalysed oxidation of sulphur dioxide in aqueous phase 56

Table II.12a: Some previous studies of sulphur dioxide oxidation catalysed by manganous sulphate solution 62

Table II.12b: Some previous studies of sulphur dioxide oxidation catalysed by some salts other than manganous sulphate 63

Table II.13: The effect of ammonia on the aqueous solubility of sulphur dioxide 76

Table II.14: Conditions for the computation of sulphate production from sulphur dioxide in the presence of ammonia 76

Table II.15: Experimental conditions used by Ibusuki 79

Table II.16: Important characteristics of aerosols 83

Table II.17: Variation of water droplet life time with initial droplet diameter in vapour-free air at 20°C 98

Table II.18: Particle diameters and coagulation coefficients 98
Table II.19: Mode of variation of droplet numbe/ concentration as a function of droplet size. 98
Table III.1: Photomultiplier stability as a function of time 138
Table III.2: Noise-to-signal ratio in the absence of aerosols 140
Table III.3: Noise-to-signal ratio in the presence of aerosols 142
Table III.4: Comparison of ZOLD parameters obtained at 9 kV and 1.2 kV photomultiplier voltage 144
Table III.5: Comparison of the M.M.D. and scattered light intensities obtained at 0.9 kV and 1.2 kV photomultiplier 144
Table III.6: Stability of the photomultiplier over a 3-hour running period 144
Table III.7: Comparison of data obtained while changing the scattering angle 146
Table III.8: A comparison of two light scattering runs carried out under identical conditions 146
Table III.9: The effect of exhaust flow instability on scattered light intensity 148
Table III.10: Photomultiplier output signal during a constant exhaust gas flow regime 148
Table III.11: Variation of aerosol ZOLD parameters with time for a constant exhaust flow regime 148
Table III.12: Filter specifications 151
Table III.13: Performance of the filters 151
Table III.14: Tube combinations and residence times 156
Table III.15: Combinations of sulphur dioxide and ammonia partial pressures and source concentrations 156
Table III.16: Scrubbing solutions for the absorption of sulphur dioxide 158
Table III.17: Sulphur dioxide absorbed by the various absorbers 158
Table III.18: Comparison of annular and tubular denuders 164
Table III.19: Experimental conditions for the comparison of various denuder coatings 164
Table III.19a: Sulphur dioxide concentration of denuder effluent 171

Table III.20: Light scattering parameters of the diffusion denuder effluent aerosols 171
Table III.21: Formaldehyde as sulphur dioxide absorbing liquid 171
Table III.22: Aerosol droplet collection techniques 175
Table III.23: The characteristics of the effluent aerosols from the droplet collecting devices 175
Table III.24: Characteristics of potassium hydrogen phthalate eluents in sulphate separation 182
Table III.25: Sulphate solution calibration 182
Table III.26: The peak areas and the corresponding sulphate concentrations for aerosol samples transfered directly from the generator 182
Table III.27: Peak areas and HPLC loop sulphate content for the eight residence times 187
Table III.28: Calibration factor for each residence time 187
Table III.29: HPLC peak areas of real aerosol samples for three experimental conditions 188
Table IV.1: Angular distribution of scattered light intensities of pure water aerosols 192
Table IV.2: Aerosol ZOLD parameters as a function of master solution concentrations 192
Table IV.3: Size parameters and droplet mass concentration of aerosols as a function of dispersion gas flow rate 200
Table IV.4: ZOLD parameters of aerosols at different relative humidities 200
Table IV.5: Variation of ZOLD parameters with residence time 207
Table IV.6: Variation of droplet number concentrations with residence time 207
Table IV.7: The comparison of the experimental and theoretical variation of droplet number concentrations with residence time 208
Table IV.8: Experimental and theoretical variations of number concentrations calculated from the aerosol M.M.D. 210
Table IV.9: Number concentration of aerosols generated from 1 mM ammoniuim sulphate solution 211

Table IV.10: Aerosol ZOLD parameters in the absence of sulphur dioxide and ammonia 214

Table IV.11: Partial pressures of sulphur dioxide and ammonia with the corresponding equilibrium state hydrogen and sulphite ion concentrations 219

Table IV.12: ZOLD parameters for droplet growth in the presence of 2 to 100 vpm ammonia and 50 vpm sulphur dioxide 221

Table IV.13: Light scattering data for $NH_3.SO_2$ particulates 227

Table IV.14: ZOLD parameters for droplet growth in the presence of 0.1 to 10 vpm ammonia and 50 vpm sulphur dioxide 230

Table IV.15: ZOLD parameters for droplet growth as a function of sulphur dioxide:ammonia ratio 232

Table IV.16: The MMD for sulphur dioxide:ammonia ratio 234

Table IV.17: ZOLD parameters of manganous sulphate aerosols in the absence of sulphur dioxide and ammonia 234

Table IV.18: ZOLD parameters of manganous sulphate aerosols in the presence of ammonia and 50 vpm sulphur dioxide 236

Table IV.19: ZOLD parameters of manganous sulphate aerosols in the presence of ammonia and 1 vpm sulphur dioxide 238

Table IV.20: The effect of ammonia partial pressure on the droplet size ratio in $MnSO_2$-SO_2-NH_3-H_2O-O_2 system 240

Table IV.21: Droplet sulphate loading obtained by HPLC analysis 243

Table IV.22: Aerosol droplet mass concentration 245

Table IV.23: Liquid water concentrations of the aerosols in Runs 6, 7 and 9 245

Table IV.24: The variation of sulphur dioxide oxidation rate with the partial pressure in the absence of ammonia and manganous sulphate 250

Table IV.25a: Variation of uncatalysed oxidation rate with ammonia partial pressure 250

Table IV.25b: Variation of manganous sulphate catalysed sulphur dioxide oxidation 254

Table IV.26: Droplet hydrogen ion concentration obtained from the gas phase ammonia partial pressure 254

Table IV.27: Experimentally determined reaction orders for Runs 6, 7 and 9 257

Table IV.28: Reaction rate constants obtained under various reactant combinations 258

List of Illustrations:

Plates:

Plate 1: The front view of the equipment 141
Plate 2: The side view of the equipment 141
Plate 3: The light scattering sampling system 141
Plate 4: The laser source and data recording system 141

Figures:

Figure II.1: The flux and burden of sulphur dioxide and other volatile S(IV) compounds in the troposphere 29
Figure II.2: Diagrammatic representation of the removal of sulphur dioxide from the atmosphere 35
Figure II.3: Droplet phase concentrations of $SO_2 \cdot H_2O$ and total S(IV) as a function of gas phase partial pressure of sulphur dioxide 43
Figure II.4: Variation of the ratios of aqueous to gas phase concentration of sulphur dioxide with the partial pressure of SO_2 in the absence of ammonia 43
Figure II.5: Variation of the equilibrium mole fractions of S(IV) specials in aqueous droplet as a function of pH 77
Figure II.6: Sulphate formation as a function of time calculated from four models 77
Figure II.7: The effect of ammonia concentration on SO_2 oxidation 78
Figure II.8: Oxidation of sulphur dioxide in solution for a limited supply of the reacting gases 78
Figure II.9: Atmospheric aerosols size spectrum 81

Figure II.10: Water-soluble inorganic ions on filter 81
Figure II.11: The effects of saturation ratio and size on growth and evaporation of salt soltuion droplets 87
Figure II.11a: Saturation ratio versus droplet size for pure water and salt solution droplets 87
Figure II.12: Change in temperature and relative humidity with size in aerosols undergoing size change by evaporation 91
Figure II.13: Effect of monodisperse coagulation on aerosol number concentration 91
Figure II.14a: The effect of temperature on the evaporation of pure water droplet 93
Figure II.14b: The effect of size and number concentration on pure water droplet life time 93
Figure II.15: Dautreband aerosol generator 103
Figure II.16: The Acorn Nebuliser 103
Figure II.17: De Vilbiss Model 40 Nebuliser 104
Figure II.18: Evaporation-condensation monodisperse aerosol generator 104
Figure II.19: Log normal distribution curves with median diameter = 3.0 microns and geometrical standard deviation = 0.1 0.2, 0.3 and 0.5 107
Figure II.20: The ZOLD curves with modal diameter = 3.0 microns and ZOLD spread = 0.1, 0.2, 0.3 and 0.5 107
Figure II.21: Radiation diagram for Rayleigh scattering 113
Figure II.22: Scattering pattern for water droplets 113
Figure II.23: Flowchart showing the basic operations of the programme SEARCH 118
Figure III.1: Block diagram showing the main components of the equipment 120
Figure III.2: Stainless steel coarse filter holder 122
Figure III.3: The construction of the aerosol generator 124

Figure III.4: The reactor and the connecting tubes - the general layout 126
Figure III.5a: The cylindrical and U-tubes of the reactor 126
Figure III.5b: Generator-to-reactor connecting tube 127
Figure III.5c: Generator-to reactor connecting tube 127
Figure III.5d: Reactor-to-sampling cell connecting tube 127
Figure III.6: Schematic diagram showing the combinations of the reactor tubes 128
Figure III.7: The wet and dry bulb hygrometer and its housing 130
Figure III.8: The aerosol light scattering sampling apparatus 132
Figure III.9: The flow diagram of light scattering cell and the exhaust system 132
Figure III.10: Laser beam collimating and expansion system 134
Figure III.11: The general arrangement of light scattering detection unit 134
Figure III.12: The photomultiplier and its housing 135
Figure III.13: Suspended glass slide for standardising laser beam intensity 135
Figure III.14: Schematic diagram of the annular denuder 162
Figure III.15: The size distributions of the electrostatic precipitator effluent aerosols as a function of voltage 165
Figure III.16: The breakthrough time of 1 vpm sulphur dioxide for different denuder coating materials 165
Figure III.17: Schematic diagram of the electrostatic precipitator 180
Figure III.18: Sulphate ion calibration curve 180
Figure III.19: Sulphate ion calibration curves for each of the eight residence times 183
Figure IV.1: Angular distribution of scattered and background light intensities of pure water mist 193

Figure IV.2: Variation of angular scattering pattern with master solution concentration 195
Figure IV.2a: The variation of droplet size with the master solution concentrations 196
Figure IV.3: Effect of dispersing gas flowrate on aerosol size distribution 198
Figure IV.3a: Variation of angular scattering pattern with the dispersing gas flow rate 199
Figure IV.4: Variation of droplet size distribution with relative humidity 201
Figure IV.5: Variation of size distribution with residence time in the absence of sulphur dioxide 204
Figure IV.5a: Variation of light scattering pattern with residence time in a non-reacting system 205
Figure IV.6: Variation of droplet number concentration with residence time for mass filteration and coagulation theory 212
Figure IV.7: Variation of size distribution with the partial pressure of sulphur dioxide 215
Figure IV.7a: Variation of aerosol modal diameter with the partial pressure of sulphur dioxide at three residence times 216
Figure IV.8: Variation of droplet size distribution with residence time for four partial pressures of sulphur dioxide 217
Figure IV.9: The effect of ammonia partial pressure on droplet size ratio in the SO_2-NH_3-O_2-H_2O reacting systems 223
Figure IV.10: Variation of size distribution with ammonia partial pressure of 1.0 vpm sulphur dioxide 224
Figure IV.11: Variation of size distribution with ammonia partial pressure for 50 vpm

sulphur dioxide at 17.2 minute residence time 226

Figure IV.12: Variation of size distribution as a function of the ratio of sulphur dioxide to ammonia partial pressures 231

Figure IV.13: Variation of droplet VMD with the ratio of sulphur dioxide to ammonia 233

Figure IV.14: Variation of size distribution with ammonia partial pressure for 1 vpm SO_2 in the presence of manganous sulphate 237

Figure IV.15: Variation of size distribution with ammonia partial pressure for 50 vpm SO_2 in the presence of manganous sulphate 239

Figure IV.16: Droplet size ratios for the manganous ion catalysed and uncatalysed reacting systems in the absence of ammonia 241

Figure IV.17: Droplet sulphate loading obtained by ion chromatography as a function of residence time with 1 vpm sulphur dioxide and ammonia 247

Figure IV.18: Droplet sulphate loading obtained by ion chromatography as a function of residence time with 1 vpm sulphur dioxide and 2 vpm ammonia 247

Figure IV.19: Droplet sulphate loading obtained by ion chromatography as a function of residence time with 50 vpm sulphur dioxide and 1 vpm ammonia 248

Appendix B : The Pasquill-Gifford dispersion coefficients versus downwind distance for various dispersion classes 284

Appendix D: Curves for various reaction rate mechanisms 293

CHAPTER 1

I N T R O D U C T I O N

Tropospheric aerosol is dominated by particles in the submicrometer size regime (Charlson et al, 1978). Available concentration and particle size measurements, however, indicate that the abundant metal cations concurrently present in sulphate - containing aerosols are present in the coarse mode above 1.0 μm (Gladney et al, 1974; Lee et al, 1968; Alkezweeny, 1978; Basset et al, 1983). The atmospheric sulphate aerosols, therefore, consist predominately of sulphuric acid and various sulphates of ammonia whose stoichiometric compositions are dependent on the ambient NH_3 mixing ratio (Weiss et al, 1977).

Chemical oxidation of SO_2 results in aerosols formed by the condensation and coagulation of transient nuclei (below 0.1 μm size range), the growth of which is too slow to account for a significant fraction reaching the coarse mode. However, a small fraction of the oxidation product may condense on pre-existing atmospheric aerosols and contribute to the coarse sulphate particles. On the whole, the bulk of the sulphate formed from SO_2 oxidation remains in the atmosphere in the accumulation size regime (0.1 to 1.0 μm).

Ferek et al (1983) have shown from field studies that the hydrogen ion plus ammonium ion equivalents equalled the sulphate ion in most areas studied; indicating that nitrate ion is a minor aerosol constituent in these samples. This is anomalous in view of the abundance of NO_x in the planetary boundary layer and the much higher rate constant for nitrate than for sulphate formation (Calvert et al., 1983). This apparent anomaly may be caused by higher removal rate of nitrate than sulphate.

Interest in sulphate aerosols and other sulphur containing species in the atmosphere stems from their potential health effects to man;

amenity and visibility degradation; effect on the terrestrial radiative balance; role as cloud condensation nuclei; and their potential role as input to acid rain precipitation. Epidemiological studies have shown that sulphate aerosols (Coffin et al, 1974) and SO_2 (Shephard et al, 1981a) cause and exacerbate respiratory diseases and that the chronically ill people, the elderly and those with pre-existing cardiopulmonary diseases are most at risk. However, controlled human exposure studies of normals and subjects with pulmonary diseases to SO_2 (Shephard et al, 1982) and sulphate (Avol et al 1979) show no significant effects at concentrations much higher than the normal urban air concentrations of these pollutants. Repeated exposure has been shown (Shephard et al, 1982) to induce tolerance or adaptation even in the most responsive subjects. The health hazards posed by high concentration episodes such as that in the Meuse Valley (Firket, 1936) may be according to Rall (1974) the synergistic effect of SO_2 and the coexisting aerosols and humidity.

Aerosols are known to alter in a physically complex manner the global radiative balance (Bundiasky, 1981). They have their greatest impact when they are low lying. They back scatter and absorb downward solar radiation and this process would result in a cooling effect on the surface - atmosphere system. Counterbalancing this is their back scattering and absorption of the portion of solar radiation reflected from the earth's surface thus diminishing the portion of radiant energy reflected back to space. The resultant heating or cooling caused by these opposing processes is determined by the earth's short wave surface albedo (Kukla et al, 1974). Within a cloud, the energy balance is also influenced directly and indirectly by the presence of aerosols suspended in it. Sulphate aerosols are important sources of cloud condensation nuclei and hence their presence and concentrations in a cloud constitute an important determinant of cloud formation.

Some of the effects of $(NH_4)_2SO_4$ and SO_2 on plants are well known. Sulphur dioxide is phytotoxic through the destruction of plant chlorophyll. Recent researches have aimed at determining the threshold of SO_2 that can effect economically important parameters of crops (Jones et al, 1977) and trees (Linzon, 1971) even in the absence of visible foliar damage. Response varied with tree or crop species but there were obvious reductions in yield which became worse as the SO_2 level increased in all the cases studied.

SO_2 and sulphate in the form of H_2SO_4 and $(NH_4)_2SO_4$ may also affect plants by acidifying the soil. Van Breeman et al. (1982) have reported acid formation from $(NH_4)_2SO_4$ in forest canopy throughfall on reaching the soil after leaching by rainwater with the production of extremely low pH.

$$(NH_4)_2SO_4 + 4O_2 = 2HNO_3 + H_2SO_4 + 2H_2O$$

The effect of the acidity is to leach out aluminium from the soil which becomes available to the plant in doses which are lethal to some plant species such as the spruce and beech. The low pH produced by this nitrification process exacerbates the known effects of acid rain on vegetation. The nitrate ion formed, however, is very readily biodegraded (Galloway et al, 1978) and hence poses no significant threat to the environment. Studies by Gmur et al. (1983) have shown that leaf exposure to $(NH_4)_2SO_4$ aerosols at levels higher than the ambient concentration causes visible foliar injury and changes in plant biomass.

Studies of the formation of tropospheric sulphate aerosols from their precursors have been carried out by computer simulations of the chemical and meterological conditions available in the polluted environment (Meagher et al, 1982, Stewart et al, 1981); in real plumes; and in smog chamber simulations. The main disadvantage of real plume studies is the fact that the atmospheric chemistry of sulphate formation is very sensitive to meteorological conditions. Though measurements in the real atmosphere are necessry to assess the general nature of the problem, the complexities and uncertainities involved in atmospheric processes are so enormous that their use in understanding the exact nature of the chemistry of the reactions and the characteristics of the products is out of the question. On the other hand, cloud chamber simulations whether of the batch or the flow type, provide an experimental means of avoiding the complexities and uncertainties of field experiments in real atmospheres. The physical and chemical characteristics of the reactants in the chamber can be accurately measured under controlled conditions not possible in nature while maintaining conditions that are representative of natural situations. It is, however, difficult to extrapolate results obtained in the cloud chamber to atmospheric condition; but a link between them could be achieved by running a parellel study involving both (Luria et al, 1983).

Aim of the Study

This study is concerned with the oxidation of SO_2 in the presence of NH_3 in submicrometer size droplets at ambient temperatures in a flow type reactor. Studies so far done on this sulphate formation mechanism were carried out in bulk solutions (Junge et al, 1958 and Holt et al, 1981); in large aqueous droplets (Van den Heuvel et al., 1963 and Miller et al, 1972); and theoretically by computer simulations in fog and cloud droplets (Scott et al., 1967; McKay, 1971; and Miller et al, 1972).

So far no studies have been reported on the evolution of size distribution and chemical composition as a result of heterogenous oxidation of SO_2 under conditions similar to those used in this study. It simulates concentrations of SO_2 and catalyst ions appropriate to a fairly diluted plume with a substantial in-mixing of NH_3. Submicrometer size droplets were chosen because in the troposphere cloud and fog droplets of similar size are more important for sulphate formation due to their longer life time than larger droplets and because of their larger surface area to mass ratio which makes the transport of gaseous reactants from the bulk gas phase to the droplet easier. This contribution to the study of the heterogeneous oxidation of SO_2 addresses itself to some aspects of the in-cloud oxidation which is the most important site for acid rain formation hitherto neglected. In particular, for the first time the synergism between NH_3 and manganese ion in SO_2 oxidation is investigated in the laboratory.

The aerosols were generated from dilute $(NH_4)_2SO_4$ and $MnSO_4$ master solutions and the oxidation monitored by both light scattering and chemical methods. The parameters measured were the ZOLD parameters (by light scattering analysis) and the molar concentrations of the sulphate (by chemical analysis) formed in the aerosol at contact times ranging from 0.65 to 25.2 minutes. The light scattering measurement method used was that developed by Carabine and Moore (1973) and sulphate analysis was by non-suppressed ion chromatography.

The basic theory of the study is discussed in Chapter II. The general experimental arrangement together with the chemical analytical methods used are described in Chapter III. The results of the experiments are stated and critically discussed in Chapter IV. In Chapter V the findings of the study are summarised and conclusions drawn.

CHAPTER II

BACKGROUND THEORY

In this chapter, the background information about this study will be examined. First, the precursors of $(NH_4)_2SO_4$ will be discussed in terms of their source and tropospheric flux, burden and removal. Then the oxidative processes that transform SO_2 to sulphate will be treated with special emphasis on those that lead to the formation of $(NH_4)_2SO_4$. Finally, the properties of aerosols will be discussed in terms of their size distribution analysis, and the processes that lead to their size distribution change and droplet removals from an aerosol stream.

II.1 Ammonium Sulphate Precursors in the Troposphere

The precursors of $(NH_4)_2SO_4$ considered are NH_3 and SO_2. Other volatile sulphur compounds of lower oxidation state such as H_2S are oxidized first to SO_2 (Hitchcock, 1984) and later to sulphate and so are included in the SO_2 discussion.

II.1.1 Ammonia

The detection of atmospheric free NH_3 in the absence of ammonium particles was first demonstrated by Junge (1956). Airborne measurements from instrumented aircraft was done by Lenhard et al (1980). Healy (1974) found that in rural Harwell, free NH_3 and SO_2 coexisted with SO_2 usually present in considerable excess. Bottger et al (1981) have estimated the source strength of NH_3 of a limited area by evaluating the chemical composition of precipitation. By integrating the results over a large area and over varying conditions simultaneously it will be possible to obtain the total NH_3 flux from the surface to the troposphere; this has been estimated at about 100 kT per annum in UK (Healey et al, 1970) with ground level concentration of around 4 μgm^{-3} (Eggleton et al, 1969). However, the total initial production rate of NH_3 at ground level could only be obtained if due consideration is given to the rate of its absorption by plants and

other surfaces, its deposition (dry and wet) rate, and all the gas phase chemical reactions that convert it into other entities.

The release of NH_3 from the land increases from the poles to the equator; is higher in the summer than in the winter; and is more in rural than in urban area (Lenhard et al, 1982). Possible NH_3 sources are animal wastes (urine, sweat and excrement); rotting organic matter (vegetation and animal tissue) (Dawson, 1977 and T.V. Larson et al, 1983); coal combustion (Sonderlund et al, 1977) and fossil fuel refining. The contribution of each source in U.K. (Healy et al, 1970) is listed in Table II.1. Figures are not available for fuel refinery effluent contribution to the atmospheric flux of NH_3 but it is likely to be substantial if coal gasification is taken into consideration. The fact that some of these sources for example, the hydrolysis of urea to give NH_3 are intensified by increase in the ambient temperature explains the geographical and temporal distribution of the release rate.

As a result of its reactivity especially with acidic substances, and high solubility, NH_3 has a very short tropospheric average residence time. The processes that remove it from the atmosphere are transformation to ammonium particles, oxidation, deposition on surfaces and absorption by moist surfaces. The oxidation of NH_3 by OH radical was shown by Stuhl (1973) to be by this mechanism:

$$NH_3 + OH \rightarrow NH_2 + H_2O \qquad \text{II.1}$$

and has a rate constant of 1.5×10^{-13} cm^3 $mole^{-1}s^{-1}$ (Perry et al, 1976). This process destroys less than 1% of the total NH_3 flux.

Of great importance is the role of NH_3 in the tropospheric formation of sulphate aerosols, which will be discussed in Section II.2.

II.1.2 Sulphur Dioxide

SO_2 exists in the atmosphere in a concentration characteristically below 0.1vpm. That this has remained fairly constant for a long time

shows the existence of a cycle that maintains a balance between its release to the atmosphere and its transport to other reservoirs. Recent studies (Koide et al 1971) have shown that the balance has been upset as a result of anthropogenic sulphur dioxide emissions which has been increasing by 2.2% per annum (Cullis et al. 1980). Its non-uniform distribution is as a result of the variability of its source and sink mechanism. Some of the estimates on the burdens and fluxes are based on sparse data of doubtful reliability and so may be in error by unknown amounts. Consequently, no attempt will be made in this study to consider the interactions and exchanges of sulphur compounds between the various reservoirs which do not directly involve the atmosphere. Authoritative reviews of the sulphur cycle exist elsewhere (Kellog et al 1972).

The atmosphere is the smallest of the natural reservoirs of sulphur compounds but at the same time the most important because atmospheric sulphur has the greatest impact on the biosphere and partly because the atmosphere is the major medium through which sulphur compounds are transferred from their source to other reservoirs. Table II.2 shows the tropospheric burden of sulphur compounds (sulphate not included) as estimated by four studies. The anthropogenic and biogenic emissions and the flux from other reservoirs constitute the source of atmospheric sulphur compounds while the flux to the crust via the pedosphere and hydrosphere constitute the sink. Fig.II.1 show the fluxes of sulphur compounds in the atmosphere in TgS per annum (Friend, 1973).

Volatile sulphides principally H_2S, $(CH_3)_2S$, CS_2 and OCS constitute the largest aggregate of sulphur input into the atmosphere. Delmas et al. (1980) and later Adams et al (1981) first investigated their emission over a large territory and long time spans, and found an exponential increase in emission from the poles to the equator. Sulphides are produced by the decomposition of amino acids containing thiol groups (Schlegel, 1974 and Nicol et al, 1970). Another biogenic source of large quantities of sulphur compounds is the anaerobic decomposition of sulphate by sulphur bacteria (Nickles, 1968).

TABLE II.1 Ammonia Source in U.K.

Source	Amount of Nitrogen Available kT yr^{-1}	Proportion Released to Atmosphere as NH_3	Amount of NH_3 Released to Atmosphere kT yr^{-1}
Animal Urine	700	10%	85
Sewage	250	Less than 1%	Less than 3
Human Sweat	5	High	Less than 5
Rotting Vegetation	100	Low	Small
Fertiliser Use	680	Less than 2%	Less than 16
Factory Leakages	750	Less than 1%	Less than 9
Coal Combustion	340	Small	Less than 10
Fossil Fuel Refinery	?	?	?

TABLE II.2 Tropospheric burden of S (TgS)

Form of Sulphur Compound	Reference			
	Friend (1973)	Meszaros (1978)	Sze et al (1980)	Moller (1984)
SO_2	0.52	0.45	0.46	0.3-0.4
H_2S	0.99	-	0.04	0.03
$(CH_3)_2S$	-	-	0.02	0.05
CS_2	-	-	2.20	0.2-0.8
OCS	-	-	0.6	8-14
Total (Tgs)	1.51	0.45	3.32	8.5-15.27

$$4H_2 + 2H^+ + SO_4^{2-} \rightarrow H_2S + 4H_2O \qquad \text{II.2}$$

The location may be continental soil or estuarine muds, tidal flats and coastal anoxic marsh sediments and bogs where oxygen supply is limited and where the sulphate is derived from sea water.

In spite of the high production of these volatile sulphides (Hitchcock, 1976) their background mixing ratio of about 2.0×10^{-4}ppm (Robinson et al, 1968) is very low. This means that they have very small tropospheric residence times of perhaps one day (Kellog et al, 1972) and are apparently quite rapidly oxidized to SO_2 alone (Delmas et al, 1978) or to SO_2 and sulphate in approximately equal quantities especially in modified marine tropical air masses (Hitchcock et al, 1984). Clarke et al (1983) have demonstrated the rapid oxidation of SO_2 in NaCl droplets even at low pH. It is most likely that H_2S or the other volatile biogenic sulphides may also be oxidized rapidly in such droplets especially in maritime and coastal environments.

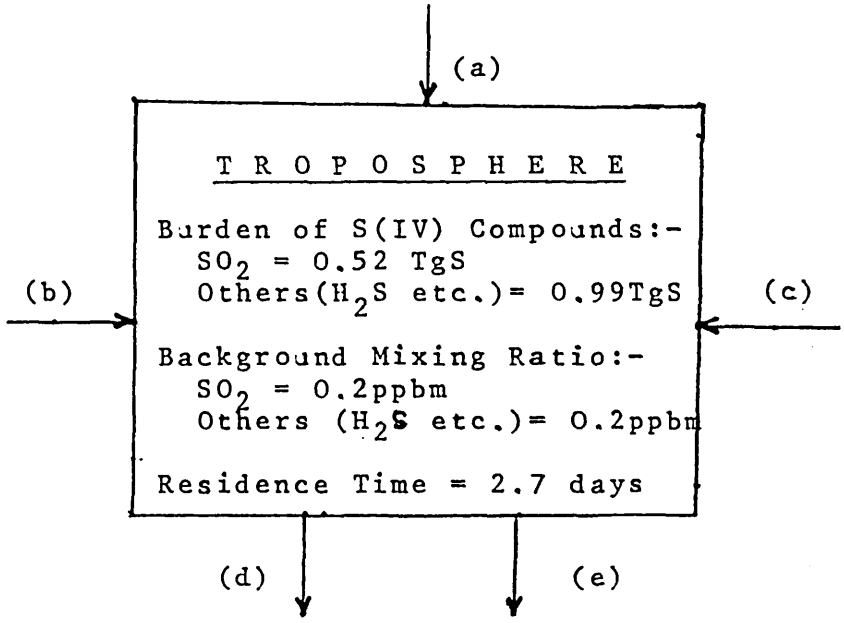
Volcanic contribution to the tropospheric sulphur flux of about 2 $TgSyr^{-1}$ is mainly in the form of SO_2 (Kellog et al, 1970). These estimates were based on the yield of magma per year of volcanoes on the assumption that the gas generated is 0.5% W/W of the lava emitted (MacDonald, 1972). Other geothermal activities such as sulphur springs contribute little compared to volcanoes (Cullis et al.1980). Generally volcanoes and geothermal activities contribute little when compared to other natural sources of atmospheric SO_2 because of the sporadic nature of their occurence. Estimates of SO_2 volcanic emission from nine studies are listed in Table II.3.

The aspect of sulphur flux into the atmosphere which is of the greatest concern and whose abatement measures have generated many studies is that of anthropogenic origin. It has been estimated at 64Tg Sy^{-1} (Robinson et al, 1968) and is almost entirely SO_2. The primary sources are listed in Table II.4 (SCEP, 1970). Coal burning is the most abundant source of man-made SO_2. Burning of petroleum products is the next with emission reaching a maximum in the heaviest fractions (Considine, 1977). Industrial activities that emit SO_2 include the smelting of non-ferrous metals (copper, zinc and lead); refinery of fossil fuels (oil and coal); the Kraft process of paper

maufacture; incineration of refuse; production of sulphur; and manufacture of H_2SO_4. Natural gas is a clean fuel with sulphur content below 5ppm (Medici, 1974).

The emission rate of anthropogenic sulphur has been increasing. Table II.5 (Cullis et al, 1980) shows an increase of SO_2 emission rate from 6.27 $TgSy^{-1}$ in 1880 to 74.44 in 1965. It also shows the change in relative weightings with coal shrinking from 97.4% of the total emission in 1880 to 68.5% while petroleum rose from 0.6% to 19.1% in the same period. This fact will be confirmed from the data on the production of the fossil fuels and other sulphur yielding products listed in Table II.6 for the same period.

Kellog et al (1972) estimated that based on the 1965 rate of the use of fossil fuels and industrial activities that the emission rate of SO_2 will reach 137 TgS y^{-1} by the year 2000. This means an increase of over 75% above the 1965 figure given by Robinson et al (1970). This is not likely to be so because a number of emission control measures are being developed and new laws on emission enacted. Some of the laws envisage stricter fuel refining strategies and comprehensive flue gas desulphurisation in all smelting and fossil fuel burning plants. Another proposition is switching to non-fossil fuel sources of energy. According to Hafele quoted by Möller (1984) whereas in 1975 up to 90% of the global energy came from fossil fuels, this fraction will fall to 67% by the year 2000 and this means that SO_2 emission will be unlikely to reach the predicted level for the year 2000. Emission reduction will eventually halt the onward trend towards increased atmospheric burden of SO_2.



Note:- (a),(b),(c),(d) and (e) are S(IV) fluxes.

(a) Anthropogenic Sources
$64 TgS\ yr^{-1}$ (Robinson and Robbins,1968)

(b) Biogenic Sources
$89 TgS\ yr^{-1}$ (Kellog et al,1972)

(c) Crustal Degassing (mainly volcanoes)
$2.0\ TgS\ yr^{-1}$ (Kellog et al,1972)

(d) Deposition (wet and dry)
$155\ TgS\ yr^{-1}$ (Junge,1968)

(e) Chemical Transformation

Figure II.1:-The flux and burden of SO_2 and other volatile S(IV)compounds in the Troposphere.

TABLE II.3 Global Volcanic SO_2 Emissions in $TgSy^{-1}$ (Moller, 1984)

Reference	Flux
Bartels	17
Kellog et al (1972)	1.5
Stoiber and Jensen (1973)	5
Friend (1973)	2
Cadle (1975)	3.75
Naughton et al (1975)	23.5
Granet et al (1976)	3
Sabroux (1980)	15
Cadle (1980)	20-30

TABLE II.4 Anthropogenic Sources of Atmospheric Sulphur

Source	Emission Rate/$TgSy^{-1}$
Coal burning	45.4
Oil burning	5.5
Industrial Activities (Smelting and Fuel Refining)	13.6
Transportation	0.4
Total	64.9

TABLE II.5 The Historical increase in SO_2 emissions ($TgSy^{-1}$)

		1880	1910	1930	1950	1960	1965
Coal	- Mass	6.1	21.05	25.65	330	47.85	61.0
	- %	97.4	90.5	85.5	79.4	736	68.5
Petroleum	- Mass	0.04	0.35	1.56	4.15	9.95	14.25
	- %	0.6	1.5	5.2	10.0	15.3	19.1
Non-ferrous ores	- Mass	0.13	1.86	2.46	3.69	6.14	6.45
	- %	2.1	8.0	8.2	8.9	9.4	8.7
Others	- Mass	-	-	0.33	0.7	1.11	1.34
	- %	-	-	1.1	1.7	0.17	1.8
Total	- Mass	6.27	23.25	30.0	41.54	65.05	83.04

TABLE II.6 The Historical production of SO_2 yielding products (in TgS) (Cullis et al, 1980)

	1880	1910	1930	1950	1961	1965
Coal	313	1055	1215	1450	1950	2040
Petroleum	4	45	147	525	1122	1511
Non-ferrous Ores	0.8	-	4.6	2.5	10.0	11.6
Others (100% H_2SO_4)	-	-		26	50	67.8

II.2 The Fate of Tropospheric SO_2

The greatest interest in the study of the fate of SO_2 released into the atmosphere has centred on the study of the plumes of a fossil fuel burning stationary source. The original policy towards the disposal of pollution sulphur emission was that of dispersion and diluting by means of high stacks with the hope that the residence distance defined by Enger and Högström (1979) as the distance where 2/3 of the emission has been removed would be well away from the geographical location of the emitting source. This measure has, however, only succeeded in creating the problem of regional and transboundary pollutant transport which is a subject of current interest in SO_2 pollution (Perhac, 1978; Ottar, 1978; Semb, 1978; Whelpdale, 1978, and Altshuller, 1976). Plume studies have been carried out by air-borne and land-based sampling (Newman, 1981; and Hegg et al, 1980) and by the remote sensing techniques (Hamilton et al, 1978; and Grant et al, 1983).

The dispersion and removal of SO_2 released in the plume of a point or diffuse source depends on the source characteristics which determine the buoyancy and, therefore, the effective emission height; the mean wind velocity which determines the rate of advection and horizontal dispersion; the time-dependent depth of the mixing layer which determines the rate and extent of vertical dispersion; and the relevant sink mechanisms such as chemical transformation and deposition. During unstable conditions of the atmosphere (moderate to strong insolation and surface wind speed under $3ms^{-1}$) (Pasquill, 1974) the height of the mixing layer can extend between 0.4 and 2 km and the plume takes a short time to mix completely. On the other hand, under stable (night-time) conditions both vertical and horizontal dispersions are minimal.

The SO_2 time-averaged concentration downwind of a point source emitting at a constant rate into a quasi-steady atmospheric flow can be described by one of the forms of the Gaussian dispersion equation. Assuming ground and inversion layer reflections (Clark, 1979) ,

$$C(x,y,z) = \frac{Q}{2\pi u \sigma_y \sigma_z} \exp \frac{-y^2}{2\sigma_y^2} \quad F(h,z,A) \qquad \text{II.3}$$

where

$$F(h,z,a) = \exp \frac{-(z-h)^2}{2\sigma_z^2} + \exp \frac{-(z+h)^2}{2\sigma_z^2}$$

$$+ \exp \frac{-(2A+z-h)^2}{2\sigma_z^2} + \exp \frac{-(2A-z+h)^2}{2\sigma_z^2}$$

$$+ \exp \frac{-(2A-z-h)^2}{2\sigma_z^2} + \exp \frac{-(2A+z+h)^2}{2\sigma_z^2}$$

where $C(x,y,z)$ = concentration at point (x,y,z) in gm^{-3}

A = Height of temperature inversion (m)

Q = source strength (gs^{-1})

u = mean wind velocity (ms^{-1})

z,y = vertical and crosswind displacements respectively (m)

σ_y, σ_z = lateral and vertical standard deviations of plume spread (m) and are functions of x, the distance downwind of the source.

h = source height (m)

These dispersion coefficients may be obtained from power law functions

$$\sigma_y = \alpha x^p$$

$$\sigma_z = \beta x^q$$

where α, β, p and q are constants having the values for the Pasquill-Gifford stability classes as shown in Appendix B.

One of the aims of the plume study is to determine the ground level concentration of pollutant at a receptor location downwind particularly with respect to potential population exposure. This is given for a vertically unbounded atmosphere by the equation in which the plume rise is taken into consideration (Clark et al, 1984),

$$C(x,y,0) = \frac{Q}{\pi \sigma_y \sigma_z u} \exp -(y^2/2\sigma_y + H^2/2\sigma_z^2) \qquad \text{II.4}$$

where $H = h_s + \Delta h$
$= $ Effective (virtual) emission height (m)
$h_s = $ Stack height (m)
$\Delta h = $ Plume rise (m)

The plume rise is obtained by the formula propounded by Briggs (1969). Pasquill (1961) estimated the location of maximum ground level concentration of SO_2 by assuming that σ_y/σ_z is a constant irrespective of the distance of the location down-wind of the source and integrating equation II.4 with respect to σ_z. He showed that this occured at a location where

$$\sigma_z \sqrt{2} = H$$

Scorer (1978) obtained the actual value of the ground level maximum concentration along the plume axis using the equation

$$C(x,0,0)_{max} = \frac{nQ}{uH^2} \qquad \text{II.5}$$

where n is a factor which is determined by the properties of the plume and has a numerical value of around 0.15.

The Gaussian plume model is limited by the simplifying assumptions on which it is based. The assumption of a quasi-steady wind direction is of course too idealised since as a result of the diurnal cycle of the atmospheric boundary layer the wind direction is time dependent. The second assumption is that of a mean wind velocity, u, which in effect neglects the vertical variation of the wind velocity. The value of u is estimated from a power-law velocity profile at the height $0.1\ z_i$, given by

$$u = u_r\left(\frac{0.1\ z_i}{z_r}\right)^p \qquad \text{II.6}$$

where $z_i = $ convective boundary layer depth

u_r = measured wind speed at a reference height z_r

p is a function of stability.

Finally, the assumption of chemical inertness of the target pollutant renders it unsuitable for use without modification in modelling SO_2 and other reactive gases. In discussing the various removal processes of SO_2 from the troposphere, the necessary modifications to equation II.5 to take care of the particular mechanism will be mentioned.

The Removal Processes of Atmospheric SO_2

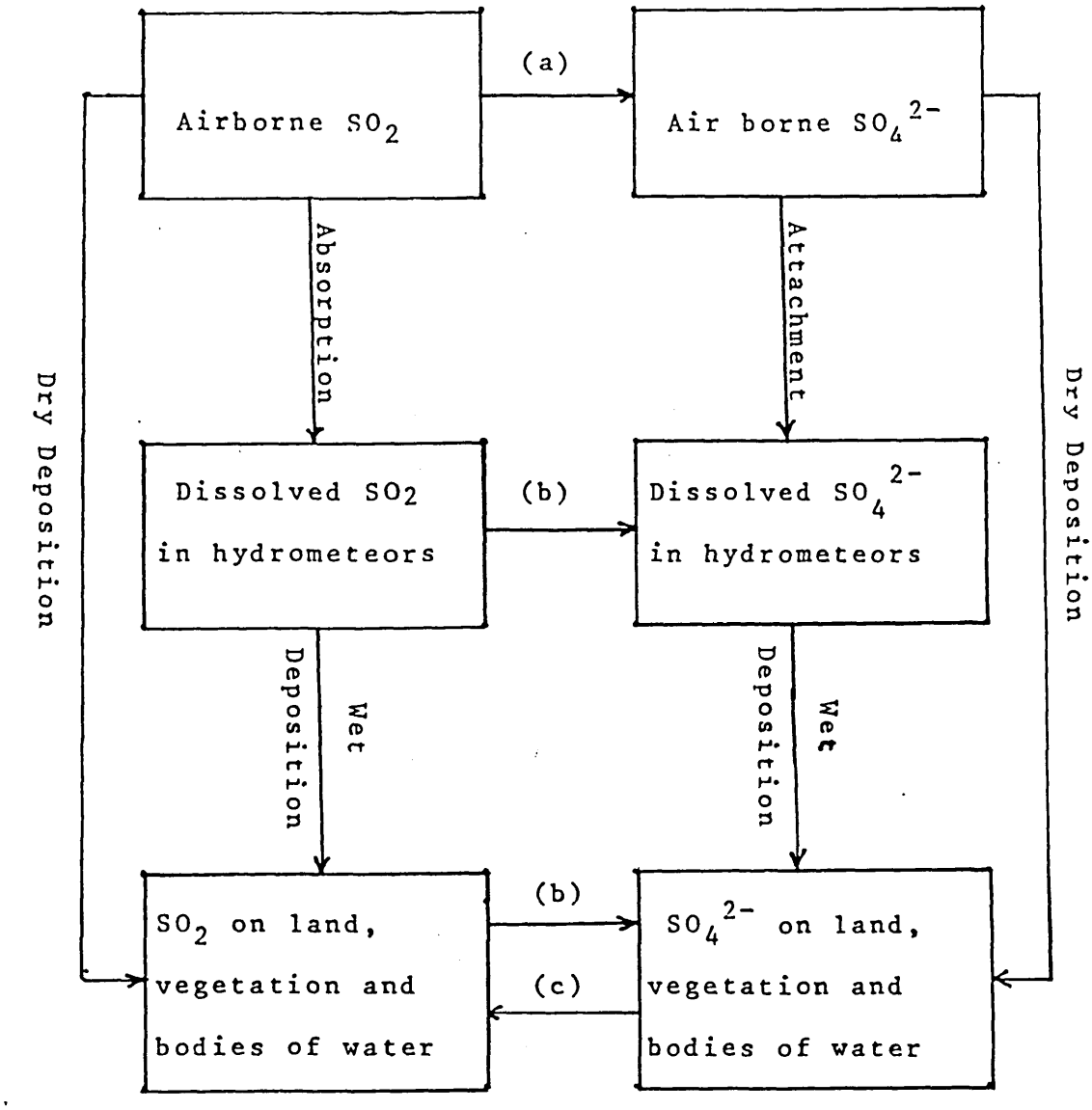
It is not possible to measure reliably in the field the transformation and deposition coefficients for atmospheric SO_2. Attempts at measurements yield results that are very variable since they are evaluated from a large number of independent controlling input variables whose values are time dependent and can vary within very wide margins.

Table II.7 shows the mechanisms of SO_2 removal from the atmosphere and the independent variables that determine the removal rate (Endlich et al., 1982). Using published data of kinetic model of atmospheric SO_2 oxidation, Moller (1980) calculated that the contributions of these processes in SO_2 removal are transformation (44%), dry deposition (45%) and wet deposition (11%). These removal processes will be considered individually with the aim of assessing their relative importance. No attempt will be made to treat then in details in this section.

Fig. II.2 is a block diagram of the sink mechanism of SO_2 in the atmosphere. The reverse of the removal processes shown in the diagram will not be discussed even though they are operating. The relative importance of these removal processes depend on conditions in the environment which will be discussed for each removal process.

Dry deposition of SO_2

There are two processes whereby SO_2 could be removed from the atmosphere by dry deposition. The first is adsorption to aerosol particles and subsequent deposition. This process is controlled by the



Note:-

(a) Homogeneous gas phase oxidation
(b) Heterogeneous aqueous phase oxidation
(c) Biogenic reduction

Figure II.2:-Diagrammatic representation of the removal of sulphur dioxide from the atmosphere.

size and type of aerosols in the mixing layer. The second process is the direct removal of the gas as a result of turbulent laminar layer between the SO_2 and the surface (soil, vegetation or water).

Direct deposition of SO_2 is governed by both transfer in the gas phase and sorption at the receiving surface. The sorption is assumed to be irreversible (Garland, 1978). For a low SO_2 mixing ratio, the sorption rate is proportional to the SO_2 concentration. If gas phase transfer processes are neglected, the SO_2 flux to the surface is given by the equation

$$F = \frac{X_s}{r_s} \qquad \text{II.7}$$

where

F = mass flux;

X_s = SO_2 concentration at a point above the surface adjacent to it

r_s = surface resistance to sorption.

The parameter r_s depends only on the nature of the surface.

Table II.8 shows the SO_2 deposition data for some surfaces obtained in experimental investigations. For water and calcareous soil surfaces, surface resistance to deposition is negligible. Liss (1971) showed that as a result of the high pH of ocean water, it is a perfect sink for SO_2 and hence the deposition velocity should be much higher than stated by Johnson (1983). Whelpdale et al. (1974) found a value of 2.2 cm s^{-1} for the water of Lake Ontario. This is expected to be higher for sea water with higher pH. A mean value of 0.8 cm s^{-1} has been suggested as applying to large areas of Europe (Garland, 1978).

Deposition velocity is measured by the concentration gradient method (Whelpdale et al. 1974; Garland, 1977; and Shephard, 1974;) which is based on equation II.7 and requires the simultaneous measurements of meteorological variables to deduce the eddy diffusivity $K(z)$ and the SO_2 concentration at different heights. Others include the tracer and the mass balance methods.

For a plume confined in a well defined mixing layer of height h, above the absorbing surface, in the absence of any other removal process, the SO_2 will decay exponentially as a result of dry deposition with a mean residence time given by

$$t_{res} = \frac{h}{V_g(z)} \qquad \text{II.8}$$

where $V_g(z) = \frac{1}{r(z)}$;

Vg(z) is the transfer or deposition velocity from a height z to a surface with a zero concentration of SO_2.

$r(z) = r_g(z) + r_s$;

$r_g(z)$ is the height dependent gas phase turbulent transfer resistance calculated from meteorological conditions. The source depletion model is used in incorporating dry deposition into the Gaussian plume model. The source strength in equation II.3 is adjusted as a function of downwind distance to reflect the amount of SO_2 lost by this process. This is given, according to Clark et al (1984) by

$$Q_d(x) = Q \{\exp F_D(x)\}^{v_g(z)/u} \qquad \text{II.9}$$

where

$$F_D(x) = -\sqrt{2}/\pi \int_0^x \frac{1}{\sigma_z} \left[\exp \frac{-h^2}{2\sigma_z^2} + \exp \frac{-(h + 2L)^2}{2\sigma_z^2} + \exp \frac{-(2L - h)}{2\sigma_z^2}\right] dx,$$

and L = mixing height (m).

Wet Deposition

Precipitation scavenging is expected to be a more efficient way of SO_2 removal from the atmosphere than dry deposition because of the much larger fall speed of hydrometeors than gas deposition velocity. This agrees with a study by Shannon (1980) using the ASTRAP model. However,

TABLE II.7 Transformation and Deposition Rates of SO_2

Parameter	Range of Variation	Independent Variable
1. Transformation Rate $SO_2 \rightarrow SO_4^{--}$ (% hr^{-1})	1% h^{-1} (winter) to 4% h^{-1} (summer)	Solar Radiation, Humidity and Chemical Composition of the atmosphere
2. Wet Deposition Rate (% hr-1) for 5 mm hr^{-1} rainfall rate	3% h^{-1} (winter) to 17% h^{-1} (summer)	Rainfall type and rainfall rate
3. Dry Deposition Velocity cm s^{-1}	0.05 - 0.85	Land characteristics, vegetation, atmospheric, stability season and time of the day.

TABLE II.8 : SO_2 dry deposition data

Surface	$V_g(z)$ (cm s^{-1})	$r_g(z)$ $s\,cm^{-1}$	r_s $s\,cm^{-1}$	Reference
Fresh Water	0.41	1.86	0.56	Garland (1977)
Ocean	0.5			Johnson (1983)
Snow	0.13 - 0.53			Johnson (1983)
Forest	0.1 - 3.6			Johnson (1983)
Calcareous soil	1.2	0.83	0.01	Garland (1977)
Sandy soil	0.6			Johnson (1983)
Grass	0.8		0.8	Shephard (1974)
Wheat	0.74	0.5	1 - 2.5	Fowler (1978)

a replicate study by Bhumralker et al (1980) using the ENAMAP-1 model made a reverse observation (Table II.9). Factors that influence the rate of wet deposition include temperature, humidity, precipitation type and intensity, cloud type and size, the location of the SO_2 relative to the cloud, its vertical concentration profile and its chemical properties.

Anderson (1967) treated wet deposition as a first order process with respect to SO_2 having a rate equation which takes both in-cloud and below-cloud processes into consideration;

$$\frac{dC_y}{dt} = -w_1 C_y - w_2 C_y \qquad \text{II.10}$$

$$= - S_1 - S_2$$

where w_1 and w_2 are the dimensionless rainout and washout rate coefficients respectively (Slinn et al, 1978); C_y = bulk gas phase SO_2 concentration; S_1 and S_2 are the cloud-borne and rain-borne SO_2 concentration.

The processes that go on in the cloud also apply to a plume. As the plume is emitted into the cold atmosphere, the water vapour condenses to form cloud-size (10 – 40 μm diameter) droplets. The droplets absorb SO_2 in a manner analogous to rain-out (incloud scavenging). Hales (1972) described a model in which the so-called pseudophysical absorption is the dominant uptake mechanism of a gas of which the spatial distribution of concentration is known. Under this model, SO_2 is treated as having absorption behaviour somewhat similar to that of a nonreactive gas because of the reversible nature and the speed of the equilibrium reactions compared to the purely physical steps (Hales, 1978). Hales (1972) treated SO_2 absorption by droplets in terms of the two-film mass transfer theory and represented it mathematically by the equation

$$J = -K_y (C_{yb} - C_{ye}) \qquad \text{II.11}$$

where

J = average molar flux of SO_2;

K_y = mass transfer coefficient based on the overall concentration driving force between the bulk gas-phase and droplet phase;

C_{yb} = mole fraction of SO_2 in the gas phase;

$$C_{ye} = H_s C_{xb} \qquad \text{II.12}$$

H_s = Henry's law constant for SO_2

C_{xb} = mole fraction of SO_2 in the bulk liquid phases

Johnstone et al (1934) have shown that II.12 is valid for SO_2 mixing ratio of between 2.6×10^{-4} and 1.7×10^{-2}. If, based on the moderate solubility of SO_2 it is assumed that the majority of transport resistance is in the gas phase, K_y could be calculated using the semi-empirical Fröessling equation (Bird et al, 1960) for purely convective-diffusive transport in the gas phase:

$$Sh = 2 + 0.6\ Re^{1/2}\ Sc^{1/3} \qquad \text{II.13}$$

where

$$Sh = \frac{K_y d}{D_y C_y} = \text{Sherwood number}$$

$$Re = \frac{d v_z}{\nu} = \text{Reynolds number}$$

$$Sc = \frac{\nu}{D_y} = \text{Schmidt number}$$

D_y and ν are the diffusivities of mass and momentum respectively in the gas phase; v_z = vertical velocity of hydrometeor ;

d and C_y are the droplet diameter and SO_2 concentration in the droplet phase respectively.

In his physico-chemical model, Postma (1970) considered the effect of the equilibrium chemical reactions on SO_2 uptake by droplets; eqns II.14, II.16, II.18 and II.20

$$SO_2 + H_2O \rightleftharpoons SO_2.H_2O \qquad \text{II.14}$$

from which

$$[SO_2.H_2O] = H_s p_{SO_2} \qquad \text{II.15}$$

where H_s = partition (Henry's Law) constant of SO_2 between air and water.

$$SO_2.H_2O \rightleftharpoons H^+ + HSO_3^- \qquad \text{II.16}$$

from which

$$[HSO_3^-] = K_{1s} H_s p_{SO_2} / [H^+] \qquad \text{II.17}$$

where K is the first ionisation constant of SO_2

$$HSO_3^- \rightleftharpoons SO_3^{=} + H^+ \qquad \text{II.18}$$

from which

$$[SO_3^{=}] = K_{2s} K_{1s} H_s p_{SO_2} / [H^+]^2 \qquad \text{II.19}$$

where K_{2s} is the second ionisation constant from which the total sulphur species in solution is given by

$$[S(IV)] = [SO_2.H_2O] + [HSO_3^-] + [SO_3^{--}] \qquad \text{II.20}$$

The effect of the equilibrium reactions on the SO_2 uptake by cloud droplet is seen from the fact that although the partition coefficient

$$\frac{[SO_2.H_2O]}{p_{SO_2}}$$

is a constant (Henry's Law constant) from equation II.17 at all concenrations, the partition coefficient

$$\frac{[S(IV)]}{p_{SO_2}}$$

is not. The equilibrium data of Johnstone et al (1934) of the SO_2 droplet-phase concentrations of the non-ionised and the total S(IV) as a function of SO_2 partial pressure (Fig. II.3) gives a straight line through the origin for the former and a curve with steeper slope at the lower concentrations for the latter. This means that the partition coefficient for SO_2 in aqueous solution decreases with concentration. Hence for S(IV) in equilibrium with gaseous SO_2 according to Freiberg (1981)

$$[S(IV)] = \eta\{SO_2 \cdot H_2O\} = \eta H_s pSO_2 \qquad \text{II.21}$$

where η = ratio of dissolved S(IV) to dissolved SO_2

$$= 1 + K_{1s}/[H^+] + K_{1s}K_{2s}/[H^+]^2 \qquad \text{II.22}$$

Equation II.22 is based on the assumption that all H^+ ions are derived from either SO_2 hydrolysis (Equations II.16,II.18) or the dissociation of water.

The decrease in partition coefficient with increase in concentration is reflected in the effect of in-cloud or in-plume scavenging on wash-out processes. Assuming no irreversible conversion of SO_2 to sulphate in the droplet phase, cloud droplets will reach a concentration of SO_2 in equilibrium with the bulk gas phase concentration defined by equation II.20 (Freiberg, 1981). The characteristic time for this process is

$$\tau_{reag} = \frac{\pi^3}{3} \eta H_s RT \tau_{da} \qquad \text{II.23}$$

where

$$\tau_{da} = d^2/4\pi^2 D \qquad \text{II.24}$$

d = droplet diameter ; D = diffusion coefficient in aqueous phase
R = the universal gas constant (atm $mol^{-1} K^{-1}$);

Since η depends on pH, the value of τ_{reag} may become quite small at the ambient pH in the cloud even for very large droplets compared to the droplet residence time. A hydrometeor from the cloud therefore will

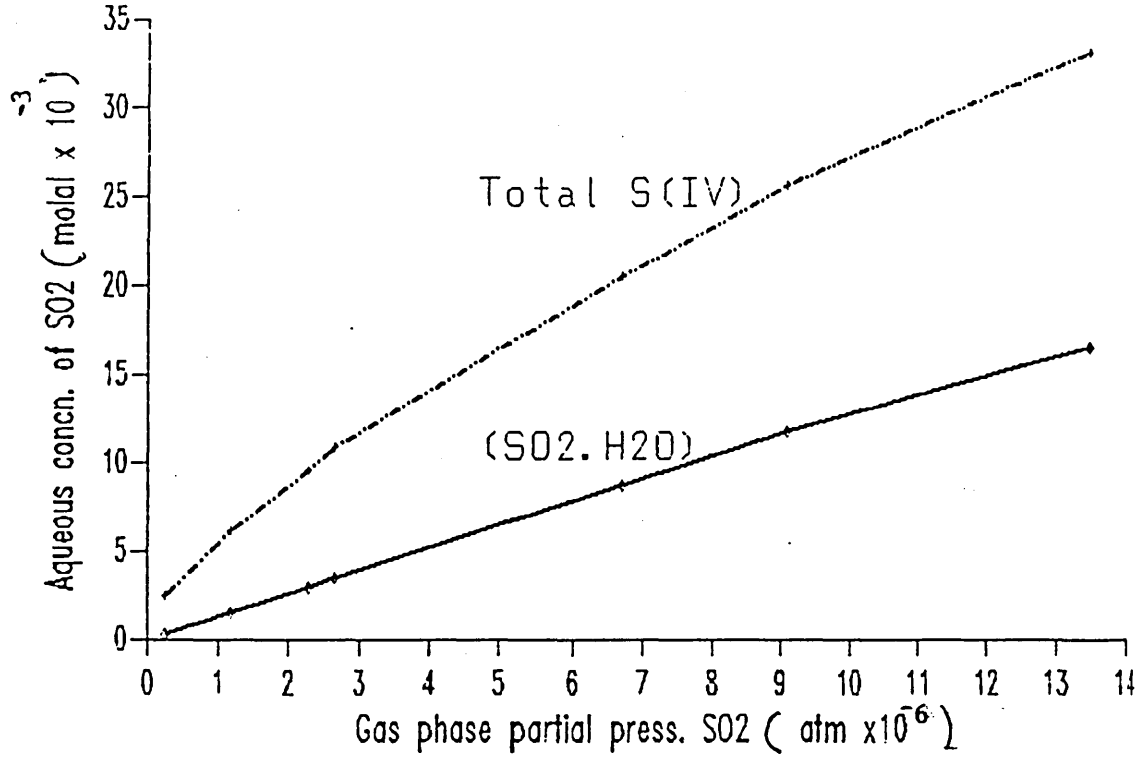


Figure II.3:-Droplet phase concentration of $SO_2.H_2O$ and total S(IV) as a function of gas phase partial pressure of SO_2.

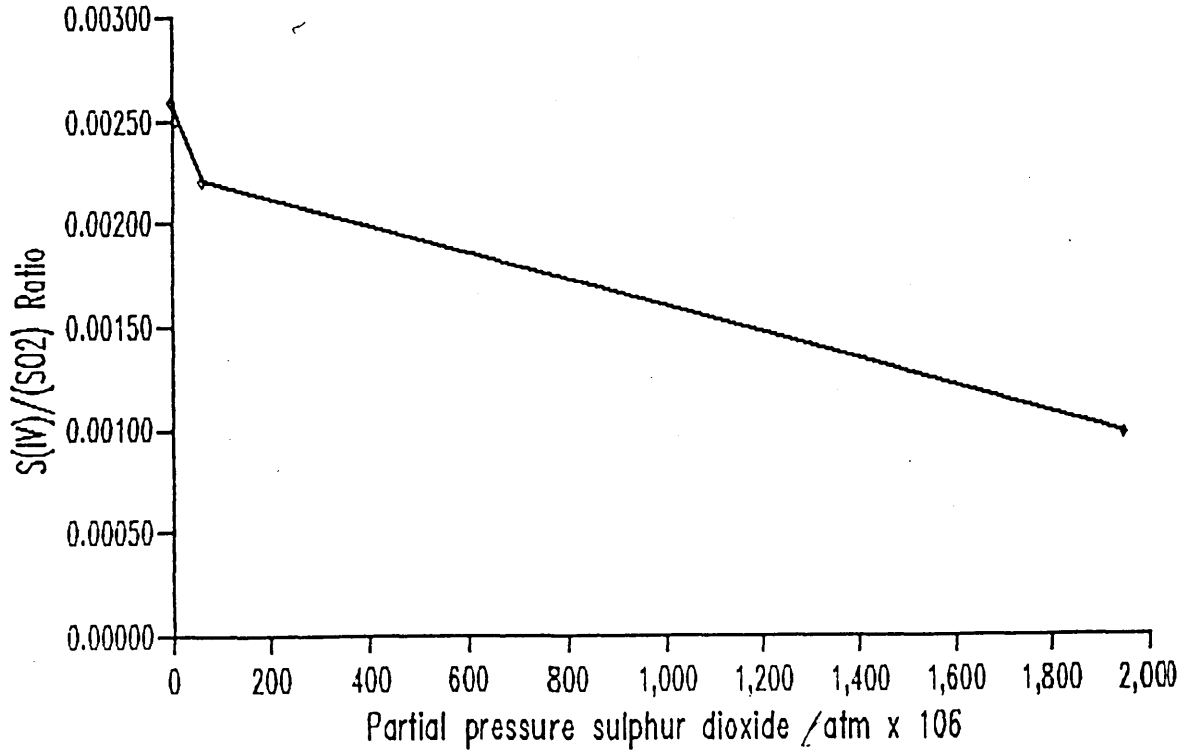


Figure II.4:-Variation of the total aqueous to gas phase concentration ratio of SO_2 with the partial pressure of SO_2 in the absence of NH_3.

have very low pH and this will tend to render it less effective in SO_2 wash-out processes.

The change in the SO_2 concentration of a droplet with time was calculaed by Garland (1978) making use of the combined approaches of Chamberlain (1960) and Postma (1970) to obtain the equation for spherical droplets

$$\frac{dC_x}{dt} = \frac{3K_y}{C_y d}(C_y - C_x^2 H^1) \qquad \text{II.25}$$

where H^1 is a solubility parameter

$$= (H_s K_{ls} M)^{-1}$$

M = molar mass of SO_2;

C_x = concentration of dissolved SO_2 in a drop of initially pure water after falling for time t through the air containing the SO_2;

C_y = concentration of SO_2 in the ambient air.

The solution of equation II.25 is

$$C_x = (H^1 C_y)^{1/2} \frac{1 - \exp(-2\gamma t)}{1 + \exp(-2\gamma t)} \qquad \text{II.26}$$

where

$$\gamma = \frac{6K_y}{d(C_y H^1)^{1/2}} \qquad \text{II.27}$$

Precipitation scavenging is not as straightforward as discussed above. Most of the models used in describing it are based on an irreversible absorption of SO_2 by the droplets and neglect the desorption process. This will tend to give higher theoretical value to the droplet phase SO_2 concentration than the real value. The effect of frictional drag on the surface of a hydrometeor as it falls through the air is also not taken into consideration. Frictional drag will tend to induce patterns of internal circulation (Pruppacher et al, 1970). This is added to by many possible secondary mixing effects brought about by oscillations and thermal perturbations induced by the drop falling through a temperature gradient. Also, account was not taken of the effect of the distortion of the bulk gas phase mass transfer

coefficient caused by the aerodynamic pattern around the falling drop. These effects affect transfer of material in the droplet in a manner that is not easy to analyse theoretically.

Field analysis of precipitation scavenging had been done by Davies (1983) by determining the SO_2 in rainwater. Högstrom (1973), Granat et al (1973) and Granat et al (1975) have undertaken measurements of SO_2 wet deposition from discrete plumes. All the studies except Hogstrom's obtained time constants of the order of 10^{-5} s^{-1} which means SO_2 scavenging by rain is very slow, confirming the conclusions of Kallend (1972) arrived at from theoretical calculations. This confirms the observations of Meurens et al (1976) quoted by Garland (1978) and Bhumralker et al (1980) that sulphur compounds in rain originate chiefly from the sulphate aerosols. Table II.10 also confirms the dominance of dry deposition in SO_2 removal from the atmosphere and also shows that a substantial part of the gas is transported away from the immediate vicinity of the source. With distance from the source, upward diffusion increases the mixing depth up to the subsidence inversion layer, thus reducing the effectiveness of dry deposition. The SO_2 under this situation is removed by other processes.

Wet deposition can be incorporated into the Gaussian plume model by assuming that rain affects the entire depth of the plume equally so that as the plume is traversing a rainy area, the source strength is effectively depleted at a uniform rate.

Chemical Transformation

Based on the data for transformation and deposition coefficients (Table II.7), chemical transformation is a slow process of SO_2 removal from the atmosphere. The rate of transformation has been estimated at a range of 0.1 to 10% h^{-1} (Harrison et al, 1975). It is controlled by the partial pressure of SO_2 and the condition of the atmosphere which includes the intensity of the solar radiation, cosmic radiation, temperature profile, humidity, and the presence and concentrations of oxidants, catalysts and particles. Chemical transformation is the best characterised process of SO_2 removal since its various mechanisms are fairly easy to simulate in the laboratory. The importance of chemical

TABLE II.9 Comparison of Dry and Wet Deposition using two models ($TgSO_2\ y^{-1}$)

Source Region	Model	SO_2 Deposition in Two receptor regions S.E. Canada Wet	S.E. Canada Dry	E. USA Wet	E. USA Dry	Total Emission
S.E. Canada	ENAMAP-1	0.45	0.77	0.12	0.26	1.9
E. USA	ENAMAP-1	0.33	0.38	4.01	6.70	14.1
S.E. Canada	ASTRAP	0.58	0.36	0.14	0.10	2.1
E. USA	ASTRAP	0.95	0.28	3.20	2.20	11.9

TABLE II.10 : The Atmospheric Sulphur Budget over N.W. Europe

Area included (km^2)	Source strength ($Mt\ Sy^{-1}$)	Dry deposition ($Mt\ Sy^{-1}$)	Wet deposition ($Mt\ Sy^{-1}$)	Wind loss ($Mt\ Sy^{-1}$)	Reference
$4x10^6$	16 - 17	6.3 (45%)	2.7 (19%)	5.0 (37%)	Garland(1977)
$4.2x10^6$	14.5	2.9 - 5.9 (20 - 41%)	4.1 (28%)	3.1 - 6.2 (21 - 43%)	Rodhe(1976)
$9x10^6$	20	11 (55%)	5.6 (27%)	3.4 (17%)	OECD (1977)

transformation in the study of the removal of SO_2 from the atmosphere is the fact that sulphate particulates have precipitation removal rate an order of magnitude more efficient than SO_2.

Typical field investigations of SO_2 to sulphate conversion rates in a steel plume (Levy et al, 1976) give data for the concentrations of SO_2 and sulphate which usually fit to expressions of the type (Freiberg, 1978)

$$C_r(x,y,z,t) = C(x,y,z)e^{-kt} \qquad \text{II.28}$$

where

$C(x,y,z)$ is given by Equation II.3;
$C_r(x,y,z,t)$ = down wind concentration of SO_2;
k is a pseudo first order rate constant;
t = time (s).

This mechanism is appropriate to a heterogeneous SO_2 oxidation process taking place in droplet solution in an expanding plume. Freiberg (1976) modelled the process as a chemical reaction occuring in an expanding volume reactor which can be equated with an elliptical plume ring which is centred about the plume's meandering centre line. The reaction rate decreases from the centre of the ring to its periphery because of the decrease in SO_2 concentration (Freiberg, 1978). However, mixing between the plume effluent and the background air controls the concentration of certain background species which are entrained and which react with SO_2 in various homogeneous oxidation mechanisms. The importance of homogeneous oxidation process should therefore increase from the plume centre to the periphery. The respective SO_2 oxidation mechanisms will be discussed in section II.2.

The contribution of chemical transformation to the time-dependent exponential decay of the plume SO_2 is expressed in terms of a chemical attenuation factor

$$\exp(-x/u\tau) \qquad \text{II.29}$$

calculated on the assumption of a first order rate mechanism

$$\frac{dC}{dt} = -kC$$

which on integration yields

$$C = C_o \exp(-kt)$$

If $t = x/u$ and $1/k = \tau$
where τ = characteristic time or time for SO_2 concentration to drop to 63% of its original value (Clarke 1985) x = distance travelled; u = mean wind velocity,
then

$$C = C_o \exp \frac{-x}{u\tau} \qquad \text{II.30}$$

or

$$C = C_o \exp \frac{-0.794x}{u\tau_{\frac{1}{2}}} \qquad \text{II.31}$$

where $\tau_{\frac{1}{2}}$ is half life and has a value of approximately two hours at 25° C and depends on the presence and concentrations of moisture, catalysts and oxidants (Meszaros et al. (1977). The depletion factor from equations II.30 or II.31 could be incorporated into the Gaussian plume model to account for SO_2 removal by chemical transformation:

$$C(x,y,z) = \frac{Q}{2\pi u \sigma_y \sigma_z} \exp \frac{-x}{u\tau} \exp \frac{-y^2}{2\sigma_y^2} \exp \frac{-z^2}{2\sigma_z^2} \qquad \text{II.32}$$

II.3 Oxidation of SO_2

The wide range in the estimated rate of the conversion of SO_2 to SO_4^{2-} (between 0.1 and 10% per hour) has been attributed to the variety of possible mechanisms for the reaction (Hegg et al, 1978). The mechanism may be grouped into two classes namely

1. Homogeneous gas-phase oxidation
2. Heterogeneous oxidation.

The former will be treated scantily with particular reference to atmospheric conditions. The latter will be treated as fully as possible.

II.3.1 Homogeneous Oxidation of SO_2

Ordinarily, homogeneous oxidation is not a very important aspect of formation of sulphate from sulphur dioxide in the atmosphere (Calvert, et al, 1978). However, in the presence of some reactive gaseous species or under intense solar radiation oxidation goes on to an appreciable extent. The results of early experimental work on homogeneous oxidation are reviewed by Leighton (1961). Four mechanisms have been delimited.

a. Oxidation of SO_2 by reactive intermediates such as atoms, free radicals and excited molecular species which are generated photochemically:- The most important atmospheric free radical is the OH. It has a steady state atmospheric concentration of 7.1×10^6 molecules cm^{-3} (Cox, 1974). It undergoes termolecular addition reaction with SO_2

$$\begin{array}{l} OH + SO_2 + M \xrightarrow{k_1} HOSO_2 + M \\ \qquad\qquad\qquad\quad \downarrow \text{Further Rxn} \\ \qquad\qquad\qquad\quad SO_4^{2-} \text{ Aerosol} \end{array} \qquad \text{II.32}$$

The reaction is irreversible and has a rate constant given by $k_1[M] = 6.0 \pm 0.8 \times 10^{-13}$ cm^3 $mole^{-1}$ s^{-1} for $[M]$ = 1 atmosphere of $N_2 + O_2$ (Cox, 1974/75). Other atmospheric free radicals and excited molecules that maybe involved in SO_2 homogeneous oxidation are

i the hydroperoxyl radical, HO_2 (Warneck, 1974)

$$SO_2 + HO_2 \xrightarrow{k_2} OH + SO_3 \; ; \; k_2 = 9 \times 10^{-16} \; cm^3 mol^{-1} s^{-1} \; ;$$

ii alkyl peroxyl RO_2 (Harker, 1975)

$$SO_2 + RO_2 \xrightarrow{k_3} RO + SO_3 \; ; \; k_3 = 9 \times 10^{-16} \; cm^3 mol^{-1} s^{-1}$$

iii triplet oxygen and alkenes. All these other species put together contribute less than 1% hr^{-1} oxidation of SO_2.

b. Oxidation of SO_2 by reactive intermediates generated in ozone-olefin thermal reaction is not important for most conditions which occur in the troposphere. The mechanism is very complex and so it is not possible to identify the reaction intermediate responsible for SO_2 oxidation. The mechanism contributes very little since a concentration of olefin of at least 50 ppb is needed for normal atmospheric background ozone concentration to produce an oxidation rate of up to 0.1% hr^{-1}.

c. Direct photo oxidation of SO_2:
Singlet (second excited state) SO_2 was shown to be chemically unreactive with even atomic oxygen but is rapidly quenched to form the reactive triplet (first excited) state by other atmospheric gases. The available quantum yield evidence of triplet SO_2 obtained by laboratory simulation using UV light of wavelength greater than 290 nm and a mixture of SO_2 and highly purified air suggests that reactions leading to oxidation occurs with only a very low efficiency under atmospheric conditions (Urone et al, 1968). Calculations based on these give oxidation rates of 0.02% hr^{-1} in sunlight at a zenith angle of 40°.

d. Direct reaction between SO_2 and some molecular species :
SO_2 has been shown to be oxidized very readily in an atmosphere of ozone and NO_x especially NO_2 (Urone et al, 1968; Doubendieck et al, 1975; Bufalini, 1971). The rate of transformation is observed to be accelerated if organic substances are added to the system.

e. Direct oxidation by cosmic ray:
Direct oxidation of SO_2 by cosmic rays and radioactivity from the ground has not been reported; however, according to Vohra et al (1984) background concentrations of radon and its daughter products are known to enhance SO_2 oxidation in the atmosphere.

It may rightly be said that homogeneous oxidation of SO_2 is mainly as a result of free radical reactions and so may be represented as

$$\frac{-d[SO_2]}{dt} = \{k_1[OH] + k_2[HO_2] + k_3[RO_2]\}\ [SO_2] \qquad \text{II.33}$$

From the tropospheric concentrations of OH and HO_2 (Castleman et al, 1974), it follows that OH is twelve times more effective as an oxidizing species than HO_2 and so the rate of homogeneous oxidation of SO_2 can be evaluated as

$$\frac{-d[SO_2]}{dt} = \beta[SO_2]$$

where $\beta = k_1[OH] = 1.2 \times 10^{-6}$
This means a conversion rate of 0.43% h^{-1} for homogeneous processes.

II.3.2 Heterogeneous Oxidation of SO_2:

Gas-droplet chemistry of SO_2 under certain conditions dominates the atmospheric transformation of SO_2 to SO_4^{2-}. Its understanding therefore is necessary for the development of atmospheric chemical models and environmental control strategies. Two oxidation mechanisms to be discussed are those on solid particles and in aqueous droplets.

a. SO_2 Oxidation on Solid Particles:

The oxidation of SO_2 adsorbed on solid particle surface is important only when the atmospheric turbidity is high. Particles likely to occur in a stack plume are metal oxides (Frank et al, 1977), siliceous materials and salt (Judaikis et al, 1973 and 1978) and carbonaceous materials (Novakov, 1974 and Tartarelli et al, 1978). A study by Liberti et al (1978) showed that the interaction between SO_2 and the solid particles was initiated by an adsorption process which has a rate constant of $4 - 5 \times 10^{-2}$ min^{-1}, and takes place to the extent of several $\mu g\ g^{-1}$ of dust which is strongly influenced by humidity. Conversion to sulphate after adsorption depends on the chemical composition and nature of the particles which can be defined in terms of pH, titrable acidity, surface area, humidity and degree of

surface coverage by adsorbed components. It does not take place to a considerable extent on siliceous and saline atmospheric particles. However, adsorption on particles from stack emission leads to quantitative conversion to sulphate if the particles are basic. On carbon particles, the oxidation mechanism involves surface radicals especially the OH radical (Yue et al, 1976) and active oxygen sites. Since the adsorption capacity of atmospheric particulates is very low, the oxidation rate is limited. Reaction is appreciable initially but as a result of fast surface covering by reaction products, the rate decreases fast until it approaches zero.

Novakov et al (1974) and Liberti et al (1978) have demonstrated the catalytic action of carboneous particulates covered by a thin film of moisture. Chang et al (1981) suggested that this process is likely to dominate SO_2 oxidation in a plume, and that it is pH-independent; first order with respect to carbon concentration and has complex dependence on the concentration of S(IV) ranging between a second and a zeroth order as the concentration increases. They proposed the rate law

$$\frac{d[S(IV)]}{dt} = k[C_x][O_2]^{0.69} f[S(IV)] \qquad \text{II.34}$$

where C_x = carbon particle concentration (g l^{-1});
$[O_2]$ = concentration of dissolved oxygen in moles l^{-1};
$[S(IV)]$ = total concentration of S(IV) species in moles l^{-1}
$f[S(IV)]$ term contains the effect of the partial pressure of SO_2 on the rate of oxidation and is given by

$$f[S(IV)] = \frac{\alpha[S(IV)]^2}{1 + \beta[S(IV)] + \alpha[S(IV)]^2}$$

$\alpha = 1.5 \times 10^{12}\ l^2 mole^{-2}$
$\beta = 3.06 \times 10^{6}\ l\ mole^{-1}$
k = Rate constant = $9.04 \times 10^{3}\ e^{-5888/T}\ Mol^{0.31}\ l^{0.69}\ g^{-1}s^{-1}$ II.

b. SO_2 Oxidation in Aqueous Droplets:

Studies have been carried out on the oxidation of SO_2 in aqueous droplets by ozone (Penkett et al, 1979); H_2O_2 (Penkett et al, 1979 and

Martin et al, 1981); and oxygen in uncatalysed systems. Working in a bulk solution system, Larson et al (1978) showed that for $p_{O_3} \simeq 10^{-6}$ atm., oxidation by O_3 was strongly pH-dependent and significantly higher than that by oxygen at a partial pressure of 0.2 atmospheres, and pH below 5.6. However, above this pH value, uncatalysed oxygen reaction would appear to dominate most of the time. Since the typical O_3 background mixing ratio is around 5×10^{-8} atmosphere (Chatfield et al., 1976) its contribution is not very important.

Middleton et al. (1980) from theoretical considerations found that under daytime conditions oxidation by H_2O_2 in the droplet phase can be the dominant sulphate production mechanism. However, with a noon concentration of 3.0×10^{10} molecules per cm^3 (Logan et al, 1981) and a night concentration of much lower value, its contribution to tropospheric conversion of SO_2 is not very important especially as the reaction rate is insensitive to catalysis or inhibition (Martin et al, 1981).

Oxidation in the droplet by oxygen under pure conditions is not an important mechanism of sulphate formation in the atmosphere (Beilke et al, 1978). However at high pH or under conditions that obtain in a polluted atmosphere it is the most important mechanism of the conversion of SO_2 to sulphate (Miller et al, 1972).

The nature of the transient species in the SO_2-H_2O system and their mode of production had been studied exhaustively by Scott (1964). The equilibrium equations II.16, II.18, II.20 and II.22 state the mode of their production. The equilibrium constants are listed in Appendix A. The rate of reaction in the droplet cloud is a direct function of the rate at which SO_2 can dissolve in the droplets. According to Judaikis et al (1973) this rate is given by

$$\frac{-d[SO_2]}{dt} = \frac{-\phi C_y u A}{4} \qquad \text{II.36}$$

where

ϕ = heterogeneous reactivity coefficient for SO_2 on water
$\simeq 5.0 \times 10^{-5}$ (Petit et al., 1977)

C_y = gas phase concentration of SO_2

u = mean molecular speed for SO_2
$\simeq 3.1 \times 10^4$ cm s^{-1} (Martin et al, 1981)

A = droplet surface area.

The total amount of SO_2 absorbed by the droplet is limited by the liquid water concentration of the droplet cloud.

The droplet phase oxidation of SO_2 by oxygen will be discussed under the following headings

i. oxidation in the absence of both NH_3 and metal ion;
ii. oxidation in the presence of metal ion alone;
iii. oxidation in the presence of NH_3 alone; and
iv. oxidation in the presence of NH_3 and metal ion combined.

i. Uncatalysed oxidation in the absence of NH_3:

In reasonably pure water solution, SO_2 oxidation does not proceed at a measurable rate. Fuller et al. (1941) had shown that uncatalysed oxidation exists. Junge et al. (1958) however, found that the the oxidation can only take place in the presence of a catalyst and that any oxidation observed in the so-called reasonably pure water was as a result of minute traces of metal ions which will serve in this capacity.

There is a disagreement among investigators as to the nature of the substrate that is oxidised. Van den Heuvel et al. (1963) formulated the oxidation as

$$2SO_2 + O_2 \rightarrow 2SO_3$$

and subsequent hydration of the SO_3 produced

$$SO_3 + H_2O \rightarrow H_2SO_4 \rightarrow 2H^+ + SO_4^{2-} ,$$

thus neglecting the equilibrium reactions between SO_2 and water molecules. This formulation is not likely to be correct in view of the equilibrium reactions equations II.16, II.18 and II.20 (Scott, 1964) whose characteristic times are much smaller than that of the oxidation step (Freiberg et al., 1981). Taking into consideration the pH dependence of the concentrations of the S(IV) species in solution,

Schroeter et al. (1963), Abel (1951), Kallend (1972) and Adamowicz et al. (1977) suggested that within the normal atmospheric droplet pH range, the dominant S(IV) species is HSO_3^- and hence is largely the species that is oxidized. Considering the strong pH dependence of the rate of oxidation however SO_3^{2-} is widely regarded as the substrate (Fuller et al, 1941; Scott et al., 1967; Beilke et al., 1978; Miller et al., 1972; and McKay, 1971); and that the retardation of oxidation by the rise in hydrogen ion concentration is as a result of the suppression of SO_3^{2-} formation by the reaction

$$SO_3^{2-} + H^+ = HSO_3^-$$

Based on the above, droplet phase oxidation in the absence of a catalyst may be stated as

$$SO_3^{2-} + \tfrac{1}{2}O_2 \xrightarrow{k_o} SO_4^{2-} \qquad \text{II.37}$$

from which

$$\frac{d[SO_4^{2-}]}{dt} = k_o[SO_3^{2-}] \qquad \text{II.38}$$

where

k_o = first order rate constant (Scott et al, 1967).

The oxidation is generally regarded as being first and zero orders with respect to S(IV) ions and to oxygen respectively over a wide range of concentration (Fuller et al, 1941; Scott et al, 1967 and McKay, 1971). However, Miller et al. (1972) Luria et al. (1982) Eggleton et al(1972) Penkett et al (1979) and Clarke and Williams (1983) suggested that the first order kinetic operates only below 10^{-6} atmosphere partial pressure of SO_2 above which zero order mechanism sets in.

The values of the rate constants obtained by nine groups of investigators are listed in Table II.11. All the values, except that of Penkett et al (1979) are within one order of magnitude. Although rate constant is temperature dependent,

TABLE II.11 Pseudo first-order rate constants (k_0) for the uncatalysed oxidation of SO_2 in the aqueous phase.

Reference	C_y/C_{IV} vpm/(M)	Liquid phase characteristics	RH (%)	pH range	Temp (°C)	$k_0(S^{-1})$
Fuller et al (1941)		Bulk solution	-	5-8	25°	1.3×10^{-2}
Schroeter (1963)		Bulk solution	-	6.95-8.2	25	2.8×10^{-3}
Beilke et al (1975)		Bulk solution	-	6	25	1.1×10^{-3}
Larson et al (1978)		Bulk solution	-	4-12	25	4.8×10^{-3}
Penkett et al (1978)		Bulk solution	-	6-9	25	1.5×10^{-5}
Scott et al (1967)*	5vpm	Droplet(.05-.25mm)	94	6-7	25	1.7×10^{-3}
Miller et al (1971)	1-4300vpm	Droplet (.4-.9mm)	94	3-4	25	3.0×10^{-3}
Marek et al (1976)	6.3×10^{-3}vpm	Droplet 2μm-120μm diameter			25	2.2×10^{-2}
Steele et al (1981)	0.45-0.9vpm	Cloud(0.1μm)	Over 100	4-7	25	10^{-4}-10^{-3}

*Based on the study of van den Heuvel et al (1963)

actual sulphate formation has very weak temperature dependence within the narrow temperature range which the tranformation was studied. This is caused by the compensating effect of the decreasing SO_2 solubility and the increasing reaction rate constant with rise in temperature.

Rate equations have however been formulated which included the explicit hydrogen ion concentration as a co-factor:

$$\frac{-d[SO_3^{2-}]}{dt} = (k_1 + k_2[H^+]^{\frac{1}{2}})\ [SO_3^{2-}] \qquad \text{II.38a}$$

where k_1 and k_2 are rate constants (Fuller et al., 1941) whose numerical values at 25° C are 0.013 and 59 respectively (McKay, 1972);

$$\frac{d[SO_4^{2-}]}{dt} = k_1[SO_3^{2-}] + k_2\ [HSO_3^-]/[H^+]^{\frac{1}{2}}$$

$$= k_1\ [SO_3^{2-}] + k_2^1[SO_3^{2-}][H^+]^{\frac{1}{2}} \qquad \text{II.38b}$$

where k_1, k_2 and k_2^1 are respectively $2.9 \times 10^{-3} s^{-1}$, $2 \times 10^{-6}\ s^{-1}\ M^{1/2}$ and $32\ s^{-1}\ M^{1/2}$ (Schroeter, 1963);

$$\frac{-d[SO^{2-}]}{dt} = k_1[HSO_3^-]/[H^+]^{\frac{1}{2}} \qquad \text{II.38c}$$

where k_1 is a function of several rate constants and has a numerical value of 1.8×10^{-6} $mole^{1/2} litre^{-1/2} s^{-1}$ (Kallend, 1972)

$$\frac{d[SO_4^{2-}]}{dt} = k_1[SO_3^{2-}]/[H^+]^{0.16} \qquad \text{II.38d}$$

where $k_1 = 1.2 \times 10^{-4}\ s^{-1}\ M^{0.16}$ (Beilke et al, 1975);

$$\frac{d[SO_4^{2-}]}{dt} = k_1[SO_3^{2-}][H^+]^{\alpha} \exp(-\beta/T) \qquad \text{II.38e}$$

where $k_1 = 3.3 \times 10^5 \pm 6.2 \times 10^5\ 1^{1.1}\ s^{-1} M^{-1.1}$

$\alpha = 1.1 \pm 0.1$

$\beta = 3.5 \times 10^2 \pm 3.3 \times 10^2$ K (Hegg et al, 1982); and

finally

$$\frac{-d[S(IV)]}{dt} = k_1[SO_3^{2-}][H^+]^{\frac{1}{2}}$$

where $k_1 = 0.32\ l^{1/2}\ M^{1/2}\ s^{-1}$ (Clarke et al, 1984)

Workers are not unanimous on the origin of the oxygen atom involved in the reaction. Winter et al (1951) and Halparin et al (1952) used labelled oxygen technique to show that only gaseous oxygen dissolved in solution was involved in the oxidation. Cunningham et al. (1975) however used the same technique to show that only oxygen atoms from the solvent molecule were involved in the oxidation. Neither of these two conflicting results considered the oxygen exchange between the solvent and the S(IV) species in solution which has been reported by Holt et al. (1981). If S(IV) is oxidized by dissolved oxygen, the observations of Cunningham et al (1975) could only be explained in terms of the exchange of oxygen atom between the dissolved S(IV) and the solvent molecule since Lloyd (1967) had shown that sulphate ion is extremely stable with respect to oxygen atom exchange with water in which it is dissolved.

Mechanisms of Uncatalysed Oxidation:

If the proposition that the so-called uncatalysed oxidation reactions are actually catalysed by trace metal ion contaminants in solution (Jung et al, 1958) then the Backstrom mechanism (Larson et al. 1978) could be used to explain oxidation where no catalyst was visibly present. Three mechanisms all of which involve free radicals have been reported to explain uncatalysed oxidation.

The mechanism put up by Bassett et al (1951) proposes the addition of O_2 by co-ordination to sulphur atom in which bisulphite radical is the chain carrier:

$$SO_3^{2-} + O_2 = [O_2 \rightarrow SO_3]^{2-}$$

or $$HSO_3^- + O_2 = [O_2 \rightarrow SO_3H]^-$$

and subsequent chain reaction to produce sulphate

$$HSO_3 + [O_2 \rightarrow SO_3]^{2-} + H_2O = 2SO_4^{2-} + 2H^+ + OH$$

$$SO_3^{2-} + OH + H^+ = HSO_3 + OH^-$$

The termination step involves the removal of HSO_3 radical. In addition to the above, a non-free radical reaction can take place between the oxygen adduct and S(IV) ion.

$$[O_2 \rightarrow SO_3H]^- + HSO_3^- = 2HSO_4^-$$

Abel (1951) proposed a free radical mechanism based on the production of HSO_3 intermediate and OH radical which subsequently react to yield H_2SO_4.

Initially, the OH^- ion from water transfers electron to oxygen to form oxygen monoradical and OH radical

$$O_2 + OH^- \rightarrow O_2^- + OH$$

The oxygen monoradical formed reacts simultaneously with SO_3^{2-} and HSO_3^- to produce hydrogen sulphite intermediate and more OH radicals

$$O_2^- + 3H^+ + SO_3^{2-} \rightarrow HSO_3 + 2OH$$

$$O_2^- + 2H^+ + HSO_3^- \rightarrow HSO_3 + 2OH$$

The OH radicals react with SO_3^{--} and HSO_3^- to produce more HSO_3

$$OH + 2H^+ + SO_3^{2-} \rightarrow HSO_3 + H_2O$$

$$OH + H^+ + HSO_3^- \rightarrow HSO_3 + H_2O$$

Finally OH and HSO_3 radicals will interact to form sulphuric acid

$$OH + HSO_3 \rightarrow H_2SO_4$$

Marek et al (1976) used this mechanism to interprete the oxidation of SO_2 in the presence of ammonia.

Another free radical mechanism for oxidation of SO_3^{2-} in aqueous solution was proposed by Hayon et al (1972) based on spectroscopic evidence. The initiation stage is the photolysis of the SO_3^{2-} ion to yield SO_3^- radical and hydrated electron. The SO_3^- reacts with oxygen to yield pyrosulphite radical.

Initiation:

$$SO_3^{2-} \xrightarrow{h\nu} SO_3^- + e^-_{aq}$$

$$e^-_{aq} + O_2 \rightarrow O_2^-$$

$$SO_3^- + O_2 \rightarrow SO_5^-$$

The propagation step involves SO_5^- and SO_3^{2-}.

$$SO_5^- + SO_3^{2-} \rightarrow SO_4^{2-} + SO_4^-$$

$$SO_4^- + SO_3^{2-} \rightarrow SO_4^{2-} + SO_3^{2-}$$

The termination reactions involve the production of non-reactive products from the radicals.

$$2SO_5^- \rightarrow$$

$$_2SO_4^- \rightarrow$$

$$SO_5^- + O_2^- \rightarrow$$

ii. Metal ion catalysed droplet phase oxidation of SO_2.

The role of metal ions in the atmospheric oxidation of SO_2 has been widely investigated because of their ubiquity in atmospheric aqueous droplets. They originate from the plumes of coal-fired furnaces and are released in the form of oxides in their highest oxidation state such as Fe_2O_3 and MnO_2 (Taylor et al., 1981). It is very likely that while suspended in aqueous droplets, considerable leaching from the particle surface takes place resulting in the formation of ions. The interest in catalysed oxidation is an attempt to define an alternative explanation for the short atmospheric residence time of SO_2 of about 8.75 h proposed by Junge, (1960) in view of the slow rate of uncatalysed oxidation in pure water droplets under normal atmospheric conditions.

Most laboratory studies (Bassett et al, 1951; Matteson et al, 1969; and Cheng et al, 1971;) made use of SO_2 and catalyst concentrations much higher than the background concentrations. This is probably because of the expected low sulphate yield. Most recent studies (Barrie et al., 1976; Kaplan et al., 1981a; and Ibusuki et al., 1984) however used the concentrations of both catalysts and SO_2 very close to the concentrations in which they occur in a polluted atmosphere. Although using concentrations that are comparable to those of the atmosphere simplifies the task of applying laboratory results to real atmosphere, the accuracy of the results is likely to be in doubt since according to Miller et al (1971) at low gas phase partial pressures, equilibrium between SO_2 and the droplet may not be established with-in the experimental time span.

Junge et al (1958) arranged some of the known catalysts in a decreasing order of effectiveness - Mn^{2+}, Cu^{2+}, Fe^{2+}/Fe^{3+}, Co^{2+},NH_4^+, Na+ and distilled water. The catalytic effects of NH_4^+, Na^+ and distilled water are very slight. Most work has been done on the catal ytic properties of manganese and iron ions; the former because of its effectiveness and the latter because of its ubiquity in the atmosphere (Trindade et al., 1981). Table II.12a shows a summary of some $MnSO_4$ catalysed S(IV) oxidation in aqueous solution. Other metal ion catalysed SO_2 oxidation mechanisms which are of peripheral interest to

Table II.12a Some previous studies of SO_2 oxidation in aqueous $MnSO_4$ solution

Reference	SO_2/S(IV) Concentration (ppm/M)	Catalyst Concentration (M)	Reaction Medium	Temperature	RH	pH	Rate Equation	First Order Rate Equation
Hoather et al(1934)	2×10^{-4} to 6×10^{-3}	3.0×10^{-6} 8.0×10^{-5}	Bulk Solution	25°C	-	3-4	$R=k_0[Mn^{++}]^{1.7}$	
Coughanowr et al (1965)	2.0×10^{-3} to	2.2×10^{-4} to 5.5×10^{-3}	Bulk Solution	25°C	-	3-4	$R=k_0[Mn^{++}]^2$	
Martin (1983)	10^{-4} to 10^{-3} less than 10^{-6}	10^{-5} to 10^{-3}	Bulk Solution	25°C	-	0-3	$R=4.7[H^+]^{-1}[Mn2+]^2$ $R=25[H^+]^{-1}[Mn^{2+}][S(IV)]$	
Ibusuki et al(1984)	$(1-5)\times10^{-6}$	5×10^{-6} to 1.5×10^{-5}	Bulk Solution	20-30	-	2.7-7.5	$R=k_0[Mn^{++}][S(IV)]$	
Johnstone et al (1958)	20-100ppm	0.03 mM-0.09 mM	Single droplet of diameter 800μM	25	100	-	$\frac{-d[S(IV)]}{dt}=k_0[Mn^{++}][S(IV)]$	2.13×10^{-3}
Johnstone and Moll (1960)	250 ppm	0.82 M	Fog Droplet 5-20 μm	25	77-96	-	$\frac{-d[S(IV)]}{dt}=k_0[Mn^{2+}][S(IV)]$	45.6
Matteson et al (1969)	2-140 ppm	6×10^{-5} - 2×10^{-4}	Aerosol droplets 2-5μm	25	96	-	$\frac{-d[S(IV)]}{dt}k^0[Mn^{2+}][S(IV)]$	0.132
Cheng et al(1971)	4.5ppm	5.2	Submicrometer	25	95	1	$\frac{-d[S(IV)]}{dt}=k_0[Mn^{2+}][S(IV)]$	0.45
Cains et al(1978)	63 ppm	0.16	Aerosol in a flow reactor 0.1-1.0μm	25	96	-	$R=k_0[Mn^{2+}][S(IV)]$	
Kaplan et al. (1981)	0.1-1.0ppm	0.45mM	Aerosol in a laminar flow reactor	25	90	-	$\frac{-d[S(IV)]}{dt}=k_0[S(IV)]$	0.027-0.066
Crump et al(1983)	>10ppm	>0.01	Aerosol in a CSTR 0.1-1.0μm	23.9-24.2	95-97		$R=k_0 / [H^+]$	(8.3 ± 2.5) $\times10^{-5}$ M s^{-1} (zero order)

Table II.12b Some previous studies of SO_2 oxidation catalysed by some salts

Reference	S(IV) Concentration (mM)	Catalyst Concentration (mM)	Reaction Medium	Temperature (°C)	pH	Rate Equation	Rate Const.
Fuller et al(1941)	12.7-14.3	Cu^{2+} 10^{-6}-0.1	Bulk Solution	25	10.6	$R=(k_1+k_3[Cu^{2+}])[SO_3^{2-}]$	$k_1=0.013\ s^{-1}$ $k_3=2.68\times10^8 s^{-1}M^{-1}$
Barron & O'Hern (1966)	45	Cu^{2+} 10^{-4}-0.1	Bulk Solution	25	7-9	$R=k_1[Cu^{2+}]^{0.5}[SO_3^{2-}]^{1.5}$	$k_1=1.2\times10^3 s^{-1}M^{-1}$
Brimblecombe et al (1974)	10^{-4}-10	Fe^{3+} 5×10^{-5} to 5×10^{-3}	Bulk Solution	25	4.9	$R=k_1[Fe^{3+}][S(IV)]$	$k_1=100 s^{-1}M^{-1}$
Sutherland (1977)	-	Fe^{3+} -	Bulk Solution	-	4.5	$R=\frac{[HSO_3^-][H^+]^n[Fe^{3+}]}{k_1 + k_2[HSO_3^-]}$	n 1.0 k_1 $k_2[HSO_3^-]$ *for small* $[HSO_3^-]$
Fuzzi (1978)	0.1-2.0	Fe^{3+} 10^{-4}-10^{-2}	Bulk Solution	20	3-8	$R=k[S(IV)]^n[Fe^{3+}]$	n=1 for pH=4 n=2 for pH=5
Barrie et al (1967)	Partial pressure of SO_2 .1 to 1upm	$MnCl_2$ 0.1	Droplet suspended on the plastic tip of Eppendorf pipette	25 & 8	3.7 & 4.5	$R=k[SO_3^{2-}]$	$9.4\times10^2\ s^{-1}$
		$FeCl_2$ or $FeCl_3$ 0.1					$5.8\times10^2\ s^{-1}$
		Equimolar $MnCl_2$ and $FeCl_2$ 0.1	Droplet diameter =1.05mm				$1.4\times10^4\ s^{-1}$
		$CuCl_2$ 0.1					Below $9.4\ s^{-1}$

this study are summarised in Table II.12b. Some of the data in the table were taken from a compilation by Kaplan et al (1981).

Bassett et al (1951) found a definite anion effect on the catalytic efficiency of these metal salts. They found, for instance that $MnSO_4$ solutions catalysed the oxidation of sulphite ion twelve times faster than $MnCl_2$ did under the same conditions of temperature and pH values; but that in the case of iron, the chloride salts produced faster oxidation rates than the sulphates. This anionic effect has been confirmed by the recent studies of Clarke and Radojevic (1983).

The catalytic effect of the salts so far studied have been shown to be independent of the concentration of oxygen at least for pH values below 8, except in cases where high concentrations of SO_3^{2-} are used (Miyamoto et al, 1930). However, oxidation mechanisms have been proposed in which oxygen is not of zero order (Backström, 1934; Yagi et al, 1962; Davies et al, 1969; Linek et al, 1970; and Sawicki et al, 1973).

Little work has been done on the dependence of catalytic effect on the pH of the medium. A complete analysis will have to consider the roles of $SO_2.H_2O$, HSO_3^- and SO_3^{2-} in the oxidation process since the concentration of each of these species in solution depends on the pH of the medium. Some studies have been carried out which yielded rates generally showing a first order dependence on hydrogen ion concentration (Brimblecombe et al, 1974; Barrie et al, 1976; Barron et al, 1966; and Freiberg et al, 1974). The most important study so far was that of Ibusuki et al (1984) which spanned the pH range between 2.7 and 7.5. The work will be discussed further in a subsequent section.

Some catalyst systems have been known to exhibit synergistic effects in admixture with another catalyst (Martin et al, 1981). Barrie et al (1974) for instance found that equimolar concentrations (on the order of 10^{-5} M) of $MnCl_2$ and $FeCl_3/FeCl_2$ produced an oxidation rate about one order of magnitude greater than that for the same molar concentrations of either $MnCl_2$ or $FeCl_3/FeCl_2$ alone. The system is complex and described by the differential equation

$$-\frac{d[S(IV)]}{dt} = ab[S(IV)]$$

where a and b are zero and first order rate constants with respect to S(IV) for Mn^{2+} and Fe^{3+} respectively. However, Johnstone et al (1958) did not observe it in a catalyst mixture.

Beilke et al (1978) observed a temperature dependence of catalysed reaction for single catalysts but not for a mixture of catalysts. In a solution of Mn^{2+}, for instance, an increase of temperature from 8° to 25° C caused an increase in oxidation rate by a factor of five to ten in the pH range 2 - 4.5. Many studies have been carried out to

determine the mechanisms of the oxidation of SO_2 catalysed by some transition metals. These studies have been characterised by inconsistent reaction rates and rate laws (Hegg et al, 1978). This is in part as a result of the different kinetics and mechanisms assumed by the various investigators. Attempts have been made to group the mechanisms into three categories:- free radical, polar and photo-assisted groups. Irrespective of the group, all start with the formation of metal ion - S(IV) complex and are distinguished only in subsequent steps.

(a) Free-radical chain mechanisms:

The mechanisms are characterised by thermal initiation followed by the addition of dioxygen and subsequently a series of one-electron transfer steps. The radicals are produced by the formation of a complex between S(IV) and a transition metal ion that has an available lower oxidation state. The metal ion considered in all the mechanisms discussed here is Mn^{2+}. The initiation step according to Schmittkunz (quoted by Larson et al, 1978)

$$M^{x+} + 3SO_3^{2-} \rightarrow [M^{x+}(SO_3^{2-})_3]^{(6-x)-} = X$$

$$X + O_2 \overset{k_1}{\rightarrow} [M^{x+}(SO_3^{2-})_3]^{(5-x)-} + O_2^-$$

$$[M^{x+}(SO_3^{2-})_3]^{(5-x)-} + SO_3^{2-} \rightarrow X + SO_3^- \qquad \text{II.39}$$

$$O_2^- + H_3O^+ \rightarrow HO_2 + H_2O \qquad \text{II.40}$$

The complex X is reformed in equation II.39 with the production of the sulphite radical which is the chain carrier.

In the Backström mechanism (Larson et al, 1978), the propagation step involves two reactions:

$$SO_3^- + O_2 \overset{k_2}{\rightarrow} SO_5^-$$

$$SO_5^- + SO_3^{2-} \overset{k_3}{\rightarrow} SO_5^{2-} + SO_3^-$$

The oxidation step involves sulphite and Caro's acid ion

$$SO_5^{2-} + SO_3^{2-} \overset{k_4}{\rightarrow} 2SO_4^{2-}$$

Three reactions are involved in the termination step:

$$2SO_3^- \overset{k_5}{\rightarrow} S_2O_6^{2-}$$

$$SO_3^- + SO_5^- \overset{k_6}{\rightarrow} S_2O_6^{2-} + O_2$$

$$SO_5^- + SO_5^- \overset{k_7}{\rightarrow} S_2O_8^{--} + O_2$$

The rate expression that could be deduced from this mechanism by Hoffman et al (83) is

$$\frac{-d[SO_3]}{dt} = k[M^{x+}]^{1/2}\,[SO_3^{2-}]\,[O_2] \qquad \text{II.41}$$

where

$k = k_2(2k_1/k)_t^{\frac{1}{2}}$
$k_t = k_5$ or k_6 or k_7

The mechanism proposed by Hayon et al (1972) is not much different from their uncatalysed oxidation mechanism except in the initiation step. The progation step after the formation of the sulphite radical in equation II.39 is

$$SO_3^- + O_2 \xrightarrow{k_2} SO_5^-$$

$$SO_5^- + SO_3^{2-} \xrightarrow{k_3} SO_4^- + SO_4^{2-}$$

$$SO_4^- + SO_3^{2-} \xrightarrow{k_4} SO_4^{2-} + SO_3^-$$

The termination step is

$$SO_5^- + SO_5^- \xrightarrow{k_5} S_2O_6^{2-} + 2O_2$$

$$SO_4^- + SO_4^- \xrightarrow{k_6} S_2O_6^{2-} + O_2$$

$$SO_4^- + SO_4^- \xrightarrow{k_6} S_2O_8^{2-}$$

The rate equation is

$$\frac{-d[SO_3^{2-}]}{dt} = k[M^{x+}]^{1/2}\ [SO_3^{--}]^{3/2} \qquad \text{II.42}$$

where

$$k = k_3(2k_1/k_5)^{1/2} \quad \text{or} \quad k_4(2k_1/k_6)^{1/2}$$

This mechanism differs esentially from that of Backström in the inclusion of the sulphate radical SO_4^- as the chain carrier.

The mechanism proposed by Schmittkunz for Mn^{2+} catalysed oxidation has both sulphite and hydroperoxyl radicals as the chain carriers. The SO_3^- propagated chain reaction follows the same mechanism as that of Hayon et al. The hydroperoxyl chain is as follows:

$$HO_2 + SO_3^{2-} \xrightarrow{k_3} SO_4^{2-} + OH$$

$$OH + SO_3^{2-} \xrightarrow{k_4} SO_4^{2-} + H$$

$$H + O_2 \xrightarrow{k_5} HO_2$$

The chain is terminated by the combination of the HO_2

$$2HO_2 \xrightarrow{k_6} H_2O_2 + O_2$$

The rate equation is

$$\frac{-d[SO_3^{2-}]}{dt} = k_3 (2k_1/k_6)^{1/2}[M^{x+}]^{1/2}[SO_3^{2-}][O_2]^{1/2} \qquad II.43$$

A comparison of the three rate equations II.41, II.42 and II.43 above shows that they have in common a half order dependence of the metal ion or its complex only. This factor in part accounts for lack of agreement in the reaction rates predicted by the mechanisms. The three mechanisms also ignored the pH dependence of the catalysed oxidation. However, since the concentrations of the different S(IV) species in solution depend on the pH, the effect of pH will depend on their rates as reactive species in the system.

(b) Polar Mechanisms:

Polar non-radical mechanisms of catalysed oxidation have been postulated by Bassett et al (1951) and Matteson et al (1969) for Mn^{2+} catalysed system and by Freiberg (1974) for Fe^{3+} ion catalysed system. In these systems, oxidation is initiated by the formation of a metal ion-sulphite complex followed by the binding of oxygen to the complex and finally electron transfer by means of two successive steps. The Mn^{2+} catalysed oxidation in the mechanism of Bassett and Parker proceeds as follows:

$$Mn^{2+} + SO_3^{2-} = MnSO_3$$

$$MnSO_3 + SO_3^{2-} = [Mn(SO_3)_2]^{2-}$$

The complex adds molecular oxygen or oxygen from the adduct $O_2 \rightarrow SO_3^{2-}$ postulated in the uncatalysed mechansm (Hayon, 1972, and Bassett et al, 1951)

$$[Mn(SO_3)_2]^{2-} + O_2 = [O_2 \rightarrow Mn(SO_3)_2]^{2-} \quad \text{or}$$

$$[Mn(SO_3)_2]^{2-} + [O_2 \rightarrow SO_3]^{2-} = [O_2 \rightarrow Mn(SO_3)_2]^{2-} + SO_3^{2-}$$

The oxygen adduct rearranges rapidly

$$[O_2 \rightarrow Mn(SO_3)_2]^{2-} \xrightarrow{k} [Mn(SO_4)_2]^{2-} \qquad II.44$$

SO_3^{2-} replaces SO_4^{2-} from the complex, being of lower electro-affinity.

$$[Mn(SO_4)_2]^{2-} + 2SO_3^{2-} \rightarrow [Mn(SO_3)_2]^{2-} + 2SO_4^{2-}$$

The sulphite complex is thereby regenerated. The effect of the catalyst here is essentially to replace the chain reactions postulated in the uncatalysed mechanism with new mechanism.

It was suggested that the presence of chloride ion interferes with the formation of the sulphite-metal complex, and also that the highly stable metal-chloride complex formed competes with the sulphite complex for the oxygen in the reactions

$$[MnCl_4]^{2-} + O_2 = [O_2 \rightarrow MnCl_4]^{2-}$$

$$[MnCl_4]^{2-} + O_2 \rightarrow SO_3^{2-} = [O_2 \rightarrow MnCl_4] + SO_3^{2-}$$

The polar mechanism proposed by Matteson et al (1969) is essentially similar to that of Bassett and Parker but has SO_2 as the sulphur species that is complexing with the catalyst ion. The choice of SO_2 is perhaps a reflection of the high acidity employed in the study.

$$SO_2 + Mn^{2+} = [MnSO_2]^{2+}$$

$$2[MnSO_2]^{2+} + O_2 = [O_2 \rightarrow (MnSO_2)_2]^{2+} = 2[MnSO_3]^{2+}$$

$$[MnSO_3]^{2+} + H_2O = Mn^{2+} + HSO_4^- + H^+$$

$$HSO_4^- + H^+ = H_2SO_4.$$

The rate determining step is the rearrangement of the oxygen adduct to give $[MnSO_3]^{2+}$.

Applying the steady state approximation the rate equation obtained is

$$\frac{-d[SO_2]}{dt} = k\,[Mn^{2+}][SO_2] \qquad \text{II.45}$$

Freiberg (1975) proposed a polar mechanism for Fe^{3+} catalysed oxidation of SO_2 in which complexes of both HSO_3^- and SO_3^{2-} are involved in two-electron transfer steps. However, according to Karaker (1963), in the presence of Fe^{3+} oxidation of SO_2 is by O_2 in a two-electron transfer process or by Fe^{2+} in a one electron transfer process simultaneously.

(c) Photoassisted Mechanisms:

A photoassisted iron catalysed oxidation in a homogeneous solution was first reported by Lunak et al (1976). It differs from photoassisted uncatalysed oxidation (Hayon et al, 1972) by the fact that the initiation is the absorption of UV by the sulphito-iron complex to form free radical. Oxidation then proceeds by the normal free radical chain mechanism.

A heterogeneous photoassisted oxidation of SO_2 on transition metal oxides suspended in water had been investigated by Frank et al (1977) using Fe_2O_3 and an irradiation of 400 nm. The rapid conversion of S(IV) to S(VI) was explained in terms of the lattice defect of Fe_2O_3. The radiation produces in the lattice two positive holes in the valence band and electrons in the conduction bend. These migrate to the surface without recombining where they react with HSO_3^- and O_2 respectively. The H_2O_2 reacts with more HSO_3^- to yield HSO_4^-.

$$Fe_2O_3 \xrightarrow[\text{surface}]{2h\nu} Fe_2O_3 + 2p^+ + 2e^-$$

$$H_2O + HSO_3^- + 2p^+ \xrightarrow{\text{surface}} HSO_4^- + 2H^+$$

$$O_2 + 2e^- + 2H^+ \xrightarrow{\text{surface}} H_2O_2$$

$$H_2O_2 + HSO_3^- \xrightarrow{\text{solution}} HSO_4^- + H_2O$$

Since atmospheric droplets contain an appreciable quantity of these oxides derived from coal burning plumes, this mechanism is likely to be

of considerable importance. However, results so far obtained using Fe_2O_3, TiO_2, ZnO and CdO by Frank et al, (1977) could not discriminate between photo-catalytic oxidation and a host of other oxidative mechanisms that are likely under the situation.

Most catalysed oxidations in the absence of sunlight have been explained in terms of the polar mechanism (Wadden et al, 1978; and Cains et al, 1978).

iii. SO_2 oxidation in the SO_2-NH_3-H_2O-O_2 system:

The earliest study of the equeous oxidation of SO_2 in the presence of NH_3 in aerosols was carried out by Junge et al (1958). Subsequent theoretical and experimental studies showed that oxidation of SO_2 in aqueous droplets was much faster in the presence of NH_3 than in its absence (Marek et al., 1976). Van den Heuvel et al (1963) confirmed this but held that the rate does not depend critically upon the concentration of NH_3 provided this is high enough to sustain the oxidation reaction. The enhancement of oxidation caused by NH_3 had been described as catalysis (Scott et al, 1967; Van den Heuvel et al, 1963; Tomasi et al, 1975; and Scott et al, 1978). However, other workers (Beilke et al., 1975; Adomowiez et al.,1977; and McLaren et al., 1970) have shown that it is a mere pH effect and results from the increase in the concentration of sulphite ion with the increase in the pH of the medium. This oxidation process therefore is a special type of uncatalysed oxidation and can therefore be expressed by the kinetic mechanisms of the uncatalysed oxidation of SO_2.

The nature of the NH_3-H_2O-SO_2 system was exhaustively studied by Scott (1966). He had shown that SO_2 and NH_3 do not exist as H_2SO_3 and NH_4OH in solution but as the solvated molecules $SO_2.H_2O$ and $NH_3.H_2O$ respectively. In addition to the equilibria shown in equations II.16, II.18 and II.20 the following equilibria also exist

$$H_2O \overset{K_w}{\rightleftharpoons} H^+ + OH^- \qquad \text{II.47}$$

$$NH_3 + H_2O \overset{H_a}{\rightleftharpoons} NH_3.H_2O \qquad \text{II.48}$$

from which

$$[NH_3.H_2O] = {}^{H_a}p_{NH_3} \qquad \text{II.49}$$

where

p_{NH_3} is the partial pressure of NH_3 in atmospheres.
H_a is Henry's Law constant for NH_3.

$$NH_3.H_2O \overset{K_a}{\rightleftharpoons} NH_4^+ + OH^- \qquad \text{II.50}$$

from which

$$[NH_4^+] = K_a H_a p_{NH_3}/[OH^-] \qquad \text{II.51}$$

For a droplet generated from very dilute $(NH_4)_2SO_4$ solution in an atmosphere containing CO_2 also, the following equilibria and dissociation reactions also exist. The assumption of 100% dissociation of $(NH_4)_2SO_4$ and the activity coefficient of unity is valid based on the low molar concentration.

$$(NH_4)_2SO_4 \rightarrow 2NH_4^+ + SO_4^{2-} \qquad \text{II.52}$$

$$CO_2 + H_2O \overset{H_c}{\rightleftharpoons} CO_2.H_2O \qquad \text{II.53}$$

$$CO_2.H_2O \overset{K_{1c}}{\rightleftharpoons} H^+ + HCO_3^- \qquad \text{II.54}$$

from which

$$[HCO_3^-] = K_{1c} H_c p_{CO_2}/[H^+] \qquad \text{II.55}$$

$$HCO_3^- \overset{K_{2c}}{\rightleftharpoons} H^+ + CO_3^{--} \qquad \text{II.56}$$

and so

$$[CO_3^{--}] = K_{2c} K_{1c} H_c p_{CO_2}/[H^+]^2 \qquad \text{II.57}$$

where

H_c, K_{1c} and K_{2c} are the Henry's Law, first and second ionisation

constants respectively for CO_2. At steady state therefore the following ions exist in the system:

H^+, NH_4^+ HSO_3^-, SO_3^{2-}, HCO_3^-, CO_3^{2-}, SO_4^{2-} and OH^-

The concentrations of these ions (H^+ and OH^- not included) are given in equations II.19,II.21,II.55 and II.57. That of the sulphate ion is the $(NH_4)_2SO_4$ molar concentration. The hydroxyl ion concentration can be expressed as (based on equation II.47)

$$K_w/[H^+] \qquad \text{II.58}$$

From the electroneutrality equation,

$$[H^+] + [NH_4^+] = [HSO_3^-] + 2[SO_3^{2-}] + [HCO_3^-]$$

$$+ 2[CO_3^{2-}] + 2[SO_4^{2-}] + [OH^-] \qquad \text{II.59}$$

If the concentrations of the ions given in equations II.19, II.21,II.52, II.55, II.57 and II.58 are inserted, an equation is obtained which on rearrangement gives a third degree polynomial

$$(1 + \frac{K_a H_a}{K_w} p_{NH_3})[H^+]^3 - 0.2[H^+]^2 - (K_w + K_{1s}H_s p_{SO_2} + K_{1c}H_c p_{CO_2})[H^+]$$

$$- K_{2s}K_{1s}H_s p_{SO_2} - K_{2c}K_{1c}H_c p_{CO_2} = 0 \qquad \text{II.60}$$

Equation II.60 is expressed in known constants and partial pressure of gases and hence could be solved for the hydrogen ion concentration. This was done using the computer programme, POLY, listed in Appendix E Kallend (1972) used the value of the hydrogen ion concentration so obtained to calculate the S(IV) concentrations in solution using the equations II.17, II.19 and II.21. Table II.13 shows the effect of NH_3 on the pH of a solution droplet and the solubility of SO_2 at 25° C. The first five rows of data show the solubility of SO_2 in the absence of NH_3, and shows how the fraction of SO_2 dissolved decreases as the partial pressure of SO_2 increases. The rest of the data show the effect of NH_3. The variations with the partial pressures of SO_2 of the

ratio of the aqueous to gas phase concentrations, Rp of a hypthetical aerosol of mass concentration 8.8437 x 10^{-6} gdm^{-3} at a temperature of 25°C are depicted in Fig II.4.

The hydrogen sulphite ion is the most abundant S(IV) species in the pH range of atmospheric droplets (below 6) as shown by Table II.13; this fact was depicted by Beilke et al (1978) as in Fig II. 5. Kallend (1972) calculated the change in the aqueous concentration of HSO_3^-, SO_3^{2-} and total S(IV) as a function of NH_3 gas phase concentration in which the SO_3^{2-} concentration increases steadily wi th the concentration of NH_3 whereas that of HSO_3^- increases sharply initally but more slowly as the concentration of NH_3 increases.

Scott et al. (1967), McKay (1971), Miller et al. (1972) and Kallend (1972) calculated the production of sulphate under given conditions of gas phase concentrations of SO_2 and NH_3. The conditions of the calculations are listed in Table II.14.

The calculated sulphate production as a function of time obtained under the conditions listed in Table II.14 are plotted in Fig II.6. The four curves look alike and hence are similar in their qualitative predictions of the effect of the partial pressures of the reacting gases on the amount of sulphate formed. However significant quantitative differences exist between these predictions. The basic asssumption on which the calculations that produced these curves were based was that the partial pressures of SO_2 and NH_3 remained constant as reaction proceeded. This will be valid in the presence of a large reservoir of the gases that was not significantly depleted as oxidation went on or in a very thin cloud with low liquid water content where only a tiny proportion of the existing gases is absorbed.

McKay (1971) and Kallend (1972) however considered a second model in which there is no replenishment of the gases as they are used up. This is a realistic model for a laminar flow reactor. Under this situation the reaction slows down as the gases are used up and ultimately stops when one or the other has been exhausted as depicted in Fig II.8. Kallend (1972) and Junge et al (1958) have however shown that in addition to exhaustion, the build-up of hydrogen ion as the droplet absorbs SO_2 also contributes to the slowing down of the reaction.

iv Catalysed Oxidation of SO_2 by Mn^{++} in the presence of NH_3

So far there is no reported study on NH_3 concentration controlled Mn^{++} catalysed oxidation of SO_2. Holt et al (1981) did a study on the isotopic exchange of O_2 in a SO_2 bulk aqueous solution oxidation system in the presence of Fe^{3+}. The study did not draw any conclusions on the effect of NH_3 on the catalysed oxidation. In considering whether NH_3 exerts merely its conventional effect (by enhancing SO_2 solubility) when Mn^{2+} is also present, the experiments of Ibusuki et al. (1984) are relevant. These workers used Mn^{2+} solutions over a wide range of pH (3 to 8) produced by adding NaOH (not NH_3). The conditions of their experiments are summarised in Table II.15; the rate constant of the SO_2 oxidation declined with increasing pH in the range 5.5 to 8.

Inhibitors:

A number of compounds have been found to inhibit the oxidation of SO_2 in aqueous solution even in quite low concentrations. Inorganic anions such as arsenites, antimonites, phosphites and cyanides have been shown to exhibit inhibitive effects on the oxidation of SO_2 (Schroeter, 1963). Organic compounds such as alcohols, glycols, amines, amides, aldehydes, ketones and phenols inhibit oxidation at concentrations as low as 10^{-6} M (Fuller et al, 1941). Their actions may be explained in terms of radical chain termination as illustrated by Larson et al. (1978).

$$SO_5^- + \text{Inhibitor} \rightarrow \text{Non-reactive product}$$

The ubiquity of these free radical scavengers makes it necessary for experiments on SO_2 oxidation to be carried out with great care. They are known to have been introduced into a reaction system through solvent water, use of rubber or plastic vessels and through the use of air and other gases that have not been rigorously treated to rid them of organic compounds. Since some of these inhibitors are likely to be present in hydrometeors, any extrapolation of labortory measurements of SO_2 oxidation should take their presence, concentration and action into consideration.

Table II.13 Effect of NH_3 on the solubility of SO_2

Partial Pressure of gases (atmospheres)			Initial Droplet $[SO_4^{--}]$ (Molar)	Droplet phase concentration of S(IV) species (mole dm^{-3})					$\frac{[S(IV)]_T}{p_{SO_2}}$
SO_2	NH_3	CO_2		pH	$SO_2 \cdot H_2O$	HSO_3^-	SO_3^{--}	Total S(IV) in Solution $[S(IV)]_T$	
7.49×10^{-9}	0	3.11×10^{-4}	10^{-3}	2.699	9.288×10^{-9}	8.08×10^{-8}	2.521×10^{-12}	9.009×10^{-8}	12.02
10^{-6}	0	"	"	2.697	1.240×10^{-6}	1.074×10^{-5}	3.336×10^{-10}	1.198×10^{-5}	11.98
10^{-5}	0	"	"	2.68	1.240×10^{-5}	1.033×10^{-4}	3.084×10^{-9}	1.157×10^{-4}	11.57
6.3×10^{-5}	0	"	"	2.62	7.812×10^{-5}	5.666×10^{-4}	1.474×10^{-8}	6.448×10^{-4}	10.23
1.953×10^{-3}	0	"	"	2.18	2.42×10^{-3}	6.378×10^{-3}	6.024×10^{-8}	8.800×10^{-3}	4.51
7.49×10^{-9}	7.49×10^{-9}	"	"	5.57	9.288×10^{-9}	6.004×10^{-5}	1.392×10^{-6}	6.144×10^{-5}	8.20×10^{3}
"	10^{-6}	"	"	7.16	9.288×10^{-9}	2.336×10^{-3}	2.107×10^{-3}	4.443×10^{-3}	5.93×10^{5}
"	10^{-5}	"	"	7.57	9.288×10^{-9}	6.004×10^{-3}	1.392×10^{-2}	1.992×10^{-2}	2.66×10^{6}
"	10^{-4}	"	"	7.93	9.288×10^{-9}	1.376×10^{-2}	7.305×10^{-2}	8.681×10^{-2}	1.16×10^{7}

Table II.14: Conditions* for the computation of sulphate production from SO_2 in the presence of NH_3

Reference	pSO_2 (atm.)	pNH_3 (atm.)	Rate equation	k
Scott et al (1967)	$7 \times 10^{-9} - 5 \times 10^{-6}$	$7 \times 10^{-9} - 5 \times 10^{-6}$	$d[SO_4^{--}]/dt = k[SO_3^{--}]$	$1.7 \times 10^{-3} s^{-1}$
McKay (1971)	$7 \times 10^{-9} - 7 \times 10^{-8}$	$3.5 \times 10^{-9} - 1.4 \times 10^{-8}$	$d[SO_4^{--}]/dt = (.031+59[H^+]^{\frac{1}{2}}[SO_3^{--}]$	-
Miller et al (1972)	$7 \times 10^{-9} - 10^{-5}$	$10^{-9} - 10^{-8}$	$d[SO_4^{--}]/dt = k[SO_3^{--}]$	$3 \times 10^{-3} s^{-1}$
+Kallend (1972)	$6.3 \times 10^{-9} - 7 \times 10^{-9}$	$1.7 \times 10^{-9} - 2.8 \times 10^{-8}$	$d[SO_4^{--}]/dt = k[HSO_3^-]/[H^+]^{\frac{1}{2}}$	1.8×10^{-6}

+ The unit of k for Kallends rate equation is $mole^{1/2}\ litre^{-1/2}\ s^{-1}$

* The atmospheric concentration of CO_2 of 3.11×10^{-4} atmosphere was used by all.

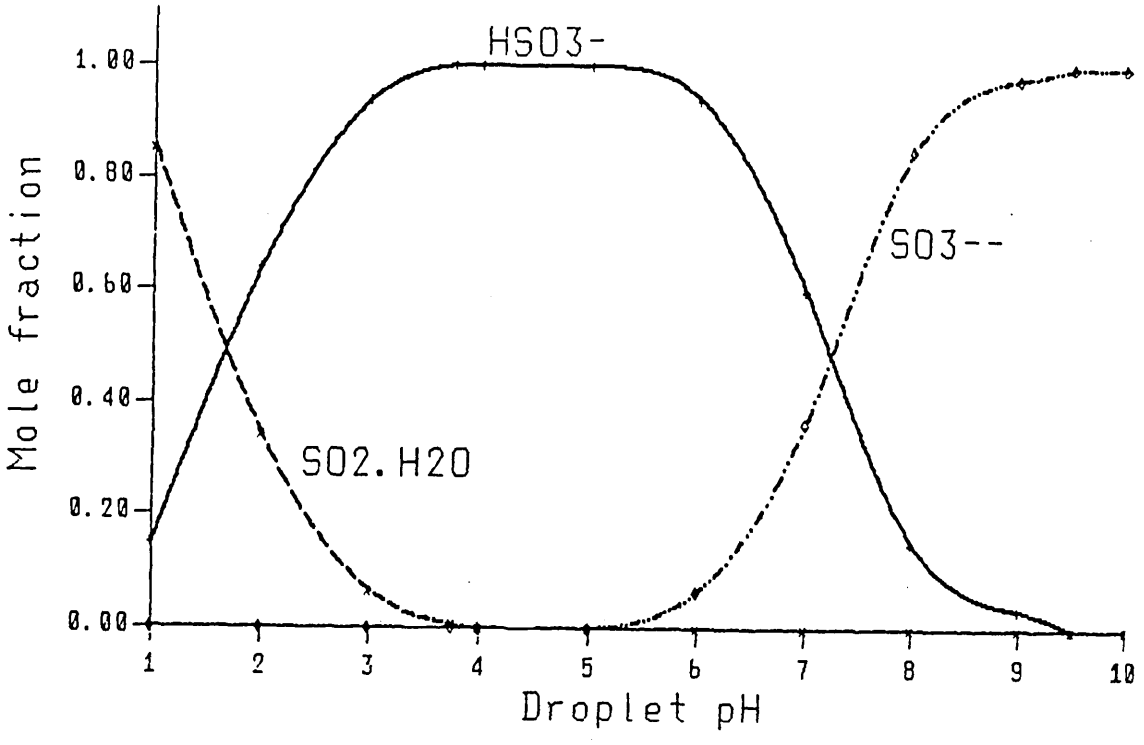


Figure II.5:-Variation of equilibrium mole fractions of S(IV) species in aqueous droplets as a function of pH.

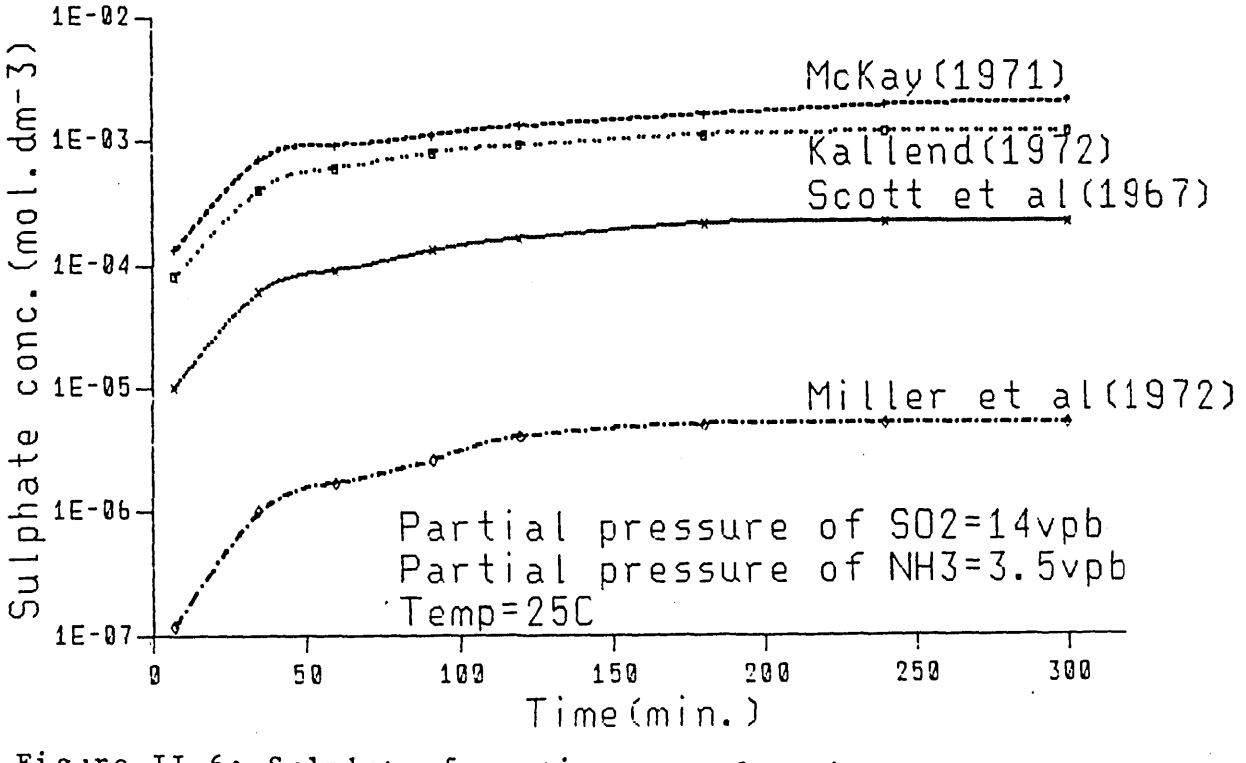


Figure II.6:-Sulphate formation as a function of time calculated from four models.

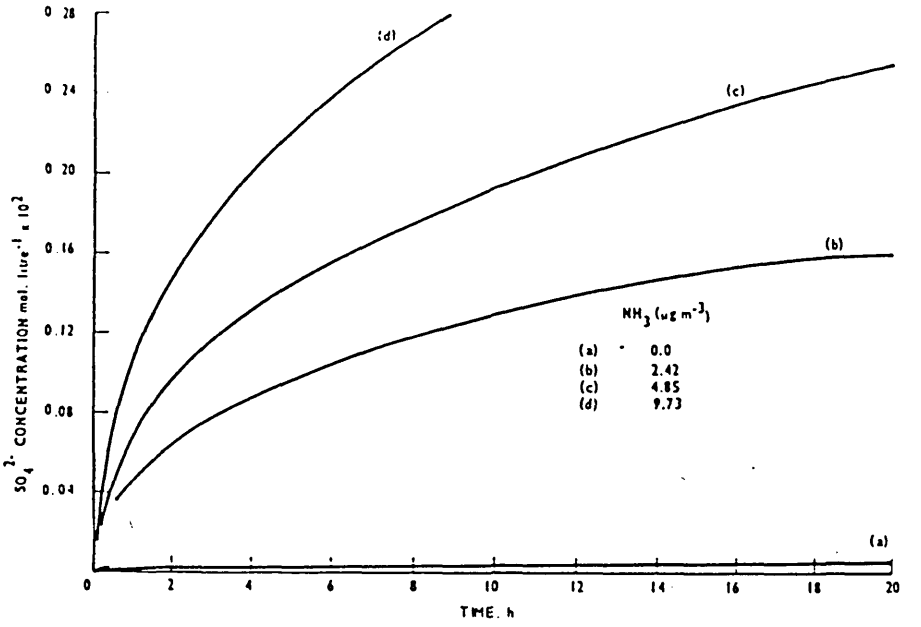


Figure II.7:-Effect of NH_3 concentration on SO_2 oxidation for $p_{SO_2}=6.3\times10^{-9}$ (after Kallend, 1972).

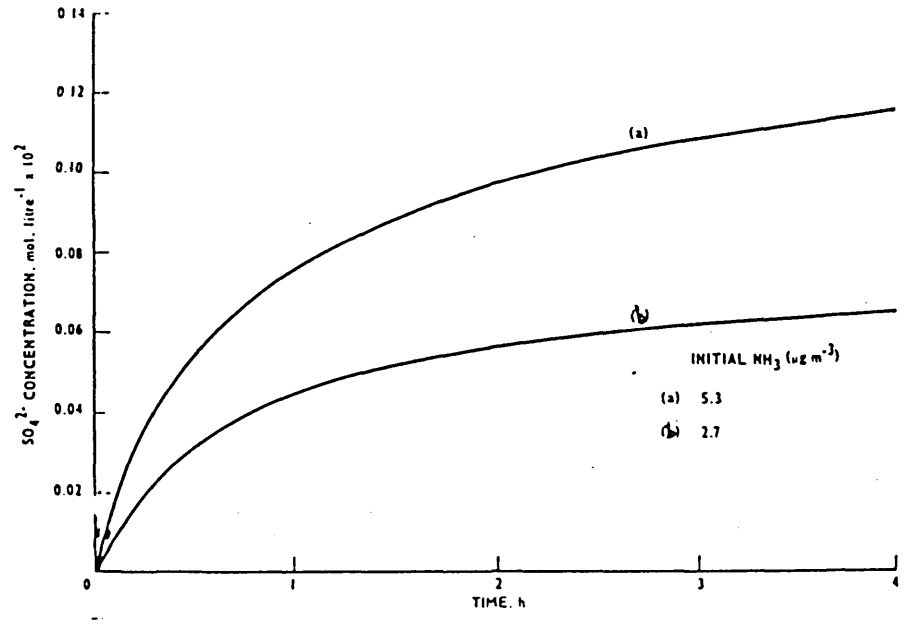


Figure II.8:-Oxidation of SO_2 in solution for a limited supply of the reacting gases. (Note the difference between these and curves (b) and (c) of Figure II.7). Initial conditions are $pSO_2=7.0\times10^{-9}$, phase volume ratio=10^{-7}. (After Kallend, 1972)

Table II.15 Experimental conditions used by Ibusuki et al. (1984).

$[Mn^{2+}]$ (M)	[S(IV)] (M)	Reaction Medium	Flow Rate ($cm^3 min^{-1}$)	Temperature (°C)	pH
$1x10^{-6}$	$1.37x10^{-5}$	Flowing	288	23.7	4.20
	$1.37x10^{-5}$	CSTR	150		
	$1.37x10^{-5}$		100		
	$7.26x10^{-6}$		288		4.32
	$7.26x10^{-6}$		80		
$2x10^{-6}$	$8.13x10^{-6}$		390		4.71
	$8.13x10^{-6}$		288		
$4x10^{-6}$	$1.362x10^{-5}$		390		4.82
	$1.362x10^{-5}$		288		

II.4 Aerosol

II.4.1 Atmospheric Aerosol

Chemical transformation of polutants in the atmosphere leads to the formation of particulates. Much of these are in the size range between 0.1 and 2 μm where sedimentation is not an important mode of removal from the atmosphere. Particulates from natural sources also contribute to the burden of atmospheric aerosols. Natural aerosols are formed by a number of processes such as the homogeneous nucleation of water in supersaturated air masses, dispersion of wind blown silicates and other materials of soil and rock origin and sea waves. Natural atmospheric particulates are also added to by waves of extraterrestrial meteoric debris (Gokhale et al, 1969) and by volcanic eruptions.

Natural atmospheric aerosols are polydisperse and multimodal - commonly trimodal. The cause of the multimodality is best understood from the knowledge of such size determining processes of aerosols as their source; deposition, coagulation, nucleation and condensation patterns; the atmospheric chemical reactions that yield them; fluid dynamic processes such as advection, convection and dispersion; and meteorological processes existing in their environment. The main cause of trimodality in natural aerosol is the mixing of aerosols from many primary sources.

Aerosol particles range from chain aggregates of molecules (0.001 μm) to fog droplets (100μm), a variation of 5 orders of magnitude in diameter. A schematic diagram of a typical atmospheric aerosol size spectrum is shown in Fig II.9.

Aitken nuclei are formed by the condensation of hot vapour to primary particles which coagulate to chain aggregates. Coagulation of Aitken nuclei leads to the formation of particles in the accumulation range. Most of the atmospheric particulates are in the accumulation mode. They are formed mostly from the chemical conversion of reactive gases into low volatility vapours which undergo homogeneous nucleation and condensation growth to form drops, which by coagulation form particles in the accumulation mode. Sulphates formed by the oxidation of SO_2 in the atmosphere are found in this mode, with $(NH_4)_2\ SO_4$ being

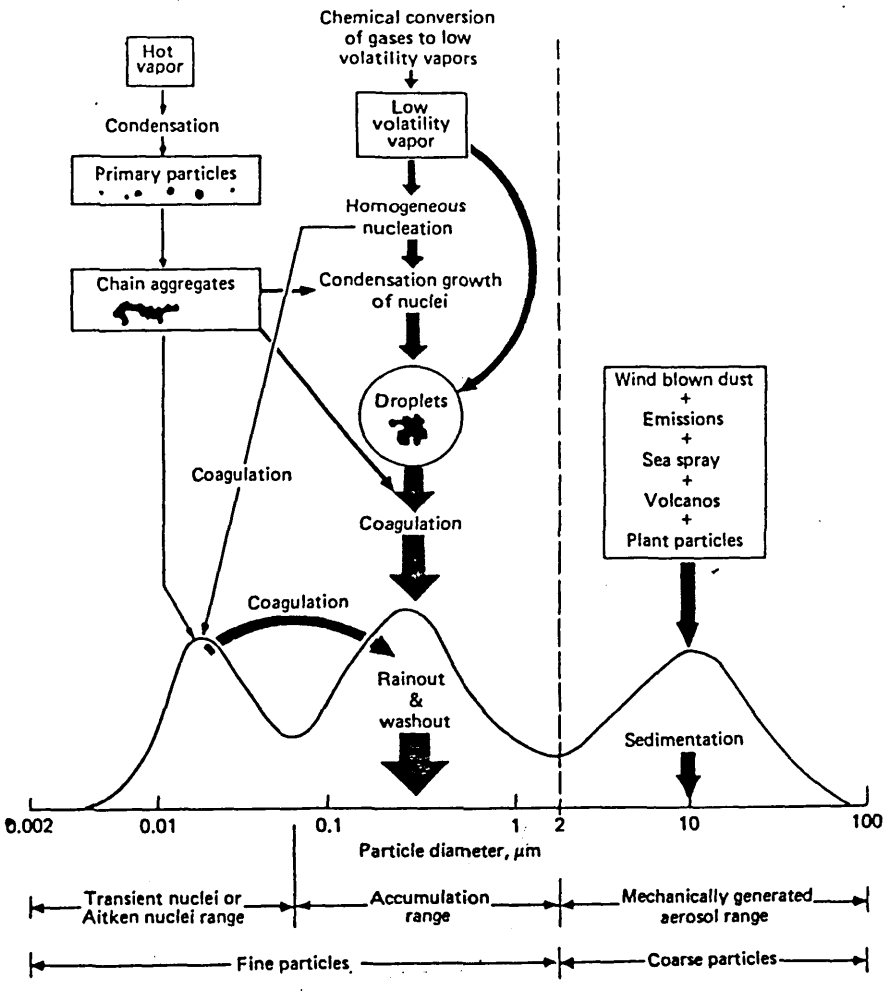


FIG.II.9:-Aerosol size spectrum(JAPCA,1979,p613)

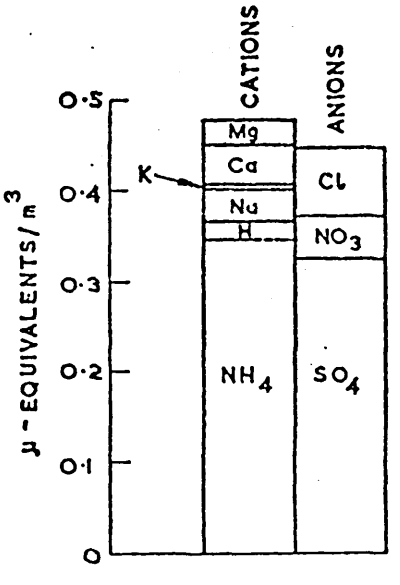


FIG.II.10:-Water-soluble Inorganic Ions on Filter(McKay,1969)

the predominant soluble component of the atmospheric aerosols (McKay, 1969 and Junge, 1953) as shown in Fig II.10. The coarse particles are mechanically generated by wind, sea spray, from volcanoes and from industrial effluents. Some important characteristics of aerosols in the three modes are listed in Table II.16.

II.4.2 Nucleation

Aerosol particles may be formed by the condensation of materials molecularly dispersed in the gas phase. The size spectrum will depend on the rate of formation of the nuclei, the rate of growth of these nuclei and the resulting particles and the rate of coagulation of these particles.

When a vapour is compressed beyond its saturation pressure to a supersaturated metastable state, aggregates containing various numbers of molecules are formed within the saturated vapour. The process of aggregation takes place by the progressive accretion of single vapour molecules. These aggregates may be considered as minute droplets and their vapour pressures will depend on their radius according to Kelvin or Gibbs-Thomson equation

$$\frac{p_i}{p_\infty} = \exp \frac{2\sigma M}{\rho R T r_c} \qquad \text{II.61}$$

where R is the gas constant; T is temperature in Kelvin; p_i is the vapour pressure of a droplet of radius r_c, p_∞ is the saturation vapour pressure, σ is the surface tension of the liquid and ρ is the density. For a given saturation ratio, the embryo droplets of radius below the critical value r_c tend to redisperse while those above it tend to grow unimpeded into macroscopic droplets. The critical radius is analogous to the activated state in ordinary chemical kinetics and the rate of nucleation is the rate of passage through this critical radius. This size (Kelvin) effect is significant only for particles less than 0.1 μm. The rate of nucleation is given by the expression (Dunning, 1960)

Table II.16 Important characteristics of Aerosols (APCA,1981)

Particle Properties	Particle Size Mode		
	Aitkin Nuclei	Accumulation Mode	Coarse Particles
1. Size Range (diameter in μm)	0.005-0.05	0.05-2	2-100
2. Method of Removal	Coagulation and formation of accumulation mode particles	Rainout and washout	Sedimentation
3. Method of size analysis	X-ray diffraction electron microscopy ultra-centrifuge and adsorption	Light scattering and turbidimetry	Sedimentation and electrical conductivity
4. Diffusion coefficient in air at 25°C and 1 atmosphere	2.5×10^{-5} - 2.5×10^{-3}	7×10^{-7} - 2.15×10^{-5}	2.4×10^{-8} - 7×10^{-7}
5. Terminal gravitational settling in air at 25°C and 1 atmosphere			
i. Reynolds number	2×10^{-11}-3×10^{-9}	3×10^{-9}-5×10^{-5}	5×10^{-5}-3
ii. Settling velocity(cms^{-1})	7×10^{-6}-7×10^{-5}	7×10^{-5}-3×10^{-2}	3×10^{-2}-48

$$J = \frac{p^2 v}{KT} \quad \frac{2\sigma}{\pi m} \quad \exp \leftarrow \frac{-\Delta G_n}{KT}$$

where m is the mass of a molecule and ΔG_n is the free energy of formation of a critical nucleus of n molecules, given by the equation

$$\Delta G_n = \frac{16\pi\sigma^3 v^2}{3\{KT\log(p/p_\infty)\}^2}$$

and the number of molecules in the embryo,

$$n = \frac{32\pi\sigma^3 v^2}{3\{KT\log(p/p_\infty)\}^3}$$

K is the Boltzman constant

Nucleation is controlled by supersaturation. J is positive for all values of supersaturation ratio greater than unity but is very small until supersaturation ratio reaches some critical value $(p_1/p_\infty)_{crit}$ above which the nucleation rate increases extremely rapidly.

Wilson (1900) working in an atmosphere entirely free of all foreign particles and ions but saturated with water vapour cooled below its saturation temperature showed that homogeneous or self nucleation of water droplet was possible. But because of supersaturation requirements, it seldomly occurs in nature and hence is not relevant to atmospheric aerosol formation. Because of its inherent instability, supersaturation is not maintained long when it is produced except at values of the order of 340% (Twomey, 1977) which never occurs naturally in the atmosphere. There is therefore no possibility of water droplets in the atmosphere or any other atmospheric particulate for that matter being formed by homogeneous homonuclear nucleation.

Heterogeneous Nucleation or Nucleated Condensation

This is the primary mechanism for cloud formation because nucleation can take place at low values of supersaturation. The atmosphere has a large population of condensation nuclei with a variety of size, composition and chemical characteristics.

Insoluble nuclei provide passive site for condensation in saturated vapour. At a given supersaturation, an insoluble nucleus

possessing a size above r_c for that supersaturation, having an adsorbed film of vapour behaves like a droplet of that size and grows infinitely by condensation. The atmospheric concentration of such particle size is relatively low and it is unlikely that very many of them will be perfectly wettable. So their role in cloud condensation is limited. Ions are singly charged clusters of air molecules formed by the action of cosmic radiation and radioactive gases from the earth. They constitute condensation nuclei at supersaturations above 2. They are, like the insoluble nuclei not important in atmospheric droplet formation.

The most important condensation nucleation mechanism is condensation on soluble nuclei. Those that occur naturally in the atmosphere include $(NH_4)_2SO_4$ from anthropogenic sources and NaCl from sea wave. Particle growth is possible even at low values of supersaturation as soon as the deliquiscence point of the salt is reached. This is the primary mechanism for water droplet formation in an aerosol system. Fig II.11 shows the effect of supersaturation on droplet size of an aerosol particle condensing on a soluble salt nucleus. The nucleus will form a droplet and grow as long as the supersaturation above S is maintained; shown by the arrow A. For saturation ratios below S, any droplet whose diameter is outside the area under the curve will at constant saturation ratio grow until it reaches the curve and then begins to grow with increase in saturation according to the curve. Conversely, any droplet whose diameter lies in the area under the curve at constant saturation ratio would evaporate until it reachs the curve and then begins to grow according to the curve with increase in saturation.

The equilibrium vapour pressure at the surface of the droplet nucleated on a soluble nucleus is reduced by an amount depending on the nature of the solute and the concentration of the solution. This is given by Raoults equation:

$$\frac{p}{p_\infty} = x_i \qquad \text{II.62}$$

where $\frac{p}{p_\infty}$ is the relative humidity and x_i is the mole ratio of the

species i. This means that condensation sets in at lower supersaturations than those required for an insoluble nucleus of the same size or a droplet of a pure solvent. The equilibrium vapour pressure, p_∞ over a droplet of aqueous solution of a single salt of radius r is given by equation II.63 (Mason 1957). For

p'_r = vapour pressure over droplet
σ' = surface tension of solution
ρ' = density of solution
p = density of pure solvent
M = molar mass of water
m = mass of dissolved salt
i = van Hoff's factor
W = molar mass of dissolved salt

$$\frac{p'_r}{p_\infty} = \exp \frac{2\sigma' M}{\rho' R T_r} \left[1 + \frac{imM}{W(\frac{4}{3}\pi r^3 \rho' - m)}\right]^{\rho/\rho'} \qquad \text{II.63}$$

This is a combination of Kelvin and Raoult's equations. For humidity near 100%, the equation above may be simplified to

$$\frac{p'_r}{p_\infty} = 1 + \frac{2\sigma M}{\rho R T_r} - \frac{8.6m}{Wr^3} \qquad \text{II.64}$$

Fig. II.11a shows saturation ratio versus droplet size for pure water and droplets containing two weights of salt, m_1 and m_2 where m_1 is greater than m_2 at 20°C. The region above each curve is a growth region and that under is an evaporation region. If two droplets of same size d_1 and d_2 of solutions containing two different weights of same salt m_1 and m_2 were kept at constant saturation ratio, d_1 would grow until it reached its equilibrium size at the point a whereas d_2 would evaporate until its equilibrium size was reached at the point b. Water droplet of the size of d_1 and d_2 under the same conditions would evaporate to zero size.

Condensational Growth

Once a stable droplet is formed by nucleation, given an infinite atmosphere maintained at constant temperature and supersaturation, it

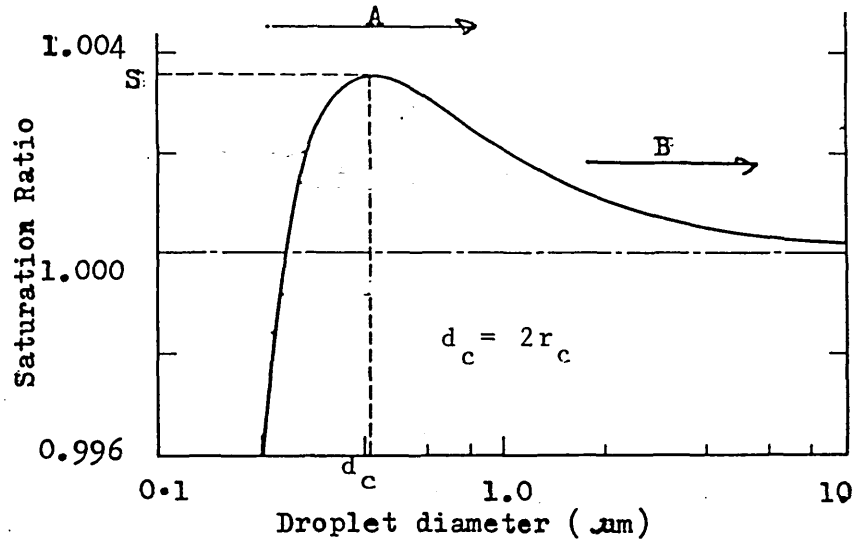


Figure II.11:-The effects of saturation ratio and size on growth and evaporation of salt solution droplet. (adapted from Hinds, 1982).

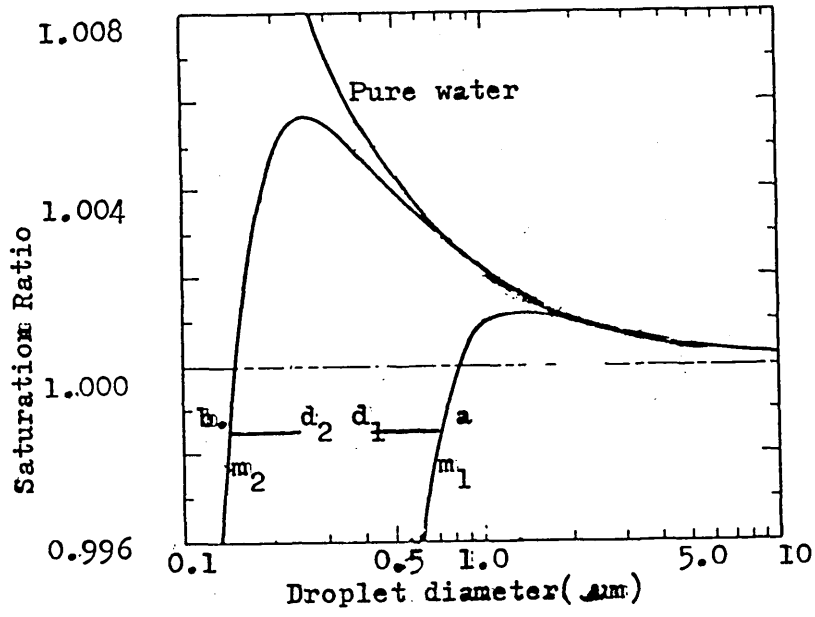


Figure II.11a:-Saturation ratio versus droplet size for pure water and salt solution droplets. (Adapted from Mason, 1971).

grows by condensation. The rate of growth depends on the saturation ratio and the Knudsen number of the particle. Initially the growth rate is governed by the rate of random molecular collisions of vapour nolecules on the droplet surface and the rate of evaporation from the droplet surface.

$$n_z = (z_{in} - z_{out})\, A_s$$

$$= \frac{\frac{\pi r^2}{4}(p - p_r)}{(2\pi mKT)^{\frac{1}{2}}} \qquad \text{II.65}$$

where

n_z is the net rate of arrival of molecules to the entire droplet surface of area A_s; Z_{in} is the arrival rate; Z_{out}, the evaporation rate; r, the droplet radius; p_r the partial pressure of the vapour at the droplet surface; m the mass of vapour molecule- and p, the partial pressure of vapour in the gas surrounding the droplet. So for Kn (the Knudsen number) greater than one, the rate of increase of droplet radius is given by

$$\frac{dr}{dt} = \frac{2M(p - p_r)}{\rho N(2\pi mKT)^{\frac{1}{2}}} \qquad \text{II.66}$$

where M is the molar mass of solvent and N is Avogadro's number.

For particles with Kn less than 1, growth depends on the rate of diffusion of molecules to the droplet surface and is given by

$$\frac{dr}{dt} = \frac{2DM(p - p_s)}{RT\rho r} \qquad \text{II.67}$$

where D is the difusivity of water molecules in the vapour state;

p_s = saturated v.p. at droplet temperature

Hence the growth rate is inversely proportional to particle size. Thus growth is rapid initially but slows down gradually as particles get larger. When $p < p_s$, negative growth or evaporation sets in.

II.4.3 Evaporation

In large droplets, the rate of evaporation is controlled by the rate at which vapour can diffuse away from the droplet, and is given by the same equation as for condensation but modified to reflect self cooling due to latent heat of vaporisation

$$\frac{dr}{dt} = \frac{2DM}{R\rho r}\left(\frac{p_\infty}{T_\infty} - \frac{p_r}{T_r}\right) \qquad \text{II.68}$$

where p_∞ is less than p_r.
In terms of decrease of surface area,

$$\frac{dA_s}{dt} = \frac{2\pi DM}{R\rho}\left(\frac{p_\infty}{T_\infty} - \frac{p_r}{T_r}\right) \qquad \text{II.69}$$

For a given temperature and partial pressure of vapour, the rate of decrease of surface area is independent of particle size. Size shrinkage will be slow initially and increase as particle size decreases.

If allowed to continue evaporation, a homogeneously nucleated droplet will reach zero size in its life time or drying time given by the equation

$$t = \frac{R\rho r^2}{2DM\left(\frac{p_r}{T_r} - \frac{p_\infty}{T_\infty}\right)} \qquad \text{II.70}$$

This is accurate for large droplets (10 - 50μm). Fuchs (1959) treated small droplets (under 0.01 μm) in terms of kinetic theory of gases operating in series with diffusion. Using an expression by Davies (1978) for the rate of mass transfer by the combined mechanisms, the rate of decrease in particle size becomes

$$\frac{dr}{dt} = \frac{2DM}{R\rho r}\left(\frac{p_\infty}{T_\infty} - \frac{p_r}{T_r}\right)\frac{r(\lambda + r)}{4r^2 + 5.33\,\lambda^2 + 6.84\,\lambda r} \qquad \text{II.71}$$

where λ is the mean free path of water molecule. The effect of latent

heat of cooling is to reduce the value of p_r and thereby slows the rate of evaporation. But this effect is negligible when the atmosphere surrounding the droplet is saturated with vapour.

From equations II.68 - II.71, drying time increases with initial droplet diameter (see table II.17) as well as with the relative humidity. Pure water droplets of submicron size range have no chance of existing even in a saturated atmosphere because of evaporation. Similarly, it is difficult to maintain pure water droplets of that size regime in a duct.

The rate of evaporation of a mono-disperse pure water droplet cloud in a tubular flowing reactor system was treated by Kousaka et al (1978). If evaporation coefficient is unity, the rate of change in droplet radius, r is given by the modified form of eqn. II.71 with a general form

$$\frac{dr}{dt} = - \frac{DM}{r\rho_s R} \eta\gamma \qquad \text{II.72}$$

where

$$\gamma = \left[\frac{p_0(T_0,r)}{T_0} - \frac{Sp_s(T_\infty)}{T_\infty} \right] \left[1 + \frac{p_0(T_0,r) + Sp_0(T_\infty)}{2p_t} \right]$$

$$\eta = \frac{Kn + 1}{1.333Kn^2 + 1.71Kn + 1}$$

p_0 and T_0 are the pressure and temperature respectively at the droplet surface; p_∞ and T_∞ are the pressure and temperature respectively of the surrounding air far away from the droplet; p_s and p_t are the saturated vapour pressure and total pressure respectively, Kn is the Knudsen number; S is the saturation ratio.

The vapour pressure at the droplet surface is given by Kelvin's equation (Equation II.61)

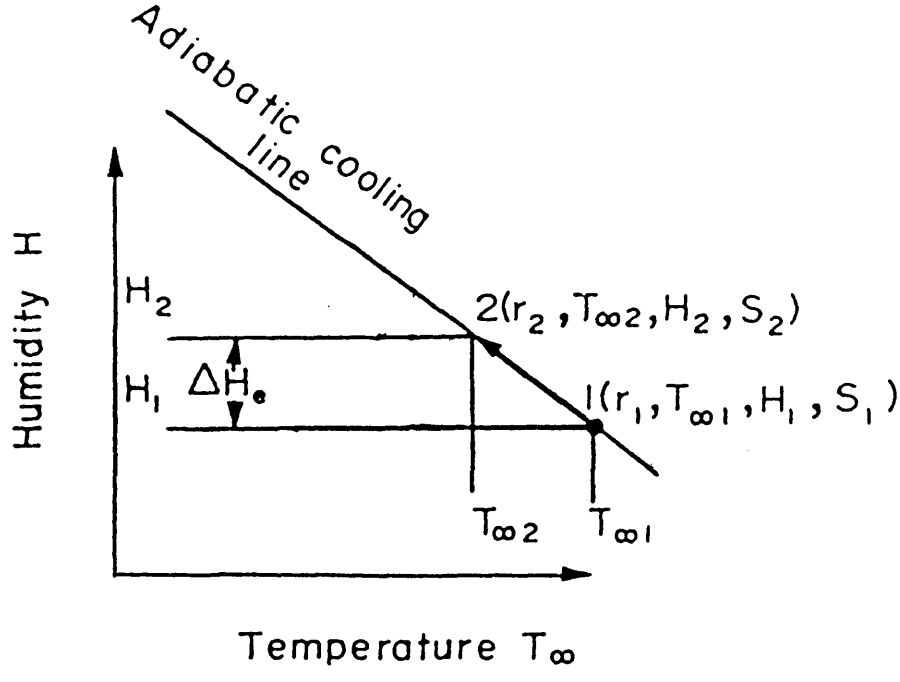


Figure II.12:-Changes in temperature and humidity with size in aerosols undergoing size change by evaporation(Kousaka et al,1978).

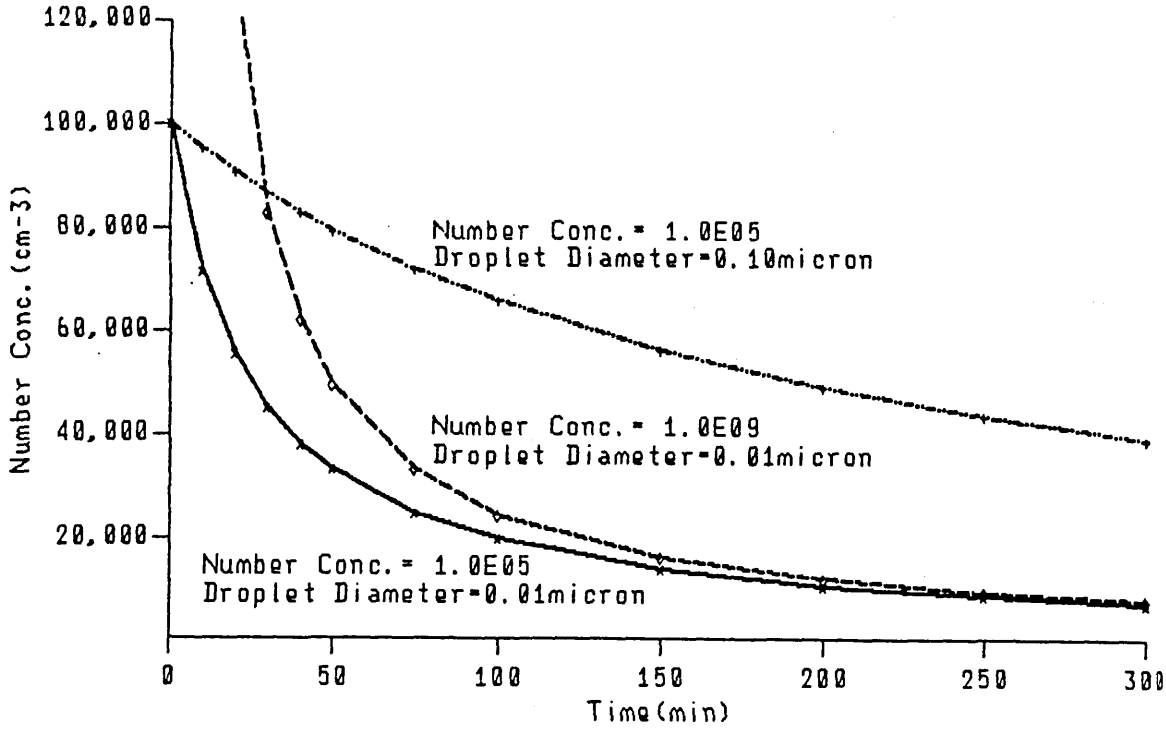


Figure II.13:-Effect of monodisperse coagulation on aerosol number concentration.

The fall in temperature of the droplet as it evaporates is given by the equation

$$T_0 = T_\infty - \frac{LDM}{KR}\gamma \qquad \text{II.73}$$

where L = latent heat of vaporisation;

K = thermal conductivity

Equations II.71 - II.73 give the rate of evaporation of a single droplet. From equation II.72, a droplet which decreases in size from r_1 to r_2 during a small time step will add water vapour to the medium per unit mass of dry air according to the equation

$$\Delta H_e = 4\pi(r_1^3 - r_2^3)\, n_w \rho / 3 \qquad \text{II.74}$$

where n_w is the droplet number concentration on mass basis.

$n_w = n_0 V_H$

n_0 = droplet initial number concentration

$\Delta H_e = H_2 - H_1$ (g of water/g of dry air)

V_H is humid volume.

According to fig II.12 as the droplet evaporates from r_1 to r_2, the temperature of the air away from the droplet surface decreases from T_{∞_1} to T_{∞_2} and the humidity increases from H_1 to H_2.

The chances of pure water droplets persisting will therefore be dependent on both the saturation of the environment and the droplet number concentration. The evaporation of water droplet clouds is depicted in Fig II.14. Fig II.14a shows the effect of temperature on the life time of droplet of diameter 0.6 μm. In Fig II.14b, the effects of droplet size and number concentration on drying time are depicted. With the increase in number concentration the rate of droplet radius decrease slows down until at a value larger than 10^5 cm^{-3} the droplets of 0.5 μm in radius seem to be almost stable because of the humdiity rise and the simultaneous temperature fall. For low values of saturation and number concentration, the quantity of water vapour produced by the evaporation is not enough to saturate the surrounding air and therefore droplets evaporate to zeros size. On the other hand, with high values of saturation and number concentration, droplets evaporate until the equilibrium vapour pressure given by

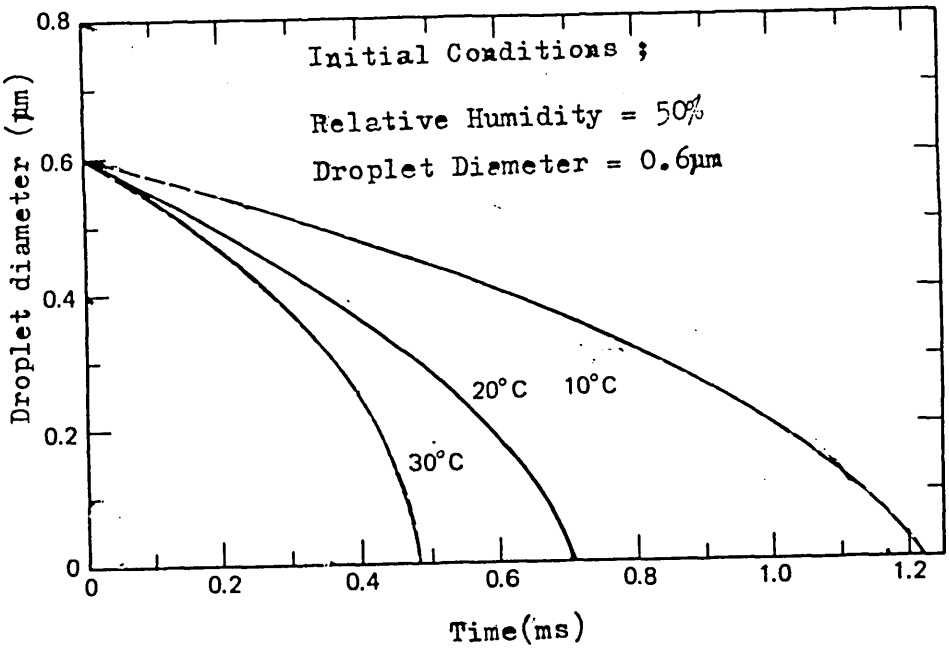


FIG.II.14a:- The effect of temperature on the evaporation of pure water droplet (adapted from Hinds, 1982).

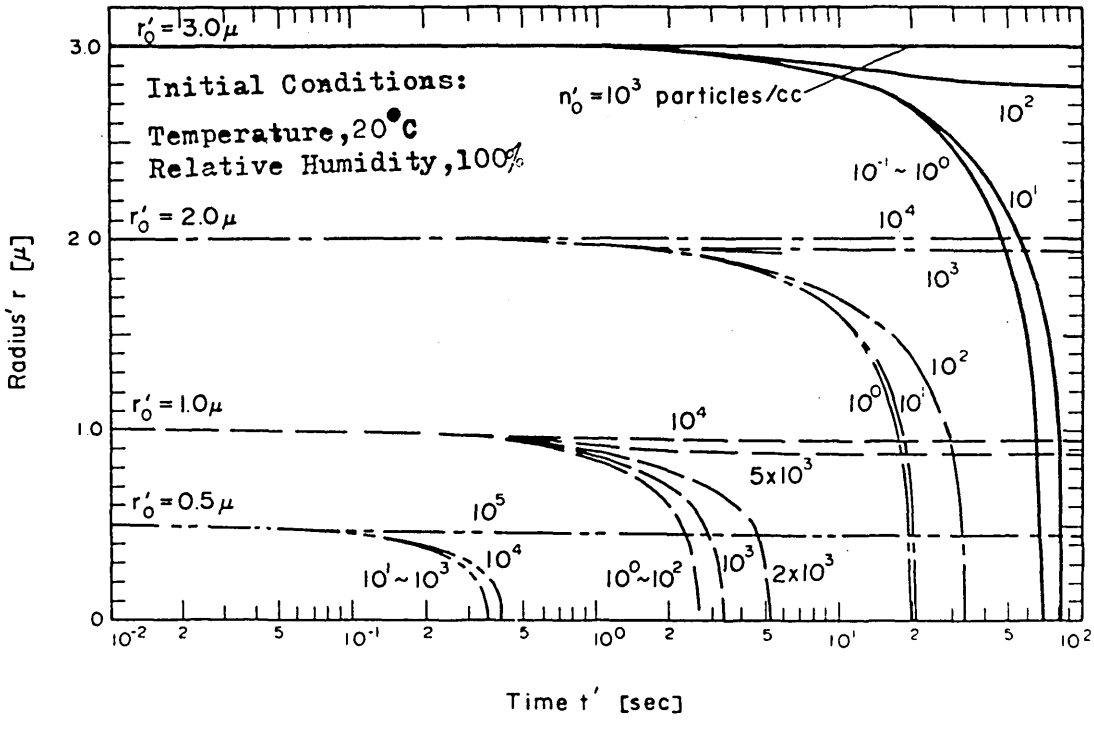


Figure II.14b:-Effect of size and number concentration on pure water droplet life-time(Kousaka et al, 1978)

equation II.61 is attained and because of the sufficient amount of water vapour source (the droplets), the droplets in this case attain stable radii after a slight change in size.

Droplets formed by heterogeneous nucleation do not dry to zero size but to the size of the original nuclei. Meadley (1971) formulated a mathematical model for the evaporation of a droplet having a soluble salt nucleus in which as the surface recedes, the concentration gradient induces a back-diffusion of the solute towards the centre as a consequences of Ficks law of diffusion. The drying rate will slow down as the droplet size gets closer to the nuclear size because the solution concentration increases and causes a reduction of the vapour pressure over the droplet surface which reduces $(p_\infty - p_d)$.

The life time of water droplets can be increased by factors of several hundreds if covered with a thin film of contaminant. Substances so far tried with success include fatty acids (Eisner, 1960). Derjaguin et al (1960) used a surface acting substance as the protective film and found not only depressed evaporation rate but also growth. The gowth is attributed to increase in the accomodation coefficient. This phenomenon has a significance in an atmosphere contaminated with oil vapour.

II.4.4 Coagulation

Aerosol particles collide with one another in an inelastic manner due to a relative motions between them to form larger particles. This leads to a continuuous decrease in number concentration and an increase in droplet size. The relative motion may be Brownian and the coagulation it produces is Brownian or thermal coagulation. It is spontaneous and ever present in aerosols. If relative motion is due to external forces or aerodynamic effects, kinematic or orthokinetic coagulaiton results. Coagulation of airborne particles was first demonstrated by Telman et al (1919).

Thermal Coagulation

Two situations in thermal coagulation are considered. The first is monodisperse coagulation while the other is polydisperse

coagulation. The description of the later is very complicated and so only a general treatment of it will be attempted here. The rate of coagulation depends on the range of particle sizes present and so the mathematics are very complicated and are incapable of explicit solution. The simplest case that involves only two sizes r_1 and r_2 where r_2 is larger than r_1 will be considered.

The equation for the number concentration N_t of droplets at time t in monodisperse aerosol of initial number concentration N_0 is given by

$$N_t = \frac{N_0}{1 + N_0 K t} \qquad \text{II.75}$$

where K is the coagulation coeficient.
For a di-disperse coagulation, K becomes $K_{1,2}$ given by the equation

$$K_{1,2} = \pi(r_1 + r_2)(D_1 + D_2) \qquad \text{II.76}$$

where D_1 and D_2 are the diffusivities of particles r_1 and r_2 respectively; with D_1 greater than D_2. Therefore $K_{1,2}$ is greater than the coagulation coefficients for either r_1 or r_2 because of the combination of the large absorbing surface of the big particle and the rapid diffusion of the smaller particle. The greater the difference in particle size, the more rapid the coagulation and this results in a new particle essentially the same size as the original larger particle while the smaller particle had dispeared.

The situation becomes much more complicated as the polydispersity increases. In such an aerosol the coagulation of a given particle has to be accounted for with particles of every other size. The situation is complicated further by the fact that the size distribution and the proportion of particles of a particular size is not static.

Monodisperse Coagulation

Monodisperse coagulation is simplified by having all the particles of equal size. Calculations developed by Smoluchowski (1916) and later verified by Whytlaw - Gray (1935) successfully described the thermal

coagulation of monodisperse liquid and solid particles in the initial stages of coagulation.

The basic approach is to focus attention on a single particle and consider how other particles of the same size diffuse to its surface. The flux of particles to the surface of this selected particle is given by Ficks first law

$$J = -D \frac{dN}{dx} \qquad \text{II.77}$$

where $\frac{dN}{dx}$ is the concentration gradient of particles at the collision surface of the selected particle. Smoluchowski's analysis of coagulation led to the conclusion that the number concentration declines at a rate given by

$$\frac{dN}{dt} = K_s N^2 \qquad \text{II.78}$$

where K_s is the coagulation rate coefficient given by

$$K_s = 8\pi rD \qquad \text{II.79}$$

in units of $m^3\ s^{-1}$.
Table II.17 gives the value of K_s for different values of droplet diameter at standard conditions.

Since from eqn.II.74, the rate of coagulation is proportional to N^2, coagulation is very rapid at high concentrations and slows as coagulation reduces number concentration as shown in Fig. II.13. Fig II.13 shows that after a given time has elapsed, the number concentration cannot exceed a certain value regardless of its initial concentration.

Particle size increases as a direct consequence of the reduction in number concentration due to coagulation. Assuming no losses, the particulate mass of a confined aerosol is conserved. Then

$$C_M = N_0 \frac{\pi}{6} \rho(2r)^3 = N_t \frac{\pi}{6} \rho(2r)^3 \qquad \text{II.80}$$

from which

$$\frac{r_t}{r_0} = \frac{N_0}{N_t}^{1/3} \qquad \text{II.81}$$

where r_0 is the initial particle radius and r_t is the particle radius at time t.

The equation shows that an eight-fold reduction in number concentration is required to double particle size by coagulation. Table II.19 shows the relationship between initial number concentration, time to reach half of it and time to double the particle size at coagulation coefficient $K = 5 \times 10^{-10}$ cm^3 s^{-1}. The table defines concentration regions where coagulation can be neglected. Hence the way to stop coagulation and freeze the particle size distribution is to rapidly dilute the aerosol to a concentration where coagulation is negligible within the experimental time.

As particles approached molecular size, thermal coagulation no longer followed equation II.74 strictly. Fuchs (1934) applied correction factors to the coagulation coefficient which gave rates of coagulation which were compatible with kinetic theory. Hidy et al (1965) developed an alternative theory which treated a particle for which Kn is equal to or greater than 10 as one component of a multicomponent gaseous system and calculated the coagulation rate according to the kinetic theory of gases.

Kinematic Coagulation

Orthokinetic or kinematic coagulation occurs as a result of relative particle motion caused by mechanisms other than Brownian motion. Some of these mechanisms are gravitational and centrifugal force fields. Others are electrical and magnetic fields which give rise to directed coagulation; sonic fields that cause acoustic coagulation; and velocity gradient which causes shear coagulation. Kinematic coagulation is not important for droplets of size below 1 μm. Of these, only shear coagulation is importance in the flow of aerosols in ducts. Particles flowing in a duct in a velocity gradient even if they are of the same size will travel at different velocities because

Table II.17 Variation of life time of water with initial droplet diameter in vapour free air at 20°C (Hinds,1982).

Initial Droplet diameter (μm)	0.01	0.1	1.0	10	40
Droplet life time (s)	2×10^{-6}	3×10^{-5}	1×10^{-3}	8×10^{-2}	1.3

Table II.18 Particle diameter and coagulation coefficients (Davies, 1945)

Diameter (μm)	0.01	0.05	0.1	1.0	10.0
Coagulation coefficient, K_s	6.7×10^{-15}	3.78×10^{-15}	8.6×10^{-16}	3.5×10^{-16}	3.0×10^{-16}

Table II.19: Mode of variation of droplet number concentration as a function of droplet size.

Initial number concentration N_0 (cm^{-3})	Time to reach 0.5 N_0	Time to double particle size ($N=0.125\ N_0$)in (s) (Hinds, 1982)
10^{14}	20μs	140μs
10^{12}	2μs	14ms
10^{10}	0.2μs	1.4s
10^{8}	20min	140s
10^{6}	33min	4hr
10^{4}	55hr	16days
10^{2}	231days	4years

of their positions on different but close streamlines. This relative motion leads to collisions as particles on a faster streamline overtake those on nearby slower streamlines. This gives rise to gradient coagulation. Shear coagulation is much smaller than thermal coagulation except for particles of size 2.5 μm or above.

II.4.5 Aerosol Sampling

In order to characterise the aerosol particles and thereby study the processes that have taken place to produce them, it is essential to collect representative sample for analysis. However, it may be necessary to analyse the aerosol in situ. This may be necessitated by equipment constraints and sometimes by the fact that sampling tends to distort some of the properties being investigated. Two techniques used in sample collection are discussed.

Filtration

The capture of aerosol particulates by filtration is a simple, versatile and economical means of collecting samples of aerosol particulates for analysis. Other uses of aerosol filtration include respiratory protection, air cleaning and processing of hazardous materials.

Two types of filters in use for aerosol sampling are depth filters and screen filters. Fibre or depth filters consist of a mat of fine fibres bonded together to form a tortuous maze of flow channels (White et al, 1964 and Kirch et al, 1978). Particulate removal is as a result of entrapment by or adsorption to the filter matrix. As the pore structure is neither regular nor defined it is not possible to quantify its retention characteristics precisely. Random matrix places no definite upper limit on size of particle which can pass through. Many formulations have been made. These include laminates of papers, pads of fibreglass wool or plastic, combinations of asbestos with coarse fibres such as cellulose, scintered metal, porcelain and diatomaceous earth. The interfibre distances are usually in relation to fibre diameter. Fibres normally occupy less than 10% of the apparent volume of the filter material. Depth filters have very high particle load capacity. The particles are retained on surface and throughout the

matrix. The operational pressure drop is usually very low but increases due to clogging as particles accumulate. Depth filters are not used for aerosol sampling as most of the particulates go through them.

Too Scrubbing.

Screen filters are so named because they retain particles on their surfaces, in much the same way as a sieve. Two types of screen filters are membrane filter and the nucleopore filter (Spurney et al, 1969). The two types are identical in most of their properties. They may be described as bundles of parallel capillaries. The structure is rigid, uniform and continuous with pore size precisely controlled during manufacture, giving well defined limits of efficiency and pressure drop. Diffusion, sieving and impaction are the main mechanism of filteration. Large particles collect on the front surface of the filter while small ones diffuse to the walls of the pores (Twomey, 1976). The high collection efficiency extends to particles much smaller than the manufacturer's stated pore size. Screen filters have low particle load capacity and clog very rapidly. They suffer from very high pressure drop. They are the best filters so far for studying aerosols in the submicron size. The nucleopore filter has the added advantage of being very thin (8 - 12 μm) and transparent and hence specially suited for light and electron microscopy. Screen filters are generally made of cellulose, esters, scintered metal, polyvinyl chloride, teflon and a host of other plastic materials.

Liquid Scrubbing

Using impingers to sample particulates is the EPA recommended method. However work done in this department showed that most of the particulates passed through the scrubbing liquid even at low sampling flow rate.

II.4.6 Generation of Aerosol

Aerosols are generated for various uses - therapeutic, industrial and for research (Topp et al, 1972). The method used in generating depends on the use to which it is to be put, the quantity of it needed and the properties it is desired to have. This section will treat mainly atomisation methods of aerosol generation and mention briefly a

new method of generating solution droplets for research. To obtain accurate results in aerosol experiments, the generator needs to deliver constant and reproducible output of monodisperse stable, uncharged, spherical aerosol particles whose size and concentration could be controlled easily.

Atomisation generators in common use may be grouped into three classes. The first is the air blast or aerodynamical atomiser in which compresed air at a high velocity is used in breaking up liquid emerging from a nozzle into droplets. The second type is based on centrifugal force generated by rotation. The liquid is fed at constant rate on to the centre of a disc, cone or top rotating at about seventy thousand rounds per minute. The liquid is carried off by centrifugal action to the edge of the disc as a thin film which forms filaments and eventually breaks into droplets. This method produces very highly monodisperse droplets.

The third type is the hydraulic or the hydrodynamical atomiser. The liquid is forced through a nozzle from where it breaks up into droplets. The atomisation depends on the physical properties of the liquid and the conditions of ejection from the nozzle and not much on the interaction between the surrounding gas and the liquid.

There are other less known types of aerosol atomisers. One of them is the electrostatic atomiser which breaks up liquid by the action of electrostatic forces and the other is the acoustic atomiser which utilizes high intensity sonic or ultrasonic vibration to atomise a liquid. These two methods are not much used except for special purposes and for demonstration.

Air blast atomiser

No attempt will be made here to treat the mechanism for liquid atomisation by airblast quantitatively. The mechanism is as follows: under the action of an aerodynamic force the liquid is drawn into narrow ligaments or film which subsequently collapses under the action of the surface tension into fine droplets (Hinze et al, 1950; and Green et al, 1957). The size of the droplets formed depends on the diameter of the liquid ligament. As the air velocity increases, the size of the liquid ligament decreases and so the droplet size decreases. In

addition to these liquid ligaments, thin liquid films are formed, they stretch and burst, thus contributing to droplet formation.

The droplets generated may suffer further disruption in the air flow which may lead to break-up into smaller droplets. They may also suffer recoelescence as a result of differential velocity at the mouth of the nozzle. These disruptive processes contribute to the polydispersity in droplets formed by air blast atomisation. This and the fact that aerosols produced are slightly charged are the only major handicap of aerosol so generated. However, the charge is so slight that there is no need to go into the trouble of discharging it. The main problem is from the polydispersity. Three types of air blast atomisers are shown in Fig.II.15 - II.17.

A common method of minimising polydispersity is to introduce impaction surfaces on which the aerosol stream impinges and the larger particles are removed by impaction. Walkenhorst et al (1964) studied the effect of such barriers on droplet size distribution. They found that not only was polydispersity removed entirely but also the aerosol particle size no longer depended on the concentration of the master solution from which it was generated. Matteson et al (1967) used a modified form of Dautreband's generator to produce aerosol whose particle sizes are log normal distributed.

Condensation Generators

This method of aerosol generation is mentioned here because of its growing use in generating monodisperse aerosols of salts that have low deliquiscence point. The salt solution is nebulized by the normal air-blast atomisation method as shown in Fig II.18 and the droplets generated passed through an evaporation chamber where complete evaporation takes place leaving behind residue particles which form condensation nuclei. The mixture of vapour and nuclei is cooled slowly downstream. A make-up vapour stream may be injected if necessary. Condensation takes place on the nuclei to produce condensation aerosol whose size and growth can be accurately controlled. The number concentration is the same for the nubulizer droplets, nuclei and condensation - formed droplet. Kaplan et al (1981a) used this method to generate $(NH_4)_2SO_4$ droplets.

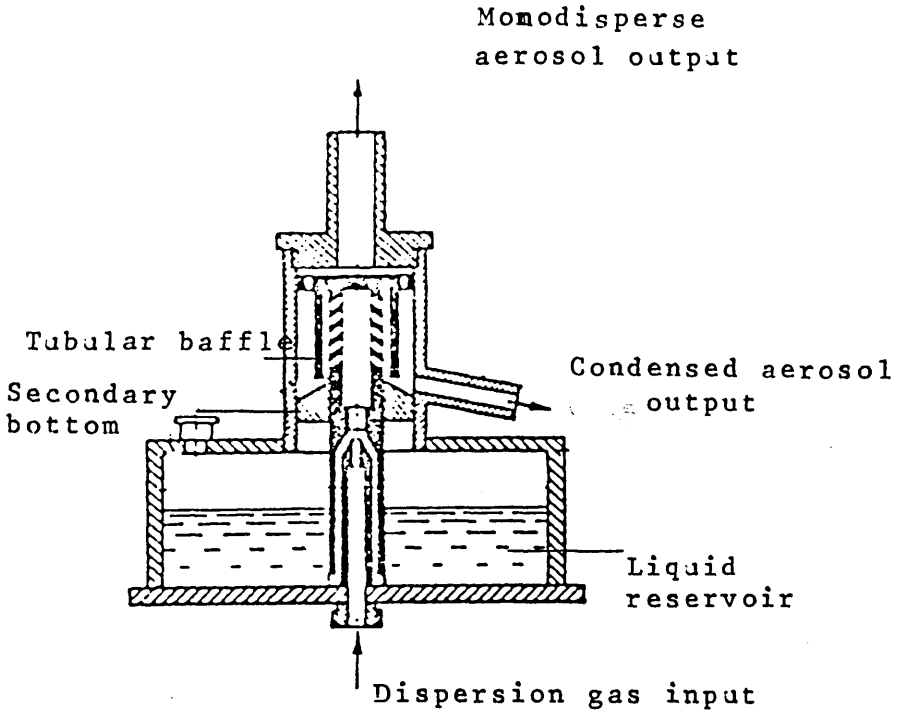


Figure II.15 :-Dautreband Generator(Walkenhorst et al,1964)

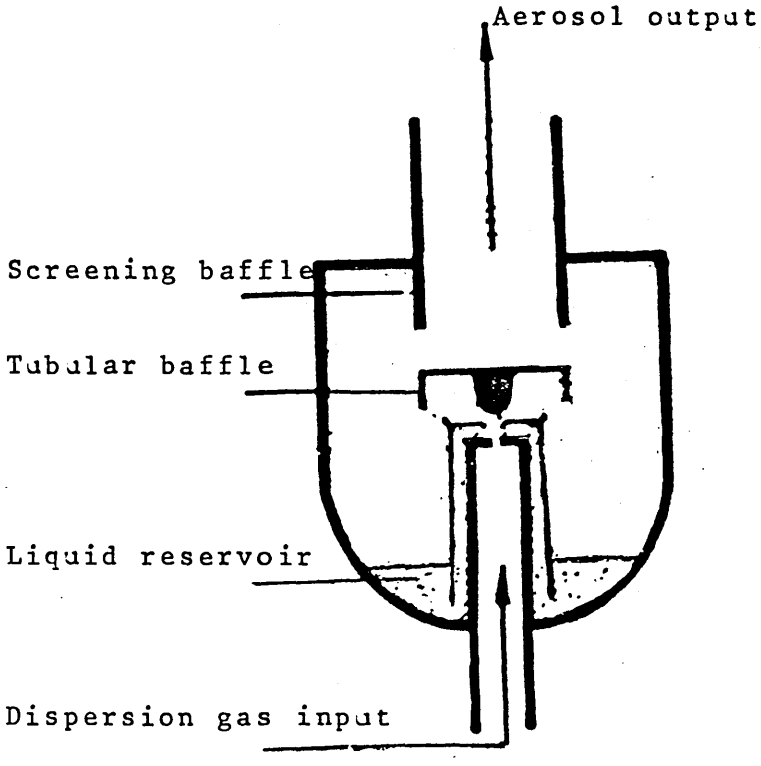


Figure II.16:-The Acorn Nebuliser.

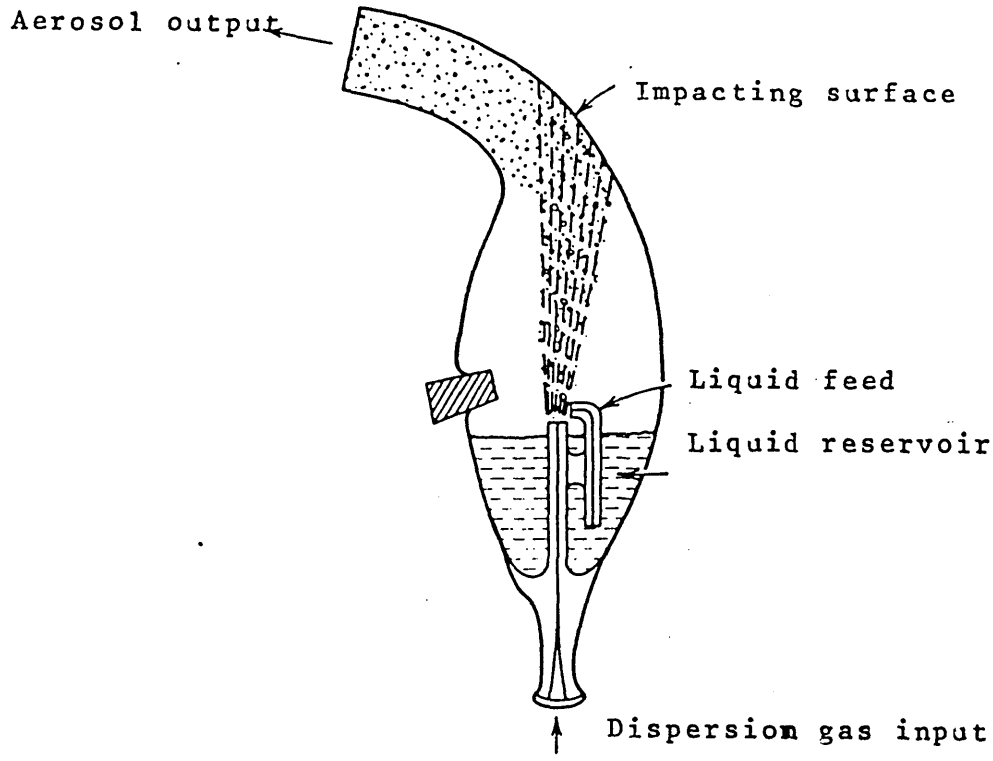


Figure II.17:-DeVilbiss Model 40 Nebuliser.

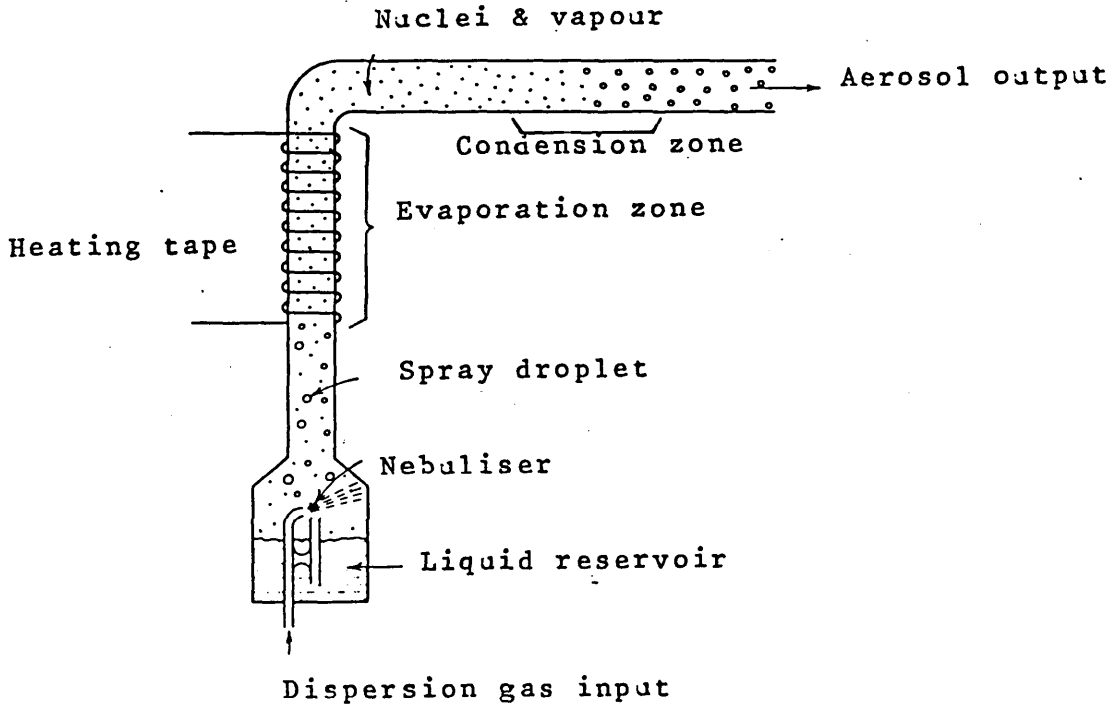


Figure II.18:-Evaporation-Condensation Monodisperse Aerosol Generator.

II.4.7 Particle size statistics

Droplet size is the most important parameter of aerosol since not only are all properties of aerosols dependent on particle size but also the nature of laws governing the change with particle size. In polydisperse aerosols, the particle sizes range over two or more orders of magnitude. Even in monodisperse aerosols where the variation coefficient of the particle size, σ/a (σ = standard deviation, a = mean diameter) is less than 0.1 there is an appreciable range in size (Fuchs, 1978). Hence the size spectrum of aerosol is best treated in terms of size distribution.

The best known and versatile distribution function is the normal distribution.

$$p(a) = \frac{1}{(2\pi)^{\frac{1}{2}}\sigma} \exp - \frac{(a - \bar{a})^2}{2\sigma^2} \qquad \text{II.86}$$

where $\bar{a}$ is the mean diameter

$$\bar{a} = \int_{-\infty}^{\infty} a\, p(a)\, da$$

and σ is the standard deviation

$$\sigma^2 = \int_{-\infty}^{\infty} (a - \bar{a})^2\, p(a) da$$

The exponential factor in equation II.86 describes a Gaussian curve and the pre exponential factor normalises the expression. Because of its symmetry, the median (value below which 50% of the population falls) and the mode are identical with the mean.

Normal distribution is not appropriate for the description of a natural phenomenon, for instance aerosol particle size distribution because naturally occuring populations are usually skewed and secondly because it admits of negative values of diameter which is a physical impossibility. The use of log normal distribution overcomes these problems since the logarithmic scale has no negative values. The function is as shown (Kerker, 1969) in equation II.87

$$p(a) = \frac{1}{(2\pi)^{\frac{1}{2}}\sigma_g a} \exp - \frac{(\ln a - \ln a_m)^2}{2\sigma_g} \qquad \text{II.87}$$

log a is normally distributed and not a. So that

$$\log a_M = \int_{-\infty}^{\infty} \ln a \; p(a) \; da \qquad \text{II.88}$$

and

$$\sigma_g^2 = \int_{-\infty}^{\infty} (\ln a - \ln a_m)^2 \; p(a) \; da \qquad \text{II.89}$$

Fig. II.19 shows four frequency curves for a log normal distribution, having the same value of median diameter but different values of σ_g (geometrical standard deviation). For sufficiently small values of σ_g ($\sigma_g < 0.14$) there is so little skewness that the frequency curve approximates to normal distribution. The skewness increases with logarithmic standard deviation and also the modal diameter moves towards smaller values as σ_g increases for a fixed value of median diameter.

Espenscheid et al (1964a) used another type of distribution which they call zeroth order logarithmic distribution (ZOLD) defined by a_M, the modal diameter and σ_0, the spread and skewness distribution given by the equation

$$p(a) = \frac{\exp\left[-(\ln a - \ln a_M)^2/2\sigma_0^2\right]}{(2\pi)^{\frac{1}{2}}\sigma_0 a_M \exp(\sigma_0^2/2)}$$

The ZOLD parameters are related to the geometrical mean, $\bar{a}$, and standard deviation, σ_g by the equations

$$\ln \bar{a} = \ln a_M + 1.5 \; \sigma_0^2 \qquad \text{II.90}$$

$$\sigma_g = a_M \left[\exp(4\sigma_0^2) - \exp(3\sigma_0^2)\right]^{\frac{1}{2}} \qquad \text{II.91}$$
$$\simeq a_M \sigma_0 \text{ (for a sufficiently narrow distribution)}$$

Figure II.20 shows four distribution curves of ZOLD having the same value of a_M but different spreads.

Other distributions have been described in the literature using factors special to them. Stevenson et al (1961) used a distribution fuction for determining particle size from the spectra of light scattering and turbidity. It is defined by the equation

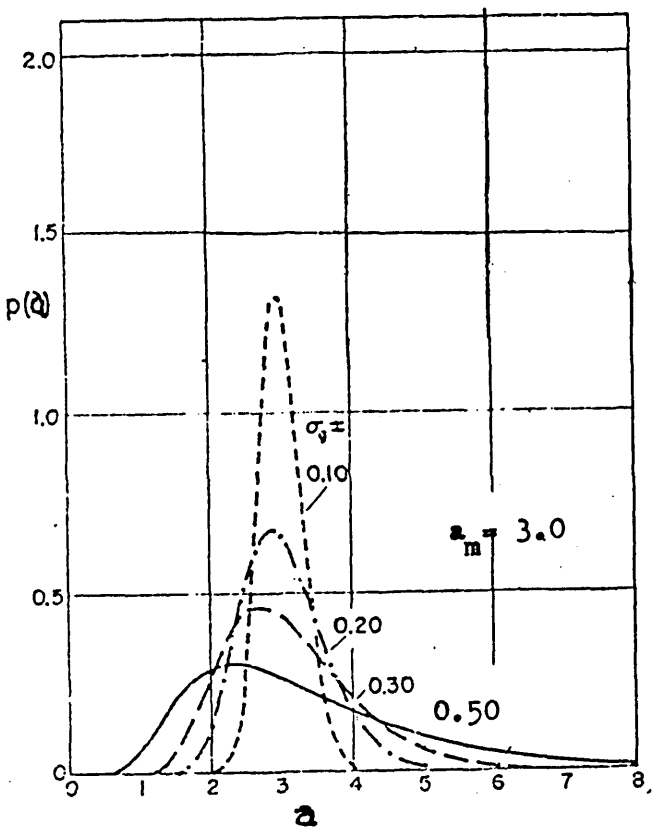


FIG.II.19:- Logarithmic normal distribution curves with median diameter = 3.0 and σ_g = 0.1, 0.2, 0.3 and 0.5 (Espenscheid et al,1964)

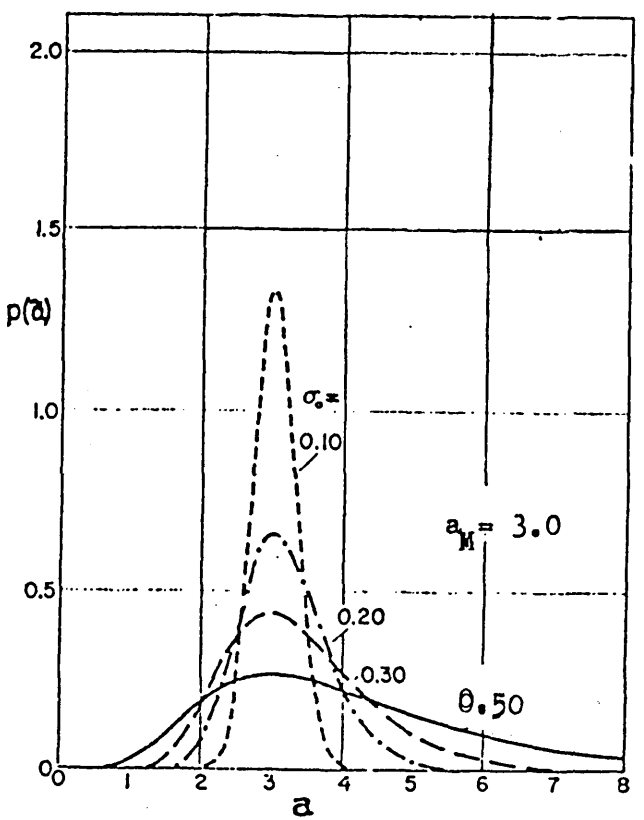


FIG.II.20:- The ZOLD distribution curves with modal diameter = 3.0 and σ_o = 0.1, 0.2,0.3 and 0.5 (Espenscheid et al,1964).

$$p(a) = c(a - a_0) \exp - [(a - a_0)/s]^3 \qquad \text{II.92}$$

where c is a normalising constant

a_0 = radius of the smallest particle present in significant concentration;

s is a factor that determines the modal diameter, half width (w) and the half spread $(a_M - a_0)$ through the relationship

$$w = 0.9015\ s$$

$$a_M - a_0 = 3^{1/3}s$$

Hilbig (1966) used a Maxwell distribution defined by

$$p(y) = \frac{2}{\Gamma[(n - 2)/2]}\ y^{n-3} \exp(-y^2) \qquad \text{II.93}$$

where $y = a/c$;

a = particle radius;

c and n are distribution parameters;

Γ is a gamma function.

Studies by Carabine et al (1971) have shown that the ZOLD is very appropriate for the study of experimental aerosols which are polydisperse and invariably unimodal. It is not suitable for the analysis of natural atmospheric aerosols which are say trimodal or artificially generated aerosols that have undergone coagulation which are bimodal. The particular advantage of ZOLD over log normal distribution is that σ_0 represents solely the spread and skewness of the distribution.

II.4.8 Optical Properties of Aerosols

The optical properties of aerosols are responsible for many spectacular atmospheric phenomena such as the colours of the sky and the back scatter of solar radiation. Degradation of visibility associated with pollution is caused by aerosols (Harrison et al, 1976). The interactions of light with aerosols can be used to measure aerosol particle size and concentration. Three of such interactions of

interest in the elucidation of aerosol properties are diffraction, extinction and scattering. Diffraction and extinction will be mentioned briefly while scattering wil be treated in terms of its use in determining particle size distribution.

When a beam of light is passed through a column of aerosol particles, some of the light is scattered and some absorbed thereby diminishing the intensity of the beam. This phenomenon is extinction and deals only with attenuation of light along an axis. It is commonly (in certain ranges of values) given by Beer-Lambert's relation

$$I = I_0 e^{-\varepsilon L} \qquad \text{II.94}$$

where I_0 and I are the incident and transmitted light intensities respectively, L is the path length of the light beam through the aerosol and ε is the extinction coefficient of the aerosol and is the fractional loss in intensity per unit pathlength associated with elemental thickness dL. The extinction coefficient is a function of light wavelength λ for particle diameter below 2 μm (Bayvel et al, 1982) and is related to the number distribution function f(a) by

$$\varepsilon = N \int_0^\infty Q_{ext} \alpha a \lambda \, f(a) \, da \qquad \text{II.95}$$

where f(a) = number size distribution function = $1/N \frac{dN}{da}$

N = particle number concentration (dm^{-3})

$\alpha = \frac{2\pi a}{\lambda}$ = size parameter

The extinction efficiency is a function of size parameter and the refractive indeces of the particle and suspending medium. Equation II.95 has the general form of

$$F(\lambda) = \int_0^\infty Q_{ext}(\alpha) \, g(a) \, da \qquad \text{II.96}$$

where

$$F(\lambda) = \frac{\varepsilon(\lambda)}{2\pi N} \qquad \text{II.97}$$

$$g(a) = a^2 f(a) \qquad \text{II.98}$$

From these, the size distribution function f(a) is calculated.

Diffraction:

Bayvel et al (1981) described a technique for particle sizing based on Fraunhofer diffraction pattern measurements valid for particles from 4 μm upwards. For an aerosol with a number distribution f(a),

$$I(\theta) = \frac{I_0}{\theta^2} \int_0^\infty i_1^2 (\alpha\theta)\, a^2 f(a)\, da \qquad \text{II.99}$$

where $I(\theta)$ is the scattered light intensity at a scattering angle θ close to zero (a maximum of 7°) i_1 is an intensity factor and I_0 is that of the incident light. Under this condition, $I(\theta)$ is independent of refractive index. From II.95

$$f(a) = -\frac{4\pi^2}{\lambda a^2} \int_0^\infty A(\alpha\theta)\, \phi(\theta)\, d\theta \qquad \text{II.100}$$

where

$$A(\alpha\theta) = \alpha\theta i_1(\alpha\theta)\, \gamma(\alpha\theta) \qquad \text{II.101}$$

$$\phi(\theta) = \frac{d}{d\theta} \frac{I(\theta)}{I_0} . \theta^3 \qquad \text{II.102}$$

This method is applicable only if

i. the distance between the aerosol droplets is greater than thrice the droplet radius;
ii. the optical path of the aerosol cloud is less than 0.1;
iii. the droplet size parameter is greater than 20; and
iv. the droplets are spherical.

This method of droplet size distribution analysis therefore is not suitable for the present study because of the droplet size limitation.

Scattering:

Size distribution of aerosol droplets can be deduced from the variation of intensity of scattered light with either the angle of

scattering (Carabine et al, 1971), the polarisation (Kerker, 1960) or the wavelength (Heller et al, 1963 and 1964). Apart from the light source and detection equipment, each method has its own particular equipment. For the method of varying the angle of scattering, three arrangements are possible for rapid scanning and detection. Maddock (1974) achieved this by using a stationary light source and single detector which was moved very precisely by means of a milling turntable. The alternative used by Moore (1974) entailed holding both light source and detector static and deflecting the incident beam by means of mirrors fixed at the series of angles. The third option was to use a stationery light source and seperate photomultipliers stationed at each scattering angle. This is likely to give the best result at a very great financial cost. In the variation of intensity with polarisation method used by Kerker (1960), the polarisation of the light was changed at every angle. In the work of Heller and Wallack, a tunable laser was used and retuned at each wavelength.

The scattering of visible light by particles of diameter less than 0.05 μm is described in terms of Rayleigh's theory of molecular or dipole scattering. Scattering by particles above 100μm can be readily treated in terms of geometric optics. Particles between these two limits are of interest in aerosol studies and can be treated in terms of Mie theory. Each particle is assumed to scatter light independent of its neighbours. The interaction of light and aerosol particles is treated in terms of the angular distribution of the scattered light, the pattern of which depends strongly on the refractive index and size parameter of the particulate.

The general theory of light scattering by aerosols was developed by Mie (1908). It gives a relationship between the incident light intensity and the intensity of light scattered at any angle θ, I(θ), by the particulate of given size parameter α and the refractive index m.

$$I(\theta) = \frac{\text{flux scattered per unit solid angle at an angle } \theta \text{ from the forward direction}}{\text{flux geometrically incident on the particle}} \qquad \text{II.103}$$

The resulting Mie equations are very complicated with particles of size greater than the wavelength of light.

For isotropic homogeneous sphere in the Rayleigh regime ($d < 0.05\mu m$) the following relation is obtained

$$I(\theta) = \frac{I_0 \pi^4 d^6}{8R^2\lambda^4} \left(\frac{m^2 - 1}{m^2 + 2}\right)^2 (1 + \cos^2\theta) \qquad \text{II.104}$$

where $I(\theta)$ is the total scattered intensity of unpolarised light at a distance R from the particle in the direction θ.
m = relative refractive index
From equation II.104,

$$I(\theta) \propto \frac{d^6}{\lambda^4} \qquad \text{II.105}$$

The scattered light is made up of two components as shown in Fig II.21. The radius vector to each curve in the diagram is preportional to the intensity scattered at the corresponding angle.
i. The scattered intensity that is polarised perpendicular to the scattering plane and given by

$$I_1 = \frac{I_0 \pi^4 d^6}{8R^2\lambda^4} \left(\frac{m^2 - 1}{m^2 + 2}\right)^2 \qquad \text{II.106}$$

It has same intensity at all scattering angles.
ii. The scattered intensity that is polarised parallel to the scattering plane and given by

$$I_2 = \frac{I_0 \pi^4 d^6}{8R^2\lambda^4} \left(\frac{m^2 - 1}{m^2 + 2}\right)^2 \cos^2\theta \qquad \text{II.107}$$

It has intensity equal to I_1 at scattering angles 0° and 180° but zero at 90°. This means that light scattered at 90° will be completely polarised perpendicular to the scattering plane. The pattern is symmetrical about 90°.

For particles in Mie regime ($d > 0.05\ \mu m$) Mie solution is applied. It is the complete solution to Maxwell's equation of the combined vector wave equations for the incident wave, the wave inside the particle and the scattered wave, subject to a set of boundary

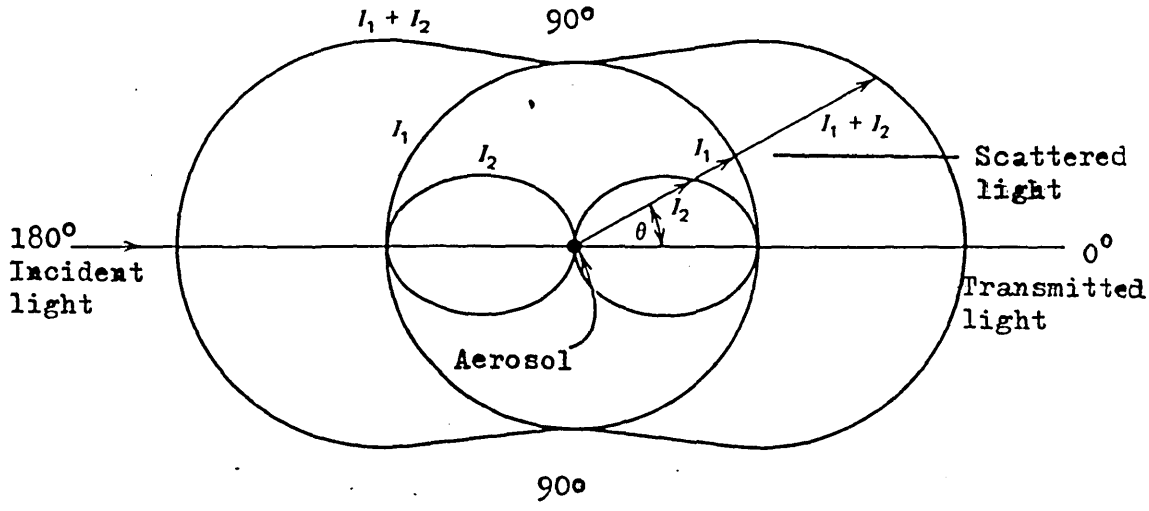


Figure II.21:-Radiation Diagram for Rayleigh Scattering (Kerker, 1969).

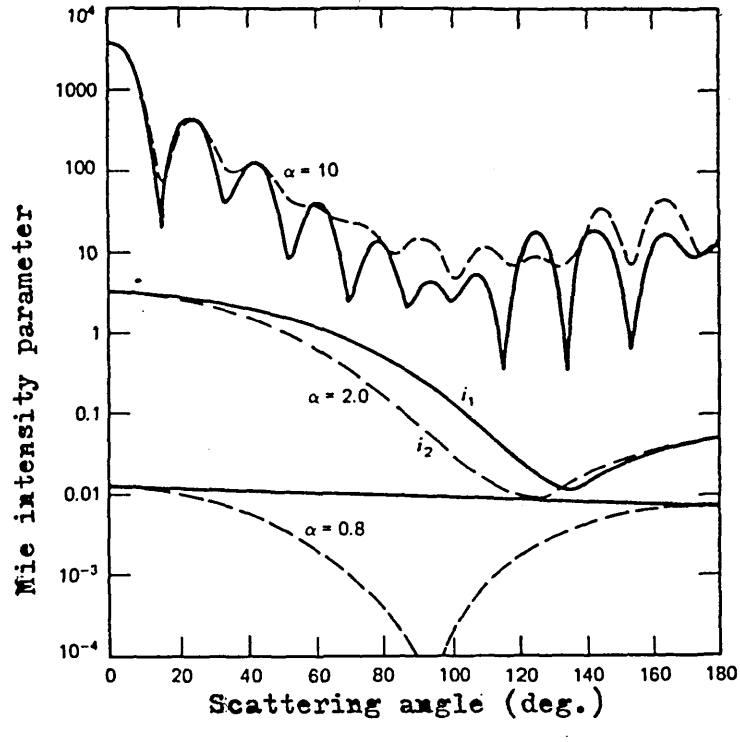


Figure II.22:-Mie Scattering Pattern for Water Droplets (Refractive index = 1.33; Size ratios = 0.8, 2.0 and 10.0). After Hinds, 1982.

conditions at the particle surface. Equation II.104 could be rewritten for a particle in the Mie regime as

$$I(\theta) = \frac{I_0\lambda^2(i_1 + i_2)}{8\pi^2R^2} \qquad \text{II.108}$$

where i_1 and i_2 are Mie intensity parameters for scattered light with perpendicular and parallel polarisations respectively. Hence for polarised light, scattered intensities are

$$I_1(\theta) = \frac{I_0\lambda^2 i_1}{4\pi^2R^2} \qquad \text{II.109}$$

and

$$I_2(\theta) = \frac{I_0\lambda^2 i_2}{4\pi^2R^2} \qquad \text{II.110}$$

for perpendicular and parallel polarisations respectively.

The intensity parameters i_1 and i_2 are functions of refractive index m, size parameter α and scattering angle θ. The relations between the three parameters are defined by a set of complicated infinite series involving Legendre polynomials and Bessel functions.

Fig. II.22 shows a plot of Mie intensity parameters i_1 and i_2 as a function of scattering angle for values of size parameter 0.8, 2.0 and 10.0; with refractive index 1.33 (a single water droplet). The diagram shows that as particle size increases, the scattering pattern becomes more and more complicated. Also as particle size increase the scattering in the forward direction becomes much stronger than at other angles. In large particles, the segment of the curve for small scattering angles below 20° consists primarily of diffracted light which is independent of the optical properties of the particle since it arises from the light passing near the particle rather than from rays undergoing reflection and refraction.

II.4.9 Particle size analysis

Particle size analysis was done to quantitatively determine the size, shape and dispersity of particles in the disperse system under

study. There are many methods of particle sizing. The choice of method depends on particle size and nature. Mention has been made at the beginning of this chapter of some of the methods that could be used in sizing particles of the size range of interest. These methods can broadly be classified as optical, mechanical, gravitational, osmotic, translational, adsorption, conductometric and such specialised methods as radiometry and pulse methods.

The oldest and the best known group of methods is optical. It ranges from microscopy (including ultramicroscopy and electron microscopy) to xray analysis and light scattering. mechanical methods include the familiar sieve analysis, the outdated ultrafiltration and its successor the gel permeation chromatography. None of these are of much use in the size range of interest. Of sedimentation methods, only ultracentrifugation method covers particle range between 1 nm and 1 μm. Centrifugation operates between 0.05 μm and 1.5 μm.

Cains (1975) and others have collected aerosol particles by means of a thermal precipitator and carried out electron microscopic analysis of their sizes. Davidson et al (1972) found that error in size determination for electron micrograph could be up to 20% too low. For $(NH_4)_2SO_4$ aerosols, electron micrography is in addition unsuitable since they are unstable in electron beam (Tu et al., 1978). They tend to vaporise with or without decomposition as they absorb energy; and so would require the cumbersome and complicated method of carrying out the operation under liquid nitrogen cooling conditions. Moore (1974) also encountered problems in electron microscopic analysis of $NH_3.SO_2$ because of partial decomposition. The most modern and one of the best methods of particle size analysis is the use of their light scattering properties. The greatest asset of this method is that analysis is done in situ which means that particle shape is not distorted by sampling. This method makes use of the principle of Mie scattering.

Kerker (1960) developed a system for sizing polydisperse aerosols which involved the measurement of the polarisation ratio of scattered intensities at nineteen scattering angles from 40° to 130° at intervals of 5°. A vast quantity of theoretical data was generated using different combinations of the values of the ZOLD parameters α_M and σ_0

and relative refractive indices m and stored in a magnetic tape. The ZOLD parameters of an aerosol could then be obtained by comparing the experimental values obtained at each of the 19 angles with the stored theoretical values. The combination of α_m and σ_0 which gave polarisation ratios that best fitted the experimental data were taken as those best describing the size distribution. This method is handicapped by its inapplicability to values of σ_0 above 0.3.

The method developed by Carabine et al (1973) utilises a direct comparison between scattered light intensities using either vertically or horizontally polarised light and those predicted by the equation

$$I_n(\theta) = \int_0^\infty p(a)\, i_n\,(\theta,\alpha)\, da \qquad \text{II.111}$$

where n = 1 or 2 for vertically or horizontally respectively polarised light, which is a general form of eqns. II.109 and II.110. The experimentally determined scattering signals are related to $I_n(\theta)$ by the equation

$$I_n(\theta) = C \sin\theta[S_\theta/S_0 - S_\theta'/S_0'] \qquad \text{II.112}$$

where C is a constant proportional to the number concentration;
$\sin\theta$ is a factor for the change in observed volume at different angles;
S_θ and S_θ' are photomultiplier signal from aerosol and the correction term for background respectively;
S_0 and S_0' are the incident beam intensities at time of measuring S_θ and S_θ'.
Light scattered from a laser source was measured at 15 angles from 15° to 165° (Moore, 1974) and the results obtained by using a least squares method to minimise the function.

$$S = \left| \frac{I_{ne}(\theta_i) - I_n(\theta_i)}{I_{ne}(\theta_i)} \right|^2 \qquad \text{II.113}$$

where n = 1 or 2 describing the polarisation of the incident radiation.
I_n is the light scattering intensity for a ZOLD distribution function

obtained from eqn II.111.

$I_{ne}(\theta_i)$ is the experimentally determined intensity of scattered light at angle θ_i.

i is the number of angles at which readings are taken.

Using horizontally polarised light yields poor results since local minima in the error function S tended to occur more frequently than in cases using vertically polarised light (Moore, 1974).

Carabine et al (1973) developed a computer programme named SEARCH which determines values of a_M and σ_0 such that the function S is minimised. Mie coefficients $i_1(\theta,\alpha)$ are determined at the fifteen angles at which measurements are taken for 1680 values of α corresponding to size range of 0.001 μm to 0.6 μm at 0.001 μm steps and 0.60-6.5 μm in steps of 0.005 μm. These values for the given refractive index are stored on magnetic tape. These values are used by SEARCH to obtain $I_1(\theta_i)$ and hence S. The flow chart of the basic operation of SEARCH is shown in Fig. II.24. The ZOLD parameters turned out by the programme SEARCH are used to compute the mass median diameter given by the equation

$$\text{MMD or VMD} = a_M \exp(2.5\sigma_0^2) \qquad \text{II.114}$$

This inversion technique has been evaluated for non absorbing particles (Polychronakis, 1978) and it was found generally that for sub-micrometer droplets, an initial choice of σ_M=0.1μm will lead more frequently to success than any other with the choice of σ_0 playing a minor role (Carabine et al, 1976).

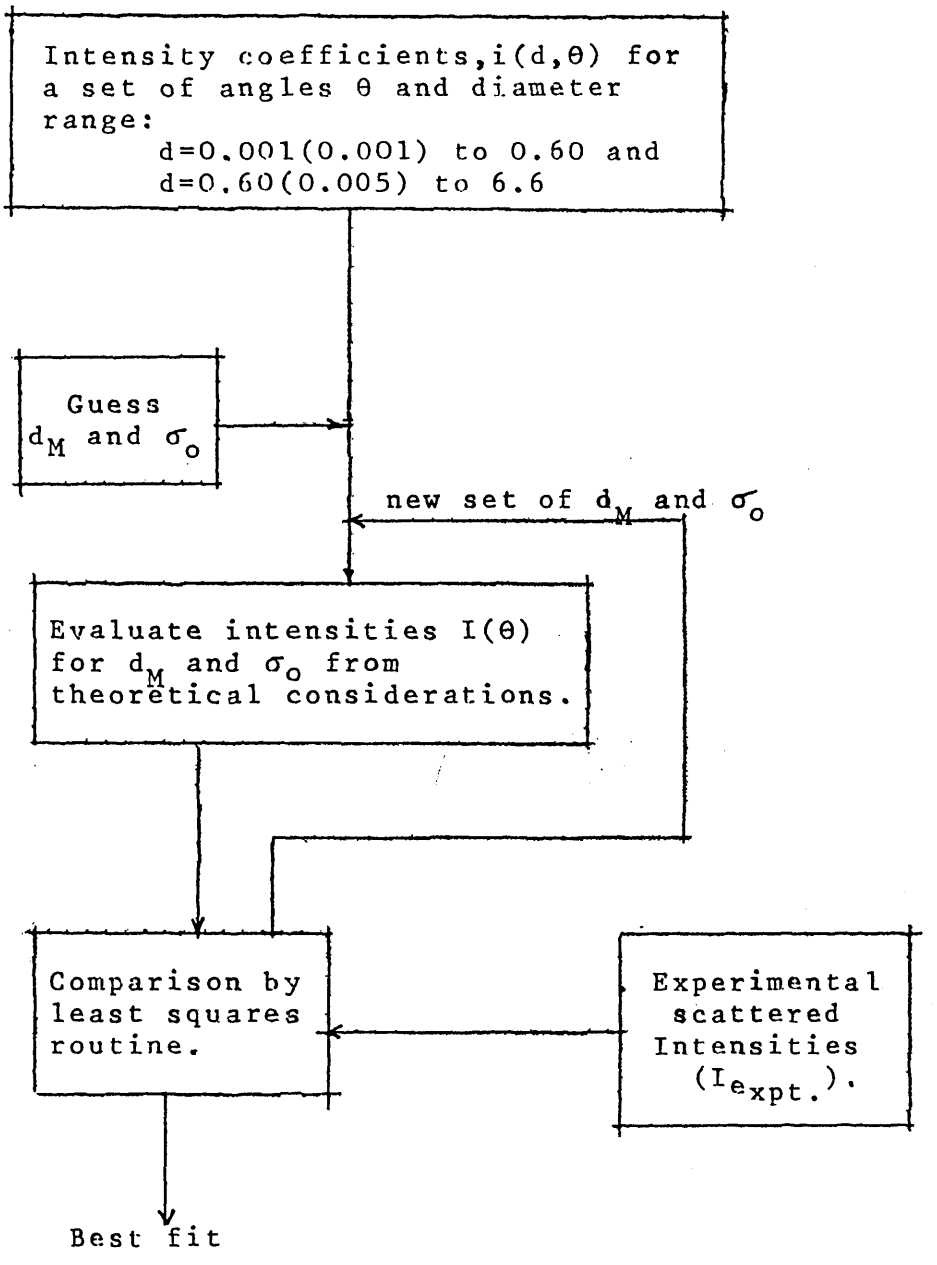


Figure II.23 :-Flowchart showing the basic operations of the programme SEARCH

CHAPTER III

Experimental Method

In this chapter, the construction and general nature of the equipment used in the study will be discussed. Preliminary experiments to optimise the equipment will be reported and steps taken to achieve reproducibility discussed. The experiments to study the behaviour of aerosols both in the reacting and non-reacting systems are reported.

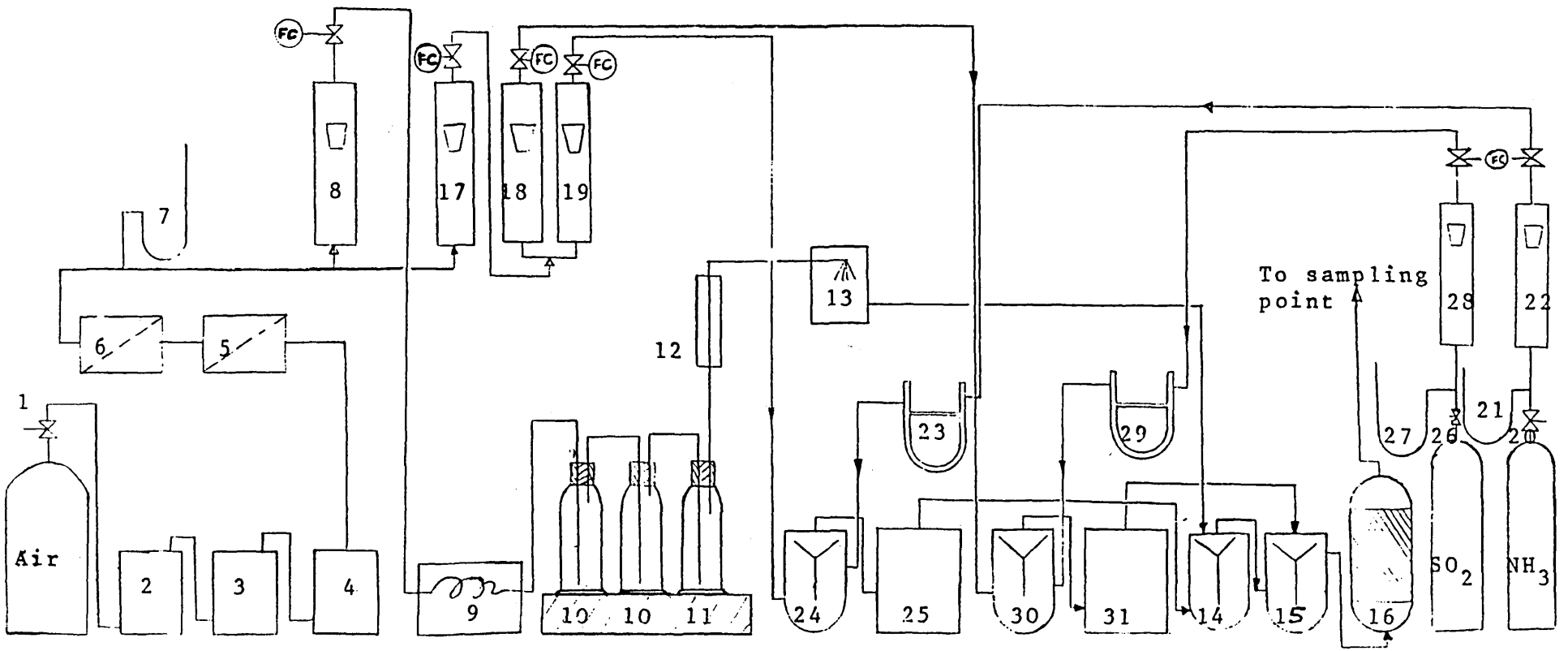
III.1 General Description

In general, aerosols were generated from a very dilute solution and made to interact with gases (oxygen, SO_2, NH_3 and water vapour) in a reactor. The product aerosol interacted with a laser beam and the scattered light was detected at scattering angles of 9° to 135° (in steps of 9°).

Fig III.1 and Plates 1 and 2 show the block diagram of the equipment used in the study. The gas system consisted of a main line carrying the air that generated the aerosol and two side lines carrying the reactant (SO_2 and NH_3) gases. The reactant gas system will be treated later.

III.1.1 The Air Supply System:

The air supply was from a size 165 compressed gas cylinder supplied by BOC. It was ordinary atmospheric air. The pressure in the main gas line was monitored by means of a Budenburg low pressure (10 psig maximum) gauge situated between the air cylinder and the scrubber unit, and a mercury open tube manometer situated between the filter unit and the main gas line rotameter (see below).



1 Two-stage Regulator (Air)
2 Scrubber (1mM-NaOH solution)
3 Scrubber (1mM-H_2SO_4 solution)
4 Scrubber (distilled water)
5 Coarse Filter
6 Fine Filter
7, 21, 27 Open-Tube Mercury Manometer
8 Metric 7p Rotameter
9 Water Bath
10 Humidifier
11 Thermally insulated empty vessel
12 Heating Coil
13 Aerosol Generator
14 Mixer (Mx3)
15 Mixer (Mx4)
16 Reactor
17, 18, 19 Size E3 Rotameter
20, 26 Corrosion Resistant Special Gas Regulator
22 Size RS Rotameter
23, 29 Carpillary Manometer
24 Mixer (Mx1)
25, 31 Holding Vessels
28 Size B Meterate Rotameter
30 Mixer (Mx2)

Figure III.1: -Block diagram showing the main components of the equipment.

The Scrubber Unit :

This consisted of three cylindrical glass vessels of 500 cm^3 capacity joined together in series. The first vessel contained NaOH which removed CO_2 (and any other acid impurities) from the air stream. The second vessel contained 0.1 M - H_2SO_4 which removed NaOH droplets and any other basic impurities from the air stream. The third vessel contained organic matter-free distilled water which washed out any acid droplet which the air stream might have picked up from the previous vessel. The scrubbing liquids were replaced with fresh ones at regular intervals.

The Filter Unit :

The unit was used in treating washed air from the scrubber and consisted of two types of filters in series. The coarse filter consisted of a stainless steel cylinder (Fig.III.2) of volume 1.09 litres loosely packed with glass wool. Its function was to remove any droplets which the air stream might have picked up from the scrubber. The fine filter consisted of a 9.0 cm diameter Whatman paper carried by a 9 cm stainless steel in-line filter holder supplied by Millipore. The filter holder had a filter area of about 45.5 cm^2 and a maximum inlet pressure of 19 kg cm^{-2} with pre-set relief valve. A Millipore filter type VMWP of pore size 0.05 μM was originally planned to be used, but was dropped because of the high back-pressure it exerted. The function of the fine filter was to remove finally any particles or droplets contained in the air stream.

Humidification:

The purified air was passed through a two-way high pressure glass tap to the side line and to the humidifier. The air to the humidifier was metred through a model metric 7p rotameter supplied by Rotameter Manufacturing Co. Ltd. with an aluminium float. The humidifier consisted of a thermostated water bath (supplied by Techne Cambridge Ltd.) and three bubblers of distilled water sealed together in series. The water bath was maintained at a temperature of 45°C and into it was immersed 150 cm of the ¼-inch glass tube coil carrying the purified air

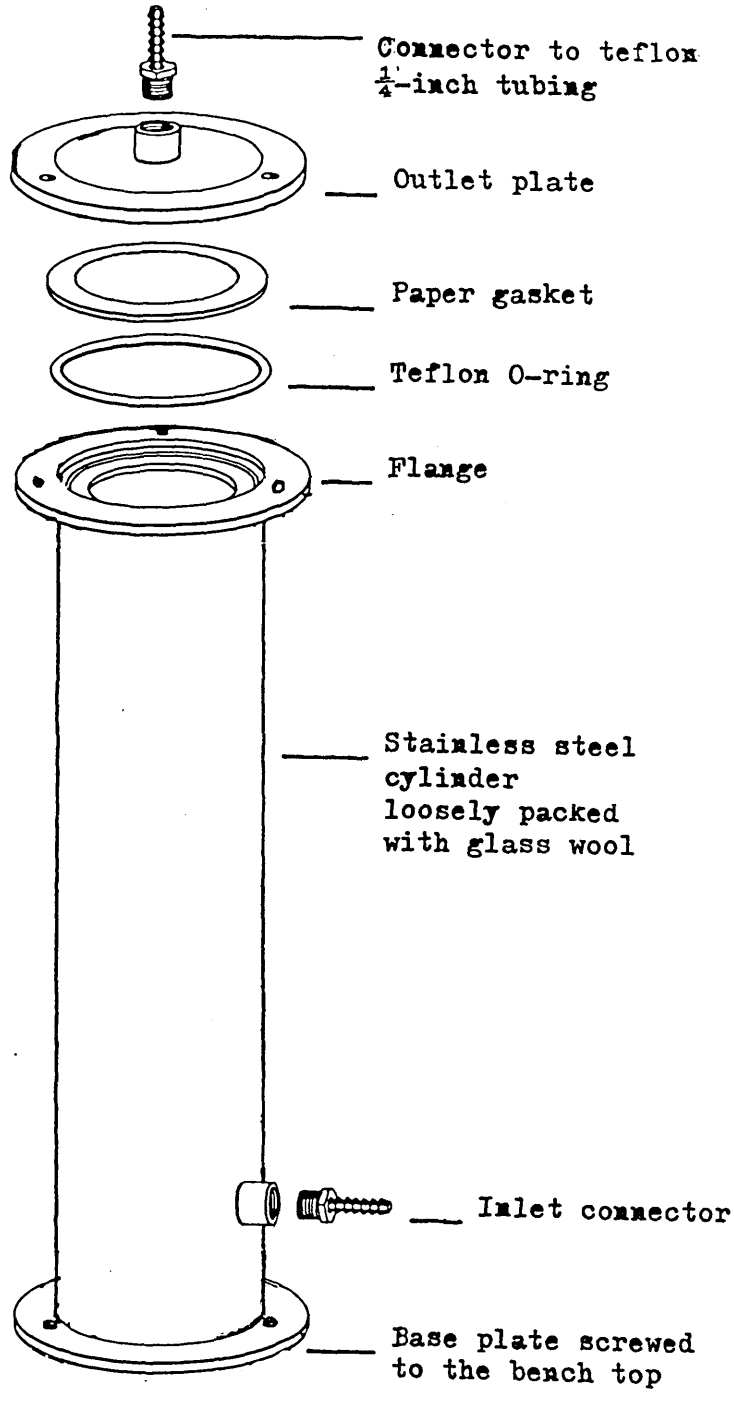


FIG.III.2:-Stainless steel coarse filter holder.

from the filter unit. This heated the air and thereby raised its capacity for water vapour prior to humidification

Cains (1975) used master solution in the humidifier to ensure that any droplet that might have come from the humidifier was of $MnSO_4$ solution. However, considering that the surface of an aqueous solution is a better sink for water vapour than pure distilled water, there was a probability that the atomising air might have left the humidifier less humid than it entered. In this work, to ensure that no liquid water passed from the humidifier into the generator and to prevent condensation in the tube that carried the humidified air into the aerosol generator, the tube was heated with a low power (140 W) heating coil. By using air at high humidity for atomisation, it was hoped that the increase in the master solution concentration in the generator during atomisation would be retarded.

III.1.2 The Aerosol Generator

The aerosol generator used in the study was the one used by Maddock (1974) and Cains (1975) and worked on the principle of air blast atomisation and liquid barrier filter. The aim of the barrier filter was to decrease the dispersity of the aerosol. The construction of the generator is shown in Fig.III.3. It had a height and a base diameter of 17 cm and 9 cm respectively. The first barrier was a glass plate which formed the distal end of the generator glass stopper, and was situated about 1.2 cm in front of the jet through which the droplet cloud was issuing. The aerosol left the generator through an intermediate glass tube of length 25 cm and diameter 1.5 cm. The topmost 4 cm length of the tube was perforated with 0.2 cm diameter holes with centre-to-centre spacing of 0.6 cm. The top was sealed with a cylindrical glass cup of diameter 2.5 cm and height 5 cm so that its base terminated the tube and its wall formed a concentric jacket around the perforated part of the tube, with its rim being about 0.8 cm below the perforated part of the tube. The base of the cup formed an impactor which forced the aerosol to change direction and exit through the holes. The aerosols issuing from the holes impinged on the wall of the cup and so changed direction sharply again and exit the gap between the rim of the cup and the tube. This constituted the third impactor. After leaving these impaction surfaces the aerosols flowed into a

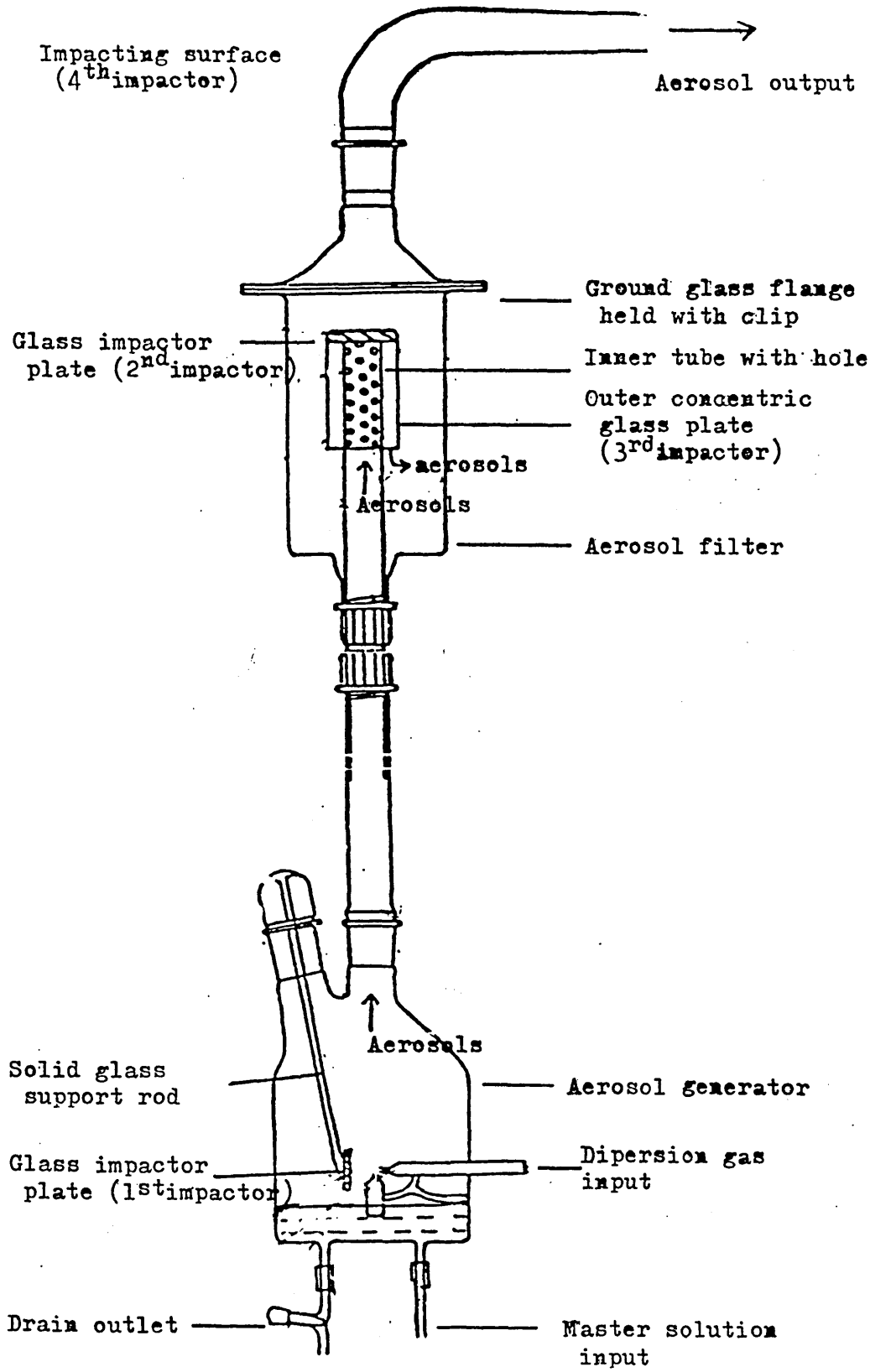


FIG.III.3.-The Construction of the Aerosol Generator

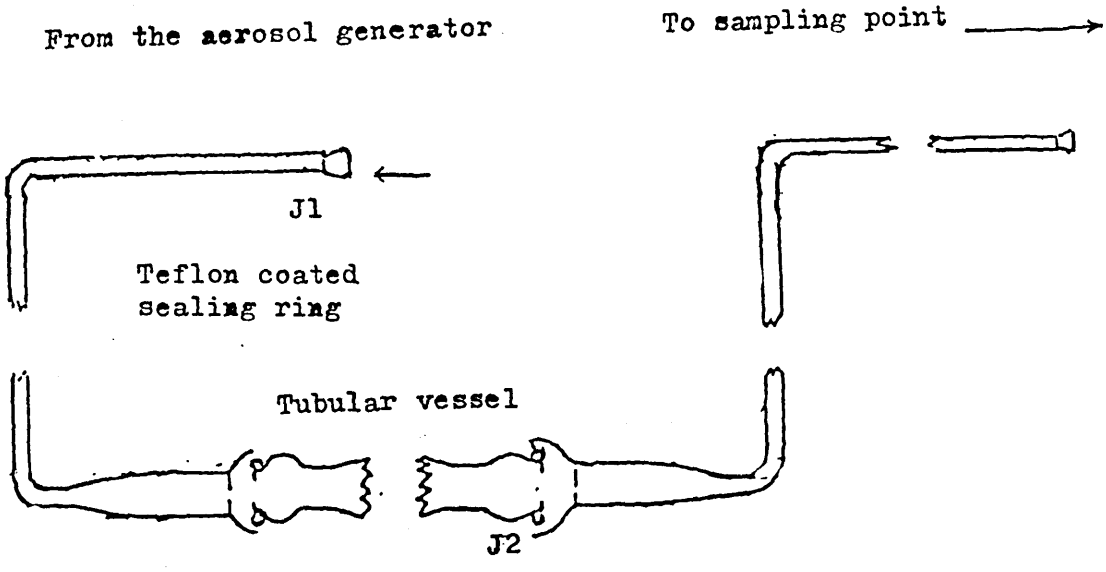
chamber of diameter and height 8.7 and 19 cm respectively. The chamber was made in two pieces joined by a flanged attachment which facilitated dismantling and cleaning.

After emerging from the filtering chamber, the aerosols flowed through a large diameter tube which had two right-angle bends. The tube was lagged with insulating materials to prevent condensation on the walls as a result of temperature fluctuations. From this tube, the aerosols flowed into a mixer (Mixer 3 in Fig III.1) which also received NH_3/air mixture from a side line. The volume of the mixer was 40 cm^3; assuming a flow rate of 4 litres per minute, the residence time was 0.6 seconds. The mixture of aerosol and NH_3 flowed into another mixer (Mixer 4 in Fig III.1) which also received SO_2/air mixture from another side line. The mixture of aerosol, NH_3 and SO_2 flowed from Mixer 4 into the reactor. Two sizes of tubes were used in carrying the aerosols from Mixer 4 to the reactor (Fig III.5b and 5c).

The Reactor

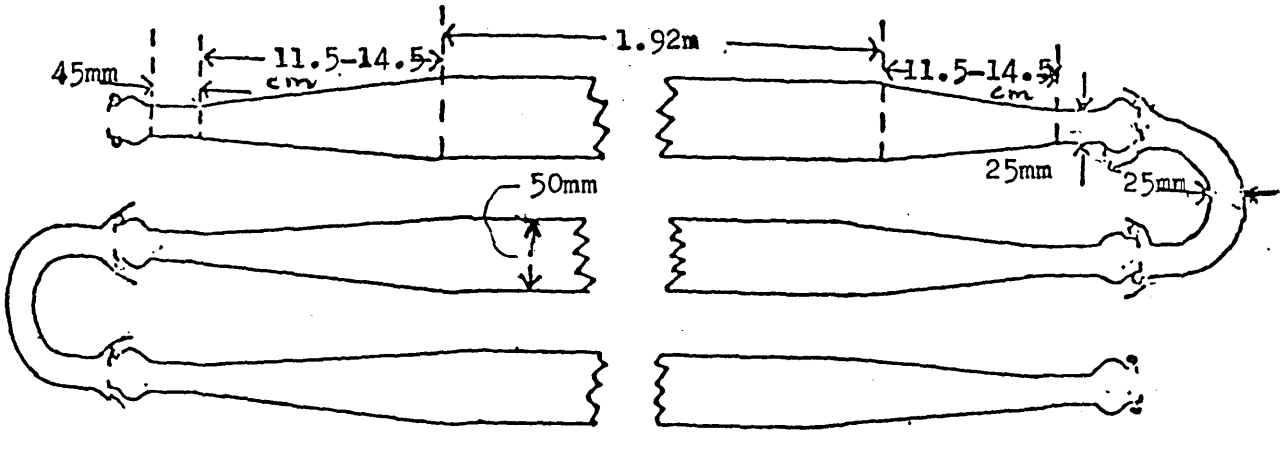
The reactor was a series of cylindrical tubes connected by Rotulex ball and cup joints. The joints were made air tight by the use of teflon-coated buna rubber sealing rings. Because of space constraints, the cylindrical tubes were joined together by means of U-tubes (Fig III.5a) to give a structure like a chain of S joined end-to-end. The U-tubes carried the cup end of the size 41/25 Rolutex joint while the cylindrical tubes carried the ball ends. This ensured flexible and leakage-free connections. Each cylindrical tube had a length of 1.9 metre; twenty-five of them had an internal diameter of 5 cm and a volume of 3.923 litres each. The small tube designated S-tube had an internal diameter and volume of 4 cm and 2.272 litres respectively. The tubes were mounted in wooden matrices (Fig. III.6).

Aerosol residence times corresponding to the following combinations of tubes were used throughout the study - S, 1, 5, 9, 13, 17, 21 and 25 tubes. The connections needed to achieve each of these combinations and at the same time ensured that the aerosols exit the reactor through the same hole position irrespective of the number of the tubes in the combination is shown in Fig III.6. The residence time and volume corresponding to each of these reactor tube combinations for



J1. 14/18 socket
J2. Ball & cup Rotulex 41/25 joint

FIG.III.4:-The Reactor and the connecting Tubes —
The general layout.



FigureIII.5:-
(a) The cylindrical and U-tubes of the reactor.

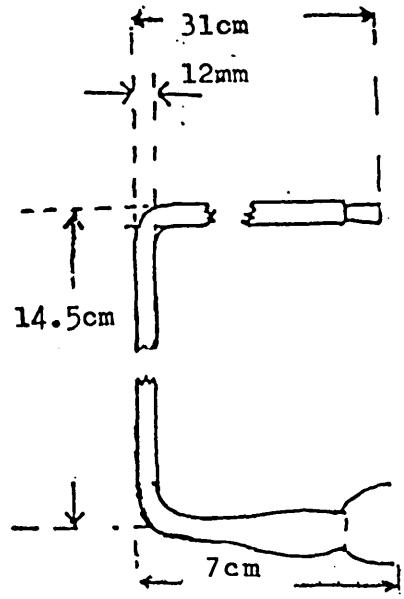


Figure III.5b:-

The tube which carries aerosols from the generator to the reactor tube in the first tube position.

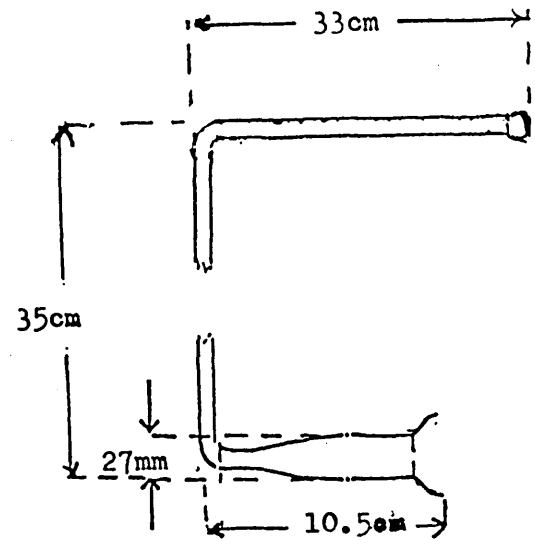


Figure III.5c:-

The tube which carries aerosols from the generator to the reactor tube in the third tube position.

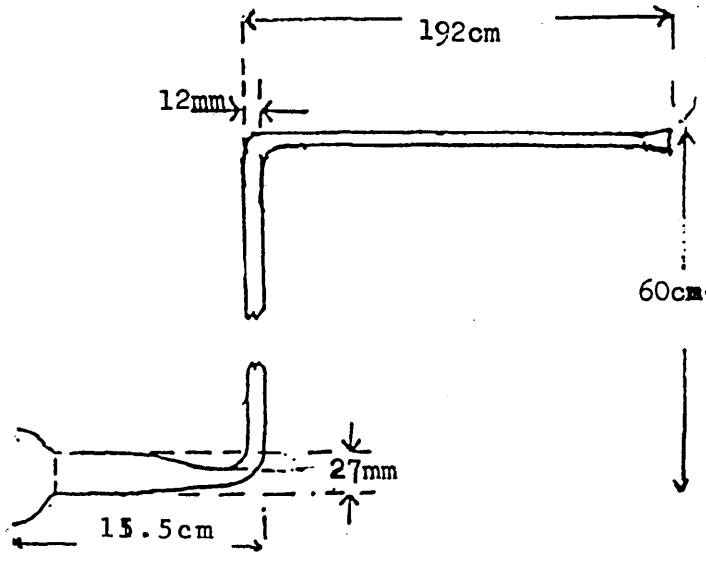
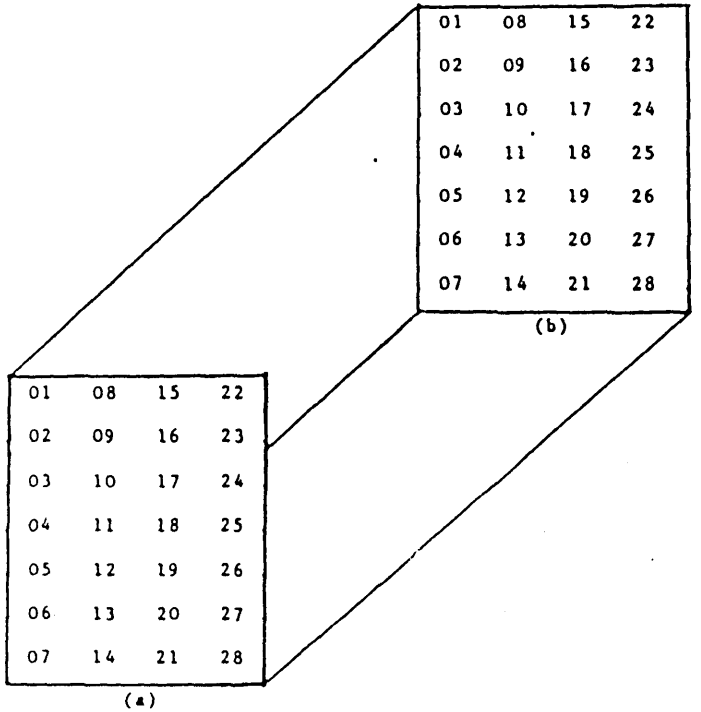


Figure III.5d:-

The tube which carries aerosols from the reactor to the light scattering sampling cell.



(a) Hole positions in the leading matrix
(b) Hole positions in the rear matrix

Mx → From the aerosol generator
LS → To the sampling point
→ U-Tube connection in the leading matrix
--- U-Tube connection in the rear matrix
... U-Tube connection in the wooden matrices
01 to 28 Hole positions in the wooden matrices carrying the cylindrical tubular reactor

S-Tube:-

Mx → 01 LS →

1-Tube:-

Mx → 01 LS →

5-Tubes:-

Mx → 03 ... 10 --- 08 ... 01 LS →

9-Tubes:-

Mx → 03 ...04 --- 05 ... 12 --- 11 ... 10 --- 09 ... 08 --- 01 LS →

13-Tubes:-

Mx → 03 ... 04 --- 05 ... 06 --- 07 ... 14 --- 13 ... 12 --- 11 ... 10
↓
LS ← 01 --- 08 ... 09

17-Tubes:-

Mx → 03 ... 04 --- 05 ... 06 --- 07 ... 14 --- 21 ... 28 --- 27 ... 20
↓
LS ← 01 --- 08 ... 09 --- 10 ... 11 --- 12 ... 13

21-Tubes:-

Mx → 03 ... 04 --- 05 ... 06 --- 07 ... 14 --- 21 ... 28 --- 27 ... 20
↓
08 ... 09 --- 10 ... 11 --- 18 ... 25 --- 26 ... 19 --- 12 ... 13
↓
01 LS →

25-Tubes:-

Mx → 03 ... 04 --- 05 ... 06 --- 07 ... 14 --- 21 ... 28 --- 27 ... 20
↓
24 ... 17 --- 10 ... 11 --- 18 ... 25 --- 26 ... 19 --- 12 ... 13
↓
23 ... 16 --- 09 ... 08 --- 01 LS →

Figure III.6:-Schematic diagram showing the combinations of the reactor tubes.

the most commonly used flow rate of 4 l min^{-1} are shown in Table III.14. The residence times were the same in both the light scattering analysis and the droplet sampling experiments.

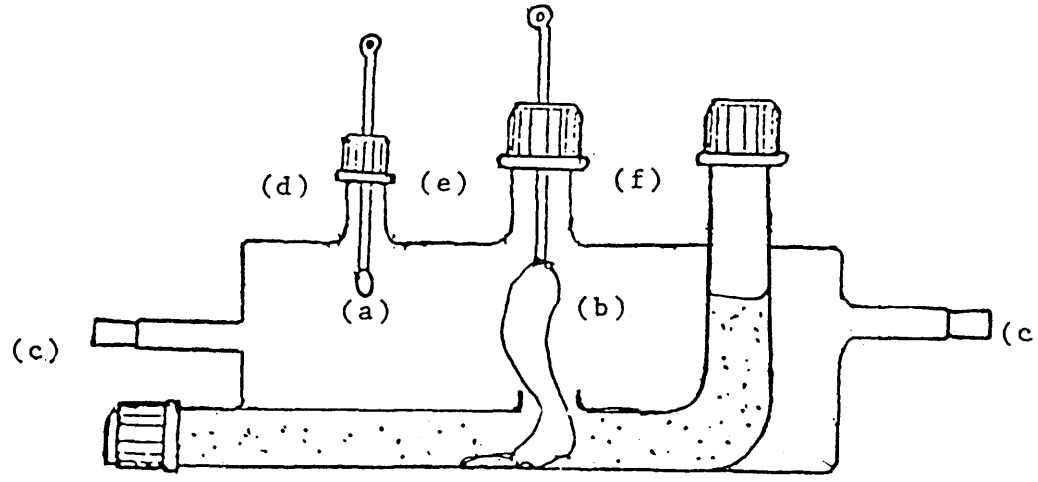
The relative humidity of the reactor was monitored by means of a Mason's Hygrometer supplied by Brannan Thermometers. It was enclosed in the vessel shown in Fig III.7. The hygrometer housing was meant to be used in-line for continuous monitoring. However, in order not to alter the aerosol characteristics it was not so used but was connected to the aerosol stream only when RH readings were needed. It took about 30 minutes to equilibriate.

The reactor was enclosed in a fibre-board box maintained at a constant temperature of 25°C by means of a heater and fan system controlled by a Thorn Automation thermostat. The thermostat was heated by four 150 watt electric bulbs in experiments that did not involve chemical reaction; and by a 2 kw heater for experiments involving SO_2 oxidation. This switch to heater was done so as to avoid possible complications from light initiated reactions. The temperature was monitored at four positions in the thermostat so chosen as to take note of possible horizontal and vertical temperature variations within the box. Aerosols from the reactor were conveyed to the sampling point for light scattering or chemical analysis by a z-shaped tube of internal diameter 3.0 cm. (Fig. III.5d).

III.1.3 The Light Scattering Unit

This was made up of the light scattering cell, photomultimplier, laser light source and the aerosol exhaust fittings.

The light scattering cell, like the one used by Maddock (1974) was constructed in two parts (Fig. III.8). The upper portion was made of two concentric glass tubes of internal diameters 1 cm and 3 cm respectively. The inner tube was a continuation of a 14/23 socket into which the cone of the z-tube from the reactor fitted. The lower portion was made of two concentric stainless steel tubes of the same diameters. The inner and outer tubes led to the exhaust treatment unit. The outer tube was welded to a brass support rod mounted on a one-metre long triangular optical bench (Plate 3). The upper portion



(a) Dry bulb thermometer.
(b) Wet bulb thermometer.
(c) 10/49 socket.
(d) Quickfit SQ18 screw-cap joint.
(e) and (f) Quickfit SQ28 screw-cap joint.

Figure III.7:-The wet and dry bulb hygrometer and its housing.

was fixed by means of a clamp and when in position there was a gap of 0.8 cm seperating the upper and the lower portions such that the laser beam intersected the gap at a position slightly nearer the upper tube. Aerosols passing this gap were contained by a sheath of nitrogen drawn though the cell annulus by suction from the upper to the lower portion, and was metred at 2.5 l min^{-1}.

Exhaust System

The effluent aerosol from the light scattering unit was pumped through a filter and ballast tank to ensure that much of its droplet content was removed before the aerosol was disposed of to the roof vent (Fig. III.9). The filter used was a 47 mm diameter microfibre glass depth filter supplied by Millipore. The ballasting tank was a 10-litre thick-walled steel tank carrying a combined pressure and vacuum guage.

The flow-rate of the exhaust gas was monitored by means of a rotameter situated downstream of the ballasting tank. It was found empirically that a flow-rate of at least the sum of the flow-rate of the aerosol and that of the nitrogen was necessary to ensure steady result. In this study, an exhaust flow rate of 9 l min^{-1} was used. This flow rate was strictly maintained in all the runs. The exhaust pump used was a type RBF Vacuum Ltd and was operated at 3000 RPM in vacuum mode.

The Laser Beam

The laser was a model 124A Spectra Physics 15mW He-Ne continuous wave laser source of 0.6328 μm wave-length, linearly polarised to better than 1 part in 1000. It was mounted on a 1.5 m long optical bench with its light exit 2.25 m from the aerosol light scattering cell. The power supply was a Model 255 DC Exciter. The beam diameter as it emerged from the laser was 1.1 mm measured at $1/e^2$ point and the divergence was 1.0 milliradian. The source was provided with a half-wave plate to facilitate the choice of beam polarisation. The vertical polarisation was used throughout the experiment. The beam was collimated and expanded to a diameter of about 4 mm by means of two

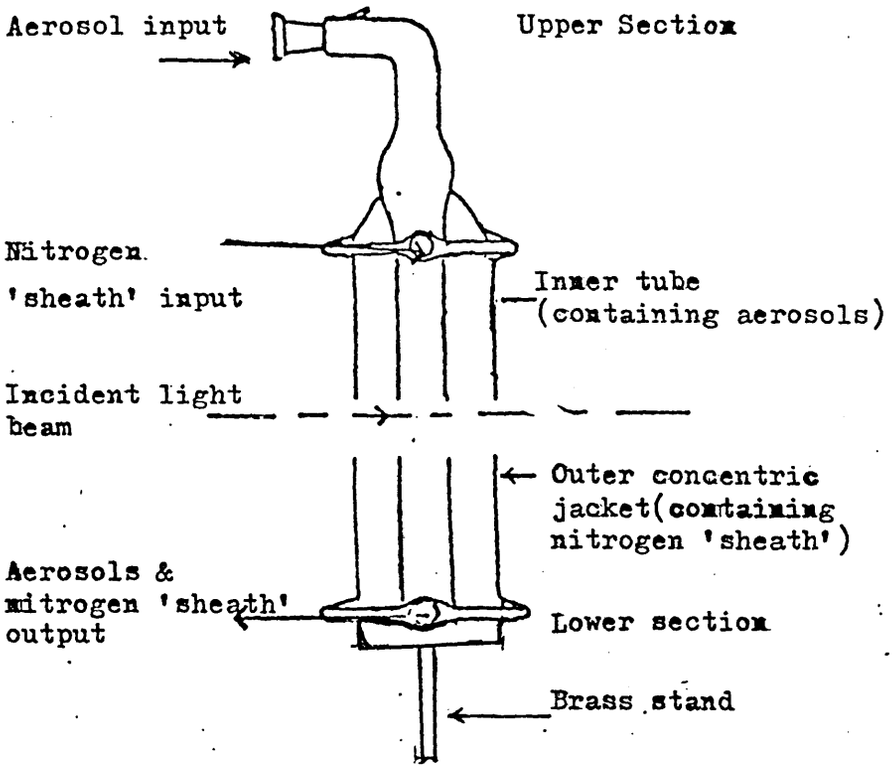


FIG.III.8:-The Aerosol Light Scattering Sampling Apparatus

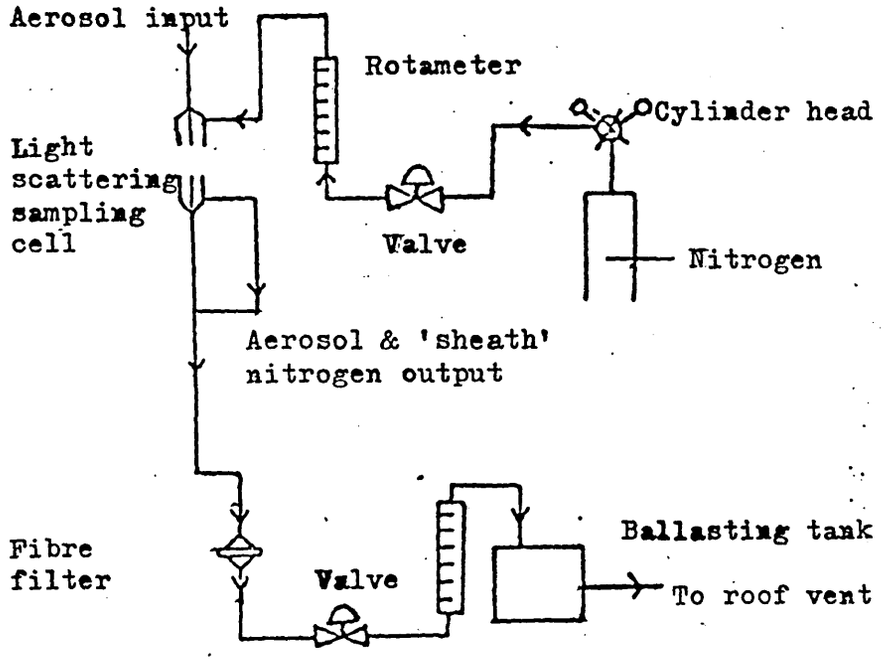


FIG.III.9 :-The Flow Diagram of Light Scattering Cell and the Exhaust System.

microscope objectives with a 10 μm pin hole located at the common focus of the two lenses (Fig III.10). For safety, the beam was passed through a paper tube of 7.3 cm diameter with the inner wall blackened (Plate 4). After traversing the sampling cell, the laser beam was intercepted by a Rayleigh Horn which was virtually a total light absorber (Plate 3 and Fig. 11). This prevented the beam from reflecting back into the sampling area and complicating the scattering pattern.

The Photomultiplier

The photomultiplier used was an EMI Type 9658 with modified S20 Cathode with a dark current of 10^{-16} amp/cm^2 and having a quantum efficiency of about 10% at the He-Ne wavelength. It was enclosed in a special light-proof metal housing which incorporated a collecting telescope which was hooded with a monochromatic Type DL85 close tolerance filter for .6328 μm supplied by Barr and Stroud Ltd. (Fig. III.12). The telecoscope received scattered laser beam and directed it onto the photosensitive area of the photomultiplier. It was operated at a high DC voltage typically between 0.9 and 1.2 KV, and the output signal integrated at 60 Hz by a digital voltmeter and typed out on a type-writer.

The photomultiplier in its housing was mounted on the aforementioned triangular optical bench so that the photomultiplier was 40 cm from the centre of the aerosol. This distance was maintained constant throughout the study. The optical bench was screwed to a 28cm diameter high precision milling turn-table supplied by Elliot Machine Tool Co. Ltd. (Plate 3). This arrangement made it possible to rotate the photomultiplier around the light scattering cell through 360°. In practice, however, only scattering angles between 9° and 135° in steps of 9° were utilised, and rotation was done manually. During data receiving no light was allowed in the room. However, if the source of the unwanted light were constant, it could be averaged out as background.

The light scattering unit was mounted on a rigid steel frame provided with shock-resistant rubber-padded height-adjustable feet.

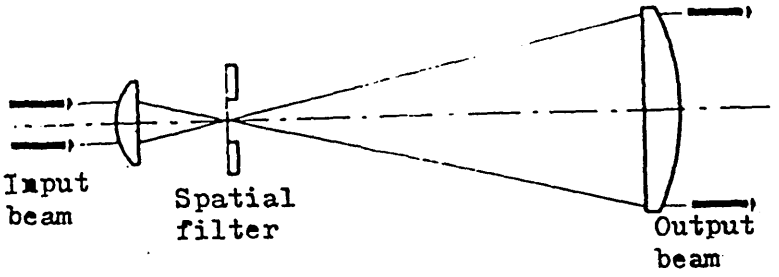


FIG.III.10:-Laser Beam Collimating and Expansion System.

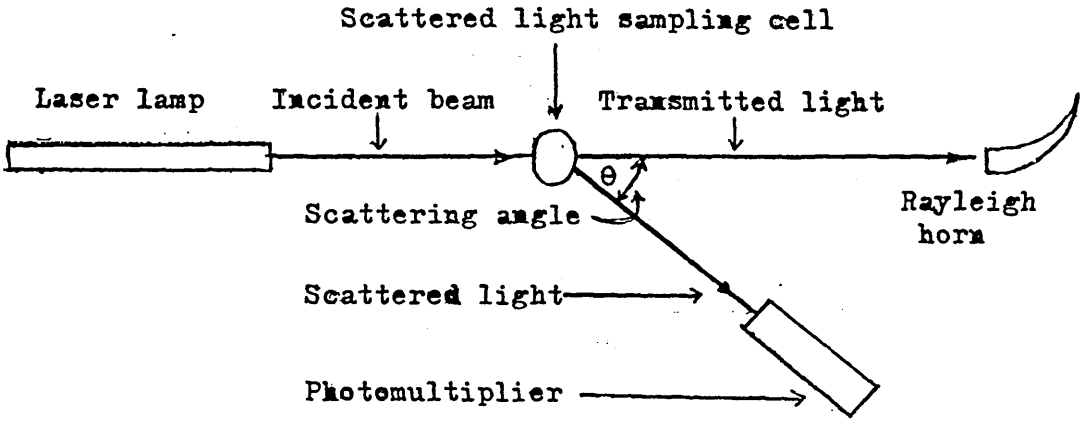


FIG.III.11:-The General Arrangement of Light Scattering Detection Unit.

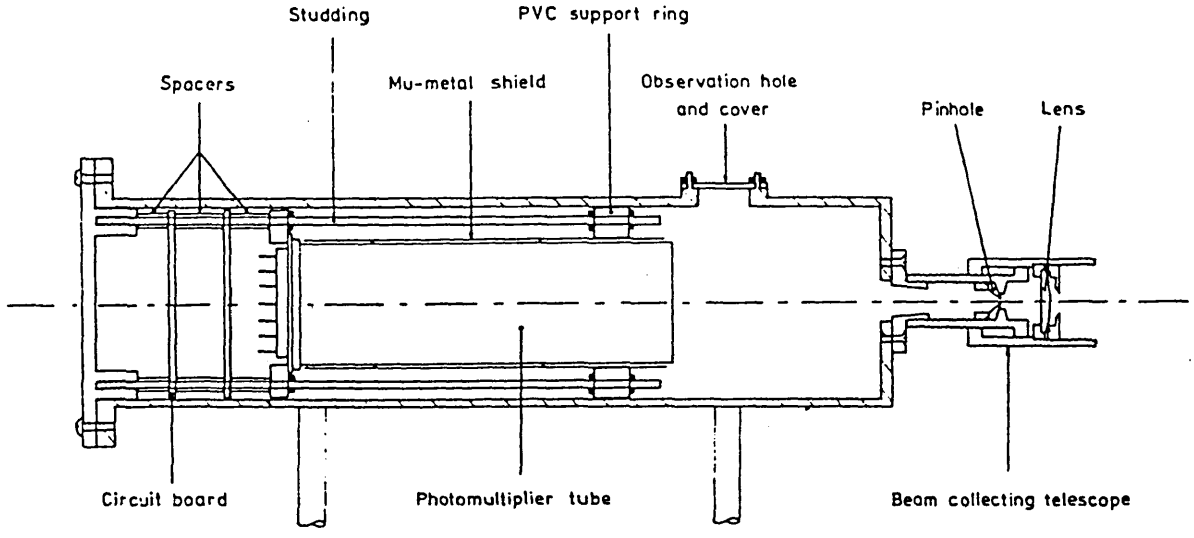


FIG.III.12:-The Photomultiplier and its Housing.

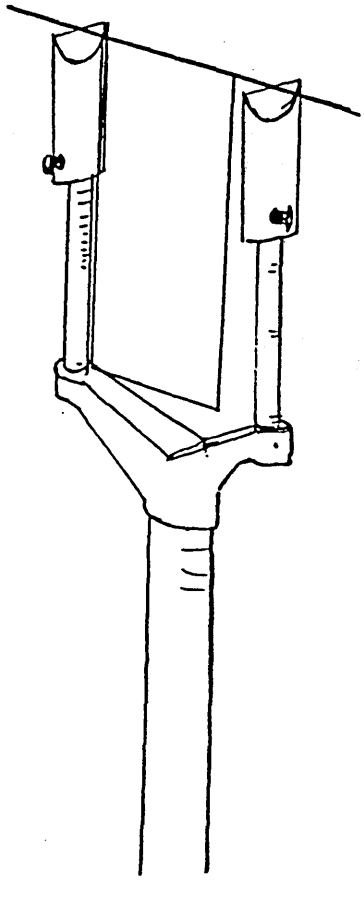


FIG.III.13:-Suspended Glass Slide for Standadising Laser Light Intensity.

The frame was 4.34 m long and 0.35 m wide at the top, broadening to 0.9 m at the base to make for stability. Optical alignment was achieved by ensuring linearity between the laser beam exit and the sampling cell and the centre of the collecting telescope of the photomultiplier. The positions of the sampling cell and the photomultiplier were located by means of brass pins.

Data Acquisition

The light intensity proportional to the voltage output of the photomultiplier was measured by a digital voltmeter which sent its output through a type writer drive unit to a typewriter (Plate 4). The digital voltmeter was a Type DM2010 instrument supplied by Digital Measurements Ltd., and could measure down to 10 μV DC. It was triggered externally by pulses from the type-writer drive unit. It was operated in the automatic mode. The type-writer used was an IBM type 11f type-writer and was set to take, say, six readings at each scattering angle.

III.2 Optimisation of the Equipment

In this section, experiments to study the characteristics of the equipment are reported. These include the operation of the laser and the photomultiplier and the efficiency of the filters used in the study.

Laser Intensity Fluctuation

The stability of the laser intensity and how it varies with time was determined by means of a microscope slide suspended in a lens holder located between the light scattering cell and the Rayleigh Horn and tilted in such a way that it reflected a part of the laser beam into the collecting telescope of the photomultiplier (Fig III.13). The readings taken for five hours at ten minutes intervals are listed in Table III.1. The overall mean is .52 and the standard deviation is .02 and the coefficient of variation of 0.04. This shows stability to an acceptable degree. If the readings were split into five parts corresponding to each hourly reading standard deviation for each hour listed in the table shows that the laser became stable after two hours and remained so for the remaining three hours. This test of intensity fluctuation was repeated from time to time in the course of the study.

Noise-to-Signal Ratio:

An important factor in the measurement of the intensity of scattered light is the presence of spurious signal. The potential origin are the laser, the photomultiplier, the aerosol and the data acquisition system. In the absence of any signal from the photomultiplier, the digital voltmeter used in this study showed a signal averaged over 210 readings of 0.07 mV. Any signal below 0.1 mV is likely to be due to digital voltmeter noise and so this effect could be easily removed by ignoring signals in this range. Cains (1978) determined the noise-to-signal ratio for the laser and found it to be of the order of 0.3% after laser stabilization. This therefore could be neglected. He also showed that noise due to aerosol flow was negligible except in the most foward scattering angles and attributed noise in this region to the presence of large particles which are strongly forward scattering.

Table III.1 Photomultiplier stability as a function of time

Time Interval (min)	Intensity Readings at 10 min intervals (volts)						Mean (volts)	SD	Coefficient of variation
1 - 60	.56	.52	.61	.50	.48	.44	.52	.055	.11
61-120	.55	.53	.57	.56	.52	.61	.56	.027	.05
121-180	.50	.50	.52	.53	.52	.50	.51	.013	.02
181-240	.50	.51	.51	.49	.50	.50	.50	.006	.01
241-300	.50	.49	.51	.51	.51	.51	.50	.006	.01
1-300							.52	.02	.04

The most important source of noise in the system is the photomultiplier. This was studied at a photomultiplier voltage of 1 KV. The laser and the photomultiplier were stabilized for two hours and then signals recorded at scattering angles of 9° to 135° in steps of 9° in the absence of aerosol. The photomultiplier noise was obtained by completely excluding any source of light to the photomultiplier and recording the voltmeter readings at fifteen scattering angles and the mean obtained. The readings are listed in Table III.2. The above operation was repeated in the presence of aerosols and the readings listed in Table III.3. From Table III.2 it will be seen that this background (in the absence of aerosol) signal has a large noise contribution, up to 50% in the central region of the light scattering angles. On the other hand, Table III.3 shows low values of noise-to-signal ratio in the presence of aerosol which scarcely exceeds 5% in the central region. In both cases the noise-to-signal ratio is highest in the middle region (around 63° scattering angle) and diminishes progressively towards the more acute and obtuse scattering angles. Its non-uniformity is as a result of higher signal intensities in the most foward and most backward scattering angles than in the middle ones.

(a) Photomultiplier Operating Voltage

Experiments were carried out to test whether results of particle size analysis obtained using two voltages .9 KV and 1.2 KV are significantly different. Aerosols were generated from a 0.1 M $(NH_4)_2SO_4$ master solution and light scattering data obtained for residence times ranging from 0.65 minutes to 25.2 minutes. The ZOLD parameters obtained from inverting the angular distribution of the intensity of scattered light are shown in table III.4. The mass mean diameter (MMD) obtained from these and the sum of the intensities of scattered light are tabulated in Table III.5.

Two-tailed t-tests were done on the two sets of modal diameters, VMD and sum of intensity of scattered light and the values of t_o are shown in Table III.4 and III.5. In the case of modal diameter, t_o is less than 1.895 at 10% level and hence, the values obtained at the two operating voltages are not significantly different. Also, in the cases of MMD and sum of intensity, the values are not significant even

Table III.2 Noise-to-signal ratio in the absence of aerosols

Scattering Angle	Signal (mV)	Noise (mV)	Noise-to-Signal Ratio (%)
9°	7.7	0.386	5
18	2.7	"	14
27	1.5	"	26
36	.98	"	39
45	.9	"	43
54	.87	"	44
63	.71	"	54
72	.9	"	43
81	.95	"	41
90	.91	"	42
99	.79	"	49
108	1.06	"	36
117	1.18	"	33
126	1.24	"	31
135	1.45	"	21
	Mean		35%

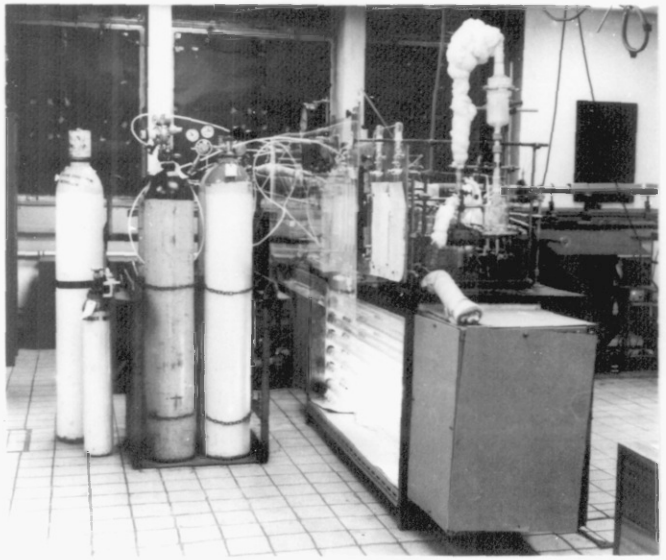


Plate 1 Front view of the equipment.

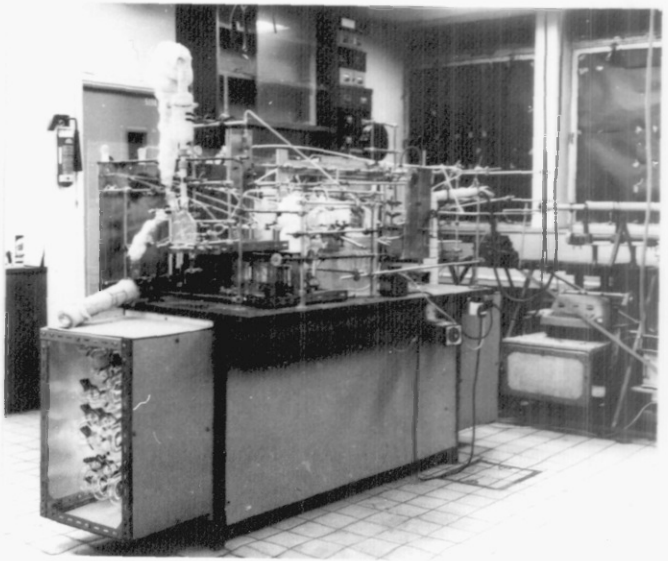


Plate 2 Side view of the equipment.

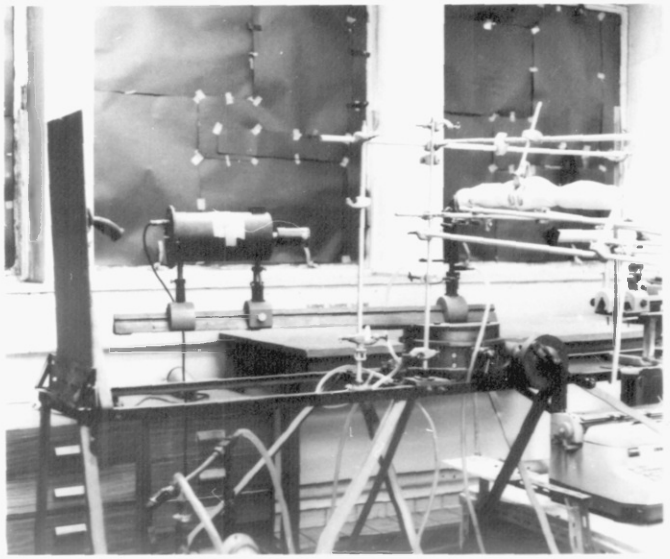


Plate 3 Light scattering sampling system.

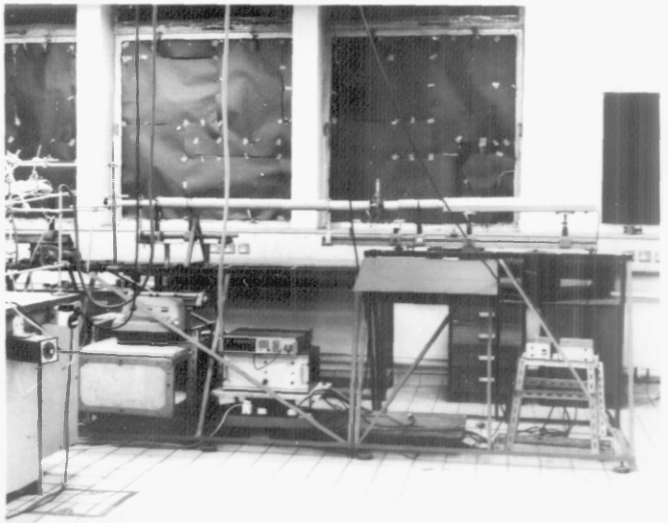


Plate 4 Laser source and data recording system.

Table III.3 Noise-to-signal ratio in the presence of aerosols

Scattering Angle	Signal (mV)	Noise (mV)	Noise-to-Signal Ratio (%)
9°	54.6	0.386	.7
18	36.7	"	1.0
27	24.2	"	1.6
36	14.6	"	2.6
45	9.9	"	3.9
54	8.5	"	4.5
63	7.4	"	5.2
72	8.3	"	4.6
81	9.6	"	4.0
90	11.3	"	3.4
99	13.3	"	2.9
108	17.7	"	2.2
117	23.7	"	1.6
126	29.2	"	1.3
135	32.2	"	1.2
	Mean		2.7%

at 20% level, and so there are no differences in MMD and sum of intensity of scattered light at the two operating voltages. However, a comprison of the t_o values for the particle size and scattered light measurements shows that the similarity in values obtained at the two voltages is less in the latter than in the former. The similarities not withstanding, since in subsequent measurements, use will be made of the values of the modal diameters in calculations other than those of the MMD, all subsequent operations of the photomultiplier, unless specifically stated were carried out at 1.2 KV, and this was strictly maintained.

(b) Photomultiplier stability

These tests were carried out to determine the stability of the photomultiplier during a running period of about three hours. The photomultiplier and the laser were first run for two hours to stabilize The light scatterer was a polyurethane foam material mounted in the path of the laser beam at the aerosol sampling point. Aerosol was not used as its fluctuations would mask the photomultiplier signal fluctuations. In the first experiment, the intensity of scattered light was sensed at a constant scattering angle of 90° at twenty minutes intervals. Six readings were taken at each interval and the means listed in Table III.6. The mean, standard deviation and coefficient of variation of the means are also tabulated. An internal consistence test was carried out and this showed that the photo-multiplier signal is stable within the experimental time.

In the second experiment, the scattered light intensity was sensed at fifteen scattering angles between 9° and 135°, first advancing from 9° to 135° and then back to 9°, taking six readings at each 9° step. The mean readings at each scattering angle was calculated and recorded in Table III.7. A two-tailed t-test done on the pair of data showed that there is no statistically significant difference between the two sets of signals.

(c) Photomultiplier Sensing Angle

Moore (1974) described the manual method of moving the photomultiplier tube to change the sensing angle as being too slow,

Table III.4 Comparison of ZOLD parameters obtained at .9KV and 1.2 kV Photomultiplier Voltage

Contact time (min)	.9KV		1.2KV	
	d mode (μm)	σ_0	d mode (μm)	σ_0
.65	.052	.688	.146	.529
1.1	.050	0646	.051	.655
5.1	.067	.627	.258	.401
9.1	.050	.921	.059	.563
13.2	.060	.941	.078	.909
17.2	.483	.482	.629	.374
21.2	.394	.425	.250	.529
25.2	.445	.406	.513	.316

For d mode : $t_0 = 0.165$; $t_{0\cdot05} = 1.895$

Table III.5 Comparison of the MMD and scattered light intensities at 0.9 KV and 1.2 KV

Contact time (min)	0.9 KV		1.2 KV	
	MMD (μm)	ΣIntensity (V)	MMD (μm)	ΣIntensity (V)
.65	0.142	0.1163	0.149	0.3016
1.1	0.170	0.341	0.294	0.123
5.1	0.179	0.598	0.386	0.244
9.1	0.417	0.428	0.131	1.678
13.2	0.549	1.036	0.615	4.645
17.2	0.863	8.366	0.892	2.808
21.2	0.619	1.244	0.503	3.564
25.2	0.672	2.778	0.658	10.779

MMD : $t_0 = 0.005$; $t_{0\cdot10,7} = 1.415$
ΣIntensity $t_0 = 0.106$, $t_{0\cdot10,7} = 1.415$

Table III.6 Stability of the photomultiplier over a 3 hour running period

Intervals	1	2	3	4	5	6	7	8	9	10
PM Reading (mV)	1.39	1.44	1.48	1.44	1.42	1.45	1.43	1.47	1.45	1.43

Mean = 1.44
Standard Deviation = 0.25
Coefficient of variation = 0.02

cumbersome and imprecise. In this experiment, the extent of this imprecision and its effects on the reproducibility of the light scattering intensities recorded at scattering angles between 9° and 135° were studied. An accuracy of 95 per cent in changing the photomultiplier sensing angle was achieved even in complete darkness with little practice.

As in the study reported in (b) above, the laser and the photomultiplier were stabilized for two hours and the light scatterer used was a piece of polyurethane foam. In one experimental run, scattered intensities were recorded at scattering angles between 9° and 135° while moving the photomultiplier in the dark (Run A). In another run, each light scattered intensity was recorded after care had been taken to ensure that the turntable was very accurately adjusted to the correct angle (Run B). Twelve readings were taken at each scattering angle in each of the two runs and the means of the twelve recorded for each run in Table III.8.

A student t-test was done to compare the two runs which showed that there was no significant difference between the two runs. The inaccuracy in adjusting the photomultiplier sensing angle which could be brought down to a value below ±0.2° is therefore not an important source of lack of reproducibility in light scattering measurements.

(d) Aerosol flow at the sampling point

Three experiments are described to show the effect of the instability of aerosol flow at the sampling point on the reproducibility of the scattered light intensity measurements. Since the aerosol flowrate was maintained constant at 4 l min^{-1} and the 'sheath' nitrogen at 3.5 l min^{-1}, the only possible varying flowrate was that of the exhaust gas.

The aerosols used were generated from a 0.005 M - $(NH_4)_2SO_4$ aqueous solution and the flow allowed to stabilize for two hours along with the photomultiplier and the laser. All the joints in the system were checked for leakage and the flowrate monitored for one hour prior to taking readings.

Table III.7 Comparison of data obtained while changing the scattering angle in opposite directions

Scattering Angle	Photomultiplier Signal (mV) Foward Direction(9°-135°)	Reverse Direction(135°-9°)
9°	18.18	18.91
18	15.66	16.88
27	14.76	15.52
36	16.39	17.05
45	17.75	17.77
54	17.35	16.76
63	15.45	15.50
72	15.61	15.94
81	15.66	15.44
90	15.30	15.32
99	19.49	19.55
108	39.68	38.86
117	96.68	91.85
126	187.4	186.5
135	290.9	290.1

$t_0 = 0.0508$; $t_{0.1,7} = 1.415$

Table III.8 A comparison of two light scattering runs carried out under identical conditions

Scattering Angle	Photomultiplier signal (mV) Run A	Run B
9	18.75	16.01
18	16.62	14.80
27	16.04	13.99
36	17.78	15.65
45	18.50	14.85
54	17.51	14.54
63	15.74	14.0
72	15.88	14.39
81	16.37	14.49
90	15.79	13.88
99	19.80	21.6
108	38.16	60.8
117	91.45	121.0
126	198.1	192.0
135	310.6	307.7

In the first run, the exhaust gas system was arranged in such a way that the exhaust flow rate decreased with time. Photomultiplier signals were recorded at intervals of fifteen minutes (twelve readings at each interval) at 90° scattering angle. The means of these readings together with the corresponding exhaust gas flow rates are listed in Table III.9. In the second run, the exhaust system was rearranged so that the exhaust flowrate remained constant at the initial value of 10 1 min^{-1}, and the readings recorded as in the first run (Table III.10). Finally, under this condition of constant exhaust flow-rate, two sets of scattered intensity readings were taken for the purpose of computing ZOLD parameters separated by an interval of twenty-one hours. The ZOLD parameters obtained from these data are listed in Table III.11. Table III.9 shows the intensity of scattered light decreasing with the exhaust gas flow-rate which affected the stability and shape of the aerosol stream. At low exhaust flow-rate, aerosol flow is random and aerosols are lost by diffusion through the nitrogen sheath and is dispersed all over the region around the sampling point. At exhaust flow-rate of 10 1 min^{-1}, however, aerosol flow through the gap between the two halves of the sampling cell becomes laminar and the aerosols are contained in the sampling area by the nitrogen 'sheath' giving reproducible readings and ZOLD parameters that reflect the actual characteristic pattern of the aerosol.

(e) Filter Efficiency

The extraction of aerosol by filtration was necessary at different stages in the study. Such operations included treatment of exhaust aerosol prior to disposal, determination of aerosol phase volume ratio and droplet number concentration and aerosol sulphate extraction as a preliminary to quantitative analysis. To this end the efficiency of three types of disc filters supplied by Millipore (UK) Ltd. were compared in terms of their collecting efficiency and the aerosol flow-rate through them. The manufacturers specifications of the filters are listed in Table III.12. The VSWP and VMWP are membrane filters whereas the AP15 is a depth filter.

First, filtered air at 4 1 min^{-1} was passed through each of them at a differential pressure of 10 psig. The flow-rates of the air

Table III.9 The effect of the exhaust flow instability on scattered light intensity

Intervals (15 min)	1	2	3	4	5	6	7
Exhaust Flowrate (1 min-1)	10	9.6	8.5	8.1	7.7	7.3	2
Photomultiplier signal (mV)	12.3	11.8	10.4	9.81	9.52	8.98	1.86

Table III.10 Photomultiplier output signal during a constant exhaust gas flow regime

Intervals (15 min)	1	2	3	4	5	6	7
Exhaust flow rate ($dm^3\ min^{-1}$)	10	10	10	10	10	10	10
Photomultiplier signal (mV)	12.6	12.3	12.3	12.6	12.1	11.9	12.3

Table III.11 Variation of aerosol ZOLD parameters with time for a constant exhaust flow regime

	d_{mode}	σ_o	Sum of squares	RMS Error
Run A	0.574	0.314	0.309	0.144
Run B	0.549	0.323	0.121	0.0896

measured downstream of the filters are recorded in Table III.13. Then aerosol generated from a 0.1 M - $(NH_4)_2SO_4$ master solution at a flow-rate of 4.0 l min^{-1} and retained in the reactor for a residence time of 25.2 minutes was passed through each of the three weighed filters. Ten litres of the aerosol was passed in each case and the differential pressure was also 10 psig. The aerosol flow-rate through each of them was measured downstream of the filters, and the weights of droplets collected by each were measured. These are listed in Table III.13.

The flow-rates of both air and aerosols were low in the membrane filters but as high in the depth filter as if the flow path contained no filter. However, the collection efficiency of the membrane filters was over one order of magnitude higher than that of the depth filter. Most of the droplets just went through the dept filter. It was therefore not used where aerosol collection for quantitative work was needed. It found very good use as a gas filter at several points in the main aerosol and reactant gas lines to remove unwanted particles from the gas stream and in the exhaust gas treatment unit where its fairly high retention capacity and its very high dirt-handling capacity were desired qualities. The membrane filters on the other hand with their very high retention capacity were suited for analytical work. The choice between VSWP and VMWP was done on the basis of balancing the slightly higher retention capacity of the former with the slightly higher flow-rate through the later; and this was in favour of the VMWP filter.

Special Precautions

Having chosen the parameters with which the light scattering unit was to be operated with optimum result, possible sources of error in these experiments were identified as leakage in the line, contamination by catalysts or inhibitors and fluctuations in aerosol flow, reactor temperature and humidity.

Leakages constituted the greatest hazard in view of the fact that quick-fit joints were mostly used and the equipment was operated at a fairly high pressure. Cones and sockets of quick-fit joints were hooked together with strong springs and the joints checked from time to

time for leakage. Flow-rates were continuously monitored using flow-meters which were carefully calibrated for the appropriate gas using a bubblemeter of size appropriate to the flow rate to be measured. Flow through the rotameters was controlled downstream. In so doing, vibrations and gas surges caused by the imperfection in the gas cylinder control were prevented from being transmitted downstream of the flow-meter. Pressures at different points in the flow-line were closely monitored by means of pressure guages and open-tube manometers. The reactor temperature and relative humidity were carefully monitored.

Of particular importance in experiments involving chemical reactions was contamination from catalysts and inhibitors. All vessels used in the experiment, up to the aerosol sampling point, were made of stainless steel, glass or teflon. Joints were grease-free. Solvent water was de-ionised and then doubly distilled water produced in the Analytical Laboratory and was of standard at least as high as that of BDH distilled water for liquid chromatography. Its pH of 6.4 and conductivity were monitored from time to time. Before the installation of the Analytcal Laboratory Aquatron still, the distilled water used was de-ionised and then double-distilled with $KMnO_4$ and tests with atomic absorption spectrometer showed no detectable amounts of Mn^{++}, iron and copper ions. All chemicals used were analytical standard.

Table III.12 Filter Specification

1. Filter Designation	Millipore VSWP	Millipore VMWP	Millipore AP15
2. Material	Mixed Ester	Mixed Ester	Borosilicate fibre bonded with resin
3. Mean Thickness (μm)	105	105	2000
3. Pore Size (μm)	0.025	0.05	2.0
4. Flowrate at 10 psi differential pressure(1 min^{-1} cm^{-2}area)	0.2	0.5	20
5. Filter Area (cm^2)	13.85	13.85	13.85
6. Porosity (%)	70	70	Not specified

Table III.13 Performance of Filters

1. Filter type	VSWP	VMWP	AP15
2. Aerosol volume sampled (litres)	10	10	10
3. Wt of droplets collected (g $l^{-1}$of aerosol)	4.2×10^{-4}	4.0×10^{-4}	1.1×10^{-5}
4. Observed aerosol flow-rate (1 min^{-1})	0.08	0.114	3.8
5. Observed air flow-rate (1 min^{-1})	1.6	2.2	4.0

III.3 Aerosol Droplet Size Analysis

The size parameters and the distribution of the intensity of light scattered by aerosols give considerable insight into the physical processes occuring during the life time of the aerosols. So, in this section, the characteristics of $(NH_4)_2SO_4$ aerosols which are undergoing size distribution change by condensation, coagulation and deposition are studied by light scattering methods. Aerosols generated from $(NH_4)_2SO_4$ master solution of specified concentration were passed through the reactor with/without the reacting gas(es) to the sampling point where the stream was intersected by the laser beam. The intensity of the scattered light was measured at fifteen scattering angles between 9° and 135° by means of a photomultiplier. Using the angular distribution of scattered light intensity, the droplet and medium refractive indices and the laser wavelength, the ZOLD parameters of the aerosol size distribution were obtained by inversion using the programme SEARCH.

In all the experiments described in this section, unless otherwise stated, the following five conditions are commonly used

i. the aerosol generation rate is 4 l min^{-1};

ii. the air thermostat is equilibriated at 25 °C for two hours prior to the start of an experimental run;

iii. the reactor is flushed with the experimental aerosols for at least one-and-a-half hours before the start of an experimental run;

iv. the reactor tubes are washed with distilled water and dried at the end of a set of related experimental runs and the generator emptied, washed and refilled with fresh master solution;

v. the photomultiplier and laser are stabilized for two hours before the beginning of an experiment.

Other conditions necessary to achieve reproducibility are described as they occur.

III.3.1 Light scattering study of $(NH_4)_2SO_4$ aerosol

Four experiments are described which studied the effect on aerosol droplet size of the master solution concentration, reactor relative

humidity, aerosol generation rate and the residence time in the reactor. Aerosols generated under specified conditions were passed through the reactor to the sampling point and the intensity of the scattering light recorded.

i. Particle size and master solution concentration:

The effect of master solution concentration on aerosol particle size and light scattering pattern was studied using master solutions of concentrations 0.0, 0.001 M, 0.005 M, 0.01 M, 0.05 M, 0.1 M and 0.5 M. The aerosols generated from them were sampled at 17.2 minutes residence time. Twelve readings were taken at each scattering angle and average, and ZOLD parameters computed.

ii. The effect of aerosol generation rate:

The effect of aerosol generation rate was studied by generating aerosols at different flow-rates of the generating air and recording their light scattering patterns. The aerosols were generated from a 0.1 M - $(NH_4)_2SO_4$ master solution and sampling was done at 17.2 minutes residence time. Twelve readings were also taken at each scattering angle and averaged.

iii. The Effect of Relative Humidity (R.H.)

The light scattering patterns of aerosols generated from a 0.05 M-$(NH_4)_2SO_4$ master solution were observed at four values of reactor humidity (20%, 78%, 82%, and 98%) with the aerosol flow-rate and residence time fixed at 4 l min^{-1} and 17.2 minutes respectively. Before the experiments, the reactor tubes were thoroughly dried by blowing warm air through them and leaving them overnight to cool. Relative humidities above 72% were obtained through a careful management of main air line humidification and make-up air moisture content. It was necessary, in addition to controlling the humidity of the air as stated above to regulate the humidity of the reactor when humidities below 72% were required. This was achieved by putting about 20.0 g of self-indicating silica gel beads into the leading reactor tube. The effect of the silica gel beads on the aerosol stream was tested by replacing it with 20.0 g of glass beads of similar grain size and observing the effect on the aerosol characterisitics. The sum of scattered intensities (1.57V and 1.60 V in the presence and absence of glass beads respectively) are identical which means that the presence

of the silica gel did not significantly affect the aerosol stream. However, there was a disparity in the values of VMD (0.692 and 0.922 in the presence and absence respectively of glass beads). The disparity might have been caused by the temporal separation between the two experiments.

iv. The Effect of Residence Time:

The residence time was calculated for the various reactor volumes based on a flow-rate of 4 l min^{-1}. The reactor volume was obtained from the separate volumes of all the components which were carefully measured by the volume of water required to fill each of them. The reactor tube combinations and the corresponding residence time are listed in Table III.14.

Aerosols were generated from a 0.1 M - $(NH_4)_2SO_4$ solution and passed into the reactor for each of the residence times shown in Table III.14. The entire eight runs were done in one day during which the generator was stopped only once for four minutes to replace spent air cylinder. After each run and change of residence time, the aerosol was allowed to flow through the reactor for thirty minutes before the readings for the new residence time were taken. Twelve readings were averaged at each scattering angle.

In order to determine the mass concentration of the aerosols and obtain samples for chemical analysis, it was necessary to device an efficient method of quantitatively sampling droplets. Neither the cloud water collector which was tested by Katz (Steele et al, 1981) nor the particle mass monitor used by Radojevic (1983) was suitable for the aerosol droplet size (sub-micron) and flow regime (4 dm^3min^{-1}) of this study. Aerosol mass concentration was therefore obtained by weighing the droplets collected on VMWP membrane filter whose specifications are listed in Table III.12. The volume of the aerosols sampled was measured by means of an Alexander Wright and Co. (Westminster) Ltd. wet gas meter located downstream of the filter. Twenty litres of aerosols were sampled each time for weighing. The filter was weighed sealed in a small (5 cm by 6 cm) light weight (under 1.0 g) plastic bag on a Sartorius 2024 MP balance with a sensitivity of 10 μg.

The droplet number concentrations of the aerosols were calculated from the mass concentration and the droplet VMD obtained from light scattering measurements.

III.3.2 Light Scattering Study of the droplet-gas interacting system

The experiments to study by light scattering methods the oxidation of SO_2 in $(NH_4)_2SO_4$ droplet and its consequent growth as a result of the increase in its sulphate content are described in this section. In the model, particle growth occurs due to the water vapour pressure lowering effect of the sulphate formed in the droplets which is a function of time.

Three sets of experiments were carried out. In the first set, the droplet phase oxidation of SO_2 in the absence of NH_3 was carried out for partial pressures of SO_2 of 10^{-6}, 10^{-5}, 5×10^{-5} and 10^{-4} atmospheres. In the second set, the oxidation of SO_2 in $(NH_4)_2SO_4$ droplets in the presence of NH_3 was carried out at partial pressures of SO_2 and NH_3 shown in Table III.15. The reacting gases were diluted from sources of different concentrations. This was done to avoid swarming the reaction medium with nitrogen from the gas mixtures when low concentrations are needed and to avoid the use of very low flow-rates in the flow dilution systems which presented enormous problems in metering and flow adjustment. The concentrations of the gas sources used are presented in Table III.15.

In the third set of experiments, the droplets in which SO_2 underwent oxidation were generated from a 1.0 mM - $MnSO_4$ solution. The partial pressures of SO_2 and NH_3 investigated were the same as those of Runs 1 to 6 in Table III.15.

The three experiments were done in the order stated here hence there was no question of cross contamination of the first and second sets by $MnSO_4$ or the first set by NH_3.

In addition to the general guidelines stated earlier, it was found that better reproducibility was obtained in a run by starting at the highest residence time and progressing to lower residence time, and to operate the entire equipment non-stop up to the end of the run. After altering the residence time, enough time was allowed for the flow pattern to normalise before taking the readings.

Table III.14 Tube combinations and residence time*

Tube Combination	Reactor Volume (dm^3)	Residence Time (s)
S-Tube	2.57	39
1-Tube	4.22	64
5-Tubes	20.43	307
9-Tubes	36.52	548
13-Tubes	52.62	790
17-Tubes	68.71	1031
21-Tubes	84.80	1272
25-Tubes	100.89	1514

* Aerosol flowrate = 4.0 dm^3 min^{-1}.

Table III.15 Combinations of SO_2 and NH_3 partial pressures and source concentrations

	Partial Pressures (x 10^6) atmospheres										
Combinations	1	2	3	4	5	6	7	8	9	10	11
SO_2	1.0	1.0	50.0	50.0	50.0	50.0	50.0	50.0	50.0	50.0	50.0
NH_3	1.0	2.0	0.1	1.0	1.0	10.0	2.0	10.0	25.0	50.0	100.0

Source Concentrations:

SO_2: Runs 1 - 3 - 1000vpm in nitrogen
Runs 4 - 11 - 10,000vpm in nitrogen

NH_3: Runs 1 - 7 - 100vpm in nitrogen
Runs 8 - 11 - 1000vpm in nitrogen

III.4 Aerosol Chemical Analysis

In this section, the experiments to quantify the sulphate formed as a result of the oxidation of SO_2 in the presence of NH_3 will be reported. First, the separation of SO_2 from the SO_4^{2-} will be treated, then the aerosol sampling technique and finally the chemical analysis.

The aerosols used in the study were generated from a master solution of either $(NH_4)_2SO_4$ or $MnSO_4$. The former was used in studying uncatalysed reactions because it is believed that it does not interfere with or affect the oxidation of SO_2 (Kaplan et al, 1981a).

III.4.1 Absorption of SO_2 by Scrubbing Liquids

SO_2 is the most important interferent in SO_4^{2-} analysis especially in a situation where the analytical method cannot distinguish between SO_3^{2-} and SO_4^{2-} ions. It is therefore necessary to use sample collection methods that exclude SO_3^{2-} ions. The extent of absorption of SO_2 by scrubbing solutions was assessed. Since the analytical method used cannot separate SO_3^{2-} from SO_4^{2-} and the two appear as total sulphur species, strict precautions were taken against oxidation in the absorbing solution. The conditions tested are listed in Table III.16.

In each case, SO_2 of appropriate flow-rate was metred into a nitrogen stream in S-tube to obtain the required SO_2 partial pressure for a total flow rate of 4 l min^{-1}. In the case of mixture B, NH_3 was also metred in addition to the SO_2. No aerosol was generated in any of the five runs. Except in mixture E, the scrubbing liquid was distilled water. For each mixture, seven samples were taken for durations listed in Table III.17. 50 cm^3 of the scrubbing liquid was used in each case. The SO_2 absorbed by each mixture for a known sampling time was determined as SO_3^{2-} by means of the HPLC (to be discussed in a later section) and tabulated in Table III.17.

Except in B and C, the amount of SO_2 that went into solution during the scrubbing was insignificant compared to the amount of SO_2

Table III.16 Scrubbing solution for the absorption of SO_2

Mixture	P_{SO_2} ($x10^6$)	P_{NH_3} ($x10^6$)	Scrubbing Soln.	Temp. of Scrubber	Effect Investigated
A	1	0	Distilled Water	20°C	Standard
B	1	1	"	"	Effect of buffering
C	50	0	"	"	Effect of P_{SO_2}
D	1	0	"	40°C	" " Temp
E	1	0	Phthalic acid Soln (pH=3)	20°C	" " pH

Table III.17 SO_2 absorbed by various eluents

Eluent flow-rate = 2.0 cm^3 min^{-1}

Loop size = 200 µl

Eluent = 10 mM - KHP buffered with $Na_2B_4O_7$

Temperature - Ambient

Sampling Duration (min)	Amount of sulphur compound in soln (mg dm^{-3})				
	A	B	C	D	E
1	2.0	89.09	2.32	1.5	.023
10	2.025	89.06	2.40	1.46	.030
20	2.01	88.2	2.18	1.56	.032
30	1.98	91.5	2.28	1.68	.030
40	2.10	90.8	3.36	1.40	.020

passed through. In all the cases, the amount of SO_2 absorbed by the scrubbing liquid was time invariant. This is as a result of the pH-controlled absorption of SO_2 in aqueous solution. Equilibrium was attained in under one minute; after which, in the absence of any chemical reaction, there was no more SO_2 absorption.

The important consequence of this observation with regards to SO_4^{2-} sampling in the presence of SO_2 by absorption into a scrubbing liquid is that under ordinary sampling condition of ambient temperature and pH of under seven, much of the SO_2 from the aerosol bulk gas phase escapes from solution. Secondly, for a sampling time of 25 minutes the amount of SO_2 absorbed from the aerosol gas phase will not differ from what it was after the first minute of sampling. However, in the presence of NH_3, a substantial amount of SO_2 was absorbed. Since in the aerosol sampling experiments, NH_3 was to be involved, it was judged necessary to remove the interfering SO_2 prior to SO_4^{2-} sampling.

III.4.2 Separation of SO_2 from Droplets

The removal of SO_2 from an aerosol stream has been studied using diffusion strippers. This is necessary especially in work involving SO_2 in a sulphate-bearing aerosol stream where accurate estimation of SO_4^{2-} is necessary and the presence of SO_2 would complicate the analysis. Under this condition, SO_4^{2-} sampling without SO_2 removal up-stream of the sampling point would create sampling artifact. Diffusion denuders have also been used in estimating the SO_2 content of a gas stream (Hickey et al, 1965; and Durham et al, 1978); and in sampling atmospheric SO_2 (Possanzini et al, 1983).

The preferential removal of SO_2 from an aerosol stream by a denuder makes use of the difference in the difusion coefficients of SO_2 and aerosol droplets. With the SO_2 diffusion coefficient of .13 cm^2s^{-1} (Fish et al, 1971) and the diffusion coefficient of droplets (diameter 0.01 to 1.0 μm) which ranges from 2.7×10^{-7} to $5.2 \times 10^{-4} cm^2s^{-1}$ (Fuchs, 1964), SO_2 will be lost by diffusion to a wall about four orders of magnitude faster than the smallest particles. Hence, if the flow of the aerosol stream through the denuder were laminar, SO_2 molecules will diffuse into the wall of the denuder while

the aerosol droplets pass through almost unchanged if other causes of droplet removal (sedimentation and impaction) were eliminated.

Gormly et al (1949) considered the case of the flow of a reactive gas with constant input concentration in a cylindrical tube whose wall was coated so that it became a perfect sink for the gas. Assuming a fully developed velocity profile, the following relationship between the input and output concentrations of the gas c_0 and c respectively was obtained

$$c/c_0 = 0.819 \exp(-14.6272\Delta) + 0.0976 \exp(-89.22\Delta) + 0.01896 \exp(-212\Delta)$$

where

$\Delta = \pi DL/4F$

L = length of the coated part of the tube

D = diffusion coefficient

F = volume flow-rate

This applies if the flow is laminar. The choice of the denuder diameter is only to ensure a laminar flow field since the Reynold nmber is related to tube diameter by the equation

$$Re = 4F/\gamma\pi d$$

where γ = kinematic viscosity of air.

Possanzini et al (1983) introduced the use of a diffusion denuder made of two co-axial tubes in which the aerosol flows through the annular space, in which the Δ depends on the annular diameter

$$\Delta_a = \pi DL/4F \times \frac{d_1 + d_2}{d_2 - d_1}$$

where

d_1 and d_2 are the inside and outside diameters of the annulus respectively;

$d_2 - d_1$ = equivalent diameter = δ.

Thus, Δ_a may be optimised by varying δ as well as L and F. Reynold number is obtained for the annular denuder according to the equation

$$Re_a = 4F/\gamma\pi(d_1 + d_2)$$

Hence using low values of the equivalent diameter and high values of the outside diameter, high values of Δ_a could be obtained without any alteration of the laminar regime. This fact gives this type of denuder a great advantage over the open tubular ones used by Durham et al (1978), Stevens et al (1978) and Ferm (1979). To demonstrate this, a tubular denuder of diameter 3.2 cm and length 29 cm was compared with an annular denuder of the same length but an equivalent diameter of 0.2 cm and an outside diameter of 3.2 cm. The flow-rate of the reactive gas (SO_2) is 100.0 cm^3 s^{-1}. The values of the Reynold numbers, Δ and the exit partial pressure of the reactive gas for an input partial pressure of 10^{-6} atmosphere are listed in Table III.18. The walls of the two denuders were regarded as being perfect sinks for the reactive gas. The exit partial pressure of the SO_2 in the annular denuder was six orders of magnitude smaller than that of the tubular denuder. As a result of the superior SO_2 removal property of the annular denuder, it was the obvious choice for this study.

The annular denuder used is shown schematically in Fig. III.14. It is similar to the one described by Possanzini et al (1983) but modified to minimise the loss of aerosols at the aerosol input end of the tube. The annulus walls were mechanically frosted to increase their surface area. The coated length was 29 cm and the internal and external annulus diameters were 3.0 cm and 3.2 cm respectively. To remove whirls caused by impaction, a 5.0 cm length of the tube near the aerosol entrance was left uncoated. This length was necessary to establish laminar flow before the aerosol reached the coated portion.

Two coating materials were tried namely tetrachloromercurate (TCM) and PbO_2. Experiments were carried out to test their ability to remove SO_2 from the aerosol stream. In each of the cases, aerosol carrying a known concentration of SO_2 was passed through the coated denuder and the SO_2 content of the effluent aerosol determined by spectrophotometric method described in the next section.

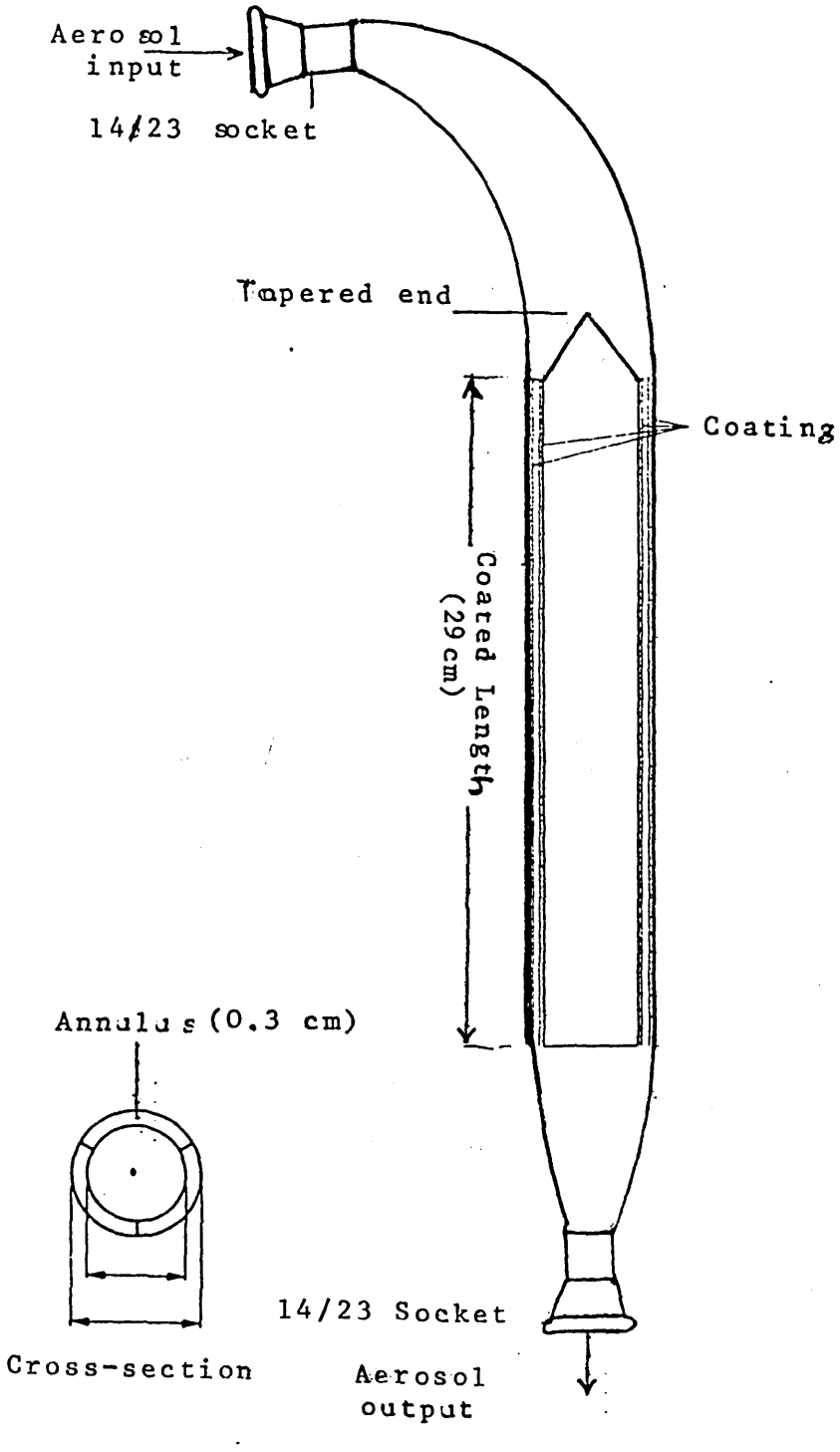


Figure III.14:-Schematic diagram of the annular denuder.

TCM removes SO_2 from a gas stream because it undergoes an exchange reaction with SO_2 (West et al, 1956)

$$[HgCl_4]^{2-} + 2SO_2 \rightarrow [Hg(SO_3)_2]^{2-} + 4Cl^- + 4H^+$$

It was buffered with phosphate to maintain constant pH as HCl was produced by the exchange reaction. For each coating, 5 cm^3 of 0.2 M - TCM in 1:1 water/MeOH solution was mixed with an equal volume of the buffer solution. The buffer solution was a mixture of 0.02 M-KH_2PO_4 and 0.02 M-Na_2HPO_4 solutions in carbon dioxide-free water/MeOH mixture. The coating solution was introduced through the exit end of the denuder into the annulus with the tube held in a horizontal position to ensure that both the internal and external walls of the annulus were coated simultaneously. The tube was rotated gently in this position about its axis until the entire walls of the annulus were coated. Much of the surplus coating solution was removed by means of a dropping pipette. The annular walls were dried by blowing a gently stream of dry warm N_2 through the annulus while at the same time rotating it slowly about its axis.

The removal of SO_2 from a gas stream by PbO_2 depends on the fact that SO_2 readily reduces PbO_2 to form $PbSO_4$. A thick slurry of PbO_2 and gum tragacanth powder in the ratio of five_to_one in MeOH was prepared. The slurry was poured into the annulus to cover the whole length of the tube while it lay horizontally on the bench. The tube was rotated gently about its axis to ensure a uniform smooth covering of the entire walls of the annulus. After removing excess MeOH with a dropping pipette, the tube was rotated further while warm dry nitrogen was blown gently through it until dry.

For each of the experimental conditions (Table III.19) a mixture of SO_2 and aerosols at a flowrate of 4 dm^3 min^{-1} were passed through the denuder which was connected directly to the mixer Mx4. The effluent from the denuder was sampled after 5, 15, 25, 35, 45 and 55 minutes by bubbling through 50 cm^3 of buffered TCM in a fritted bubbler for five minutes. The samples were analysed using the spectrophotometric method described in the next section. The SO_2 concentration of the effluent aerosols and its variation with time for different denuder tube conditions are shown in Fig III.16 and Table III.19a.

Table III.18 Comparison of annular and tubular denuders

	Re	Δ	C_{exit}(atmosphere)
Tubular Denuder	261.7	.031	5.266×10^{-7}
Annular Denuder	135.1	.9603	6.501×10^{-13}

Table III.19 Experimental conditions for the comparison of various denuder coating

Experiments	Number of Runs	SO_2 Partial Pressure x 10^6	Denuder Coating Material
A	6	1.0	Uncoated
B	6	50.0	Uncoated
C	6	1.0	Buffered TCM
D	6	1.0	PbO_2
E	6	50.0	TCM
F	6	50.0	PbO_2

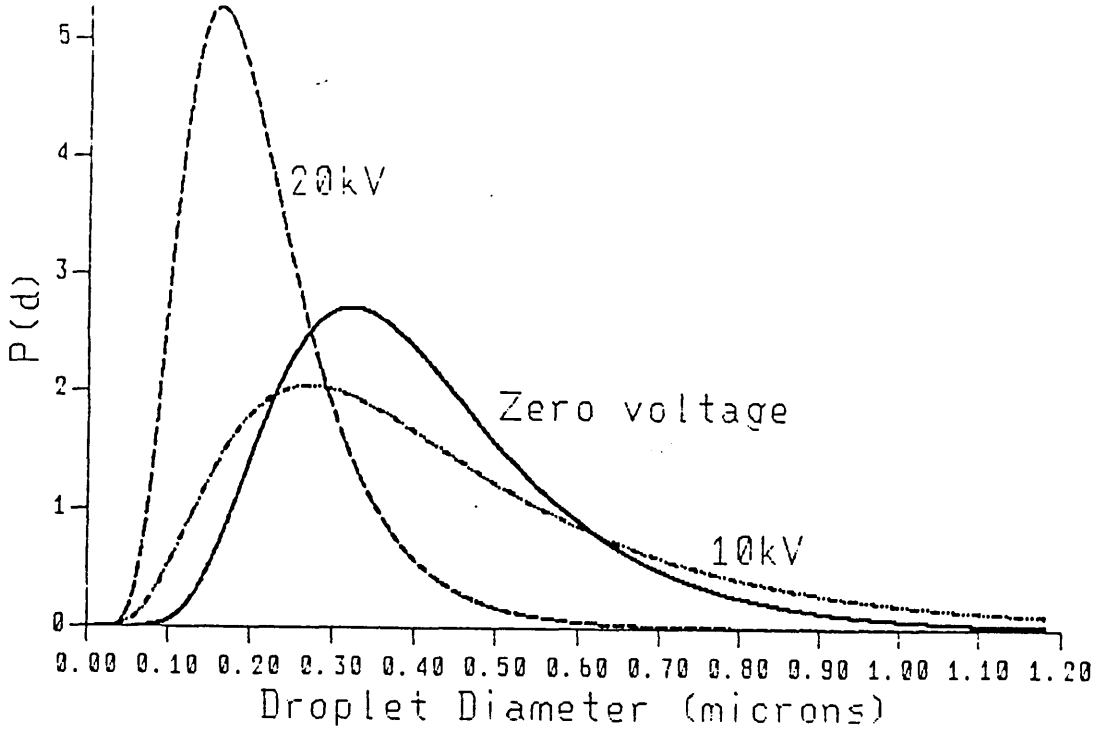


Figure III.15: - The size distributions of the effluent aerosols of an electrostatic precipitator as a function of the voltage.

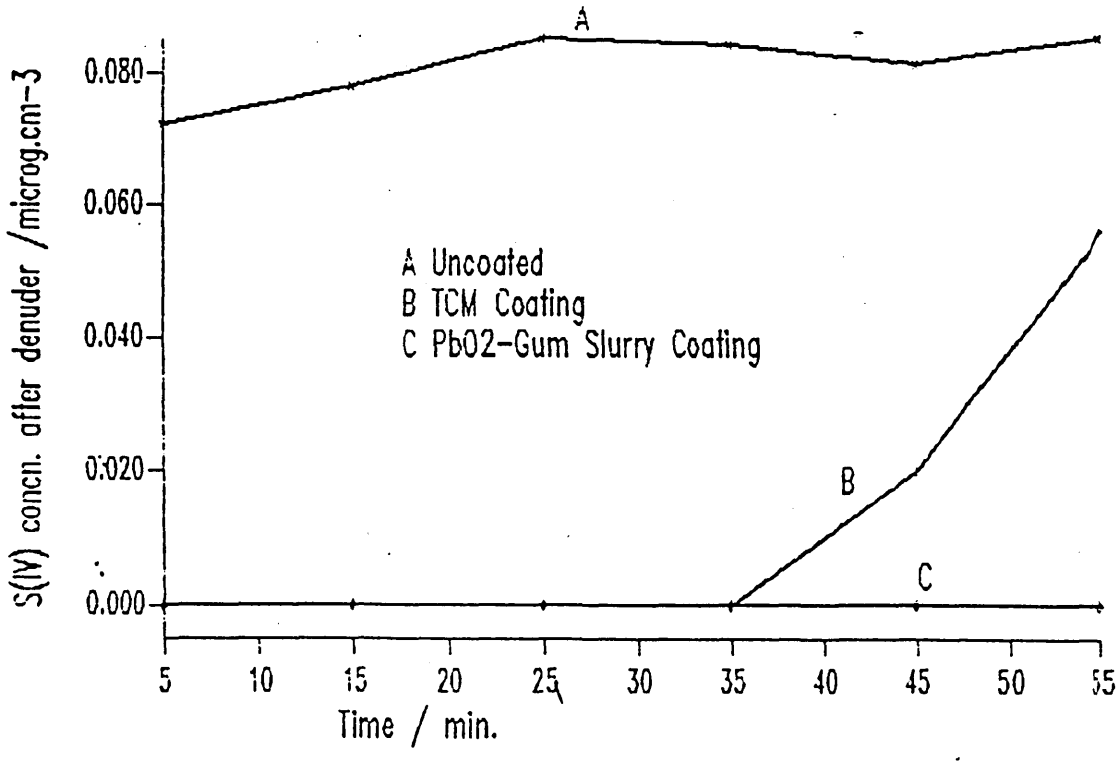


Figure III.16: - The break through-time of SO_2 of partial pressure 1vpm for different absorbing materials.

The graphs for the coated tubes show the extent of the breakthrough with the coating materials. For 1 ppm SO_2 the break through occurs after thirty-five minutes in the tube coated with buffered TCM and did not occur at all in the one coated with PbO_2 slurry. On the other hand, for 50 ppm SO_2, the break through occured after five minutes and values of effluent SO_2 concentration approaching that of the uncoated tube was observed after twenty-five minutes with buffered TCM. PbO_2 coating proved to be a perfect SO_2 sink for 1 vpm SO_2 and also for 50vpm SO_2 and was used for the whole study.

The mechanism of the operation of the denuder is that as the gas phase SO_2 is depleted by absorption by the coating material, the droplet phase SO_2 is desorbed into the bulk gas phase to maintain the equilibrium in the reversible reaction

$$SO_{2(g)} + H_2O_{(l)} \underset{\text{desorption}}{\overset{\text{absorption}}{\rightleftharpoons}} SO_2 \cdot H_2O$$

The result is that both the gas phase and the droplet phase SO_2 are removed by the denuder.

One of the most likely shortcomings of the diffusion denuder is aerosol loss to the wall of the denuder. This will not only diminish the amount of droplet and hence sulphate collected for analysis but will cover sites for the absorption of SO_2. Loss may be caused by three phenomena namely diffusion, sedimentation and impaction on obstacles and irregularities in the annular wall coating. Loss by sedimentation was eliminated in this study by using the denuder in a vertical position, and loss by impaction, by ensuring smooth coating of the annular walls. Loss by diffusion is a function of droplet diameter which in this study ranges from 0.01 μm to 1.0 μm and hence diffusion coefficients of between 5.2×10^{-4} and 2.7×10^{-7} $cm^2\ s^{-1}$, so loss by diffusion is unimportant. No quantitative experiment was carried out to confirm this. However, a qualitative experiment was carried out to compare the scattered light intensity, light scattering pattern and the ZOLD parameters of an aerosol stream that was passed through a coated denuder ~~coated~~ with an identical one that was not. The data are listed in Table III.20. In run A, the aerosol was passed into the uncoated denuder in a vertical position and through the Z-tube to the light

scattering cell. In run B, the denuder was coated with PbO_2 - gum tragacanth slurry and the aerosol after passing through it for ten minutes was sampled at the light-scattering cell. Run C was the same as B but the aerosol flowed through the denuder for one hour before sampling was done. There was no significant difference between the three runs as far as the ZOLD parameters and the intensity of scattered light of the aerosols were concerned. Possanzini et al (1983) recorded a loss in the denuder of under 0.2% for the smallest droplets.

Another possible source of error is the flaking off of the wall coating which might be carried into the sample. This problem is encountered in some cases where PbO_2 is used as the coating material especially when a substantial quantity of $PbSO_4$ has been formed. The $PbSO_4$ with a solubility of 4.25 mg per 100 cc of water at 25°C would introduce a detectable amount of sulphate even when only a small grain of it was introduced. However, the presence of the gum tragacanth serves as a binding material for the particles.

The commonest and most obvious source of error is the loss of removal efficiency due to saturation. It is therefore imperative to determine the breakthrough time of a coating material before use. The denuder used in this study has a breakthrough time of at least one hour for the highest partial pressure of SO_2 utilized and so was adequate for obtaining at least two samples of 100 litres of aerosol each. Sampling more than twice was not attempted. The coating was removed after two samples by rinsing first with water, then dilute nitric acid and finally with a large quantity of distilled water. This is inconvenient and hence there is a need for a denuder material with longer breakthrough time. The solution to it may lie in the use of the PbO_2 powder in stainless steel mesh used by Kaplan et al (1981b).

III.4.3 SO_2 Analysis

Methods of SO_2 determination include titrimetry spectrophotometry and ion and gas chromatography. Gas chromatography is the easiest since samples do not need preanalysis treatment and so can be used in-situ and on-line. Ion chromatography, titrimetry and spectrophotometry on the other hand entail intricate sample collection and preparation

some of which are prone to introduce error. However some methods of SO_2 collection on specially prepared filters (Huygens et al, 1963) or in special solutions (West et al, 1956) and (Dasgupta et al, 1980) have minimised these errors.

For a long time, the determination of SO_2 in atmospheric samples had been done by titrimetric methods. The SO_2 is absorbed in a suitable solvent system, usually NaOH or iodine solution or H_2O_2 and then titrated. In the EPA method 6 in which SO_2 is absorbed in H_2O_2 solution and propanol and titrated with standard $Ba(ClO_4)_2$ using thorin indicator, the minimum detectable limit is 1.2 vpm; it suffers interference from free NH_3 and does not give sharp colour change at the end point. Hence neither it nor any or the other titrimetric methods was used in this study.

A gas chromatograph with a flame photometric detector (FPD) calibrated with gravimetric primary standard gas samples from permeation tube gives very good accuracy if the correct operating conditions and correct gas flow-rates are used. Cains (1975) used the United Analyst Gas Council (LRS) Odorant Chromatrograph which operates in the 1 - 20 vpm range of sample concentration. This instrument however is not sensitive enough for this study.

The latest chromatographic method for SO_2 analysis is the ion chromatography. Sulphite ion in solution is separated from other ions by means of a special low capacity ion exchange resin and detected by means of a conductivity detector (Pohl et al, 1980). This method in the Dionex system has a special advantage in SO_2 pollution studies in that it separates and detects both S(IV) and S(VI) species (Hansen et al, 1979; and Dasgupta et al, 1982). Its major handicap is interference caused by the on-column oxidation of S(IV) to S(VI) which is almost linearly dependent on the retention time. A way of inhibiting oxidation and stabilize S(IV) with HCHO has been reported (Dasgupta, 1980) to have accelerating effect on the deterioration of column and hence is not advisable. The ion chromatographic method available for this study, the non-suppressed method using the Vydac system failed entirely to separate S(IV) from S(VI). So, ion chromatography was not used as a specific method for S(IV) determination in this study.

Spectrophotometry offers several of quick and routine ways of SO_2 analysis in solution. Scott (1964) used both UV and IR in characterising and quantifying S(IV) species in solution. In this study, IR spectrophotometry was not used because only few IR cells are insoluble in water and these are very expensive and very fragile.

The best spectrophotometric method for accurate determination of SO_2 is the UV/visible spectrophotometric technique which is based on the red-violet colour produced when p-rosaniline hydrochloride - HCl mixture and HCHO are added to a solution containing SO_2. The basis of the most successful method of environmental SO_2 determination is the work of West et al (1956) in which $HgCl_4^{2-}$ (TCM) is used as the SO_2 absorber/stabilizer and para rosaniline hydrochloride as the dye. The few refinements made to the original method to improve its reproducibility include studies on the purity of the dye (Pate et al, 1962); interference due to ozone, NO_x and transition metal ions (Pate et al, 1965); and the use of HCHO as an alternative absorbing/stabilizing solution (Dasgupta, 1980).

Dasgupta et al (1980) made use of buffered HCHO as the absorbing solution. HCHO absorbs SO_2 to form hydroxymethane sulphonate

$$HCHO + SO_2 + H_2O = HOCH_2SO_3H$$

The pH is maintained at a value of about 4.2 by 1 mM solution of potassium hydrogen phthalate. Dasgupta and his co-workers showed that the SO_2 in hydroxymethane sulphonate was thirty times more stable to oxidation than in disulphito mercurate (II) ion formed with TCM. They also showed that using a single bubbler, the absorption efficiency of the buffered HCHO varied from 100% with samples of 1 ppm SO_2 and sampling rate of 0.4 l min^{-1} to 99% with 98.8 ppm SO_2 and a sampling rate of 5 l min^{-1}. Finally, colour development was shown to be three times faster and the final colour more stable than in the West-Gaeke Method. These facts coupled with the fact that no $HgCl_2$ was used makes this a very attractive method.

However, when the method was tried in this study, SO_2 absorption was not much better than with water as the absorber. When 1 ppm SO_2 in a gas stream was bubbled at a flow rate of 1 dm^3 min^{-1} through 50 cm^3

of HCHO/KPH solution which was 7 mM in HCHO and 1 mM in KHP and which exhibited a pH of 4.2, for sampling times of 1, 5, 10, and 15 minutes respectively, the samples obtained failed to show SO_2 absorption better than the water absorber described earlier (Tables?II.16 and III.17). The amount of SO_2 absorbed by buffered HCHO is listed in table III.21. The failure of the KHP-bufered HCHO to achieve absorption efficiency claimed by Dasgupta et al could not be traced to any failure in equipment or methodology used in this study. This technique therefore was not used in spite of its attributes.

The West-Gaeke (1956) method which included some aspects of its modification by Scaringelli et al (1967) was used. Interference from O_3, NO_x and heavy metals was not expected and so no precautions were taken against them. The few variations to West-Gaeke method are in the concentration of the dye and the use of H_3PO_4 to control pH to which the colour is highly sensitive.

The instrument used was the Perkin Elmer Model 554 UV-visible spectrophotometer. It was operated at a slit width of 1 and a fixed wavelength of 548 μm and both in absorbance and concentration modes. All the chemicals used except the dye were analytical reagent grade. The dye was not assayed but believed to be impure enough to warrant purification in order to remove the violet colour that contributed to the blank.

A working solution of the dye was obtained by purifying 0.1 g of the dye according to the method of Scaringelli et al (1967) and treating 20 cm^3 of this mixture with 25 cm^3 of 3M-H_2PO_4 and diluting to 250 cm^3 with distilled water. The absorbing solution, 0.1 M-TCM was prepared by dissolving a mixture of 0.1 mole and 0.2 mole of AR grade $HgCl_2$ and NaCl respectively in distilled water and making up to the 1 dm^3 volume. A 0.2% solution of HCHO was prepared by making 5 cm^3 of the 40% solution up to 1 dm^3 with distilled water.

Table III.19a SO_2 concentration obtained after passing SO_2 through denuders under conditions shown in Table III.19

Experiments	[S(IV)] in effluent aerosol stream ($\mu g\ cm^{-3}$) 5 min	15 min	25 min	35 min	45 min	55 min
A	0.073	0.078	0.085	0.084	0.081	0.077
B	4.22	3.58	3.68	4.30	4.00	3.85
C	0.0	0.0	0.0	0.0	0.0	0.056
D	0.0	0.0	0.0	0.0	0.0	0.0
E	0.0	2.05	3.48	3.63	3.98	3.87
F	0.0	0.0	0.0	0.0	0.0	0.056

Table III.20 Light Scattering parameters of the effluent aerosols of the diffusion denuder (Master solution = 1mM-$(NH_4)_2SO_4$; residence time = 0.65 min)

Run	d_{mode} (μm)	σ_0	ΣIntensity (v)	VMD (μm)	Dysmmetry
A	0.24	1.00	2.103	0.295	9.504
B	0.24	1.00	2.098	0.293	8.501
C	0.23	1.00	2.092	0.276	7.704

Table III.21 HCHO as the absorbing liquid

Sampling Durations (min)	Range ($\mu g\ cm^{-3}$)	Mean ($\mu g\ cm^{-3}$)	No. of Samples
1	2.48 - 2.86	2.65	4
5	2.5 - 3.2	2.75	4
10	2.2 - 3.0	2.73	4
15	1.9 - 3.1	2.40	5

Calibration

The standard sodium sulphite solutions were prepared from AR standard $Na_2SO_3.7H_2O$ of assay 96% and specially prepared water. The deionised and double-distilled water was boiled and sparged with nitrogen and finally cooled in an atmosphere of nitrogen. A solution of the sodium sulphite which contained exactly 0.082 g of the salt in 1 dm^3 corresponding to 20.0 μg of SO_2 in 1 cm^{-3} of solution was prepared. Ideally, the calibrating Na_2SO_3 solutions should be standardised by iodine titration. This was not done in view of its high purity and the corrections made for the impurity. 10.0cm^3 of the freshly prepared standard solution was pipetted into a 100 cm^3 volumetric flask and made up to the mark with the 0.1-TCM solution. Aliquots were taken from this 20.0 μg cm^{-3} standard solution to prepare calibration standards that contained 15.0, 10.0, 5.0 and 1.0 μg cm^{-3} of SO_2 using the TCM solution. To 10.0 cm^3 of each of the calibration standards, 1.0 cm^3 of acid p-rosanilin and HCHO solutions were added. A blank of 10 cm^3 of the TCM solution was similarly treated. The colour was left for thirty minutes to develop after which the absorption was determined using distilled water in the reference cell.

After blank corrections, the absorbance was plotted as the abscissa against the concentration in μgcm^{-3} of the corresponding calibration standard and the line of best fit obtained. The slope of this line was the calibration factor which was subsequently used in calculating the sample concentration from peak height. Alternatively, the calibration factor could be stored in the memory of the instrument so that when it was operated in the concentration mode, the sample concentration could be read off directly from the ordinate display panel of the spectrophotometer.

Sample Analysis

Samples were collected by drawing the gas stream containing the SO_2 at the rate of 4 l min^{-1} through an impinger equiped with a fritted bubbler and containing 50 cm^3 of the absorbing solution. Unless otherwise specified, the absorbing solution was the TCM solution. Enough gas was sampled each time to get into solution at least 1.0 μg cm^{-3} of SO_2. 10.0 cm^3 of the sample was treated exactly in the same

manner as the calibration standard and the absorbance determined. The sample concentration was computed from the peak height and the calibration factor.

III.4.4 Droplet Sampling Methods

In this section, four techniques for droplet collection after the SO_2 content had been removed by means of denuders are described and compared in terms of convenience and efficiency in sample collection. The methods include filtration, passing an aerosol stream through a liebig condenser, an electrostatic precipitator and collection by bubbling through a scrubbing solution. Filtering, especially with a small pore size membrane filter would have been the best technique in terms of its sample collection efficiency. However, as a result of its resistance to flow which necessitates the use of vacuum pump downstream of the filter and in the absence of an ultrasonicator to recover the sample from the filter, it is cumbersome as a method for sampling droplets for routine sulphate analysis.

The conditions under which the other sampling techniques were studied are listed in Table III.22. In each case, aerosol was generated at 4 l min^{-1} from a 1 mM solution of $(NH_4)_2SO_4$ and passed through the sampler and the effluent from the sampler subjected to particle size determination by light scattering to determine qualitatively the extent of aerosol removal by the sampler.

i. The Condenser

The condenser used was an ordinary liebig condenser with a jacket diameter of 4.4 cm and a length of 39 cm. The inner tube was a quarter-inch coiled glass tube of 35 coils. The outer tube had one inlet through which water of a desired temperature could be introduced. It was hoped that aerosol could be deposited in the wall of the coiled glass tube as a result of impaction. In filling the outer tube with water at 90°C, it was expected that SO_2 would desorb at this temperature and would pass through the tube as the droplets were deposited in the tube. The ZOLD parameters and the sum of intensities of the scattered radiation of the aerosol emerging from the condenser are shown in Table III.23.

ii. The Electrostatic Precipitator

The precipitator consisted of two condensers, each of which had a straight inner tube lined internally with a thin aluminium sheet connected through a thick copper wire lead to a Bradenburg type MR/50R high volt generator capable of generating up to 50 KV of 1.0 amp maximum current. The outer tube was lined externally with thin aluminium sheet also and connected to the earth terminal of the generator (Fig. III.17). The outer chambers of the two condensers were joined in series by means of a plastic tube. The aerosol flowed through the outer tubes where the droplets became charged by the high current density and so drifted to the electrode as a result of coulonb forces and turbulent diffusion relative to the ionised gas motion. The voltage of the precipitator was measured by means of a Scalamp electrostatic voltmeter supplied by W G Pye and CO. Ltd. Since the precipitator geometry and polarity and aerosol flow-rate were constant, the effect of current density on droplet removal was investigated. This was done by subjecting the aerosol stream as it left the precipitator to light scattering analysis and comparing the characteristics under different conditions of voltage. The results are recorded in Table III.23.

iii. The Scrubber

The scrubber used was a single 60 cm^3 capacity impinger carrying a 24/29 socket that took a dreschel bottle head provided with a sintered bubbler of medium pore size. The scrubbing liquid was 30 cm^3 of distilled water. The scrubber effluent aerosols were subjected to light scattering analysis after passing through the scrubber under conditions shown in Table III.22. The light scattering characteristics are shown in Table III.23.

The sum of the background intensity, the mass mean diameter (MMD), the sum of the scattered light intensity and the ratio of the scattered intensity to the background intensity are calculated and tabulated for all the conditions investigated in Table III.23. The following comments on the trends of the characteristics of the effluent aerosols show the suitability or otherwise of the different methods of aerosol collection.

Table III.22 Aerosol Droplet Collection Techniques

Condenser

A Dry

B With water at 90° C in the outer jacket

Electrostatic Pecipitator

C Zero voltage

D 10 kV

E 20 kV

F Dilute aerosol at zero voltage

G Dilute aerosol at 20 kV

Scrubber (100 cm^3 dreschel bottle)

H Empty

J Containing scrubbing liquid (water) at 29° C

K Containing scrubbing liquid (water) at 20° C

Table III.23 The characteristics of the effluent aerosols from the droplet collecting device

Runs	Sum of [a] Background Intensity (V)	d_{mode} (μm)	σ_o	VMD (μm)	Sum of [b] Experimental Intensity (V)	b/a
A	0.018	0.133	0.689	0.44	0.450	25.0
B	0.018	0.310	0.545	0.65	0.463	25.7
C	0.021	0.320	0.420	0.49	4.37	208.1
D	0.017	0.269	0.605	0.43	1.81	106.5
E	0.022	0.160	0.434	0.41	1.93	87.7
F	0.020	0.113	0.770	0.50	0.572	28.6
G	0.021	0.050	0.913	0.40	0.149	7.1
H	0.016	0.050	0.691	0.17	0.164	10.3
J	0.023	0.051	0.790	0.24	0.054	2.3
K	0.018	0.050	0.644	0.14	0.019	1.1

Under the two conditions investigated in the condenser, there is almost no removal of droplet from the aerosol since the sum of scattered intensity is significantly higher than the background in the two experiments carried out with the condenser. This was therefore rejected.

The characteristics of the aerosol as it exits the electrostatic precipitator were observed at zero, ten and twenty KV. For the effluent aerosol at zero volt, the intensity of the scattered light after equilibration was very high and remained constant at 4.372 volts for as long as it was observed. As soon as the voltage was increased to 10KV, the intensity rapidly decreased to the background level. After a short time, it rose again and reached a steady value of 1.934 volts after ten minutes. This meant a reduction in intensity by a factor of 2.26. However, a two-fold increase in voltage did not produce much reduction in intensity. Rather it produced an increase in modal diameter and decrease in spread (Fig. III.15). Droplet removal up to 10 KV was mostly by electrostatic precipitation and the removal after 10KV was likely to be by diffusion since it appears that the smaller particles were removed (increased modal diameter and decreased spread) leaving the larger ones. It appears the precipitator became saturated with droplets at 10 KV and hence could not collect more by electrostatic processes. To test this, a highly diluted aerosol was analysed after passing through the precipitator at zero voltage and at 20 KV. The aerosol showed decreased size and intensity and increased spread. Despite the low value of the intensity at zero volt, the intensity was still significant at 20 KV; that means that droplet removal was inefficient. Larsen et al (1984) attributed deficiencies in the particle removal properties of an electrostatic precipitator on the effect of secondary flow in the form of axial roll of the gas. Axial roll results from non-uniform electric fields and is determined by current density, electrode geometry and aerosol axial flow-rate. At high flow-rate, the precipitator efficiency is expected to be low primarily because of high roll strength. At low flow-rate, efficiency is also low primarily because of high turbulence and less organised secondary flows. The precipitator could therefore only be optimised by the careful management of the flow-rate and current density simultaneously. Since the flow-rate in this experiment is limited by the generator flow-rate, no attempt was made to optimise the

precipitator efficiency by varying it. Under the situation therefore the precipitator was not an efficient method of aerosol droplet sampling and hence was not used.

Using a single scrubber, a substantial decrease in scattered light intensity was achieved. When two scrubbers were connected in series, the intensity was that of the background which means total droplet removal. This is therefore the most efficient of all the techniques tried and hence was used in this study for droplet sampling.

III.4.5 Sulphate Analysis

Titrimetric and instrumental methods have been used for sulphate determination in environmental samples. Sulphate precipitation as $BaSO_4$ and the determination of the light transmited through the precipitate as a function of the sulphate concentration (turbidimetry) or measuring the intensity of the scattered light as a function of the sulphate concentration (nephelometry) has been in use for low sulphate concentration analysis (Barnes et al, 1949). However, the techniques have not enjoyed wide use because they are very difficult to replicate. The titrimetric method that is sensitive enough for low sulphate concentrations is the $Ba(ClO_4)_2$ - Thorin titration used in the EPA Method 6 (1977). The minimum detection limit of this method is 0.05 ng cm^{-3}. In spite of its low detection limit it is not suitable for this study since ammonia interferes. A spectrophotometric method for sulphate determination was first described by Bertolacini et al (1957). It is based on the reaction between sulphate ion and barium chloroanilate, $BaC_6Cl_2O_4$ at a pH of 4 to yield a highly coloured acid - chloroanilate ion that absorbs at 530 mμ. Carlson et al (1967) achieved increased sensitivity by lowering the pH of the system by usingg phosphate buffer. However when this method was attempted, it was not easy to achieve reproducibility.

Since its introduction by Small et al (1975), ion chromatography has offered the analytical chemist a fast and reliable method of quantitative separation and determination of anions in aqueous solution. The first form of it was a combination of ion exchange, eluent suppression and conductimetric detection. It made use of alkaline eluents e.g. NaOH which facilitated the separation of anions

on an anion-exchange column and whose background conductance could be suppressed by the exchange of their cations for hydrogen on a cation-exchange column (Pohl et al, 1980). The separated anions could then be determined quantitatively in their acidic form by conductimetric method in a matrix of de-ionised water. The system is very good for the analysis of environmental sulphur ions because of the good resolution obtainable for sulphite and sulphate ions in combination (Sawicki et al, 1977; Hansen et al, 1979; and Dasgupta et al, 1982). In general, suppressed ion chromatography has several disadvantages (Miller, 1982). The first is the necessity for background suppression of the eluent which must be an alkali so that after neutralisation by the suppressor column it will have a low conductance. Regeneration of the rapidly exhausted suppressor column, a time consuming step is a periodic necessity. The suppressor column also reduces the conductivity of weak acid anions such as cyanide and borate rendering them difficult to determine except at high concentrations or using other types of detectors. The suppressor column contributes greatly to the band broadening of the system and so impact both resolution and detection limit through unnecessary peak broadening. Finally, the phases available for the columns are low pressure materials and are not compatible with most conventional HPLC.

The non-suppressed ion chromatography was proposed independently by Gjerde et al (1979) and Harrison et al (1979). In the two systems, good resolution and sensitivity of detection were achieved for various anions on specially prepared low capacity anion exchange resin by using eluents with very low conductance so that the detectors signal due to the sample anions are significantly above the background. The two systems make use of a specially designed high performance conductivity detector with a wide dynamic range and high electronic suppression but differed in the material of the ion exchange column. Harrison et al. used the Vydac 302 I.C. column while Gjerde et al used the XAD-1,2,4. Non-suppressed ion chromatography is performed using conventional liquid chromatograph instrumentation.

In this study, sulphate analysis was done by means of non-suppressed ion chromatography. The system used consisted of a Perkin-Elmer Series 4 liquid chromatograph, a Vydac Model 302 IC4.6 low

capacity anion separator column, a Model 21 liquid chromatograph conductivity detector and a Linseis XT strip chart recorder. Injector loop volume was 0.5 cm^3 and samples of 1.0 cm^3 were injected with a Hamilton Co. gas-tight No. 1001 microlitre syringe. Operation was at ambient temperature which fluctuated much at 23°C ± 1.5° but the column was thermally isolated to minimise the effect of the temperature fluctuation and the detector was provided with temperature compensator to correct base-line drift. Seven potassium hydrogen phthalate (KHP) eluents with pH range of 4.5 to 6.0 and a concentration range of 0.5 mM to 10mM were prepared. The pH adjustment was done with solid $Na_2B_4O_7$. The eluent description and the retention time which each eluent gave for a sample containing sulphate only are shown in Table III.24. The eluents were degassed by sparging with helium at a pressure of 2 bar for twenty minutes before starting the pump. Eluent flow rate used in all the runs was 2 $cm^3\ min^{-1}$ and the pump was run for at least one hour to equilibrate before the injection of the sample. The process of degassing and equilibrating was repeated each time the eluent was changed.

It was observed that eluents of concentrations below 10.0 mM failed to elute sulphate. The reason could not be traced and so only eluents of concentration of 10 mM were used.

Calibration

As a preliminary to determining the sulphate content of the aerosols, a calibration curve was obtained for sulphate ion (Fig. III.18) using sulphate ion concentrations (μM) and HPLC operationg parameters listed in Table III.25. The sulphate ion was derived from $(NH_4)_2SO_4$ of AR standard solutions. The calibration factor obtained from the slope of the line is 5.75×10^{-7} M mm^{-2}

Since there was a substantial loss of aerosol as a result of impaction at bends in the flow reactor, a condition which escalated as the number of tubes increased, method of calibration was devised to relate the concentration of sulphate measured in the solutions used to absorb the aerosols, to the actual sulphate concentrations in the droplets. To this end, with foreknowledge of the mass concentration of droplets in the aerosol (measured by membrane filter deposition to be

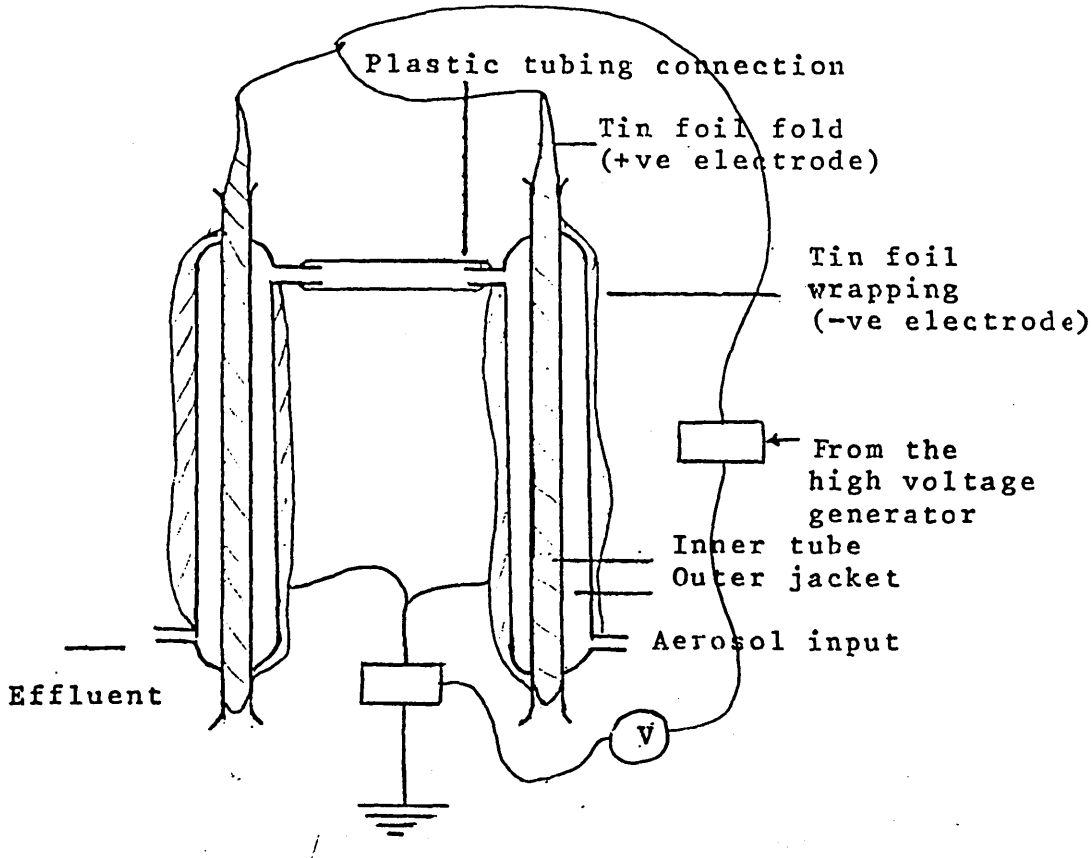


Figure III.17:-Schematic diagram of the electrostatic precipitator.

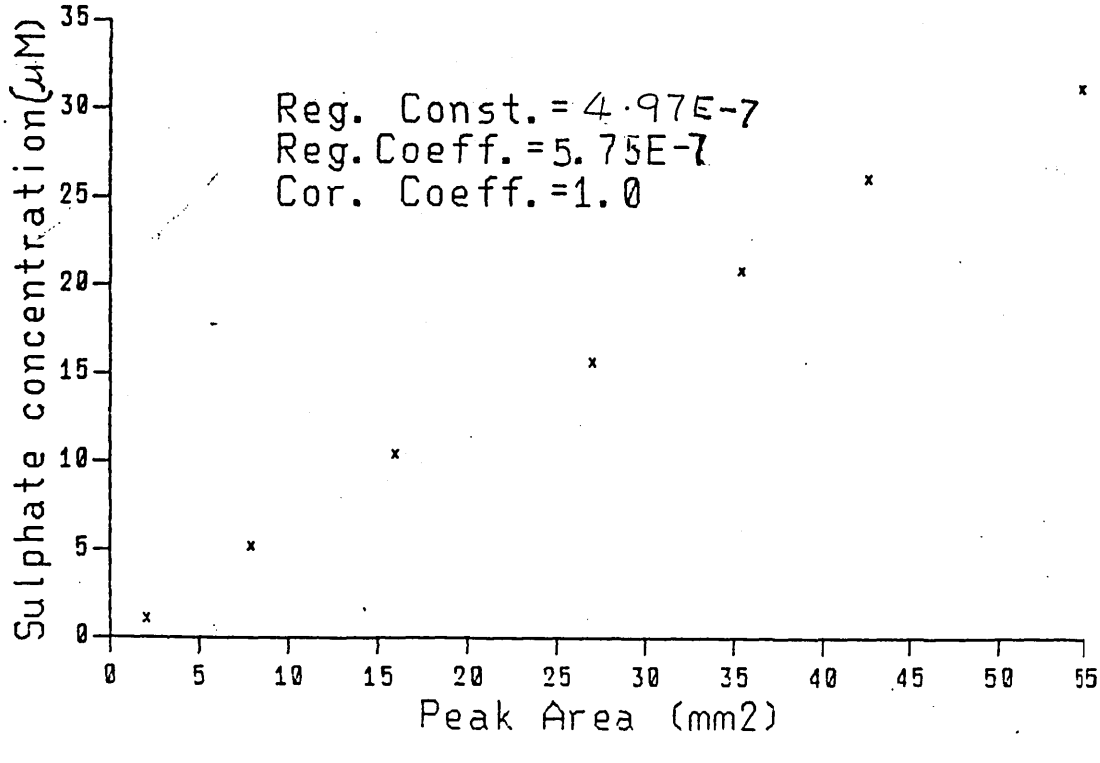


Figure III.18:-Sulphate ion calibration curve.

1.6 g m^{-3}), solutions of sulphate of convenient concentrations (1.875, 2.2 2.5 and 2.8 mM) were used as master solutions in the generator. The absorbing solution was divided between the dreschel bottles arranged in series and carrying sintered bubblers. 100 dm^3 of each of the four calibration aerosols were passed directly from the generator to the absorber and the sulphate concentrations were determined by ion chromatography using the calibration factor obtained from Fig. III.18. The peak areas and the coresponding sulphate concentrations of the four aerosol samples are listed in Table III.26. The data for the tube combinations used in the experiments are given in Table III.27 in the form of chromatography peak areas (the declining values illustrate the effect of aerosol deposition).

The loop sulphate content for each aerosol transfered directly without deposition occuring and the corresponding HPLC peak area for each of the eight reactor tube combinations were fitted into regression lines (Fig. III.19); the reciprocal of the slopes of which are the calibration factors and are listed in Table III.28.

Sample Collection and Analysis

Real aerosol samples were collected for the following reacting gas partial pressures-

a. 1 ppm SO_2 and 1 ppm NH_3

b. 1 ppm SO_2 and 2 ppm NH_3

c. 50 ppm SO_2 and 1 ppm NH_3

The SO_2 and NH_3 flowed through two side gas lines, and were subjected to two-stage dilution to obtain the concentrations at which they were used in this study. Both gases were obtained from BOC gas cylinders of concentration 1000 vpm in nitrogen. The cylinder regulators were the Matheson two-stage corrosion-resistant special gas regulators. The gases were filtered at the cylinder heads by means of qualitative standard filter papers held in a 13-mm stainless steel filter holders. The pressure in each of the gas lines was monitored by means of an open tube mercury manometer. After filteration, the gases, NH_3 and SO_2 were metered into mixers labelled Mx1 and Mx2 respectively in the block diagram by means of rotameters (size B for NH_3 and size RS for SO_2) supplied by Meterate GPE. Downstream of the rotameters, capillary manometers made in the departmental glass work shop were used for

Table III.24 Characteristics of KHP eluents in sulphate separation

pH	Eluent Conc. (mM)	Retention Time (min)
6.0	0.5	-
6.0	1.0	-
5.1	5.0	-
4.5	10.0	9.5
4.8	10.0	8.0
4.9	10.0	7.5
5.0	10.0	6.5

Table III.25 Sulphate solution calibration

Sulphate ion concentration ppm	Sulphate ion concentration μM	HPLC Peak Areas (mm^2)
0.1	1.04	2.1
0.5	5.21	8.0
1.0	10.42	16.0
1.5	15.63	27.0
2.0	20.83	35.4
2.5	26.04	42.6
3.0	31.25	54.9

Ion chromatographic parameters:
Eluent: KHPhthalate ; 10mM and pH = 4.9
Eluent Pumping Rate: 2 cm^3 min^{-1}
Sample loop size: 500 μl
Recorder voltage: 1 V
Detector Range: 10

Table III.26: The peak areas and corresponding sulphate concentrations for the aerosol samples tranfered directly from the generator

Master Solutions Concentrations (M)	1.87	2.20	2.50	2.80
Aerosol Volume sampled (dm^3)	100	100	100	100
Scrubbing solution volume (cm^3)	30	30	30	30
Sample Peak areas (mm^2)	17.39	20.40	23.18	25.96
Sample Concentrations (μM)	10.00	11.73	13.33	14.93

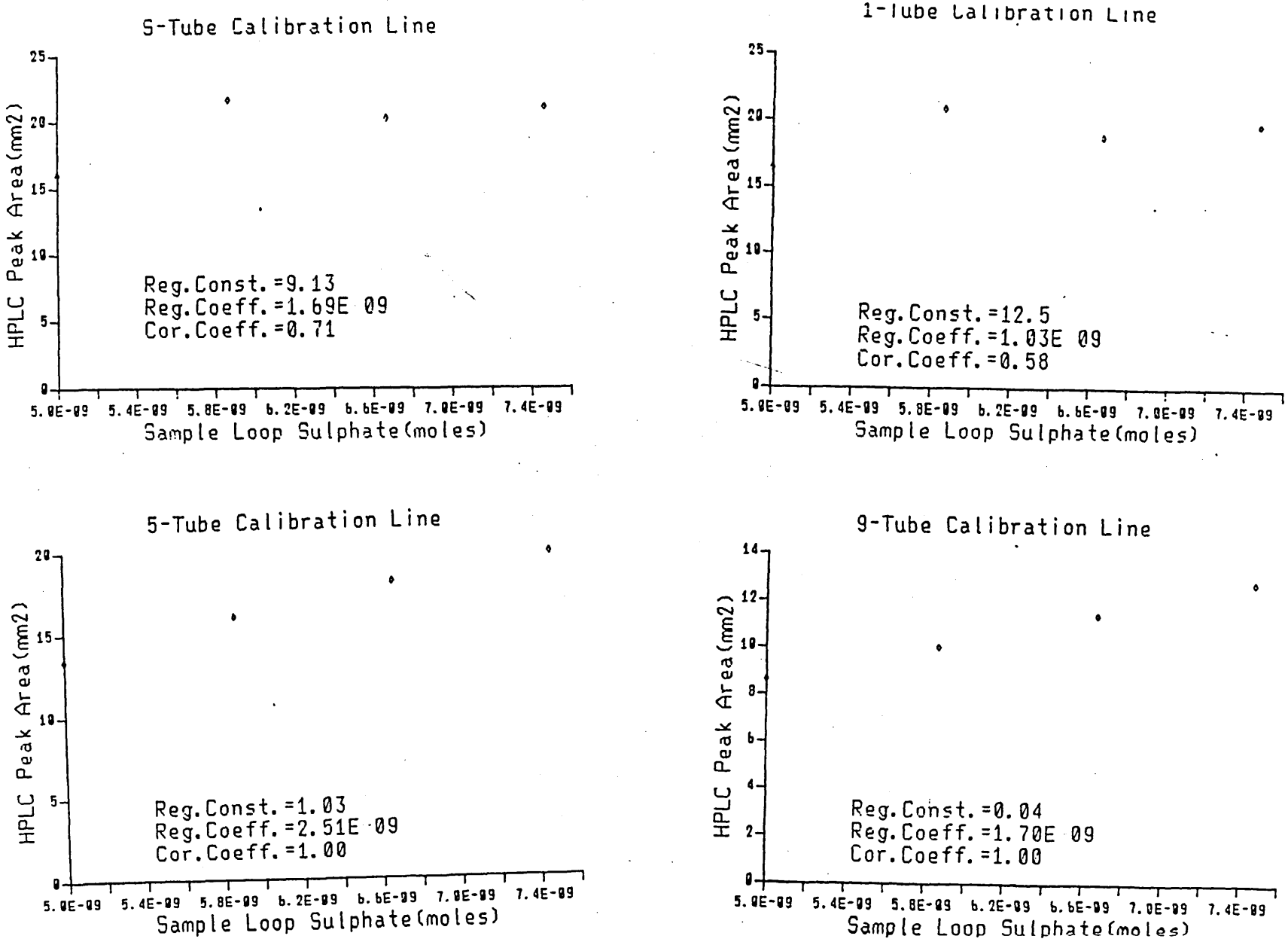


Figure III.19:-The sulphate ion calibration curves for eight residence times.

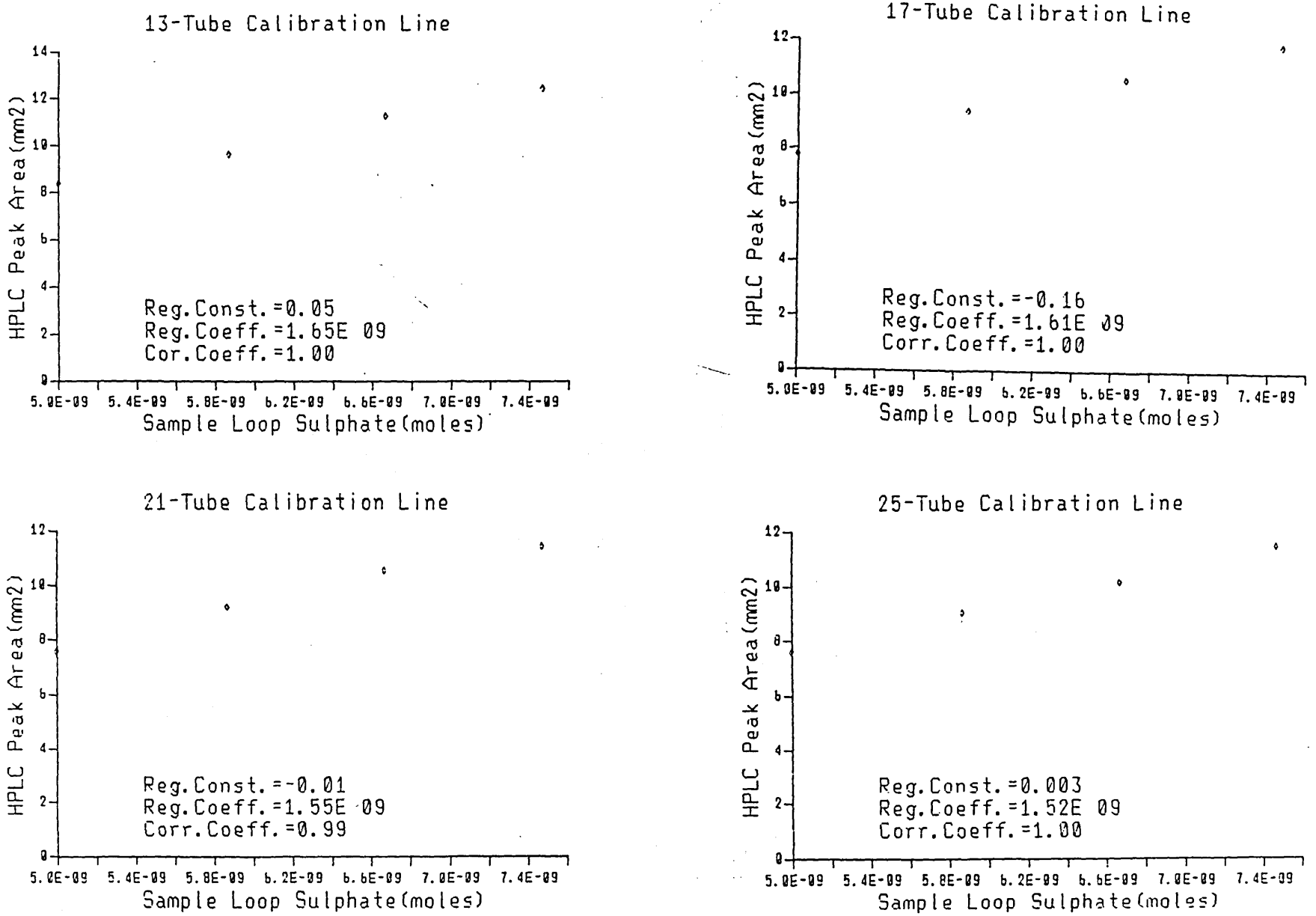


Figure III.19:-The sulphate ion calibration curves for eight residence times (contd.).

metering very low flow rates where the rotameters were not sensitive enough. Scrubbed filtered air from a point up-stream of the humidifier in the main air line was also metered into each of the two mixers by means of a size E3 rotameter supplied by GEC-Elliott Process Instruments at such a flow rate as to make up a total flow-rate of 250 cm^3 min^{-1} each for the required volume mixing ratio of the reacting gases. The air diluted gases were each let into a one-litre equilibriating chamber composed of two 0.5 dm^3 dreschel bottles connected in series. In the case of NH_3, the diluted equilibriated gas flowed into the mixer labelled Mx3 into which aerosol from the generator also flowed. The mixer had a volume of 30 cm^3. The mixture of NH_3 and aerosol flowed into Mx4 into which the equilibrated SO_2 flowed. The reacting aerosol was then directed into the reactor from where it was sampled after contact times of 0.65, 1.1, 5.1, 9.1, 13.2, 17.2, 21.2 and 25.2 minutes.

The sampling procedure which was also used in sampling for calibration is described more fully at this point. The aerosol flow-rate (4 l min^{-1}) and the conditions of reactor temperature (25°C) and humidity (98%) were maintained throughout sampling. The sampling procedure aimed at achieving a quantitative capture of SO_4^{2-} in droplet at an aerosol flow-rate appropriate to the parameters of the study with simultaneous exclusion of unreacted SO_2. Exclusion of SO_2 was efficiently achieved by the use of PbO_2-coated diffusion denuder described earlier. Unreacted NH_3 was not an interferent and hence presented no problem. However, re-entrainment of droplets that passed through the absorbing solution into the air-stream was a major obstacle to quantitative capture of SO_4^{2-} when samples were obtained by scrubbing the aerosol with a suitable absorbing solution. Experiments on the use of a scrubber to capture aerosols reported earlier showed that the scrubbing solution was not a perfect aerosol sink but that a small but significant quantity passed through the solution. This is consistent with the observtions of Hryneiwiez (Ferm, 1979). The solution to the problem was the use of two scrubbers in series with up to two-thirds of the scrubbing solution in the first scrubber. After sampling, the fritted bubblers and the tube connecting them were washed with the scrubbing solution in the second scrubber and adding the washing to the first scrubber. Step taken to accumulate sufficient sample for chemical analysis was choosing a sampling time of

twenty-five minutes during which time one hundred litres of the aerosol was sampled. Finally, the sampling method aimed at minimal contamination during sampling and sample handling.

The scrubbing solution and the volume of aerosols sampled were the same as those of the calibration aerosols. Samples were obtained in duplicate and after the HPLC analysis the peak areas were averaged and listed in Table III.29. Using these peak areas and the calibration factors (Table III.28), the aerosol sulphate concentrations of the runs (6, 7 and 9) were calculated from the emperical formula

$$[SO_4^{2-}]_A = pfv/lV$$

where

$[SO_4^{2-}]_A$ = aerosol sulphate concentration (moles dm^{-3} aerosols)
f = calibration factor (moles mm^{-2})
p = peak area (mm^2)
v = volume of scrubbing solution after sampling (cm^3)
l = sample loop volume (cm^3)
V = volume of aerosols sampled (dm^3)

This formula can be modified to express the SO_4^{2-} yield in terms of the volume of droplets sampled if the aerosol mass concentrations were measured.

Table III.27 Calibration Curves - Peak areas and HPLC loop sulphate content (loop size = 500µl)

Sample $[SO_4^{2-}]$ (moles dm^{-3})	10 µM	11.73 µM	13.33 µM	14.93 µM
loop SO_4^{2-} content (moles)	5.0×10^{-9}	5.87×10^{-9}	6.67×10^{-9}	7.47×10^{-9}
Reactor tube combinations				
S-Tube	16.0	21.6	20.2	21.0
1-Tube	16.4	20.8	18.8	19.8
5-Tubes	13.4	16.0	18.0	19.6
9-Tubes	8.6	10.0	11.4	12.8
13-Tubes	8.4	9.6	11.2	12.4
17-Tubes	7.8	9.4	10.6	11.8
21-Tubes	7.6	9.2	10.5	11.4
25-Tubes	7.6	9.0	10.1	11.4

Table III.28 Calibration factor for each Residence Time (based on the sample loop SO_4^{2-} content)

Tube Combination	Residence Time (min)	Calibration factor (moles mm^{-2})
S	0.65	2.96×10^{-10}
1	1.1	3.23×10^{-10}
5	5.1	3.95×10^{-10}
9	9.1	5.84×10^{-10}
13	13.2	6.04×10^{-10}
17	17.2	6.30×10^{-10}
21	21.2	6.45×10^{-10}
25	25.2	6.58×10^{-10}

Table III.29 HPLC Peak areas of real aerosol samples

Residence Time (min)	Peak Areas (mm^2) Run 6 P_{SO_2}=1, P_{NH_3}=1	Run 7 P_{SO_2}=1, P_{NH_3}=2	Run 9 P_{SO_2}=50, P_{NH_3}=1
.65	9.7	10.18	9.52
1.1	9.6	10.20	9.80
5.1	10.10	12.90	10.70
9.1	9.90	11.82	9.80
13.2	9.60	11.56	9.48
17.2	9.40	11.22	9.84
21.2	9.36	12.08	9.88
25.2	9.28	12.14	9.98

CHAPTER IV

Results and Discussions

In the previous chapter, the equipment and experimentation were described for the following investigations -

i. the light scattering pattern and size distribution of $(NH_4)_2SO_4$ aerosols;

ii. the oxidation of SO_2 in $(NH_4)_2SO_4$ droplets in the presence of NH_3 and

iii. the oxidation of SO_2 in $MnSO_4$ droplets in the presence of NH_3.

In this chapter, the results obtained in those experiments are discussed and explained in terms of the physical and chemical processes that interplay in the aerosol stream. The processes could in principle include oxidation, condensation/evaporation, coagulation, and droplet removal from the stream through sedimentation, diffusion, thermophoresis and impaction at reactor tube bends.

In the first section, the light scattering pattern of $(NH_4)_2SO_4$ solution aerosols and their size distribution are discussed. In the second section, the characteristics of $(NH_4)_2SO_4$ and $MnSO_4$ aerosols in the presence of reacting gases (SO_2, NH_3 and O_2) are discussed. The particle size distribution was characterised by the ZOLD parameters (defined in section II) obtained in each case by inverting the experimental light scattering intensity using the programme SEARCH. The chemical analysis of the sulphate produced by the oxidation of SO_2 is discussed and a contribution made towards elucidating the rate constant of the reaction. Finally, the results obtained in this study are applied to the dispersion and reaction of SO_2 in a stack plume.

IV.1 Description of the Model on which the Present Work is Based

Sulphur dioxide and NH_3 of known partial pressures and oxygen from air are simultaneously absorbed in submicrometer size aerosol droplets of known size distribution and phase volume ratio in which the SO_2 is oxidized to sulphate ion. The droplets generated from master solutions

of known sulphate concentrations have concentrations equal to those of the master solutions. Only the droplet phase oxidation is considered; gas phase oxidation being negligible because of the absence of sunlight and such highly reactive oxidants as O_3, H_2O_2 and free radicals. The phase volume ratio of the aerosols is so small that for most SO_2 and NH_3 partial pressures used in the study the gases are not significantly depleted within the time span of the experiment.

The entire aerosol system is modelled as a plug flow reactor. Each droplet, however approximates a batch reactor with an expanding volume the reactants in which are being continuously reinforced by diffusion from the bulk gas phase. As a result of their small size, the characteristic diffusion time is so small compared to the time of the chemical processes that mass transfer processes are neglected both in the gas and aqueous phases. Hence only the pertinent chemical reactions intrinsic to the system are considered. They include equilibrium (absorption, hydrolysis and ionisation) and non-equilibrium (oxidation) reactions with the latter being much slower then the former. Their rates are independent of most physical situations but depend on such chemical properties of the system as pH and the concentration of the reacting species as well as the temperature through its relation with the equilibrium and rate constants. The rate equation for the uncatalysed system is taken from the model of Scott et al (1967)

$$SO_3^{2-} + \tfrac{1}{2}O_2 = SO_4^{2-} \; ; \qquad (1)$$

$$\frac{d[SO_4^{2-}]}{dt} = k_0[SO_3^{2-}] \qquad (2)$$

that is sulphite ion is the substrate for attack by oxygen and the reaction is first and zero orders with respect to SO_2 and oxygen respectively.

As SO_2 is oxidized to sulphate and the total sulphate loading of the droplet increases, it grows by the accretion of water vapour from the bulk gas phase as a result of Raoult's solute effect. Thus, neglecting coagulation and interactive forces that affect size distribution, increase in droplet size is equated to the droplet sulphate loading resulting from the oxidation of SO_2.

IV.2 Light Scattering Study of $(NH_4)_2SO_4$ Aerosol

The changes that took place in $(NH_4)_2SO_4$ aerosol as a result of changes in master solution concentration, aerosol generator flow_rate, relative humidity and residence time are discussed and explained with reference to condensation and coagulation. Other processes that determine the evolution of particle size distribution and the mass and number concentrations such as loss in the tube are not taken into consideration since calculations on the simultaneous effects of these are very complicated. (Okuyama et al, 1980).

IV.2.1 The Effect of Master Solution Concentration

An attempt was made at generating aerosols from distilled water. The angular distribution of scattered light intensities obtained are listed in Table IV.1. A two-tailed t-test was carried out to determine the significance of the scattered light intensity in comparison with the background intensity. With t_0(=1.495) less than t 0.05, 14 (=1.761), the scattered light intensity is not significantly different from the background intensity. This is also reflected in the close similarity of the curves of the angular distribution of the background and scattered intensities (Fig. IV.1). This means that the aerosols did not reach the sampling point. When followed by means of a laser beam it was discovered that they disappeared before reaching the reactor tube. When the exit was blocked to create high pressure in the reactor and then opened suddenly to release the pressure, aerosols were observed momentarily throughout the length of the reactor. The sudden lowering of pressure in the reactor caused adiabatic cooling of the water vapour ladden air stream resulting in supersaturation and consequently nucleation of water molecules. The initial diameter of the droplets formed was likely to be below 0.1 μm and consequently were subject to Kelvin size effect. Since the saturation ratio in the reactor was usually below 1.0, in the absence of stabilizing condensation nuclei, the droplets quickly evaporated since their life-time of 4.7×10^{-5} seconds (calculated from equation II.70) is very short. However, Kousaka et al (1979) observed a longer life-time for pure water droplets grown on inert nuclei. They showed that there

Table IV.1 Angular Distribution of Scattered Light Intensities

Scattering angle	Background Intensity(mV)	Scattered Intensity(mV)
9	30.51	40.97
18	13.29	9.04
27	11.56	10.07
36	8.70	8.91
45	7.14	6.37
54	5.73	5.14
63	5.05	6.10
72	4.77	5.74
81	5.37	5.69
90	5.62	6.85
99	6.33	6.71
108	7.06	9.13
117	9.14	11.04
126	12.37	17.49
135	20.97	23.34

Table IV.2 Aerosol ZOLD parameters as a function of master solution concentration

Run	Master Soln (M)	d_{mode} (μm)	σ_0	*MMD(μm)
1	0.001	0.061	0.442	0.0994
2	0.005	0.085	0.641	0.237
3	0.01	0.333	0.310	0.423
4	0.05	0.417	0.361	0.578
5	0.10	0.458	0.280	0.557
6	0.50	0.504	0.314	0.645

*MMD or VMD = $d_{mode}\exp(2.5\sigma_0^2)$ (Carabine et al, 1978)

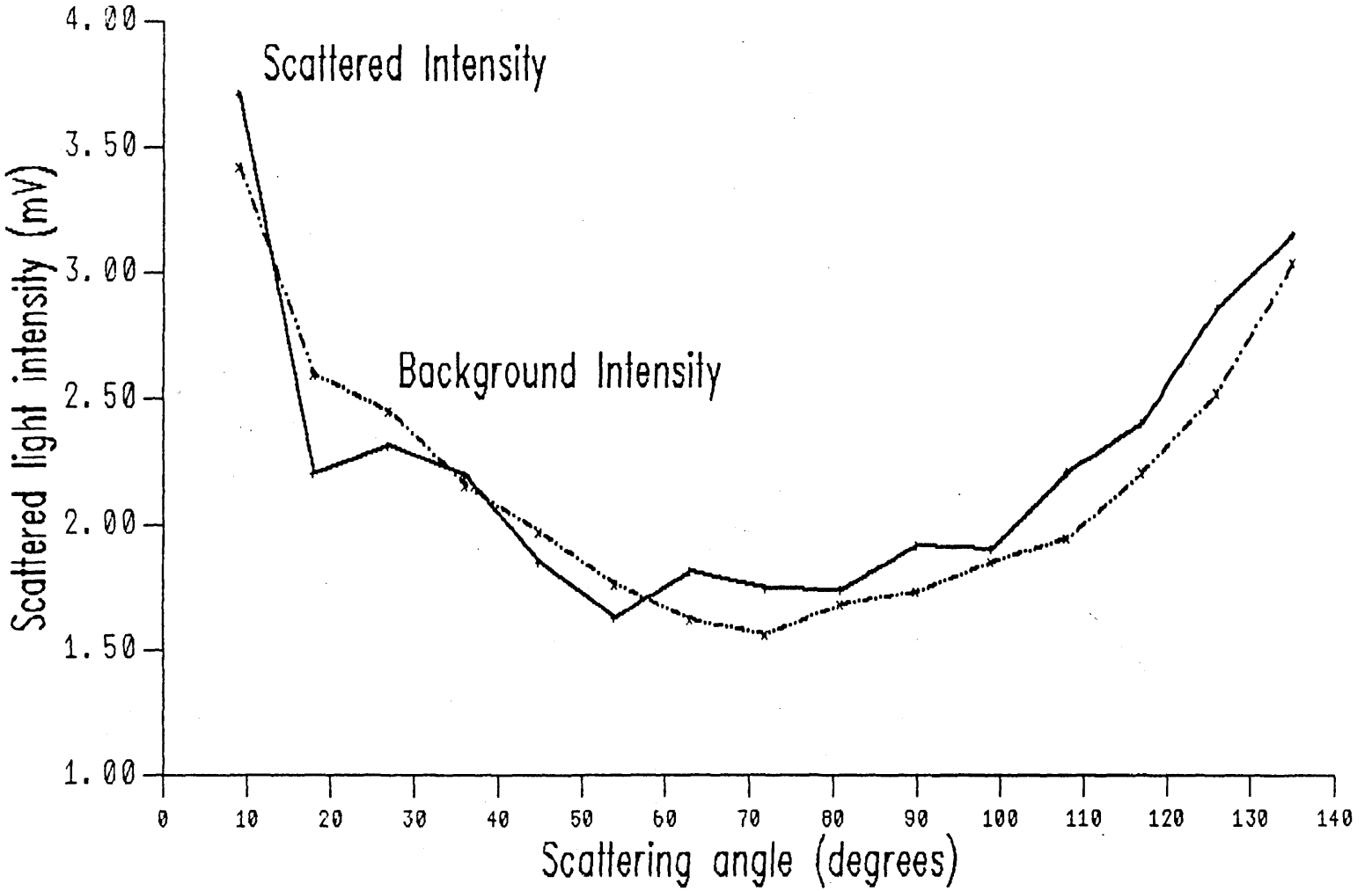


Figure IV.1:-Angular distribution of scattered and background intensities of pure water mist.

was no appreciable change in size distribution of such droplets after 4.0 seconds residence time. This was explained in terms of the droplet number concentration of the aerosol; the stabilizing effect of the inert support was not considered.

On the basis of the lack of stability of pure water droplets, the data in Table VI.1 was not inverted to obtain the ZOLD parameters. Use was not made of pure water droplets in this study.

Aerosol samples generated from $(NH_4)_2SO_4$ master solutions of concentrations ranging from 1 mM to 0.5 M were studied by the light scattering method. Fig. IV.2 shows the angular distributions of the scattered light intensities for the various concentrations of master solutions. The curves in the figures did not show any characteristic inflection points and hence no approximate conclusions can be drawn from their shapes. The ZOLD parameters obtained from inverting these angular distribution of scattered light intensities are listed in Table IV.2.

Droplet size increased with master solution concentration (Fig. IV.2a). Since the droplet size of aerosols generated by air-blast atomisation has a strong dependence on generator parameters (Tu et al, 1978) but a weak dependence on the master solution concentration through its viscosity and density, droplet size should be independent of master solution concentration if generation conditions are constant. These facts however were not verified in this study because the factors that alter the aerosol characteristics could not be eliminated unless the aerosols were analysed as they emerged from the jet. Granting that the initial droplet size was independent of the master solution concentration the observed difference in size after a residence time is explained in terms of the dependence of the stable droplet size on P/Q (the ratio of moles of solute to water in the master solution) and the relative humidity given by the equation

$$RH = \left[1 + i\ P/Q\right]^{-\rho/\rho'} \exp \frac{4\sigma' M}{\rho' RTd} \qquad \text{IV.1}$$

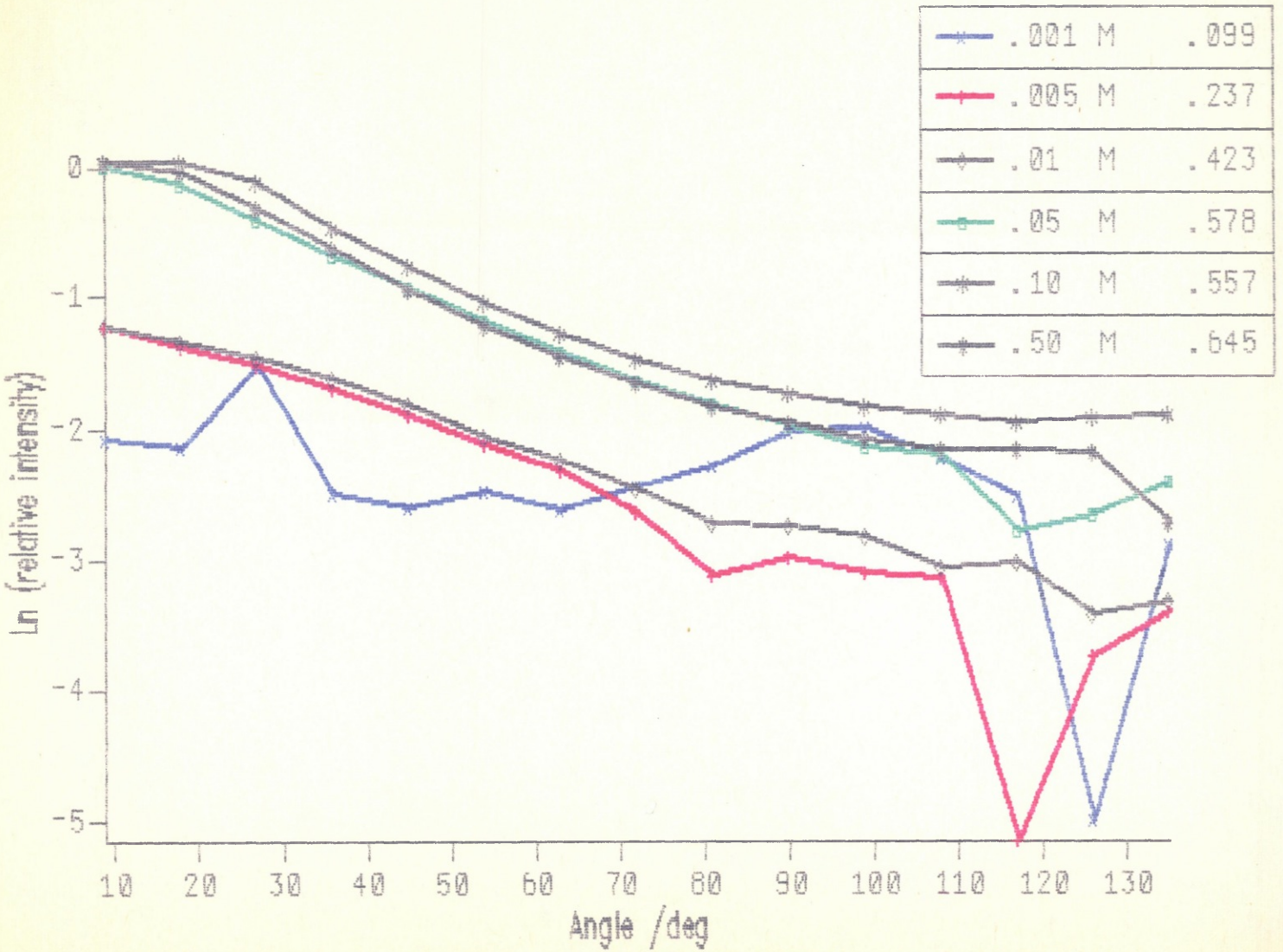


Figure IV.2 Variation of scattered light intensity pattern with the master solution concn.

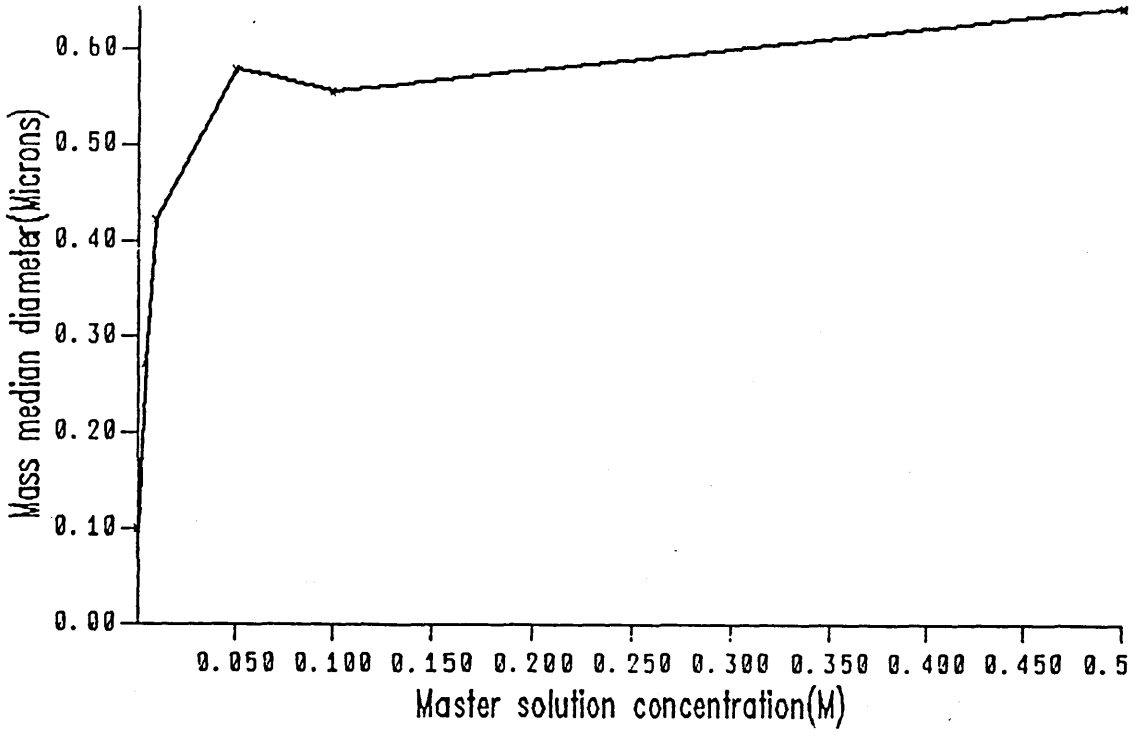


Figure IV.2a:-The variation of droplet size with the master solution concentration.

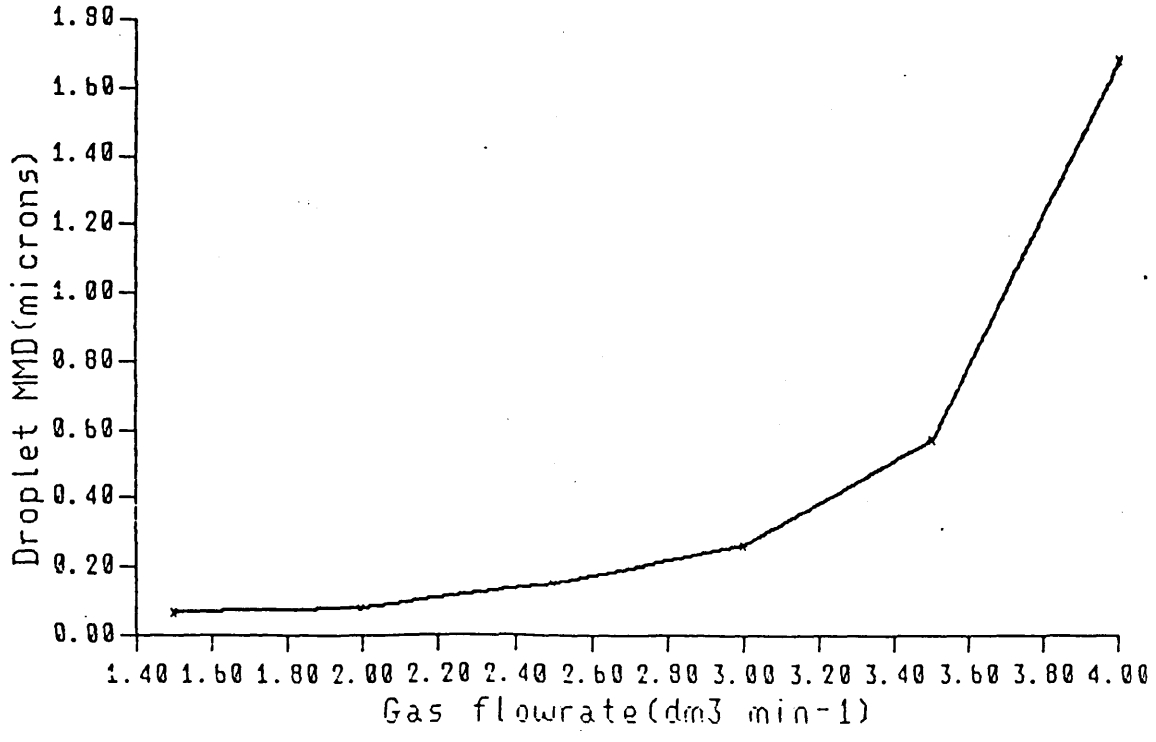


Figure IV.3b:-Variation of droplet size with the dispersion gas flowrate (Master solution 0.1M-$(NH_4)_2SO_4$).

(Vohra et al, 1970) which is a modified form of equation II.63. This is valid only for residence times smaller than the characteristic time for growth by condensation.

The ZOLD spread does not show any characteristic trend and so it is not easy to determine the part played by coagulation in determining the size distribution. This is not likely to be much.

IV.2.2 The Effect of Generator Flow-rate

The effect on size distribution of flow rate in the generator was studied in the range 1.5 to 4.0 dm^3 min^{-1}. The ZOLD parameters, and droplet mass concentration of the aerosols collected from each of the flow-rates studied are listed in Table IV.3.

No aerosols were formed at a flow-rate of the dispersion gas below 1.5 dm^3 min^{-1}. Between the generator flow-rates of 1.5 and 3.0 dm^3 min^{-1} the modal diameter showed no trend (Fig. IV.3). This is contrary to the observation by Maddock (1974) of changes in modal diameter in this flow regime. The reason is that in the latter work the master solution was highly hygroscopic (as a result of high concentration) H_2SO_4 and hence grew by condensation at a much shorter time than the $(NH_4)_2SO_4$ solution. However, a graph of VMD against generator flow_rate (Fig. IV.3b) (see p 196) shows a steady increase in droplet size with flow_rate. Between 3.0 and 4.0 dm^3 min^{-1}, the modal diameter increased very much. At 4.0 dm^3 min^{-1} the volume of aerosol generated was so excessive that the walls of the generator and the reactor were soon covered with droplets and the level of the master solution in the nebulizer decreased appreciably thereby affecting the parameters of the generator. The increase in size with generator flow-rate was presumably caused by the increase in efficiency of the generator. The expected decrease of droplet size with increasing generator flow-rate (Fuchs et al, 1966) was not realised in this study, probably because the flow-rates utilised were too low to exhibit that trend.

Fig. IV.3a shows the scattering patterns of the aerosols. For dispersing gas flowrate below 2.5 dm^3 min^{-1} there was no characteristic scattering pattern showing the inefficiency of aerosol generation at these flowrates.

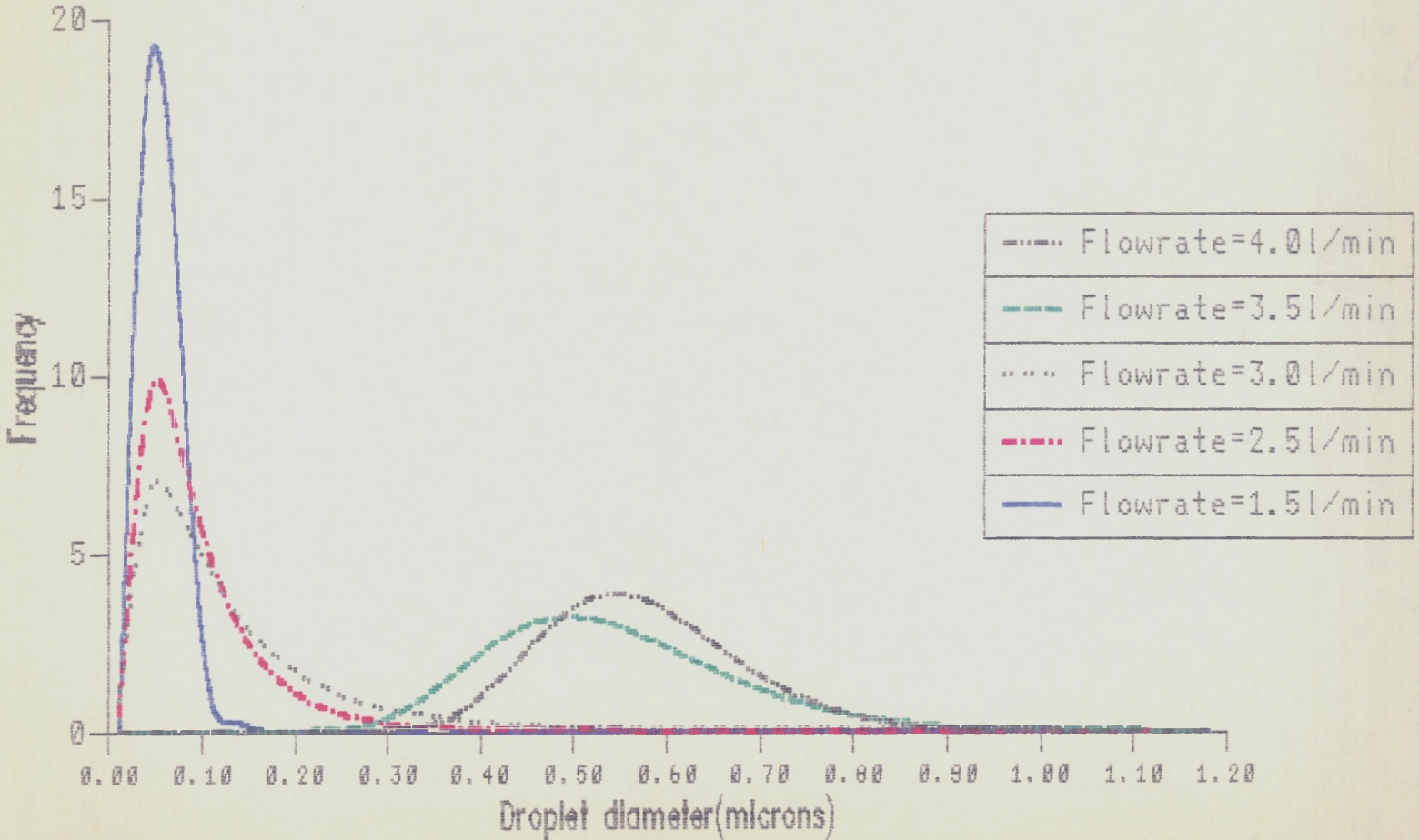


Figure IV.3:-Effect of dispersing gas flowrate on aerosol size distribution.

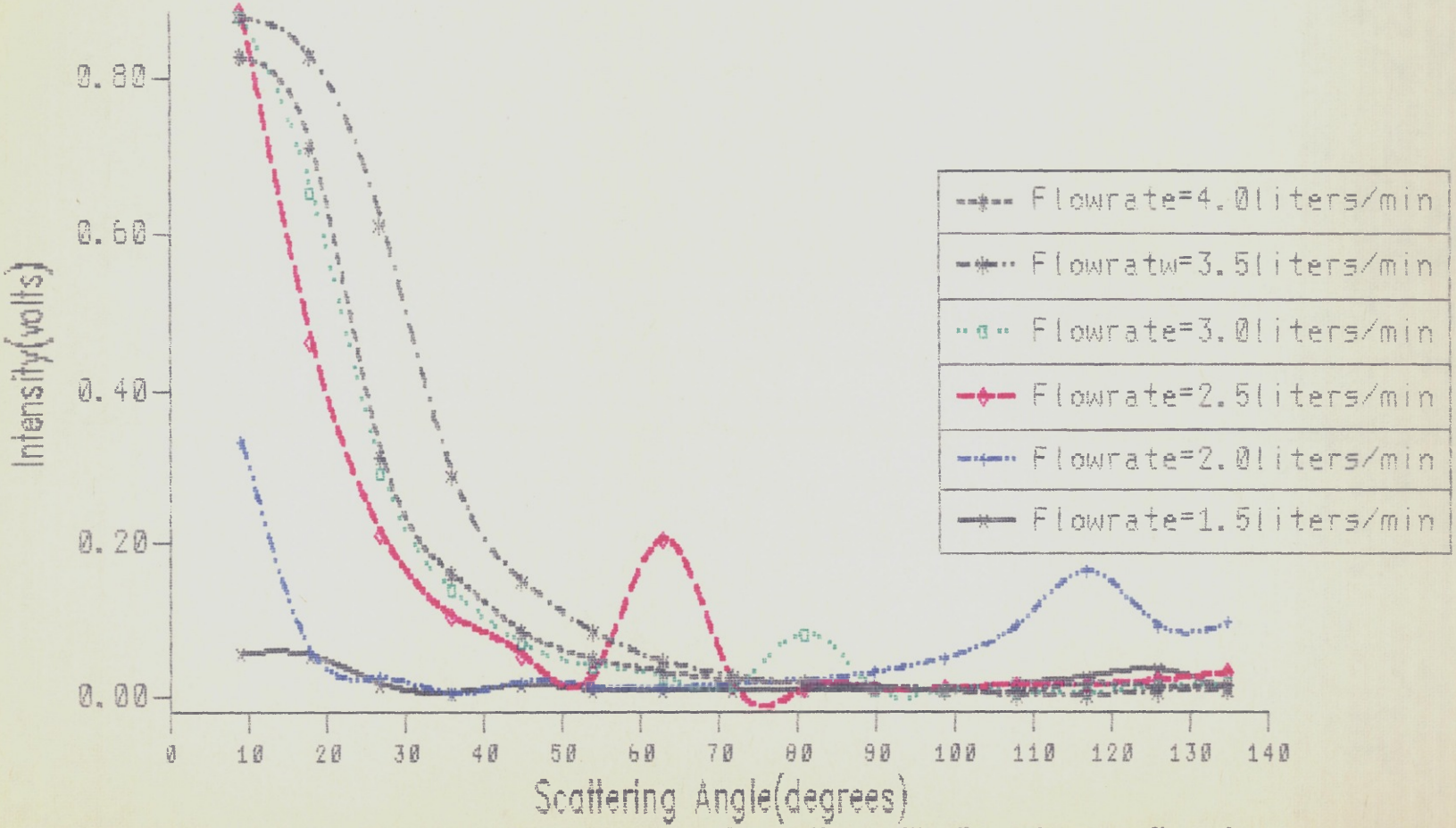


Figure IV.3a:-Variation of angular scattering pattern with dispersing gas flowrate.

Table IV.3 Effect of dispersion gas flow-rate on the size parameters and droplet mass concentration of aerosols
(master solution 0.1 M - $(NH_4)_2SO_4$)

Run	Flow-rate (dm^3 min^{-1})	d_{mode} (μm)	σ_0	Droplet mass conc. (g cm^{-3})
1	1.5	0.05	0.324	$1x10^{-8}$
2	2	0.052	0.403	$1.2x10^{-8}$
3	2.5	0.050	0.660	$6.3x10^{-8}$
4	3.0	0.051	0.811	$1.0x10^{-7}$
5	3.5	0.493	0.243	$3.8x10^{-7}$
6	4.0	1.543	0.186	$3.0x10^{-6}$

Table IV.4. ZOLD parameters of Aerosols at Different relative humidities; Master solution concentration 0.1 M;
Residence time = 1031 seconds.

Run	%r.h.	d_{mode} (μm)	σ_0	VMD
1	20	0.231	0.104	0.238
2	78	0.179	0.551	0.382
3	82	0.241	0.448	0.398
4	98	0.401	0.296	0.499

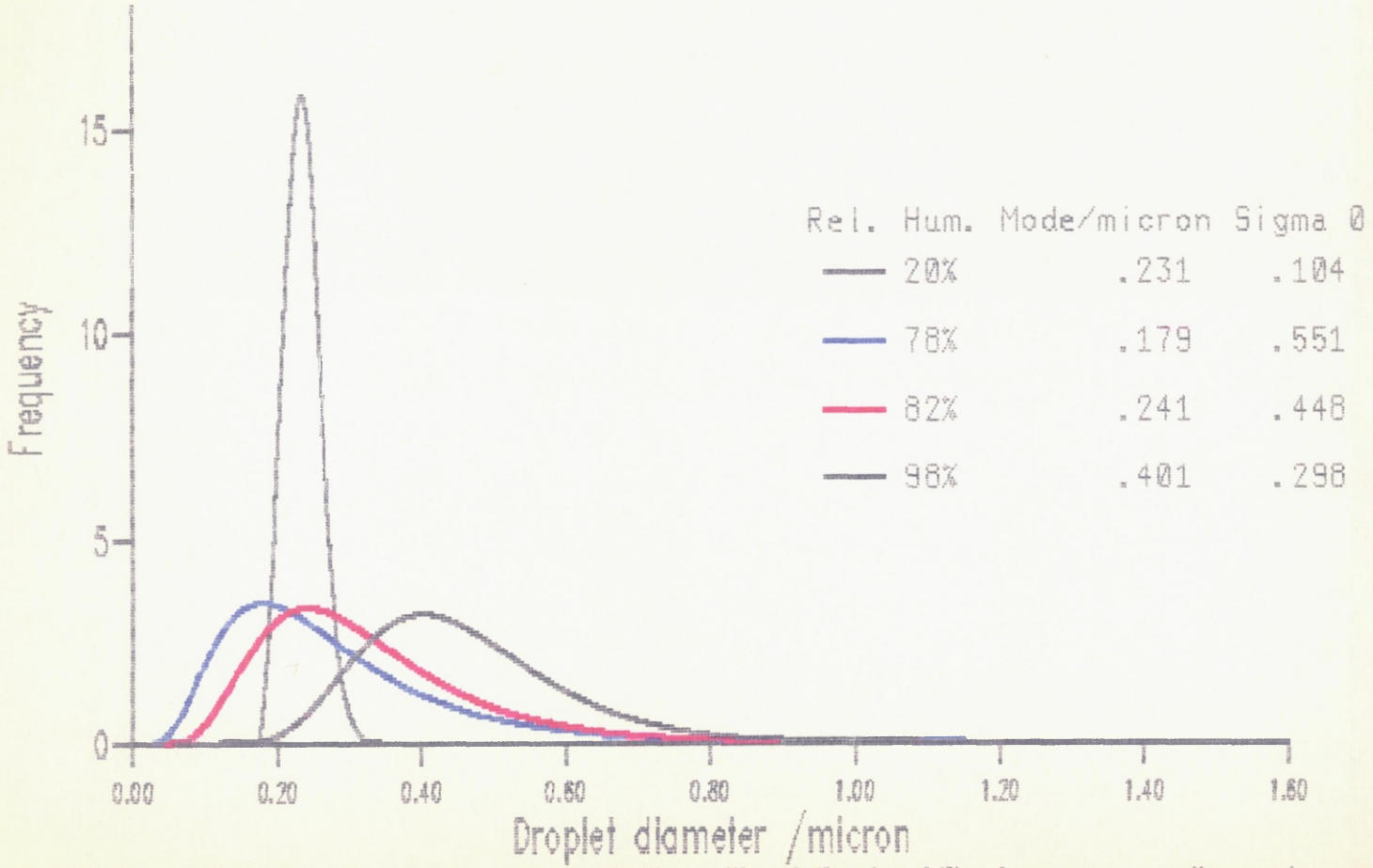


Figure IV.4 Variation of droplet size distribution with relative humidity, for a non-reacting system

IV.2.3 The Effect of Relative Humidity

Table IV.4 shows the characteristics of the aerosol droplets as a function of relative humidity in the reactor in which the humidity was varied between 20% and 98%. The variation of size distribution with relative humidity is depicted in Fig. IV.4.

The growth in droplet size is attributed to nucleated condensation. Maddock (1974), using the partial differential equation for the diffusion of water vapour into H_2SO_4 showed that a droplet of diameter 1.0μm would attain equilibrium diameter in about 0.01 seconds after exposure to an atmosphere of 50% relative humidity at 20°C. Cains (1975) obtained a value of 0.002 seconds for a 0.5 μm droplet of $MnSO_4$ under identical conditions. It is likely therefore that equilibrium diameter was attained in this experiment in under one second. Sinclair et al (1974) explained the size distribution pattern in terms of differences in coagulation rates at the different humidities and loss in the reactor. This explanation was not verified in this study since the experiment was not designed to study coagulation and loss of aerosols in the reactor. Another plausible explanation is as follows. $(NH_4)_2SO_4$ is a deliquescent salt which undergoes a clear-cut phase transition at a relative humidity of about 81% and room temperature from the dry crystal to a solution droplet (Charlson et al, 1974). Below this therefore, the aqueous droplet from the aerosol generator loses water by evaporation; but above it, the droplet grows by the accretion of water vapour and coagulation to a large size on a large time scale. However, an increase of approximately 1/(1-rh) times the original volume after the deliquescence relative humidity mentioned by Cooper et al (1973) was not observed. The prospects of an indefinite growth of a droplet above a certain relative humidity was mentioned by Carabine et al (1976).

IV.2.4 The effect of Residence Time

In this context, when reactive gases were absent, the variation of aerosol properties (size distribution and number and mass concentrations) is discussed in terms of coagulation only. The

mechanisms that contribute to aerosol loss in the reactor were not studied and so are regarded as not affecting the properties of the aerosols. In the last section, it was seen that the diffusion of water vapour to aerosol droplets was so fast and the relaxation time so short that the effects of condensational growth could not be measured in this set of experiments.

The aerosol size distribution and light scattering pattern at four residence times are shown in Fig.IV.5 and Fig.IV.5a respectively. The scattering in the backward direction continues to diminish in importance as the residence time increases.

Table IV.5 shows the variation of ZOLD parameters with residence time of aerosols generated from 0.1 M $(NH_4)_2SO_4$ solutions. There is an increase in modal diameter with residence time. The higher size in Run 7 than 8 may be attributed to the lower relative humidity in Run 8 than in Run 7. Between Run 1 and 4, the modal diameter increased by a factor of over forty while the spread decreased by about one-third in about nine minutes. Such a rapid size increase and spread decrease is consistent with polydisperse coagulation. At Run 4, the aerosol had acquired a highly monodisperse size distribution as a result of the disappearance of small particles as they were rapidly collected by large ones. This process is helped by the combination of the large absorbing surface of the big particle and the rapid diffusion of the small ones; and so the greater the difference in particle size the greater the effect. Between Run 4 and Run 8, size increase was slower and the ZOLD spread was fairly constant as residence time increased. The increase in droplet size accompanied by increase in dispersity is consistent with monodisperse coagulation in which some particles get larger and so experience enhanced coagulation. However, it will be observed that the change in both size and dispersity with time in this region is very slow, and approximates to a stable size distribution which Friedlander (1977) termed the self-preserving size distribution. According to Hinds (1982) it occurs at a GSD of about 1.5. The interpretation of a stable size distribution is based on the removal of small particles by coagulation and the removal of large ones by sedimentation and impaction at bends.

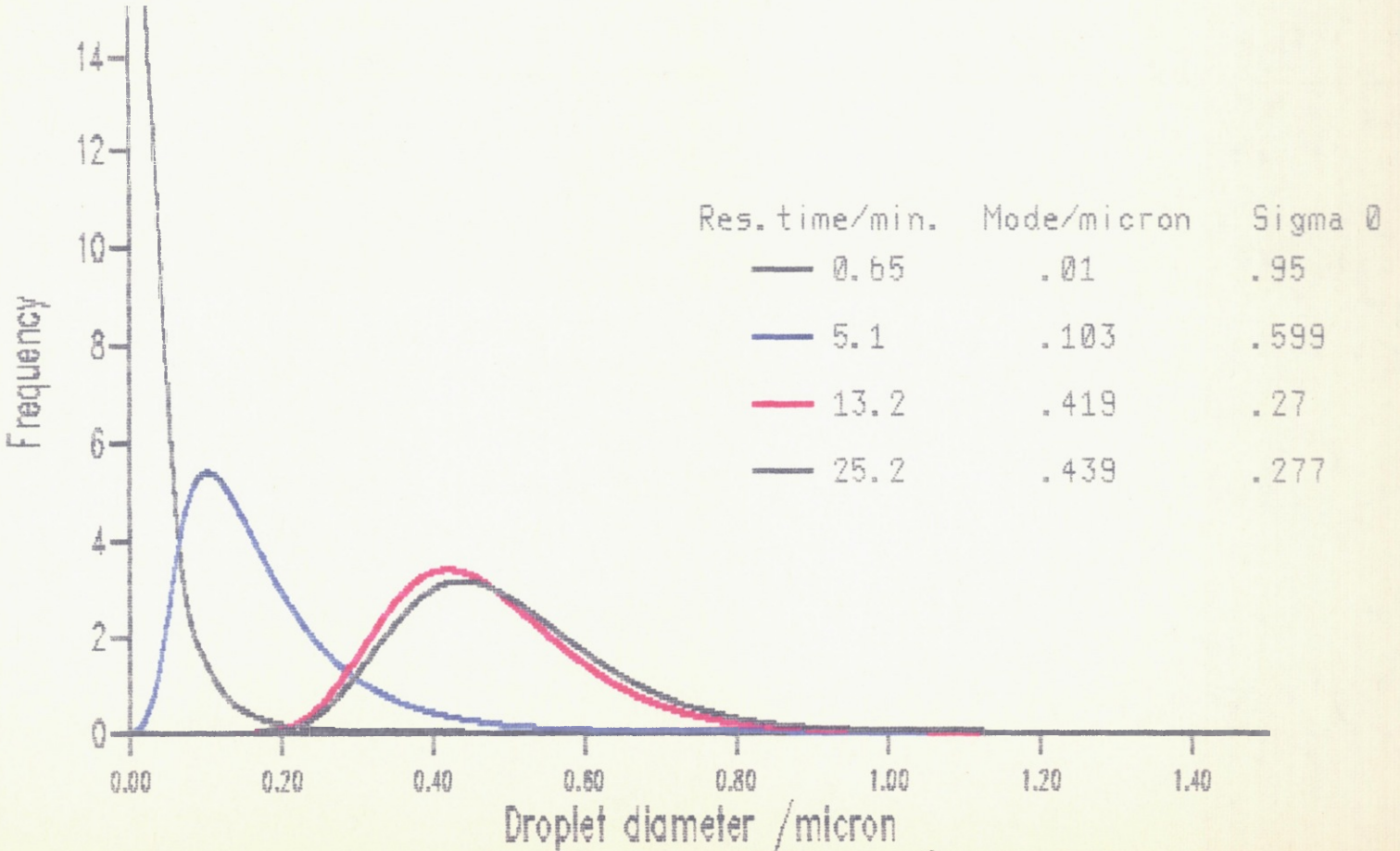


Figure IV.5 Variation of size distribution with residence time with SO2 absent (master soln. 0.1 M ammonium sulphate)

FigIV.5a:- Variation of Light Scattering Pattern with Residence Time in a Non-Reacting System.

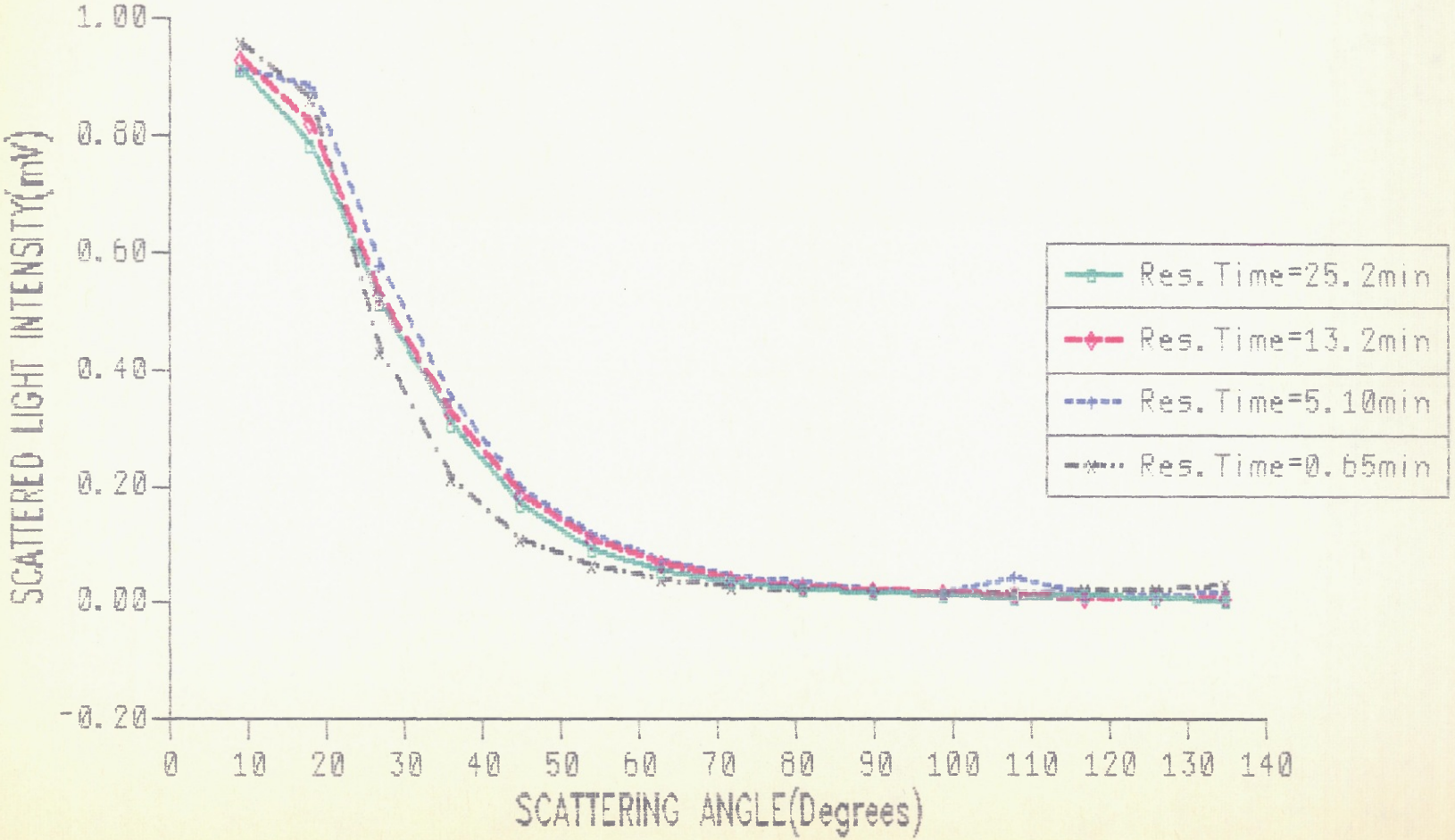


Table IV.6 shows the aerosol mass concentration and number concentration for all the tube combinations. The mass concentration was determined by the method described in III.3.1. If there were no loss, the mass concentration should be time invariant. However, it decreased slightly as residence time increased. This is more a systematic than a random error and is likely to be caused by the loss of aerosol in the reactor by sedimentation and impaction. As expected from equation II.75.

$$N_t = \frac{N_0}{1 + N_0 K t}$$

the droplet number concentration declined as the residence time increased and coagulation went on. N_0 and N_t are number concentrations at a reference time, t_0 and after a time span t. The reference time, t_0 is the residence time of the aerosols in s-tube. The decline was very rapid initially when the droplet concentration was very high but slowed down as coagulation reduced the number concentration.

The experimental results were compared with theoretically calculated variation of number concentration with residence time. Three sets of theoretical data were obtained based on three assumed modes of coagulation. In the first set, a monodisperse coagulation of particles of initial size 0.01 μm (the modal diameter of the droplets at 39 seconds residence time) and a number concentration of 3.05×10^{12} cm^{-3} was assumed. In the second one, a polydisperse coagulation between droplets of diameter 0.01 μm and 1.0 μm and a number concentration of 3.05×10^{12} cm^{-3} was assumed. The polydisperse coagulation coefficient was calculated from Eqn II.76. In the third set, a combination of polydisperse and monodisperse coagulation was assumed to operate in relay. Polydisperse coagulation was dominant from Run 1 to Run 3 while monodisperse coagulation dominated from Run 3 to Run 8. These sets of data conditions are designated A,B and C in Table IV.7. The calculations are based on Eq II.75.

The experimental values are higher than all the sets of theoretical values by at least one order of magnitude. The significance of this becomes more obvious if the loss of droplets in the tube (as shown by the decreasing mass concentration as residence

Table IV.5 Variation of ZOLD parameters with Residence Time

Master solution concentration = 0.1M - $(NH_4)_2SO_4$

Runs	Residence Times (sec)	Temp (°C)	RH (%)	d_{mode} (μm)	σ_0	VMD
1	39	24	98	0.01	0.95	0.095
2	64	25.5	82	0.015	0.866	0.098
3	307	24.5	98	0.103	0.599	0.253
4	548	25.0	98	0.415	0.262	0.500
5	790	25.0	98	0.419	0.270	0.503
6	1031	24.75	98	0.424	0.270	0.509
7	1272	24.5	98	0.464	0.247	0.540
8	1514	25.0	90	0.439	0.277	0.532

Table IV.6 Variation of number concentration with residence time

For aerosols generated from a 0.1M-$(NH_4)_2SO_4$ solution

Run	Residence Time (s)	Droplet Diameter (μm)	Coagulation Coef., K($cm^3 s^{-1}$)	Droplet Mass Conc(g cm^{-3})	Number Concentration (cm^{-3})
1	39	0.01	6.68×10^{-9}	1.60×10^{-6}	3.05×10^{12}
2	64	0.015	4.51×10^{-9}	1.62×10^{-6}	9.15×10^{11}
3	307	0.103	8.59×10^{-10}	1.58×10^{-6}	2.76×10^{9}
4	548	0.415	4.2×10^{-10}	1.54×10^{-6}	4.11×10^{7}
5	790	0.419	4.12×10^{-10}	1.56×10^{-6}	4.04×10^{7}
6	1031	0.424	4.08×10^{-10}	1.45×10^{-6}	3.63×10^{7}
7	1272	0.464	4.00×10^{-10}	1.40×10^{-6}	2.67×10^{7}
8	1514	0.439	4.05×10^{-10}	1.11×10^{-6}	2.50×10^{7}

Table IV.7 The comparison of the experimental and theroetical values of the variation of number concentration with residence time

Run	Tube(s)	$t(t_n-t_0 s)$	N_t(Experimental (cm^{-3})	N_t(Theoretical) (cm^{-3}) A	B	C
1	s	0	$3.05x10^{12}$	$3.05x10^{12}$	$3.05x10^{12}$	$3.05x10^{12}$
2	1	25	$9.15x10^{11}$	$5.988x10^{6}$	$2.222x10^{6}$	$2.222x10^{6}$
3	5	268	$2.76x10^{9}$	$5.586x10^{5}$	$2.073x10^{5}$	$2.073x10^{5}$
4	9	509	$4.11x10^{7}$	$2.941x10^{5}$	$1.091x10^{5}$	$1.713x10^{5}$
5	13	751	$4.04x10^{7}$	$1.993x10^{5}$	$7.398x10^{4}$	$1.459x10^{5}$
6	17	992	$3.63x10^{7}$	$1.509x10^{5}$	$5.6x10^{4}$	$1.272x10^{5}$
7	21	1234	$2.67x10^{7}$	$1.213x10^{5}$	$4.502x10^{4}$	$1.127x10^{5}$
8	25	1475	$2.50x10^{7}$	$1.015x10^{5}$	$3.766x10^{4}$	$1.011x10^{5}$

A = Monodisperse coagulation; coagulation coefficient = 6.68×10^{-9} cm^3 s^{-1}

B = Polydisperse coagulation; coagulation coefficient = 1.80×10^{-8} cm^3 s^{-1}

C Combination of monodisperse and polydisperse coagulations

Polydisperse coagulation coefficient = 1.80×10^{-8} cm^3 s^{-1}

Monodisperse coagulation coefficient = 4.2×10^{-10} cm^3 s^{-1}

time increases) is taken into consideration. The monodisperse coagulation and the combination of monodisperse and polydisperse coagulation assumptions give results that are identical to each other and closer to experimental values than the wholly polydisperse coagulation.

The disparity between theory and experiment may be attributed to the simplicity of the model in which condensational growth is totally ignored; and the droplet size distribution is inadequately considered (i.e. the modal diameter is regarded as representing the droplet diameter, and the contributions of the other particle sizes in the distribution are neglected).

In another approach, particle number concentrations were calculated from the droplet volume mean diameter (VMD) and the experimental mass concentrations and used in obtaining the coagulation patterns based on monodisperse, polydisperse and a combination of polydisperse and monodisperse coagulation assumptions. These are listed in Table IV.8. A better agreement is obtained between theory and experiment as shown in Fig. IV.6 using droplet size based on volume mean diameter. The higher theoretical than experimental values in E (Table IV.8) are expected in view of the observed non-conservation of droplet mass concentration. This closer agreement is attributed to the fact that size distribution was taken into consideration. However, the model does not take into consideration the intermediate sizes created in the course of the coagulation. A more comprehensive model such as that of Suck et al (1979) would produce theoretical results in closer agreement with experimental results.

Considering the number concentrations of the aerosols generated from 0.1M-$(NH_4)_2SO_4$ master solution, the droplets were likely to be so close to one another that their polarisation fields interacted. Even if the droplets were so separated that this did not happen the possibility of multiple scattering which would tend to distort the scattering pattern was very high. Added to these was the fact that coagulation would be an important factor in the evolution of droplet size distribution. Hence aerosols generated from this concentration of master solution was not considered suitable.

Further work in this study was done with aerosols of lower number concentrations than the ones described above. They were generated from 1 mM-$(NH_4)_2SO_4$ solution and possessed characteristics as listed in Table IV.9.

Table IV.8 Experimental and theroetical variation of number concentration calculated from MMD values

Run	VMD	N_t(Experimental (cm^{-3})	N_t(Theoretical) (cm^{-3}) D	E	F
1	0.095	3.557×10^9	3.557×10^9	3.557×10^9	3.55×10^9
2	0.098	3.281×10^9	4.118×10^7	1.790×10^9	1.790×10^9
3	0.253	1.860×10^8	3.883×10^6	3.072×10^8	3.072×10^8
4	0.500	2.348×10^7	2.045×10^6	1.687×10^8	7.888×10^6
5	0.503	2.336×10^7	1.386×10^6	1.161×10^8	3.987×10^6
6	0.509	2.096×10^7	1.050×10^6	8.858×10^7	2.672×10^6
7	0.540	1.695×10^7	8.439×10^5	7.156×10^7	2.009×10^6
8	0.532	1.405×10^7	7.607×10^5	2.528×10^7	1.608×10^6

D = Monodisperse coagulation; coagulation coefficient = 9.6×10^{-10} cm^3 s^{-1}

E = Polydisperse coagulation; coagulation coefficient = 1.1097×10^{-11} cm^3 s^{-1}

F = Combination of polydisperse and monodisperse coagulations.
Polydisperse coagulation regime; $K_{1,2} = 1.1097 \times 10^{-11}$ cm^3 s^{-1}
Monodisperse coagulation regime; $K = 5.126 \times 10^{-10}$ cm^3 s^{-1}

Table IV.9 Number concentrations of aerosols generated from 1mM-$(NH_4)_2SO_4$ solution

Residence Time (min)	.65	1.1	5.1	9.1	13.2	17.2	21.2	25.2
MMD(μm)	0.112	0.156	0.137	0.118	0.170	0.432	0.423	0.349
Mass Conc ($x10^6 gdm^{-3}$)	8.844	8.844	8.844	8.844	8.844	8.844	8.844	8.844
Number Conc (dm^{-3})	$1.20x10^{10}$	$4.45x10^9$	$6.57x10^9$	$2.54x10^9$	$3.44x10^9$	$2.10x10^8$	$2.23x10^8$	$3.97x10^8$

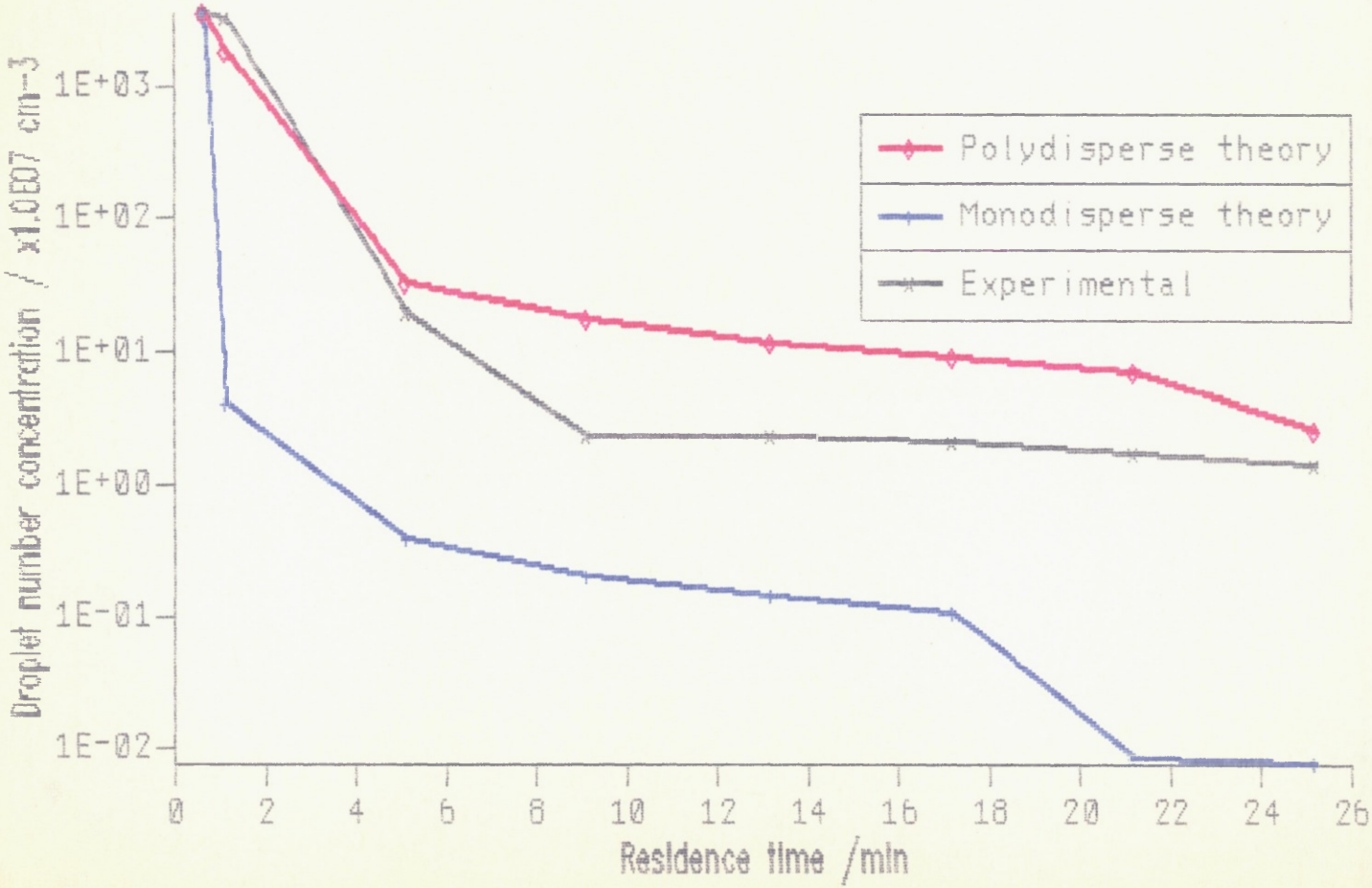


Figure IV.6 Variation of droplet number concentration with res.time, from mass filtration and from coagn. theory

IV.3 Light scattering of gas-droplet interacting aerosol systems

Three SO_2 oxidation mechanisms were investigated as described in section III.3.2, namely

i. oxidation in the absence of NH_3;

ii. oxidation in the presence of NH_3;

iii. metal ion-catalysed oxidation in the presence of NH_3.

The particle size obtained by light scattering is a reflection of the total sulphate loading of the droplet. The relationship is embodied in the equilibrium state equation (Wagner, 1978) which is a form of Equation II.63

$$\frac{p_r'}{p_\infty} = A.\exp Z$$

where

$$A = 1 - \frac{6imM}{\rho\pi M_N d^3};$$

$$Z = \frac{4M\sigma}{\rho RTd}$$

IV.3.1 Size Analysis of Oxidation product of SO_2 in the absence of NH_3

The effect on the droplet size distribution of varying the partial pressure of SO_2 was investigated briefly. The partial pressures used were 1.0, 10.0, 50.0 and 100.0 vpm. In Table IV.10 are shown the ZOLD parameters obtained at different contact times for these partial pressures, with the results in the absence of SO_2 included as the base line. Fig IV.7 and 8 show the variation of droplet size distribution with SO_2 partial pressure and residence time respectively. The following trends in droplet size were observed.

i. Particle size increased with residence time in all the cases. The increase in size in the run without SO_2 was the most regular, and the spread in the distribution showed a general increase after a contact time of 5.0 minute. This shows that the increase in size in the run without SO_2 was mostly as a result of coagulation. The

Table IV.10 Aerosol ZOLD parameters in the absence of NH_3 and Mn^{++}

Master solutions is 1mM-$(NH_4)_2SO_4$

Contact time/min	Run 0 p_{SO_2} = 0			Run 1 p_{SO_2} = 1 vpm			Run 2 p_{SO_2} = 10 vpm			Run 3 p_{SO_2} = 50 vpm			Run 4 p_{SO_2} = 100 vpm		
	d_{mode}	σ_0	MMD	d_{mode}	σ_0	MMD	d_{mode}	σ_0	MMD	d_{mode}	σ_0	MMD	d_{mode}	σ_0	MMD
.65	.015	.895	.111	.052	.655	.152	.020	.818	.107	.052	.66	.16	.051	.67	.16
1.1	.050	.781	.230	.053	.718	.192	.053	.624	.140	.075	.56	.16	.068	.58	.16
5.1	.054	.655	.158	.065	.592	.156	.051	.797	.250	.064	.79	.31	.055	.69	.18
9.1	.051	.728	.192	.068	.582	.159	.065	.59	.16	.070	.79	.33	.061	.67	.18
13.2	.052	.748	.211	.066	.671	.203	.054	.767	.235	.066	.66	.18	.075	.56	.16
17.2	.057	.781	.262	.072	.649	.206	.081	.59	.19	.080	.56	.17	.078	.569	.17
21.2	.069	.758	.290	.083	.60	.20	.15	.47	.25	.089	.76	.37	.092	.49	.17
25.2	.077	.638	.213	.12	.56	.26	.10	.53	.21	.173	.57	.39	.104	.53	.21

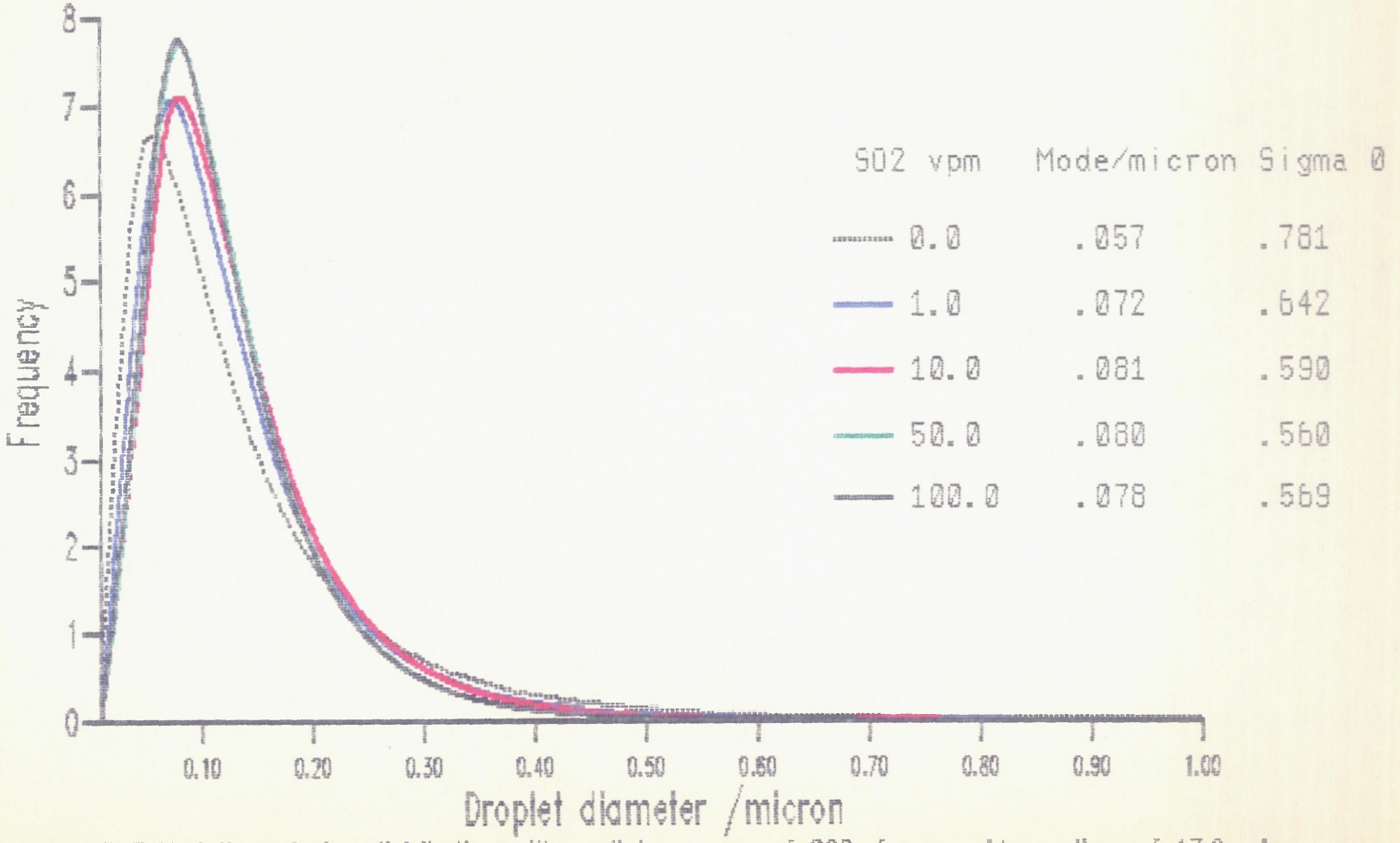


Figure IV.7 Variation of size distribution with partial pressure of SO2, for a residence time of 17.2 min.

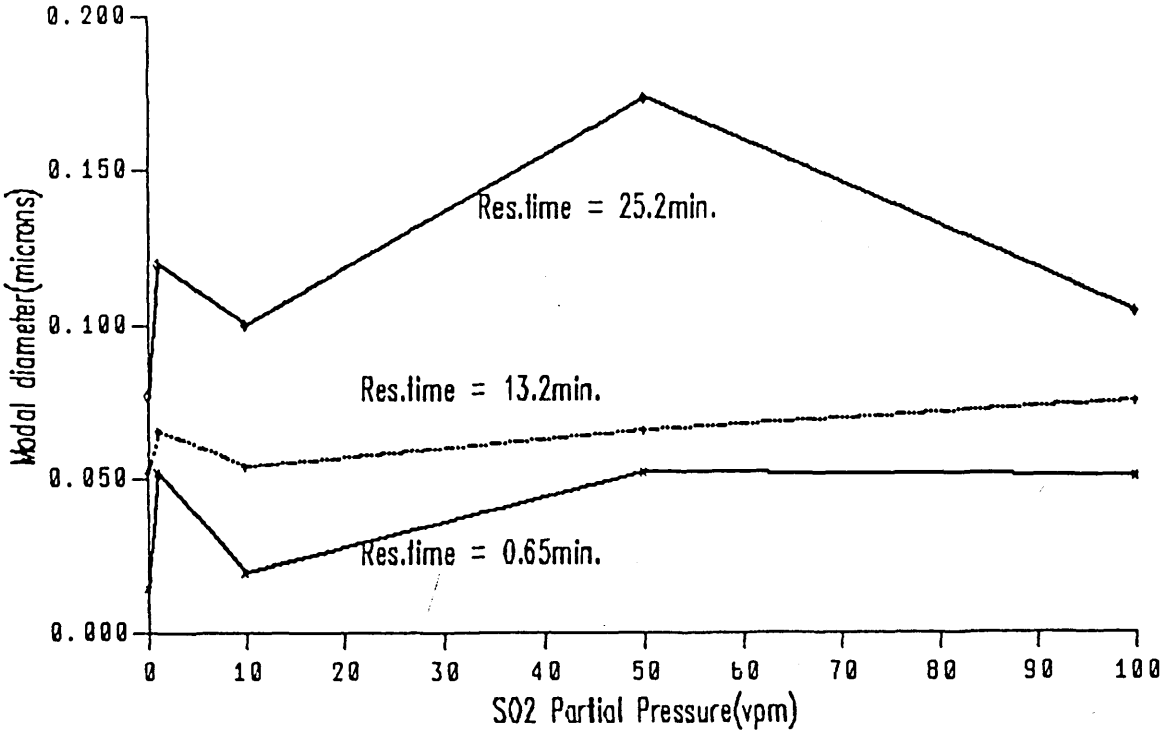


Figure IV.7a:-The variation of aerosol droplet diameter with SO_2 partial pressure in a SO_2-O_2-H_2O system at three residence times.

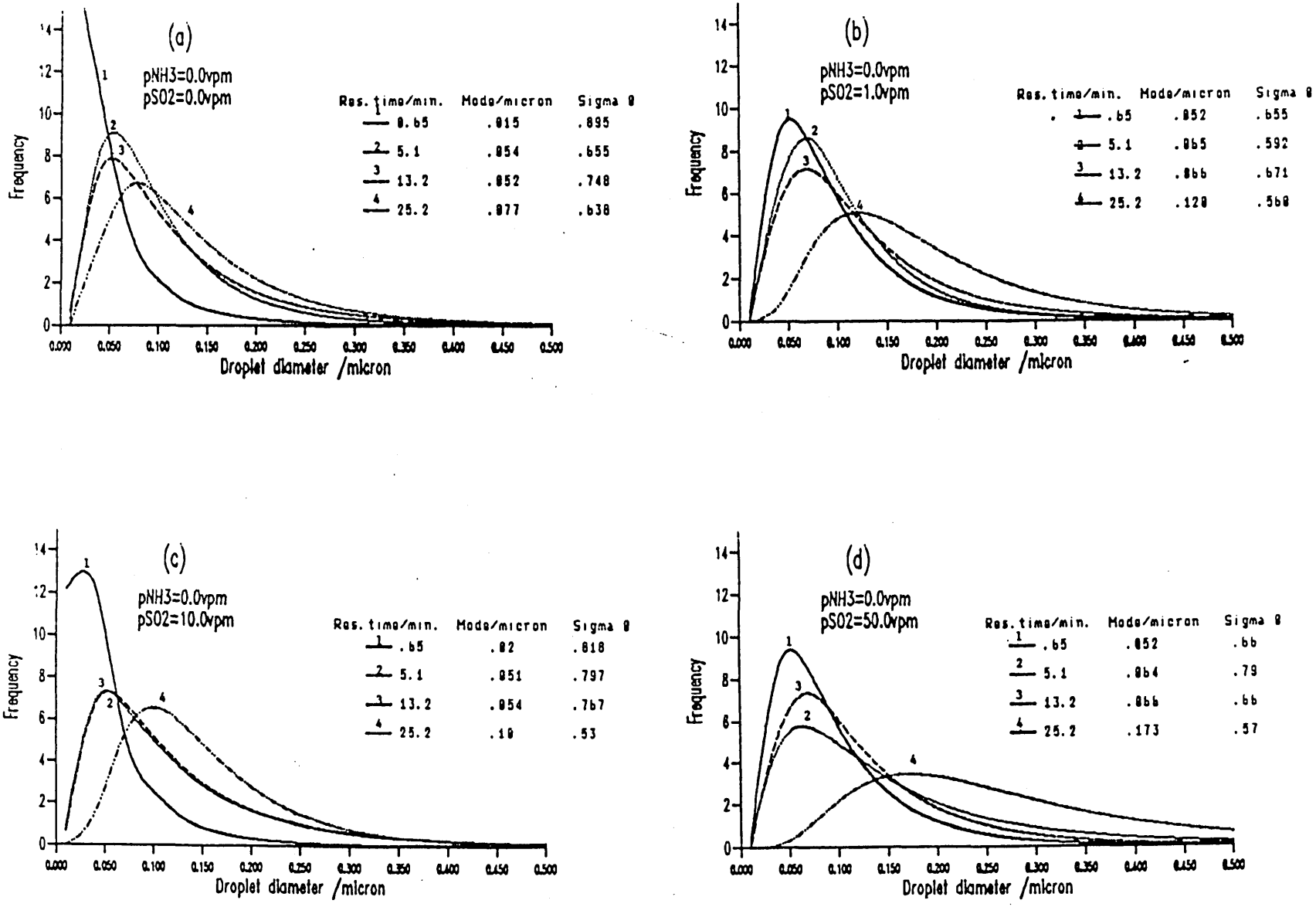


Figure IV.8:-Variation of droplet size distribution with residence time

magnitude of the effect of coagulation was however small. The spreads in the distributions of the other runs (1 - 100 vpm SO_2) showed a general decrease as the modal diameter increased with contact time. This shows a preponderance of condensational growth over coagulation. Hence increase in modal diameter in these runs was as a result of the increase in the amount of sulphate ion in the droplet formed by oxidation. However, an attempt to obtain rate constant from the droplet size variation based on this assumption and that of equilibrium between the gas phase and the droplets yielded unrealistically high values of pseudo first order rate constants for 1.0 and 100 vpm.

2. Fig. IV.7a shows the variation of the aerosol modal diameter with the partial pressure of SO_2 for three residence times.Droplet size increased generally with SO_2 partial pressure. However, comparing the 1 vpm and 100 vpm runs, the change in modal diameter is far less than the cube root of 100. This anomaly of slow growth at 100 vpm could be justified even if the widely accepted (Scott et al, 1967 and Beilke et al, 1975) model of first order with respect to sulphite ion were to apply at all SO_2 gas phase partial pressures in this range. By this argument, the suppression of the sulphite ion formation by the hydrogen ion furnished by the absorption and dissociation of SO_2 would depress the sulphate formation below the level expected at high gas phase partial pressures. On the other hand, if it were accepted that the reaction is first order only at SO_2 gas phase partial pressure not exceeding 1 vpm (Miller et al, 1972 and Luria et al, 1982), then with the partial pressure of 100 vpm well outside this regime, the oxidation may well not depend on the sulphite ion concentration.

3. The droplet size is generally very small compared with Table IV.5 and means that growth was not high. This is a result of low sulphate yield.

IV.3.2 SO_2 Oxidation in the Presence of NH_3

Three combinations of the partial pressures of SO_2 and NH_3 were used to study the effect of ammonia on the oxidation of SO_2. These combinations and the respective equilibrium concentrations of hydrogen and sulphite ions in the droplets are listed in Table IV.11. The aerosols were generated from 1 mM-$(NH_4)_2SO_4$ solution. The partial pressures of the reacting gases were chosen to reflect the condition of SO_2 dilution a few meters downwind of an intense SO_2 source (BNL,

Table IV.11 Partial pressures of NH_3 and SO_2 with the corresponding equilibrium state concentrations of H^+ and SO_3^{2-} (moles dm^{-3}).

Combination	P_{SO_2}	P_{NH_3}	$[H^+]_e$	$[SO_3^{2-}]_e$
(a)	50	0.0	2.442×10^{-3}	1.129×10^{-8}
		2.0	2.3828×10^{-6}	0.0118
		10.0	1.0955×10^{-6}	0.0561
		25.0	7.1147×10^{-7}	0.133
		50.0	5.1693×10^{-7}	0.252
		100.0	3.7828×10^{-7}	0.470
(b)	50	0.1	1.0531×10^{-5}	6.07×10^{-4}
		1.0	3.3498×10^{-6}	5.999×10^{-3}
		10.0	1.0955×10^{-6}	0.0561
(c)	1	0.5	7.2994×10^{-7}	2.53×10^{-3}
		1.0	5.2593×10^{-7}	4.87×10^{-3}
		2.0	3.8266×10^{-7}	9.19×10^{-3}
		10.0	1.8981×10^{-7}	0.037
		0.0	2.0107×10^{-3}	3.33×10^{-10}

1972). In the experimental arrangement, the NH_3 was introduced into the aerosol stream before the SO_2 in a mixer wherein the residence time for the experimental aerosol flow rate used was 0.45 seconds. The characteristic time associated with the gas phase diffusion of the equilibrium NH_3 concentration to the droplet is given by the equation (Freiberg et al, 1981)

$$\tau_{reag} = \frac{\pi^3}{3} \eta H_a RT \tau_{dg}$$

where

$$\tau_{dg} = d^2/4\pi^2 D_g$$

d = droplet diameter; D_g = gas phase diffusivity of NH_3;

$$\eta = 1 + K_a/[OH^-] = 1 + \frac{K_a[H^+]}{K_w}$$

K_a = ionisation constant of NH_3;

K_w = water dissociation constant;

H_a = Henry's Law Constant for NH_3;

R = Universal gas constant (atm M^{-1} K^{-1})

T = absolute temperature

For a droplet of diameter 1.0 μm, this gives the values of τ_{reag} for NH_3 of 1.47×10^{-3} and 5.65×10^{-6} seconds for gas phase partial pressures of 0.1 and 100.0 ppm respectively. These time spans are negligible compared to the residence time of the aerosol in the mixer and so the equilibrium concentration of NH_3 in the droplets was achieved before the droplets reached Mx4 where contact with SO_2 took place.

The effect of increase in NH_3 partial pressure on sulphate yield was studied using the data for the experimental combinations in group (a) of Table IV.11. The ZOLD parameters obtained by inverting the light scattering data are listed in Table IV.12. The variation of size distribution with the partial pressure of NH_3 for a residence time of 17.2 minutes is shown in Fig. IV.11. The curves for 2 and 10 vpm NH_3 appear as one curve. The size ratios, I(d) were also calculated and tabulated. Size ratio in this context is the ratio of the droplet VMD

Table IV.12 ZOLD Parameters for Droplet Growth in the Presence of 2.0 - 100.0 ppm NH_3 and 50 ppm SO_2

	ZOLD PARAMETERS																	
Run				10			11			12			13			14		
P_{NH_3} (10^{-6})	0.0			2.0			10.0			25.0			50.0			100.0		
Res. Time	1	2	3	1	2	3	1	2	3	1	2	3	1	2	3	1	2	3
.65 min	0.013	0.623	0.22	0.051	0.886	2.33	0.066	0.775	1.90	0.060	0.768	1.68	0.055	0.754	1.46	0.052	0.789	1.58
1.1 min	0.015	0.873	0.64	0.050	0.905	2.45	0.19	0.51	5.98	0.089	0.755	2.34	0.20	0.50	4.49	0.120	0.531	1.54
5.1 min	0.027	0.707	0.52	0.072	0.797	1.94	0.35	0.50	4.38	0.167	0.599	2.27	0.14	0.69	2.02	0.13	0.66	2.64
9.1 min	0.043	0.686	0.76	0.077	0.87	2.14	0.43	0.41	1.98	0.058	0.934	2.79	0.18	0.55	2.48	0.13	0.85	3.53
13.2 min	0.051	0.608	0.79	0.87	0.91	1.80	0.079	1.0	2.28	0.203	0.584	2.90	0.087	0.96	2.31	0.239	0.526	3.79
17.2 min	0.059	0.632	0.94	0.554	0.466	5.61	0.550	0.466	5.57	0.377	0.385	3.21	0.723	0.314	5.44	0.467	0.416	4.24
21.2 min	0.064	0.589	0.90	0.54	0.39	2.20	0.483	0.461	4.86	0.383	0.464	3.88	0.385	0.454	3.82	0.22	0.46	4.66
25.2 min	0.086	0.591	0.99	0.53	0.28	2.88	0.58	0.35	3.52	0.51	0.38	3.11	0.586	0.238	3.25	0.16	0.78	3.75
Mean			0.72			2.67			3.81			2.77			3.16			3.22
Std. Deviation			0.24			1.15			1.53			0.63			1.26			1.10

1 = d_{mode}
2 = σ_0
3 = I(d)

at a given partial pressure of SO_2 and NH_3 to that of a droplet obtained under the same experimental conditions of temperature, relative humdiity and residence time but in the absence of the two gases.

There is generally an increase in droplet size ratio with NH_3 partial pressure at all residence times. This is rapid initially and reaches a maximum at an NH_3 partial pressure of 10^{-5} atmospheres in all but a few of the residence times studied. This trend is depicted in Fig. IV.9. This increase however does not match the corresponding value of the calculated equilibrium concentration of sulphite ion in the droplet shown in Table IV.11. This disparity may be caused by several factors. First, the assumptions on which the sulphite concentration was calculated may be too idealized to reflect the true sulphite concentrations in the droplet. The formation of sulphite ion is an absorption followed by instantaneous reversible reaction and hence the rate can be expressed in terms of the pH, the appropriate equilibrium constants, and the partial pressures and diffusivities of the reacting gases. Since the droplets are in submicrometer size regime, complete internal homogeneity is assumed and hence mass transfer of species within the droplet is not limiting since the time constant for it is very short (of the order of μs). Freiberg et al (1981) however, calculated the time it would take to achieve the equilibrium S(IV) concentration in the droplet of size used by Scott et al (1967) and concluded that steady-state condition was not fulfilled under the conditions of the experiment. The departure from steady state increased with droplet size and may be caused by surface resistance to interfacial mass transfer (Beilke et al, 1978). It is not likely to be important in the size regime of this study. Another assumption in the calculation of SO_3^{2-} ion concentration was that the droplet surface was a perfect SO_2 absorber. This assumption is valid in view of the high partial pressure of NH_3, by analogy to the absorption of SO_2 into alkaline solutions like the ocean water (Liss, 1971 and Liss et al, 1974). Any condition that detracts from this assumed condition of high droplet pH and the specified gas phase partial pressure of SO_2 will cause a corresponding deviation of the real from the calculated values of the equilibrium SO_3^{2-} ion concentration. Such a condition can be caused by any process including parasitic reactions in the gas phase which would remove any of the components from the reaction medium .

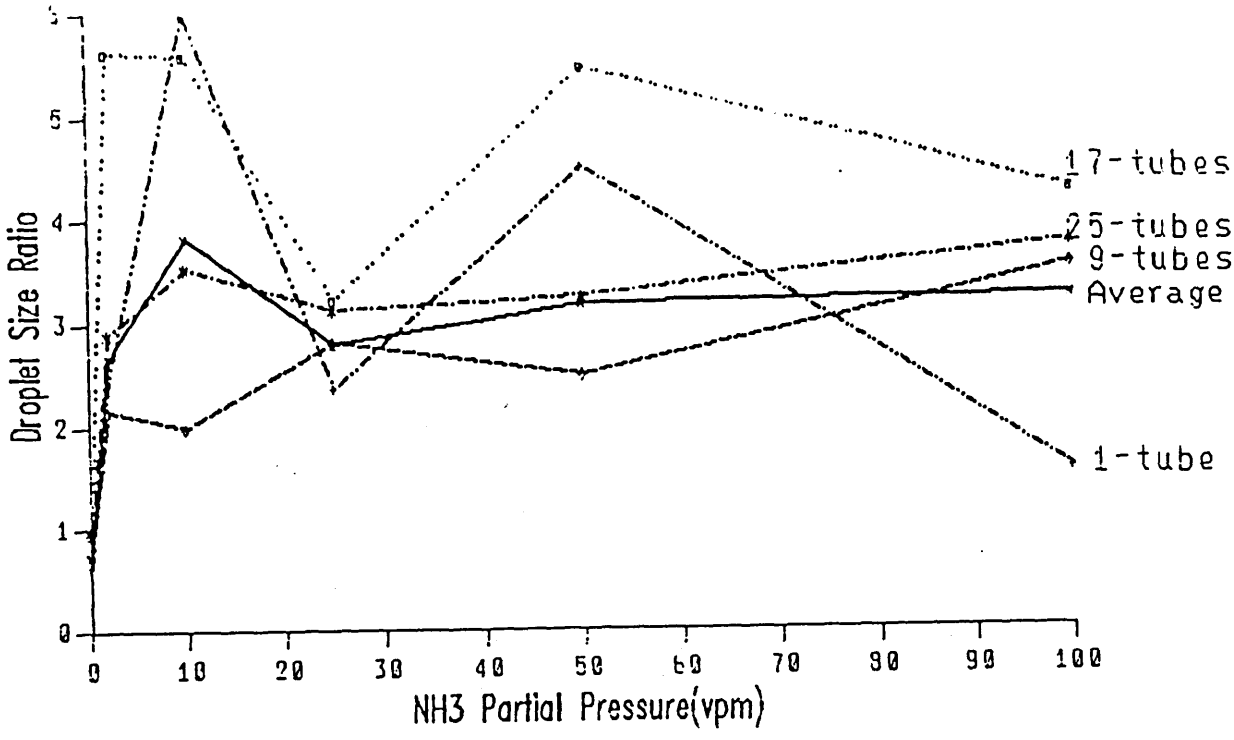


Figure IV.9:-The effect of NH_3 partial pressure on droplet size ratio in the SO_2-NH_3-H_2O-O_2 reacting system for the partial pressure of NH_3 0.1 to 100vpm.

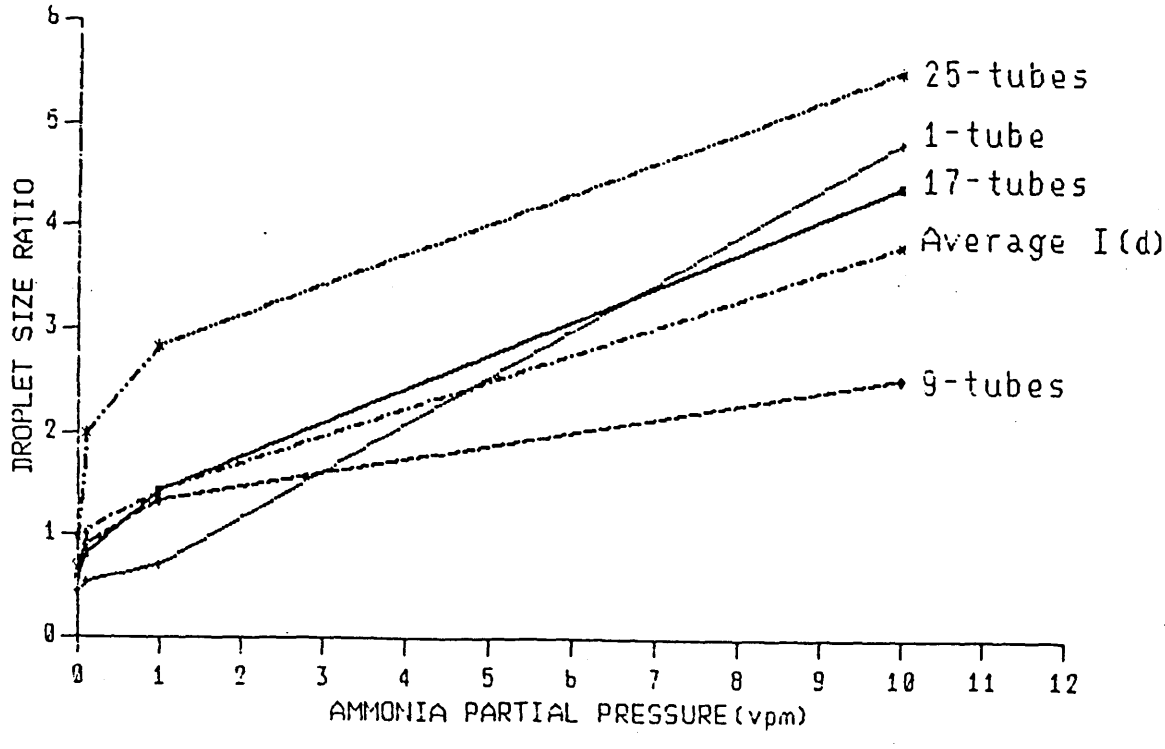


Figure IV.9a:-The effect of NH_3 partial pressure on droplet size ratio in the SO_2-NH_3-H_2O-O_2 reacting system for the partial pressures of of of NH_3 0.1 to 10.0 vpm.

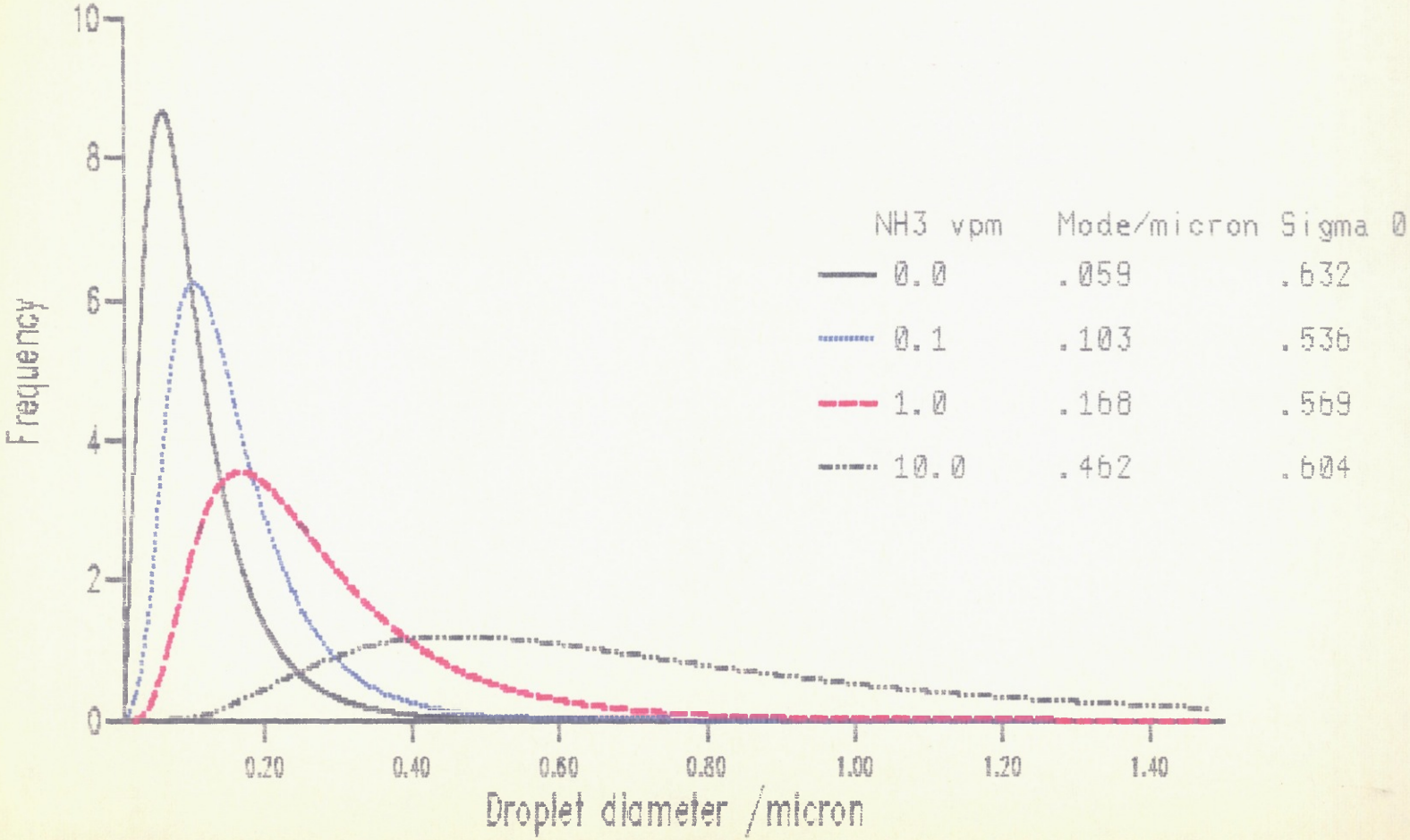


Figure IV.10 Variation of size distribution with NH3 partial pressure; 1.0 vpm SO2, res. time 17.2 min.

Scott et al (1969), Carabine et al (1973) and Polychronaikis (1979) found that gaseous NH_3 and SO_2 react to form solid products in the presence of moisture.

$$NH_3 + SO_2 \xrightarrow{H_2O} NH_3.SO_2$$

Carabine et al (1973) and Polychronaikis (1979) however used concentrations of the reacting gases much higher than are used in this study.

To investigate further the extent of and the conditions for this reaction, a set of qualitative experiments were carried out. The sum of the intensities at a range of angles of scattered light was determined as a function of the partial pressures of SO_2 and NH_3 and the relative humidity of the reactor. The experimental conditions and results are listed in Table IV.13. Since the experiments were carried out in the absence of stable aerosols from the generator, the light scattering must have been done by the adduct particles. Distilled water aerosol was used in C merely to boost the humidity since it has been shown earlier that distilled water droplet disappeared very fast by evaporation under the temperature and saturation ratio that are available in the reactor. In Run A, drying of the gas was not rigorous since a substantially high humidity is required to trigger off the reaction at the temperature (25°C) and the reacting gas partial pressures of this experiment (Scott et al, 1969). Ordinarily passing the gas from the cylinder through a long tube containing silica gel prior to passing it into the reactor was sufficient to achieve the desired degree of dryness. Nitrogen instead of air was used so as to avoid the formation of $(NH_4)_2SO_4$. The light scattering data were not inverted for the ZOLD parameters. The results show that under the conditions of the experiment on particle size as a function of NH_3 partial pressure, except at high partial pressures of the reacting gases and high humidity, no significant amount of SO_2 and NH_3 was lost in adduct formation. The adduct formation dependence on the humidity and NH_3 partial pressure found here is in agreement qualitatively with the observations of Arrowsmith et al (1973), namely a positive correlation between the rate of formation of this adduct and

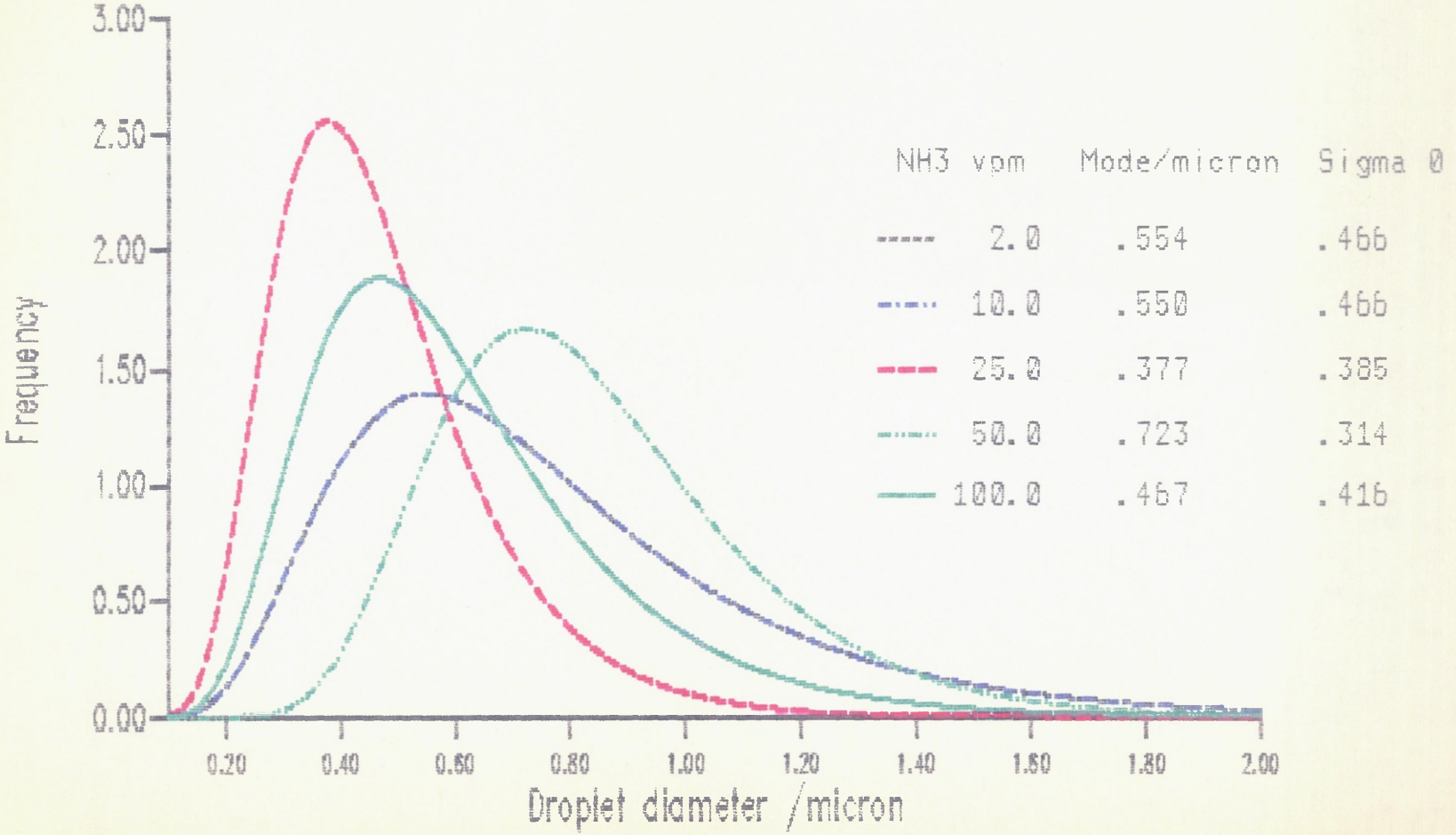


Figure IV.11 Variation of size distribution with partial pressure of NH3; res. time 17.2 min, with 50 vpm SO2

Table IV.13 Light scattering Data for $NH_3.SO_2$ particulates

Humidity Conditions	Partial Pressures x 10^6 SO_2	NH_3	Sum of Scattered Intensity (Volts)	Comments
A Dried N_2	50	100	Background[a]	No particles formed
B Humidified N_2	50	25	Background[a]	No particles formed
	50	50	Background[a]	No particles
	50	100	1.69	Particles formed
C Distilled Water	50	10	Backgound[a]	No particle formed
Aerosol	50	100	1.69	Particles formed

[a] No difference between the experimental and background intensities.

the relative humidity of the reactor and the partial pressure of NH_3. Granting the validity of this finding, the reaction could deplete both NH_3 and SO_2 to a substantial extent only in Run 14. Hence with high partial pressures of the reactant gases and the relative humidity of around 98%, an unquantified amount of the gases would be lost as a result of this parasitic reaction thus distorting the real effects of NH_3 partial pressure on droplet size. This however does not account for decrease in droplet size after the NH_3 partial pressure of 10 vpm.

The role of temperature fluctuation in keeping droplet size low is ruled out because any variation that occurred would have produced two opposing effects that tended to compensate each other. Increase in temperature, would have increased the mass transfer coefficient in the gas phase of the reacting gases but lowered the solubilities of the gases. The absorption-desorption reversibility of the gas-droplet interaction distorts the aqueous phase concentration calculated from the gas phase mole ratios.

Even if the calculated sulphite concentration reflected very closely the actual value of the ions in the droplets, errors may also occur as a result of the aerosol sampling and analysis. Carabine et al (1973) obtained experimental accuracy of within ±4% for the modal diameter and ±10% for the spread from data inversion in similar experiments. Hence accuracy for the MMD cannot be better than 20%. Another likely source of error is the value of the droplet refractive index used for the data inversion which was always taken as being equal to that of the master solution. According to Moore (1974) an accuracy of 0.02 is necessary. In a reacting growing droplet the instantaneous values of the refractive index are not possible to determine. The error which is introduced by this uncertainty in the value of refractive index is likely to be insignificant because although the total sulphate loading of the droplet increases the relaxation time for the diffusion of water vapour to the droplet is so small (Freiberg et al, 1981) that the instantaneous droplet sulphate concentration is virtually constant.

Since it is not easy to pinpoint the cause of this decrease of droplet size above an NH_3 partial pressure of 10vpm, it may be

attributed to a systematic sampling error special to the conditions of these experiments or to an unknown process which might have come into play to alter the S(IV) oxidation mechanism.

The variation of droplet size as a function of the partial pressure of NH_3 was further studied by varying the NH_3 partial pressure over two orders of magnitude at 0.1, 1.0 and 10.0 ppm. The resulting ZOLD parameters for these experiments utilising 50 vpm SO_2 and NH_3 of these mixing ratios are listed in Table IV.14. Fig. IV.9 shows the variation of droplet size ratio with the partial pressure of NH_3 at specified residence times. As shown in Fig. 9a, there is an increase of size ratio with the NH_3 partial pressure in this case with a more pronounced effect. This is also depicted in Fig. IV.10 which is the droplet size distribution at a residence time of 17.2 minutes for the partial pressures of NH_3 of 0.1, 1.0 and 10.0 vpm. This shows that the utilisation of NH_3 for the enhancement of SO_2 oxidation in the droplet phase is more efficient at lower ~~than at~~ partial pressures of NH_3 above than 10^{-5} atmosphere.

The group of experimental runs in C (Table IV.11) were used in investigating the effect of the ratio of NH_3 to SO_2 on SO_2 oxidation. The ZOLD parameters for the runs using 1 ppm SO_2 and NH_3 of concentrations 0.0, 0.5, 1.0 and 2.0 ppm corresponding to a SO_2 to NH_3 ratios of 1:0, 2:1, 1:1 and 1:2 respectively are listed in Table IV.16.

The droplet size distributions of the aerosols at 17.2 minutes contact time are shown in Fig. IV.12. If the SO_2:NH_3 ratio had an effect on droplet size, the size change between the 2:1 and 1:1 gas mixtures would differ appreciably from that between 1:1 and 1:2, and it would mean that one of the two forms of the sulphate of ammonia, namely $(NH_4)_2SO_4$ (a 1:2 compound) or NH_4HSO_4 (a 1:1 compound) was formed exclusively. This was verified by plotting residence times against the MMD for the mixtures 2:1, 1:1 and 1:2 on the same axes, and observing their relationship.

Fig. IV.13 (the variation of droplet size with SO_2 :NH_3 ratio) shows that the MMD of the 1:1 mixture corresponds approximately to the value of the means of the MMD of the 2:1 and 1:2 mixtures. It means therefore that apart from the general increase of MMD with the partial pressure of NH_3, there is no definite trend in droplet size as a

Table IV.14 ZOLD Parameters for Droplet Growth in the Presence of 0.1 - 10.0 ppm NH_3 and 50 ppm SO_2

Run	3			8			9			23		
$p_{NH_3} \times 10^6$ atm	0.0			0.1			1.0			10.0		
Res. Time(min)	d_{mode}	σ_0	Size Ratio	d_{mode}	σ_0	Size Ratio	d_{mode}	σ_0	Size Ratio	d_{mode}	σ_0	Size Ratio
0.65	0.013	0.623	0.31	0.019	0.834	0.98	0.026	0.771	1.04	0.051	0.869	3.06
1.1	0.015	0.873	0.44	0.030	0.755	0.54	0.033	0.825	0.7	0.093	0.996	4.83
5.1	0.027	0.707	0.60	0.064	0.639	1.12	0.041	0.801	1.29	0.202	0.643	3.59
9.1	0.043	0.686	0.73	0.050	0.706	0.91	0.104	0.601	1.34	0.223	0.558	2.53
13.2	0.051	0.608	0.61	0.095	0.622	1.18	0.075	0.732	1.36	0.259	0.773	5.47
17.2	0.059	0.632	0.61	0.103	0.536	0.81	0.168	0.569	1.44	0.462	0.604	4.39
21.2	0.064	0.589	0.53	0.106	0.570	0.82	0.217	0.500	1.40	0.484	0.588	1.15
25.2	0.086	0.591	0.97	0.25	0.46	1.99	0.34	0.48	2.84	0.528	0.565	5.51
Mean			0.60			1.04			1.43			3.82
Std. Deviation			0.20			0.43			0.62			1.53
Coefficient of variation			0.33			0.41			0.44			0.40

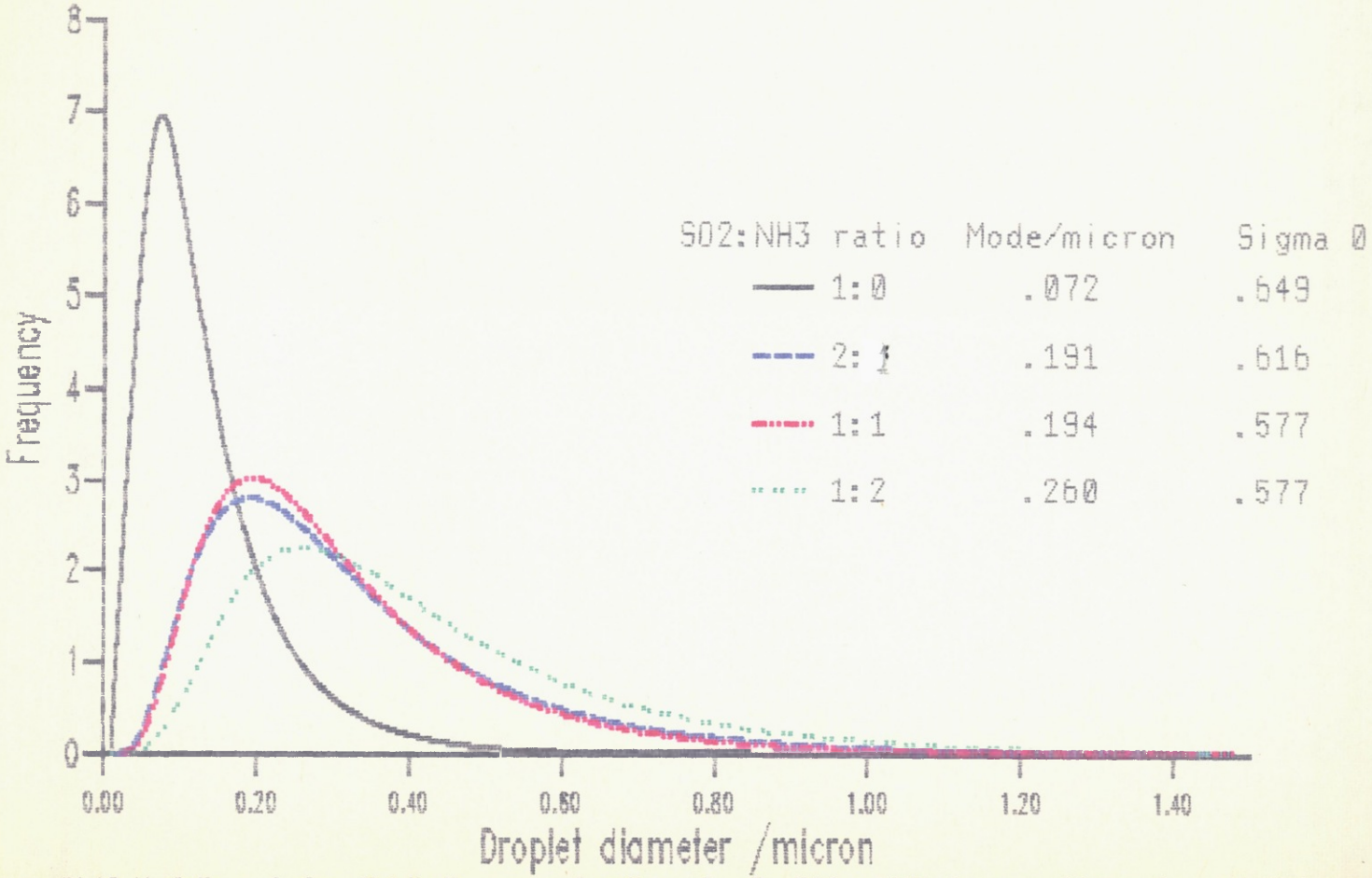


Figure IV.12 Variation of size distribution as a function of ratio SO2 : NH3, for a residence time of 17.2 min.

ZOLD Parameters

Run	1			5			6			7		
SO_2:NH_3	1:0			2:1			1:1			1:2		
Res. Time	d_{mode}	σ_0	VMD	d_{mode}	σ_0	VMD	d_{mode}	σ_0	VMD	d_{mode}	σ_0	VMD
.65 min	0.015	0.895	0.111	0.054	0.655	0.158	0.051	0.728	0.192	0.066	0.680	0.210
1.1	0.039	0.681	0.124	0.078	0.594	0.188	0.082	0.612	0.209	0.077	0.638	0.213
5.1	0.053	0.713	0.189	0.084	0.545	0.177	0.102	0.554	0.220	0.099	0.603	0.246
9.1	0.073	0.619	0.190	0.052	0.748	0.211	0.119	0.589	0.283	0.158	0.529	0.318
13.2	0.066	0.671	0.203	0.118	0.547	0.249	0.172	0.595	0.417	0.238	0.601	0.587
17.2	0.072	0.649	0.206	0.191	0.616	0.493	0.194	0.577	0.446	0.260	0.577	0.598
21.2	0.084	0.735	0.324	0.203	0.586	0.479	0.227	0.567	0.507	0.284	0.554	0.612
25.2	0.156	0.776	0.703	0.223	0.604	0.555	0.264	0.570	0.595	0.256	0.667	0.779

Table IV.15 ZOLD parameters of droplet growth as a function of SO_2 to NH_3 ratio.

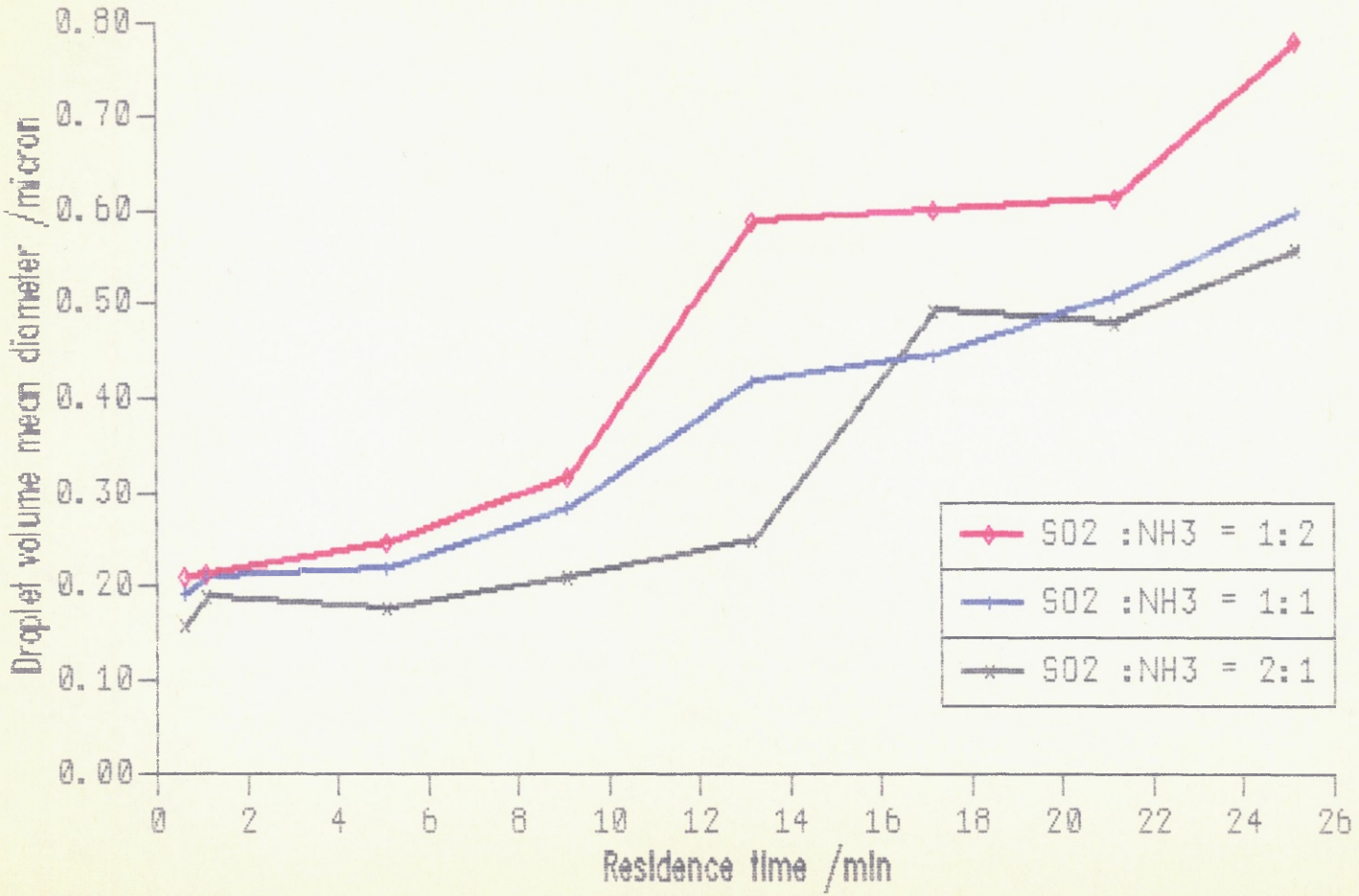


Figure IV.13 Variation of droplet volume mean diameter with ratio of SO2 to NH3, and with residence time (1 vpm SO2)

Table IV.16 The mean MMD for SO_2:NH_3 ratios of 2:1, 1:1 and 1:2 (Master solution 1 mM - $(NH_4)_2SO_4$)

	Volume Mean Diameter			
Residence Time (min)	2:1	1:1	1:2	Mean
0.65	0.158	0.192	0.210	0.184
1.1	0.188	0.209	0.213	0.201
5.1	0.177	0.220	0.246	0.212
9.1	0.211	0.283	0.555	0.247
13.2	0.249	0.417	0.587	0.418
17.2	0.272	0.446	0.598	0.435
21.2	0.493	0.507	0.612	0.553
25.2	0.479	0.595	0.779	0.629

Table IV.17 ZOLD paramters of $MnSO_4$ aerosol in the absence of the reacting gases

Residence time (min)	d_{mode}	σ_0	MMD(μm)
0.65	0.022	0.778	0.0999
1.1	0.026	0.777	0.118
5.1	0.034	0.769	0.149
9.1	0.055	0.631	0.149
13.2	0.067	0.584	0.157
17.2	0.059	0.591	0.141
21.2	0.065	0.592	0.156
25.2	0.072	0.572	0.165

function of the ratio of the SO_2 and NH_3 in the reacting mixture. This means that $(NH_4)_2SO_4$ and NH_4HSO_4 were formed in the reaction with equal probability. Junge (1960) observed atmospheric NH_4^+ to SO_4^{--} ratios that correspond to a mixture of the two ammonium sulphate species. Charlson et al (1974) had used light scattering methods to show that NH_4HSO_4 formed 60 - 70% of the atmospheric ammonium sulphate. This is probably as a result of the lower ambient mixing ratio of NH_3 than SO_2 (Healy et al, 1970). Since the experiments were carried out at a constant humidity of 98%, it was not possible to distinguish between the formation of the deliquescent $(NH_4)_2SO_4$ whose humidogram always shows an inflection at 81% relative humidity (Charlson et al, 1974) and that of the hygroscopic NH_4HSO_4.

IV.3.3 Mn^{2+} ion catalysed oxidation of SO_2 in the presence of NH_3

Two series of combinations of SO_2 and NH_3 partial pressures were used in studying the effect of NH_3 on the manganese ion catalysed oxidation of SO_2. These were p_{SO_2} = 1 vpm with p_{NH_3} = 0, 0.5, 1.0 and 2.0 vpm (Runs 15, 17, 18 and 19); and p_{SO_2} = 50 vpm with p_{NH_3} = 0, 0.1, 1.0 and 10 vpm (Runs 16, 20, 21 and 22). The ZOLD parameters are listed in Table IV.18 and Table IV.19. Using the M.M.D of 1mM-$MnSO_4$ aerosols listed in Table IV.17 as the base line, size ratios, I(d) were calculated from Tables IV.18 and IV.19 and listed in Table IV.20.

The catalytic effect of $MnSO_4$ in the absence of NH_3 was studied by comparing the droplet size obtained in the SO_2-$MnSO_4$-H_2O-O_2 system with that of SO_2-$(NH_4)_2SO_4$-H_2O-O_2 system under indentical experimental conditions. Fig. IV.16 ~~and Fig. IV.16b~~ shows that size variation with residence time was similar in aerosols generated from the two salts. This is contrary to earlier observation by Junge et al (1958). Since no studies were carried out on pure water droplets, it was not possible to determine whether there was any significant difference between the effects of $MnSO_4$ and pure water.

Figures IV.14 and IV.15 show the variation of droplet size distribution of the Mn^{2+} catalysed system for a contact time of 17.2 minutes for 1 vpm and 50 vpm SO_2 respectively with NH_3 partial pressure. In both cases, droplet size was higher in the presence than in the absence of NH_3 up to p_{NH_3} of 1 vpm. However, above this value, droplet size decreased as the partial pressure of NH_3 increased. This rather unexpected trend is discussed further later in the chapter.

Table IV.18 ZOLD parameters of $MnSO_4$ aerosols in the presence of NH_3 and 1 ppm SO_2

Runs	15			17			18			19		
P_{NH_3}	0.0			5×10^{-7} atm			10^{-6} atm			2×10^{-6} atm		
Res. time (min)	d_{mode} (μm)	σ_0	MMD (μm)	d_{mode} (μm)	σ_0	MMD (μm)	d_{mode} (μm)	σ_0	MMD (μm)	d_{mode} (μm)	σ_0	MMD (μm)
0.65	0.057	0.65	0.16	0.039	0.68	0.12	0.032	0.70	0.11	0.051	0.608	0.128
1.1	0.051	0.68	0.16	0.09	0.60	0.22	0.015	0.99	0.18	0.052	0.741	0.205
5.1	0.053	0.71	0.19	0.06	0.79	0.29	0.059	0.59	0.14	0.054	0.794	0.261
9.1	0.059	0.72	0.21	0.10	0.73	0.39	0.061	0.67	0.18	0.053	0.755	0.220
13.2	0.077	0.60	0.19	0.15	0.52	0.30	0.062	0.73	0.23	0.054	0.742	0.214
17.2	0.078	0.56	0.17	0.12	0.57	0.27	0.074	0.91	0.58	0.056	0.718	0.192
21.2	0.19	0.39	0.27	0.16	0.61	0.41	0.084	0.74	0.32	0.058	0.779	0.264
25.2	0.12	0.64	0.34	0.22	0.61	0.53	0.022	0.55	0.46	0.150	0.522	0.296

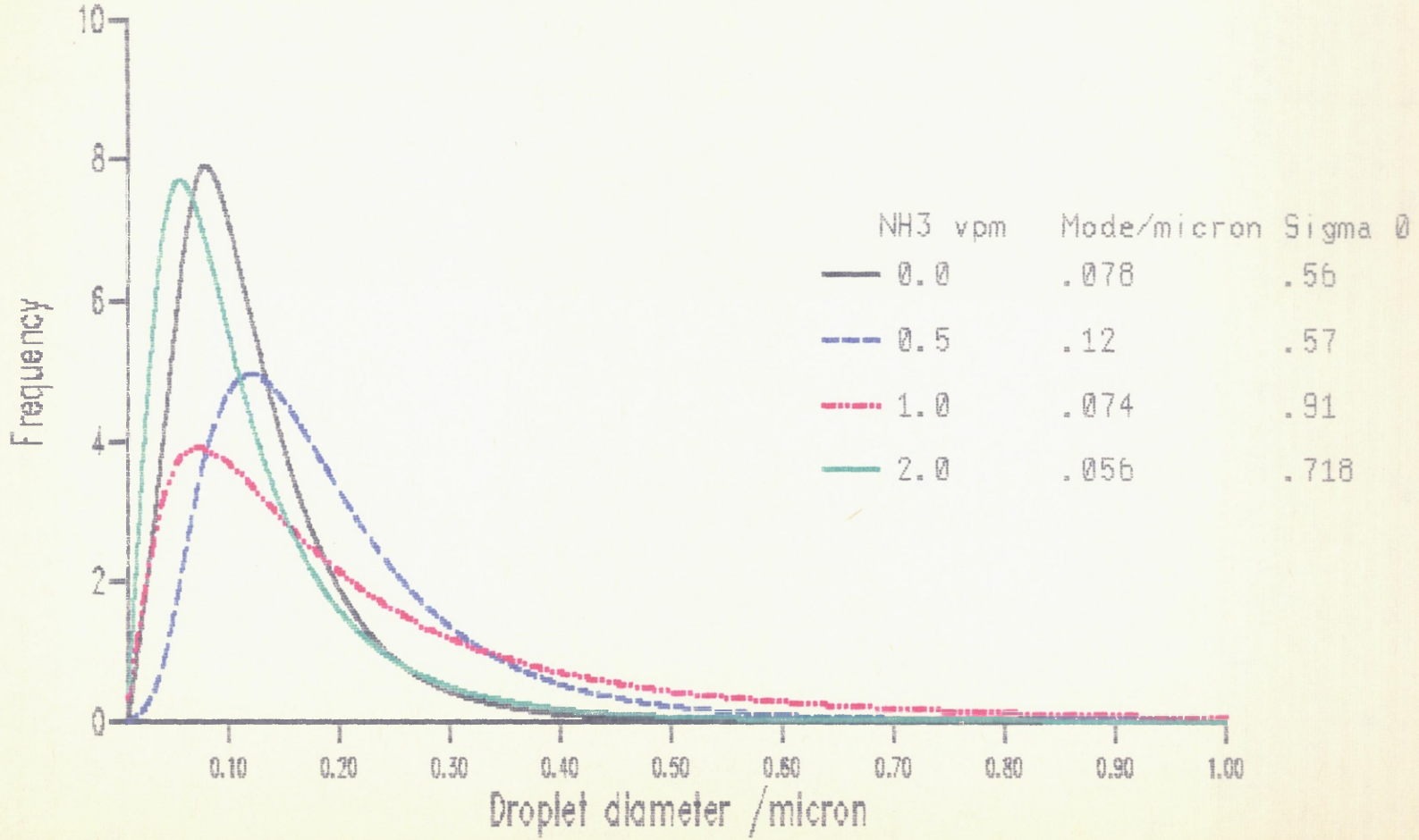


Figure IV.14 Variation of size distribution with NH3 partial pressure; 1 vpm SO2, res. time 17.2 min, Mn2+ catalysed

Table IV.19 ZOLD parameters of $MnSO_4$ aerosol in the presence of NH_3 and 50 ppm SO_2

Run	16			20			21			22		
p_{NH_3} (atm)	0.0			10^{-7}			10^{-6}			10^{-5}		
Res.Time (min)	d_{mode} (μm)	σ_0	MMD (μm)	d_{mode} (μm)	σ_0	MMD (μm)	d_{mode} (μm)	σ_0	MMD (μm)	d_{mode} (μm)	σ_0	MMD (μm)
0.65	0.053	0.68	0.17	0.053	0.718	0.192	0.048	0.706	0.167	0.013	0.848	0.078
1.1	0.051	0.75	0.21	0.066	0.818	0.352	0.059	0.806	0.299	0.035	0.785	0.163
5.1	0.056	0.81	0.28	0.072	0.840	0.420	0.032	1.00	0.390	0.050	0.672	0.155
9.1	0.058	0.76	0.24	0.078	0.853	0.481	0.062	0.874	0.419	0.051	0.668	0.156
13.2	0.061	0.67	0.18	0.092	0.494	0.169	0.034	0.998	0.977	0.067	0.584	0.159
17.2	0.07	0.63	0.19	0.264	0.563	0.584	0.081	0.998	0.977	0.067	0.584	0.157
21.2	0.069	0.64	0.19	0.336	0.481	0.599	0.036	0.994	0.426	0.071	0.572	0.161
25.2	0.154	0.60	0.37	0.352	0.495	0.649	0.202	0.701	0.690	0.058	0.659	0.172

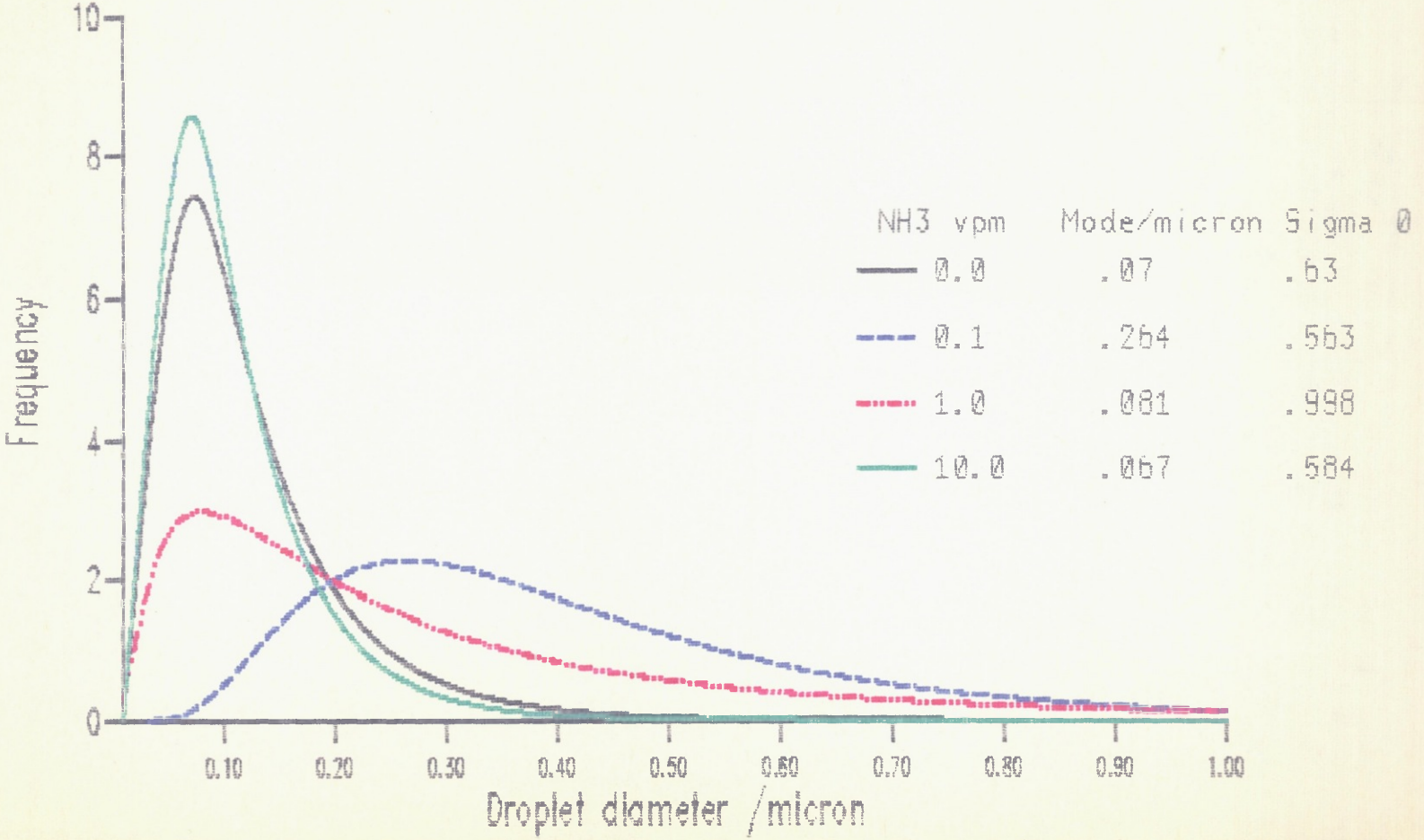


Figure IV.15 Variation of size distribution with NH3 partial pressure; 50vpm SO2, res. time 17.2 min, Mn2+ catalysed

P_{SO_2}	5×10^{-5} atm				10^{-6} atm			
P_{NH_3}	0.0	10^{-7}	10^{-6}	10^{-5}	0.0	5×10^{-7}	10^{-6}	2×10^{-6}
Res. time (min)	(Run 16)	(Run 20)	(Run 21)	(Run 22)	(Run 15)	(Run 17)	(Run 18)	(Run 19)
0.65	1.56	1.92	1.67	0.78	1.09	1.57	1.66	1.28
1.1	1.34	2.98	2.53	1.38	1.49	1.39	1.78	1.74
5.1	1.21	2.82	2.62	1.04	0.946	2.07	1.90	1.75
9.1	1.23	3.23	2.81	1.02	1.05	2.22	1.64	1.48
13.2	1.48	1.08	2.61	1.01	1.22	1.15	1.17	1.36
17.2	1.21	4.14	7.07	1.11	1.37	1.23	1.33	1.36
21.2	1.62	3.84	2.73	1.03	1.30	2.37	1.24	1.69
25.2	2.07	3.93	4.18	1.04	1.26	2.37	2.27	1.79

Table IV.20 The effect of ammonia partial pressure on the droplet size ratio, I(d) in the $MnSO_4$-SO_2-NH_3-H_2O-O_2 system.

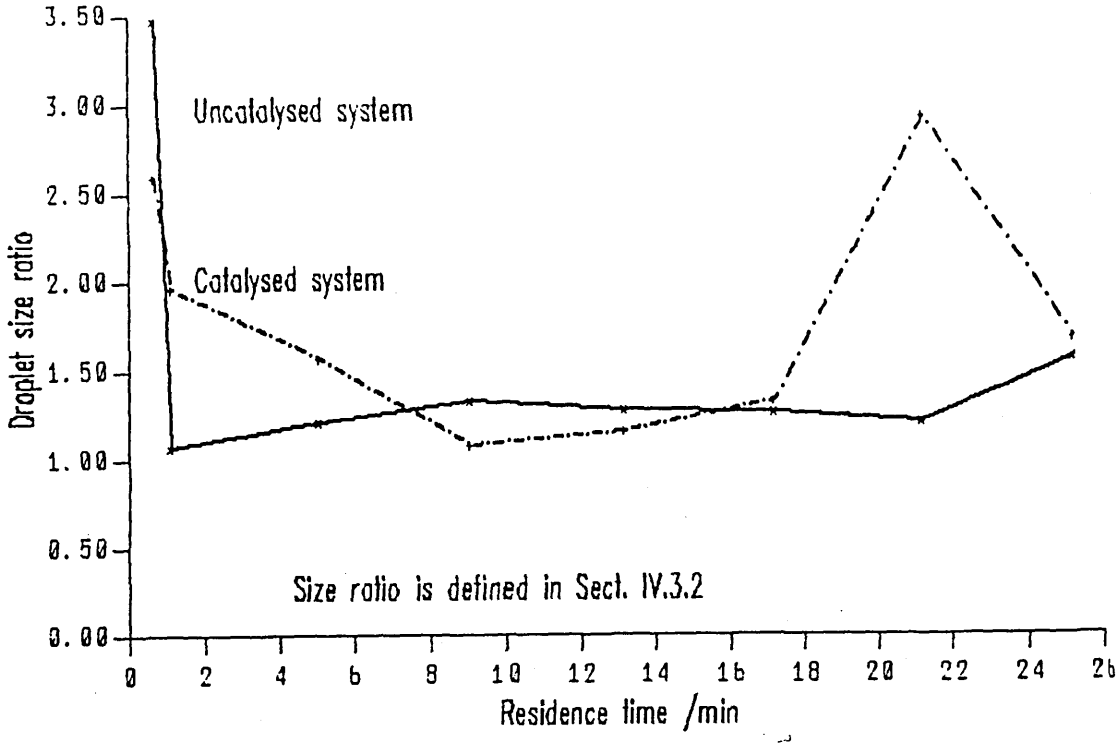


Figure IV.16:-Droplet size ratios for the Mn^{2+} catalysed and the uncatalysed systems with NH_3 absent

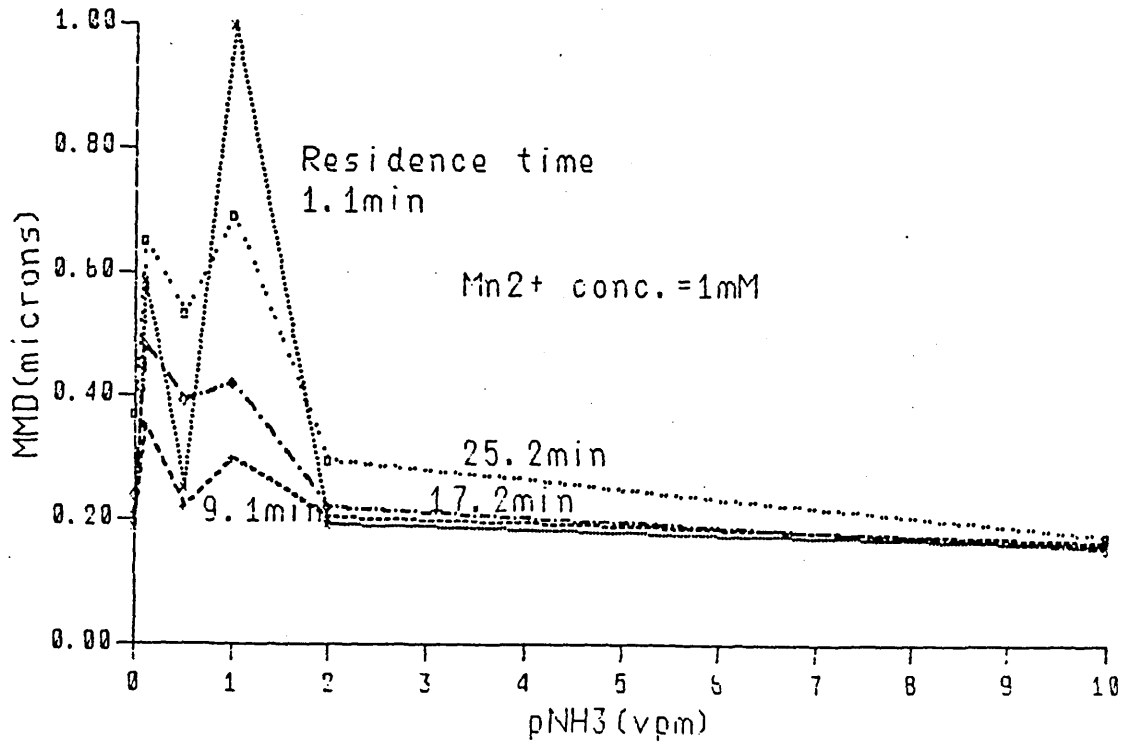


Figure IV.16a:-Variation of droplet size with the partial pressure of NH_3 in Mn^{2+} system.

IV.4 SO_2 Oxidation Monitoring by Chemical Method

In this section the yield of SO_4^{2-} from SO_2 oxidation measured by ion chromatographic analysis are reported. The peripheral question of determination of the liquid concentration of the aerosols is also discussed. Finally the sulphate concentrations obtained are used in calculating the oxidation rates and rate constants. The values are discussed in terms of the oxidation enhancement by NH_3 and Mn^{2+}.

IV.4.1 Sulphate concentration

The sulphate concentrations of the aerosols in runs 6, 7 and 9 are listed in Table IV.21. In view of the uncertainty in the experimental value of the liquid water content of the aerosol, the sulphate concentration is based on the entire volume of the aerosol. The sulphate loading of other runs were not determined directly by HPLC analysis but by a technique discussed in Appendix C and are listed in Appendix C2, C3 and C4.

IV.4.2 Aerosol liquid water concentration

The liquid water concentration of the aerosols obtained experimentally are listed in Table IV.22. The values vary within approximately one order of magnitude. The increase with master solution concentration shows qualitatively the Raoults Law solute effect.

Attempts to quantify the sulphate produced by oxidation in Runs 6, 7 and 9 using the changes in the liquid water mass concentration was not successful. One of the likely reasons for the failure is the narrow range of variation in sulphate produced in the small time interval studied. The more important reason is the loss of droplets in the reactor bends which distorted the pattern of droplet mass change with contact time. A droplet mass concentration of 1.59 g m^{-3} of aerosols was accepted for runs 6, 7 and 9 for all residence times. This was the value obtained for the residence time of 1.1 minutes in run 6 and which, within the degree of accuracy imposed by the balance used did not vary for other residence times or runs.

Table IV.21 Droplet sulphate loading obtained by HPLC analysis

	SO_4^{2-} Loading (moles dm^{-3} of aerosols x 10^9)		
Run	6	7	9
P_{SO_2} (vpm)	1.0	1.0	50.0
P_{NH_3} (vpm)	1.0	2.0	1.0
Contact time (min)			
.65	1.73	1.82	1.70
1.1	1.86	1.94	1.92
5.1	2.39	3.05	2.53
9.1	3.47	4.14	3.43
13.2	3.47	4.17	3.53
17.2	3.55	4.24	3.72
21.2	3.62	4.68	3.83
25.2	3.66	4.78	3.94

The liquid water concentrations of the aerosols in runs 6, 7 and 9 were calculated from the experimental sulphate concentrations (Table IV.2) using the modified (McDonald, 1953) form of Raoults' equation

$$m = \frac{im'H}{1 - H}$$

where m and m' are the masses of water and solute respectively in the droplet, H is the relative humidity, i is the vant Hoff's factor. A value of 3 i.e. the number of ions per molecule of $(NH_4)_2SO_4$ was used. Using the relative humidity value of 98% the liquid water concentrations of the aerosol calculated are listed in Table IV.23.

These values calculated from the sulphate concentration of the aerosols are on the average lower by at least one order of magnitude than the value measured by filteration for run 6 at a contact time of 1.1 minutes and adopted as the appropriate value for all the other runs. The exclusion of the solute mass though contributory is not a critical cause of this discripancy. It may be that the aerosol mass concentration was overestimated or the sulphate loading of the aerosols was underestimated. If the latter were the cause, it might have been as a result of loss of aerosol droplets in the denuder.

Table IV.22 Aerosol droplet mass concentrations.

Master solution concentration(M)	0.001	0.01	0.05	0.1	0.5
Relative humidity (%)	96	95	97	94	96
Reactor temperature (^{o}C)	23.6	23.8	23.7	23.3	24.8
Droplet mass concentration (gdm^{-3} $x10^{5}$)	0.834	1.67	3.1	1.6	3.0
MMD (microns)	0.1	0.42	0.58	0.56	0.65

Table IV.23 Liquid water concentration of the aerosols in runs 6, 7 and 9

Contact time (min)	Mass concentrations ($g\ dm^{-3}$ of aerosols) x 10.E05 Run 6	Run 7	Run 9
0.65	3.36	3.53	3.30
1.1	3.61	3.77	3.73
5.1	4.64	5.92	4.91
9.1	6.74	8.04	6.66
13.2	6.74	8.10	6.85
17.2	6.89	8.31	7.22
21.2	7.03	9.09	7.44
25.2	7.11	9.28	7.65

IV.5 Reaction rate and rate constants

An attempt was made to obtain the oxidation rate and the rate constant from the droplet size using the time for fractional increase (analogous to half-life) in droplet size. However, the oxidation rates obtained by this method could not be brought to the same basis in terms of units with those obtained by other workers and hence no comparison could be made. Hence it became necessary to invert droplet sizes into sulphate concentration using a strategy discussed in Appendix C. In the treatment of oxidation rates and rate constants that follows runs 4 and 8 are omitted owing to the erratic nature of the data.

The aerosol sulphate concentration determined experimentally (runs 6, 7 and 9) are plotted against residence time as shown in Fig. IV.17 - IV.19. In all the cases, the curves are steep initially and flattened out after about thirteen minutes, showing that reaction was very fast initially but slowed down as time went on to an asymptote. This is in agreement with the findings of a plume study by Hegg et al (1981) and the interactive cloud model of Easter and Hobbs (1974). The model of Scott et al (1967) predicted a similar trend but with a longer linear interval than was observed in this study. The shape of the curves after thirteen minutes may be attributed to the self-limiting property of SO_2 oxidation. This according to Junge et al. (1958) results from the accumulation of acidity or the exhaustion of the reacting species. Product analysis of runs 6, 7 and 9 however showed that the reactants were not exhausted within the duration of the experiments. Also that the accumulation of acidity was not responsible for the observed sulphate profile is demonstrated by the existence of such profile in buffered runs. A likely explanation is that initially there is a rapid droplet growth resulting in enhanced absorption of the reactant gases and hence enhanced reaction rate. Enhanced absorption of reactant gas during condensation of a humid gas stream on droplets had been reported by Matteson et al (1978). But as residence time increases, the growth rate falls off, most likely as a result of lowered R.H. resulting in depressed reactant absorption and hence lowered reaction rate.

The reaction rates were the regression coefficients obtained by fitting the first five points of the graphs in Fig.IV.17 to IV.19 to a regression line. Those for the other runs were calculated similarly and listed in Table IV.24 and IV.25a.

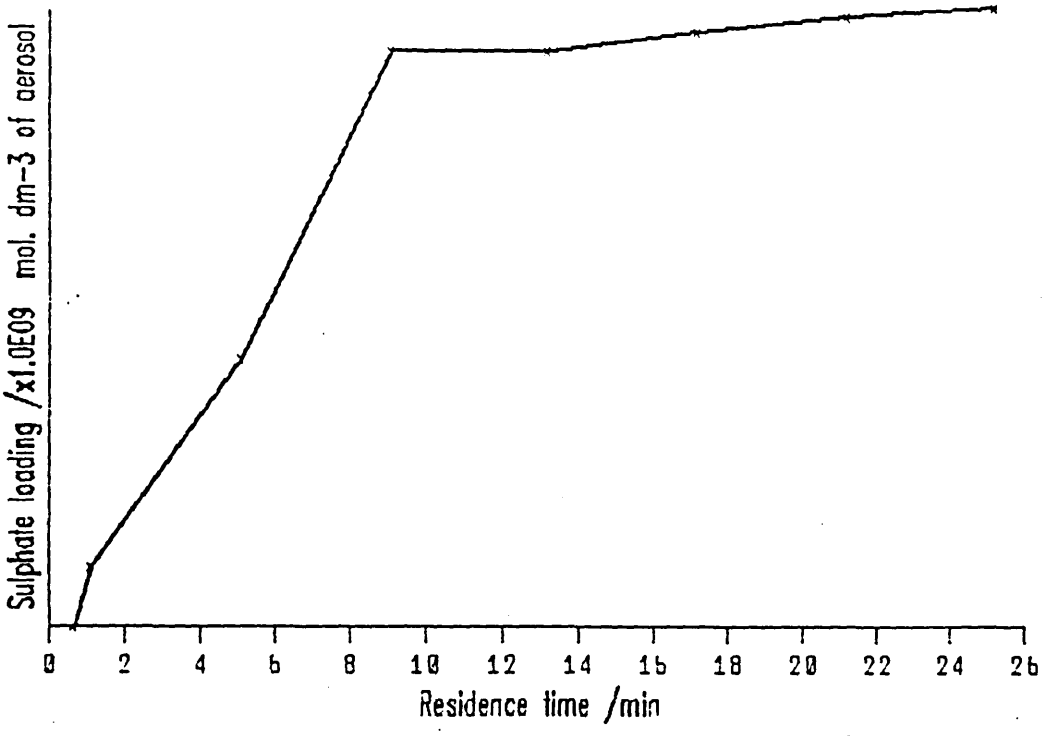


Figure IV.17:-Droplet sulphate loading obtained by ion chromatography as a function of residence time, with 1.0 vpm SO_2 and NH_3.

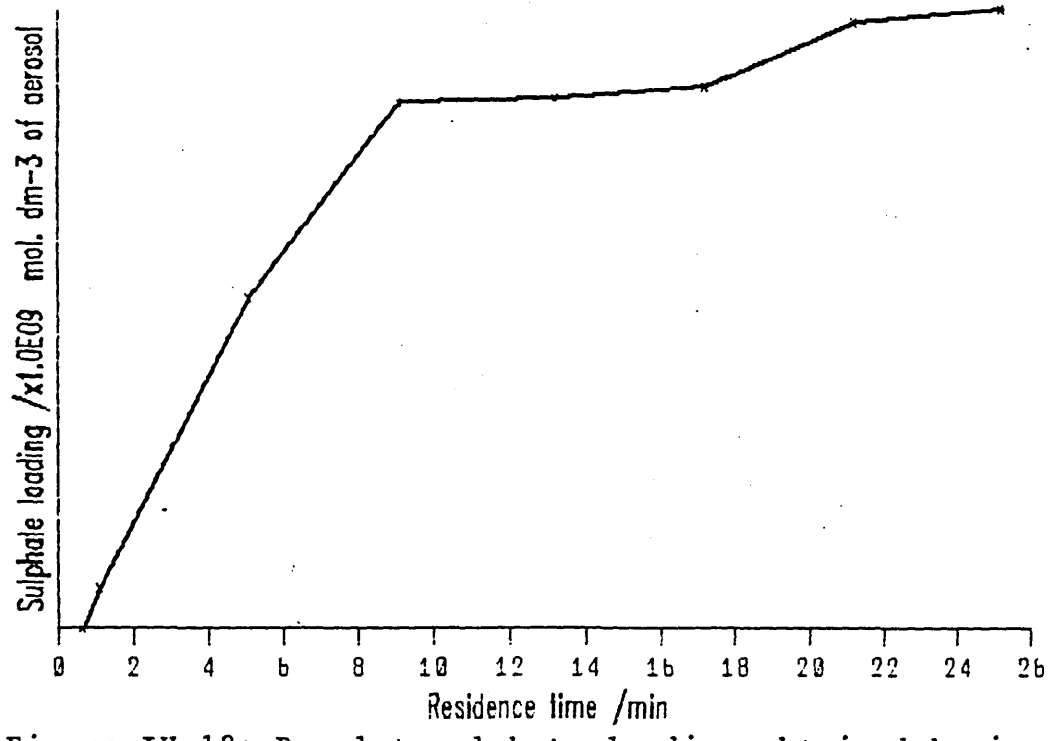


Figure IV.18:-Droplet sulphate loading obtained by ion chromatography as a function of residence time ,with 1vpm SO_2 and 2vpm NH_3.

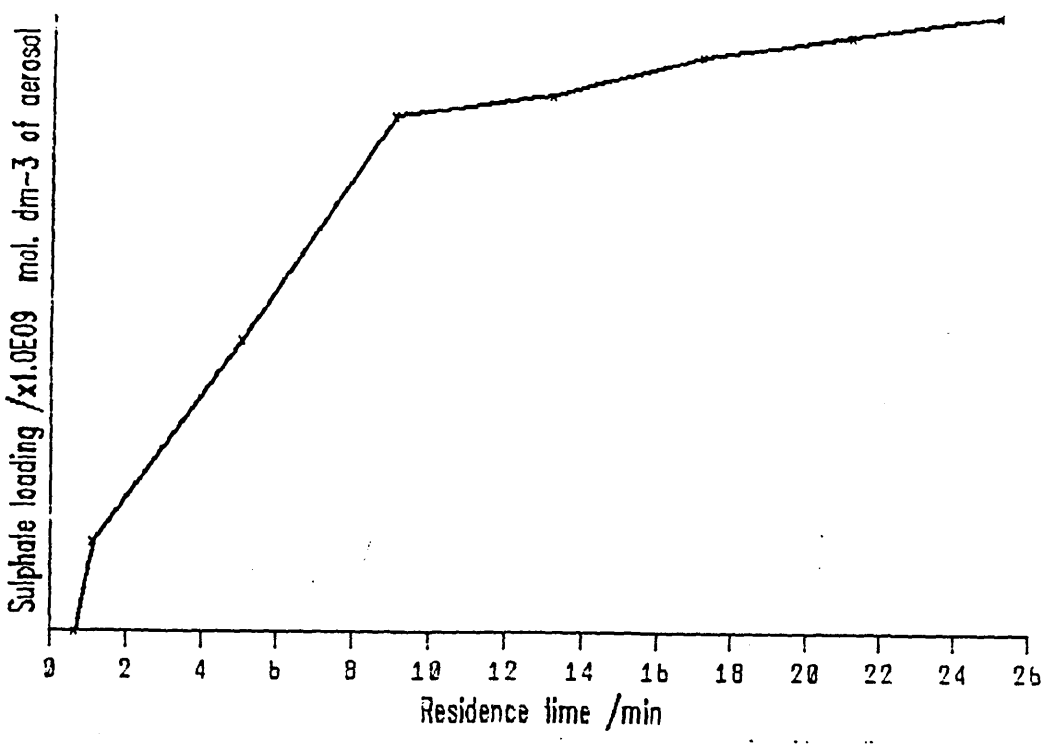


Figure IV.19:-Droplet sulphate loading obtained by ion chromatography as a function of residence time (50vpm SO_2, 1vpm NH_3)

Trends in Reaction Rates:

The trends in reaction rates will now be discussed in terms of the presence or absence of Mn^{2+} and NH_3. The reaction rates of the uncatalysed system show a slow increase by a factor of two for a two order of magnitude increase in the gas phase partial pressure of SO_2 (Table IV.24). This means that the SO_2 partial pressure dependence of the oxidation is very weak in the region investigated (1 to 100 vpm). This is consistent with the findings of Miller et al (1972).

That the presence of NH_3 has enhanced the SO_2 oxidation is demonstrated by comparing the reaction rates in runs 1 and 6. The reaction rate in run 6 for ammonia concentration of 1 vpm was thirteen times faster than in run 1 in which NH_3 was absent. An increase in NH_3 partial pressure by a factor of two produced an increase in rate by a factor of 1.5. The increase in rate with NH_3 partial pressure results from the pH dependence of the equilibrium concentration of hydrogen sulphite and sulphite ions according to the physico-chemical model of Scott and Hobbs (1967). In addition to this, the model put foward by Wang and Himmelblau (1964) which suggests a further production of hydrogen sulphite from $SO_2.H_2O$ as a result of the reactions with OH^-

$$SO_2.H_2O + OH^- \rightleftharpoons HSO_3^- + H_2O \qquad \text{IV.7}$$

is likely to yield oxidation rate higher than is predicted by the model of Scott and Hobbs.

The variation of reaction rate with NH_3 partial pressure is shown in Table IV.25a. Reaction rates showed a general increase below NH_3 partial pressure of 10 vpm. However, at 10 vpm NH_3 concentration, a maximum reaction rate was attained, which remained fairly invariant as gas phase concentration of NH_3 increased. This trend as pointed out earlier was caused at least in part by gas phase reaction between SO_2 and NH_3. Another possible cause of the failure of oxidation rate to keep pace with sulphite ion concentration after a p_{NH_3} value of 10 vpm was the dependence of the SO_2 oxidation in this pH regime on oxygen concentration which was suggested by Hegg et al (1978).

Table IV.24 The variation of SO_2 oxidation rate with the partial pressure of SO_2 (NH_3 and Mn^{2+} absent).

Runs	p_{SO_2} (vpm)	pH	Reaction Rates (Ms^{-1})
1	1.0	2.7	4.33×10^{-13}
2	10.0	2.6	4.53×10^{-13}
3	50.0	2.6	6.13×10^{-13}
4	100.0	2.4	8.50×10^{-13}

Table IV.25a The effect of NH_3 partial pressure on the oxidation rate of SO_2 (Mn^{2+} absent)

Runs	p_{SO_2} (vpm)	p_{NH_3} (vpm)	pH	Reaction Rates (Ms^{-1})
5	1.0	0.5	6.1	1.87×10^{-12}
6	1.0	1.0	6.3	3.27×10^{-12}
7	1.0	2.0	6.4	4.56×10^{-12}
8	50.0	0.1	5.0	1.69×10^{-12}
9	50.0	1.0	5.5	3.23×10^{-12}
11	50.0	10.0	6.0	7.79×10^{-11}
12	50.0	25.0	6.1	2.29×10^{-11}
13	50.0	50.0	6.3	5.38×10^{-11}

The influence of NH_3 on Mn^{2+} catalysed oxidation:-

The reaction rate of the Mn^{2+} catalysed oxidation of 1 vpm SO_2 in the absence of NH_3 is about one-and-a-half times faster than the oxidation under similar conditions in the absence of Mn^{2+}. The variation of catalysed SO_2 oxidation rate with NH_3 partial pressure is listed in Table IV.25b. For the 1 vpm SO_2 reaction rate decreases with increasing partial pressure of NH_3. The same trend exists for the 50 vpm SO_2. Ibusuki et al (1984) observed pH-dependent oxidation rates using NaOH buffered solution (Table II.15, p79) instead of NH_3. These authors interpretations are similar (see (c) below) to only one of the possibilities which the NH_3 additive implies.

A parasitic reaction which would scavenge any or all of the three reacting components (NH_3, SO_2 and Mn^{2+}) from the system may be operating in the system. The formation of $NH_3.SO_2$ adduct had been adequately discussed earlier. It is not likely to be the major cause of depressed oxidation rate, at least, in the experimental runs that involve low partial pressures (below 2 vpm) of the reacting gases. In the runs that made use of high partial pressures of the gas (p_{SO_2} = 50 vpm, p_{NH_3} 2 vpm) at the worst, adduct formation would degrade the concentrations of the reacting gases to low levels leaving enough NH_3 still to play an enhancing role in the oxidation process. However, it is not realistic to suggest that the presence of Mn^{2+} in the solution would in any way affect this gas phase process. The following hypotheses have therefore been put foward to explain the observed trend in oxidation rate.

(a) The formation of a complex between Mn^{2+} and $NH_3.H_2O$ could be a factor responsible for the decreasing oxidation rate as the NH_3 concentration increases. Octahedral complexes of the type $[Mn(NH_3)_6]^{2+}$ exist between NH_3 and some manganous salts (Cotton et al., 1980). Such a complex is likely though not yet reported between Mn^{2+} from $MnSO_4$ and NH_3. If it exists, S(IV) would be in competition with NH_3 for the Mn^{2+} ion, to the extent as to depress the concentration of the $[Mn\ S(IV)]^{2+}$ complex which is formed at the initiation step of the mechanism of Matteson et al.

(b) The oxidation trend shown in Table IV.25b could also be interpreted in terms of the S(IV) species involved in complex formation with Mn^{2+} and the dependence of the relative concentrations of these

species on the droplet pH (Beilke et al, 1978). As in other mechanisms of droplet phase oxidation of SO_2, there is a lack of consensus on the S(IV) species that forms the Mn^{2+}-S(IV) complex in the rate determining step. The observed rate trend is consistent with oxidation proceeding through the formation of a complex between Mn^{2+} and a S(IV) species whose concentration decreases with increasing pH, and this species is most likely to be HSO_3^-.

(c) Another likely cause of the depressed reaction rate observed in the catalysed SO_2 oxidation in this study is the sequestration of Mn^{2+} and OH^- ions through the formation of the insoluble $Mn(OH)_2$ which has a solubility product of 4×10^{-14}M. In the system, the aerosols were contacted with NH_3 and consequently the equilibrium concentrations of $NH_3.H_2O$, NH_4^+ and OH^- were already established before SO_2 was let in. Even if SO_2 and NH_3 were introduced into the aerosol stream at the same time, it is still possible that the NH_3 could dominate the solution chemistry of the system initially. This is because NH_3 is more soluble and is absorbed much faster than SO_2. The faster rate of absorption is a consequence of the fact that the process is gas phase controlled and the gas phase diffusivity of NH_3 is twice that of SO_2 (Appendix A). Hence before the introduction of SO_2, the following equilibria between NH_3 and aerosol exist:

$$MnSO_4 \rightarrow Mn^{2+} + SO_4^{2-} \; ;$$

$$H_2O \overset{K_w}{\rightleftharpoons} H^+ + OH^- \; ;$$

$$NH_3 + H_2O \overset{H_a}{\rightleftharpoons} NH_3.H_2O \; ;$$

$$NH_3.H_2O \overset{K_a}{\rightleftharpoons} NH_4^+ + OH^- \; ;$$

$MnSO_4$ is assumed to be completely dissociated and hence

$$[Mn^{2+}] = [SO_4^{2-}]$$

From electroneutrality equation,

$$[H^+] + [NH_4^+] = [OH^-]$$

Consequently, using the partial pressure of NH_3, the hydrogen ion concentration could be calculated from the equation

$$[H^+] = \left(\frac{K_w}{\frac{K_a}{K_w}.H_a p_{NH_3} + 1} \right)^{\frac{1}{2}} \qquad \text{IV.2}$$

The values of hydrogen ion concentrations obtained for the partial pressures of NH_3 used are listed in Table IV.26. Given that a hydrogen ion concentration of at least 1.56×10^{-9} mol dm^{-3} given by the equation

$$[H^+] = K_w \left(\frac{Mn^{2+}}{K_{sp}} \right)^{\frac{1}{2}} \qquad \text{IV.3}$$

was required to prevent the precipitation of $Mn(OH)_2$, it will be seen from Table IV.26 that in all the NH_3 partial pressures used, this value of hydrogen ion concentration was not attained and therefore Mn^{2+} removal by precipitation as $Mn(OH)_2$ is likely. The hydroxide is very readily oxidized in alkaline medium (Cotton et al, 1980) to yield the hydrated oxide

$$Mn^{2+} + 2OH^- \overset{K_{sp}}{\rightleftharpoons} Mn(OH)_2 \rightarrow MnO.OH \qquad \text{IV.4}$$

thus ensuring the removal of Mn^{2+} and OH^- ions from solution. Since data on the oxidation rate of $Mn(OH)_2$, which according to Cotton et al (1980) is pH-dependent are not available, it is not possible to calculate the characteristic time and thereby elucidate the effect of the increase in the hydrogen ion concentration of the droplet when it absorbed SO_2 later in the line. However, the likely effect was to slow down the $Mn(OH)_2$ oxidation and thereby slow down the rate of removal of Mn^{2+} and OH^- ions by precipitation. We may interprete the results as follows, for highly alkaline medium ($p_{NH_3} > 2$vpm), the concentration of the hydrogen ion furnished by the SO_2 was not sufficiently high to prevent the removal of Mn^{2+} and OH^- ions so that the catalytic effect of Mn^{2+} and the enhancement effect of NH_3 were severely reduced. On the other hand, for the mildly alkaline medium (p_{NH_3} below 2 vpm), the hydrogen ion concentration was suficiently high to prevent the precipitation of $Mn(OH)_2$ while at the same time maintaining a pH high enough to cause enhanced oxidation of SO_2. Based on this model, two modes of synergism

Table IV.25b Variation of Mn^{2+}-catalysed oxidation rate with NH_3 partial pressure

	Reaction Rate (moles dm^{-3} of aerosol s^{-1}) x 10^{12}					
p_{SO_2} (vpm)	1.0				50.0	
p_{NH_3} (vpm)	0.0	0.5	1.0	2.0	1.0	10.0
Mn^{2+} absent a	0.14	5.50	1.62	2.28	2.09	154
Mn^{2+} present b	0.19	5.48	0.65	0.38	6.86	1.55
b/a	1.35	1.0	0.4	0.17	3.28	0.01

Table IV.26 Droplet hydrogen ion concentrations obtained from the gas-phase NH_3 partial pressures

NH_3 partial pressure (vpm)	H^+ ion concentration (mol dm^{-3}) x 10^{10}	pH	OH^- ion concentration (M) x 10^5
0.1	10.00	9.0	1.01
0.5	4.48	9.3	2.25
1.0	3.17	9.5	3.18
2.0	2.24	9.6	4.50
10.0	1.00	10.0	10.10

are proposed to operate in the system to yield an enhanced sulphate production at hydrogen ion concentrations above the value given by equation IV.3, and a depressed sulphate formation below this value. Ibusuki et al (1984) working with $MnSO_4$ bulk solution of concentration between 10^{-6} and 5×10^{-6} M and S(IV) of concentration between 5×10^{-6} and 1.5×10^{-5} M found that rate constant was depressed at pH values between 5 and 8 and explained it partially in terms of $Mn(OH)_2$ formation. This, however has no theoretical basis since the solubility product of $Mn(OH)_2$ cannot be exceeded under the catalyst concentrations and the pH values used in the study.

Since it is not possible that the entire Mn^{2+} ion in the droplet phase would precipitate out as $Mn(OH)_2$ it is likely that the decrease in reaction rate with increase in NH_3 concentration is as a result of a change in reaction mechanism. Coughanowr and Krause (1965) found a second order rate dependence on Mn^{2+} concentration at very low Mn^{2+} concentrations. Hence it is valid to assume that at high values of NH_3 partial pressures with the consequent high droplet pH, the Mn^{2+} concentration was so reduced that the rate equation could be

$$R = k_2[Mn^{2+}]^2 \qquad \text{IV.12}$$

Reaction Order

The attempt made at determining the reaction orders of runs 6, 7 and 9 (Appendix D) by fitting the experimental sulphate and initial sulphite concentrations into the integrated zero, half, first and second order rate equations failed to indicate precisely the orders of the reaction from the shapes of the curves except in run 9 where a zero order was indicated. A calculation of the numerical values of order (Appendix D) also gave values (Table IV.27) that are inconsistent with any known values in the literature. A suggestion of a third order rate equation is not countenanced on theoretical grounds. The contradiction in the reaction orders of run 9 obtained by two techniques (zero by graphical method and 2.6 by calculation) underscores the unreliability of the calculated values.

A first order relation was expected for runs 6 and 7 and zero order for run 9 judging from the partial pressures of SO_2 in the three runs (Miller et al, 1972 and Luria et al, 1978). If runs 6 and 7 are regarded as being of similar order judging from the similarity of the calculated values to that of 9 (even though definitely faulty), they may as well be regarded as being of zero order. If that is so, it means that even at 1vpm gas phase concentration of SO_2 the oxidation is zero order with respect to SO_2. This will be in agreement with the findings of Clarke and Radojevic (1983).

Rate Constants

Pseudo-first order rate constants were derived for the runs and listed in Tables IV.28. In some of the runs namely 1, 3, 15, 16 and 21 the SO_4^{2+} produced was too high to be accounted for in terms of sulphite ion as the only readily oxidised S(IV) species. That the concentration of sulphite ion was small in these runs may be attributed to low pH in the absence of the buffering effect of NH_3. In runs 15 and 16 in the presence of catalyst and under 1 vpm NH_3, the rate of oxidation was SO_3^{2-} limited since $[SO_3^{2-}] < [SO_4^{2-}]$. Calculation of rate constants in thes runs was done on the basis of the total concentration of SO_2 in the aerosol stream. Runs 4, 8, 10 and 14 were not analysed because of the inconsistency of the data. The rate constants listed in Appendix D and Table IV.28 are discussed in terms of the different combinations of reactants.

A variation in pseudo first order rate constant of over four order of magnitude is observed ranging from low $9.35 \times 10^{-8} s^{-1}$ for an uncatalysed reaction in $(NH_4)_2SO_4$ droplets in the absence of NH_3 to high $1.27 \times 10^{-3} s^{-1}$ for an uncatalysed reaction in the presence of NH_3. This means a characteristic time ranging from high 123.8 days to low 13 minutes. However, in the individual reactant combinations (Table IV.28), the range of variation is much narrower.

For runs in reactant combination A, that is the $(NH_4)_2SO_4$ droplet phase oxidation of SO_2 in the absence of Mn^{2+} or NH_3, a pseudo-first

Table IV.27 Order of the Reaction obtained from experimental conditions

	Run 6	Run 7	Run 9
Rate	1.29×10^{-6}	2.14×10^{-6}	1.60×10^{-6}
[S(IV)]	4.83×10^{-3}	9.19×10^{-3}	6.9×10^{-3}
Order	2.54	2.78	2.61

Table IV.28 The Pseudo-first order rate constants obtained under various combinations of reactant concentrations

Reactant Combinations	Run(s)	Rate Constant (s^{-1})	Coefficient of Variation	SO_2 oxidation	Characteristic time
A					
$(NH_4)_2SO_4$ droplet	1, 2				
NH_3 an Mn^{2+} absent	and 3	3.08×10^{-6}	0.19	1.1% hr^{-1}	90.2 min
B					
$(NH_4)_2SO_4$ droplet	5, 6, 7				
NH_3 present	9, 11				
Mn^{2+} absent	12 and 13	4.5×10^{-4}	0.92	2.7% min	37 min
C					
$MnSO_4$ droplet	15				
Mn^{2+} present	and				
NH_3 absent	16	1.23×10^{-6}	1.31	0.44% hr^{-1}	9.4 days
D					
$MnSO_4$ droplet	17, 18				
Mn^{2+} present	19, 20				
$P_{NH_3} \leq$ 2 vpm	and 21	2.55×10^{-4}	1.6	1.5% min^{-1}	65.4 min
E					
$MnSO_4$ droplet					
Mn^{2+} present					
P_{NH_3} = 10vpm	22	7.59×10^{-7}	-	0.27% hr^{-1}	15.2 days

order rate constant of 3.08×10^{-6} s^{-1} with a coefficient of variation of 0.19 was observed. This is definitely a low value compared to the values listed in Table II.13 especially those of them in which the reaction took place in pure water droplet (Steele et al., 1981 and Miller et al, 1972). Since none of the runs made use of pure water droplet, it is not possible to determine the effect of $(NH_4)_2SO_4$ on the rate constant under the experimental conditions used in the study. However, based on the low value of the rate constant, it is not likely that $(NH_4)_2SO_4$ acted as a catalyst in the oxidation. The likely effect of $(NH_4)_2SO_4$ on droplet phase oxidation of SO_2 is the stabilization of the droplet towards evaporation thereby maintaining high liquid phase concentration of S(IV) species. This means in effect that any condition that is capable of stabilizing the droplet and maintaining the same pH as $(NH_4)_2SO_4$ would produce a similar effect.

In the reactant combination B, the rate constant is 4.50×10^{-4} s^{-1} with a coefficient of variation of 0.92. The time constant of 2.7% min^{-1} for runs in which NH_3 is involved in the absence of Mn^{2+} is in good agreement with the value of 2.5% min^{-1} obtained by van den Heuvel and Mason (1963). However, it is lower than most values listed in Table II.13.

In combination C, that is $MnSO_4$ catalysed oxidation of SO_2 in the absence of NH_3 the rate constant of 1.23×10^{-6} s^{-1} is lower than the 8.3×10^{-5} s^{-1} obtained by Crump et al (1983) and in most other studies (listed in Table II.14a). That the rate constant obtained in this combination is lower than in combination A is inexplicable in view of the well characterised catalytic effect of Mn^{2+}. When considered along with the value of 2.55×10^{-4} s^{-1} obtained in combination D it becomes certain that the enhancement effect of NH_3 also extends to Mn^{2+} catalysed system. However, a comparison with the rate constant in combination B with D shows the synergistic effect of NH_3 and Mn^{2+} in admixture. In view of the known dependence of the relative concentrations of the S(IV) species on pH, it becomes likely that SO_3^{2+} is involved in the SO_2-Mn^{2+}-NH_3-H_2O-O_2 oxidation system. If SO_3^{2-} complexes most readily with Mn^{2+} of all the S(IV) species in aqueous solution as was suggested by Bassett and Parker (1951) then the higher rate constant in the presence of NH_3 than in its absence is explained in terms of increased SO_3^{2-} concentreation as a result of higher pH. However, it is not likely

that SO_3^{2-} is the complexing S(IV) species in view of the low value of the rate constant (7.59×10^{-7} s^{-1}) in Combination E where SO_3^{2-} is expected to be the dominant S(IV) species. Also, $SO_2.H_2O$ is unlikely to be the complexing S(IV) species as suggested by Matteson et al (1969) in view of the fact that its equilibrium mole fraction at pH values above 5.0 is zero. On the other hand, although the mole fraction of HSO_3^- decreases as pH increases above 5.0, it still exists in a substantial concentration at pH values below 9.0. It is the most abundant S(IV) species in solution in the pH range between 2.0 and 7.0. Hence the trends in the rate constants in the Combinations D and E may be explained in terms of the formation of complex between Mn^{2+} and HSO_3^- in the initiation step of the free radical mechanism of Schmittkunz or that of the polar non-radical mechanism of Bassett et al (1951).

IV.6 Application to stack plume

The results obtained in this study show that the rate of heterogeneous droplet phase oxidation of SO_2 in aerosols is affected by the presence of NH_3, catalyst and water vapour. Since a stack plume or at least one that passed through a rural agricultural district and had undergone a substantial inmixing with NH_3 satisfies these conditions, an examination will be made of the changes in the S(IV) composition of a stack plume as it is advected by the mean wind with dispersion and dilution.

Stack effluent SO_2 concentration of the order of 10^3 vpm have been measured by Brookhaven National Laboratory (1972). In addition, a host of other components which participate in SO_2 oxidation exist and these include water vapour, acidic gases (NO_x), basic oxides (CaO and MgO), transition metal oxides, NH_3 and inert siliceous fly ash particles of sizes in the nuclei and accumulation mode. As the effluent exits the stack, there exists an induction period during which it cools down to ambient temperature and the aerosol droplets are formed by water vapour condensation on either pre-existing inert particulates or sulphate CCN formed in the stack effluent by homogeneous gas phase processes. Peuschel and van Valin (1978) measured a rate of formation of such CCN of 10^{15} to 10^{16} s^{-1} in a stack plume at a supersaturation of 1% early in its emission. Since the droplets formed on inert supports are invariably large, they are easily lost from the plume by sedimentation and hence do not play much part in the heterogeneous droplet phase oxidation of SO_2. Droplets formed on sulphate CCN persist for a very long time and play important role in droplet phase oxidation since as a result of their small size, absorption of SO_2 by them is not limited by aqueous phase diffusion.

The situation simulated in this study and which is discussed here exists at some distance downwind of a source where the plume gas phase SO_2 has been depleted down to 50 vpm and droplets in the accumulation mode of number concentration 10^9 cm^{-3} have been formed. Assuming an unlimited supply of oxygen, the conversion rate will depend on the rate of SO_2 uptake by the droplet which as was shown in the study depends on temperature and the control of the droplet pH either by the buffering action of NH_3 or dilution, but not critically on the SO_2 partial

pressure. Only first order rate equations with respect to SO_2 were considered.

The rate equation involving Mn^{2+} is

$$\frac{-d[SO_2]}{dt} = k'[SO_2][Mn^{2+}]$$

and for SO_2 alone

$$\frac{-d[SO_2]}{dt} = k[SO_2] \qquad \text{.....IV.13}$$

The sulphate yield at time t is given by

$$[SO_4^{2-}]_t = [SO_2]_0 \{1 - \exp(-kt)\} \qquad \text{.....IV.14}$$

This suggests that in-plume conversion becomes total at infinite time, $t = t_\infty$ i.e.

$$[SO_4^{2-}]_{t_\infty} = [SO_2]_0 \qquad \text{.....IV.15}$$

Equations IV.14 and IV.15 can adequately explain batch systems in which the volume is constant. Freiberg (1976) used a modification to the fixed volume system of SO_2 oxidation in the presence of Fe^{3+} to formulate conversion in a plume. Applying the modification to equation IV.14,

$$(SO_4^{2-})_t - (SO_4^{2-})_0 = (SO_2)_0\{1 - \exp[\frac{k}{b}(\frac{1}{t} - \frac{1}{t_0})]\} \qquad \text{.....IV.16}$$

where (SO_4^{2-}) and (SO_2) are the SO_4^{2-} and SO_2 loadings of an eliptical plume (of Freiberg's model)

$$(SO_2) = V[SO_2]$$

V = volume of the reactor (the eliptical plume) and depends on the plume horizontal and vertical dispersion coefficients, σ_y and σ_z;
b is a constant which depends on the local meteorology;
t_0 is a dispersion parameter and is a reference time at which $V = V_0$.

The residence time of the plume SO_2 is obtained by substituting the left hand side of equation IV.16 with $(1 - 1/e)(SO_2)_0$, and solving for t,

$$\tau_{res} = kt_0/k - bt_0 \ln e \quad \ldots\ldots IV.17$$

where τ_{res} is the residence time, the time when the plume SO_2 had decayed to 1/e of the original concentration. The corresponding residence distance χ_{res} is given by

$$\chi_{res} = ukt_0/k - bt_0 \ln e \quad \ldots\ldots IV.18$$

where u = mean wind velocity.
At τ_{res} the plume SO_2 had decayed to 1/e of the original value. At $t = t_\infty$, equation IV.16 becomes

$$(SO_4^{2-})_{t_\infty} - (SO_4^{2-})_0 = (SO_2)_0[1 - \exp(-k/bt_0)] \quad \ldots\ldots IV.19$$

This means that the conversion to SO_4^{2-} in the expanding plume does not proceed to completion but to an asymptotic limit. This is in good agreement with the results of this study.

Based on the above, it is likely that conversion is very rapid near the source. As the plume is diluted downwind, conversion is quenched to an extent which depends on the partial pressures of the residual SO_2, NH_3 and water vapour, the dispersion characteristics and the aerosol droplet size. The significance of the asymptotic nature of the oxidation profile to SO_2 long range transport is that based on heterogeneous droplet phase process alone, even in the presence of adequate supply of NH_3, SO_2 will persist in the atmosphere for long distances from the source in an appreciable concentration unless degraded to the background level by other depletion processes.

CHAPTER V

Conclusions and suggestions for Further Research

In this study, experiments have been designed to study in situ by light scattering methods some properties of aerosols which are relevant to atmospheric pollution. The evolution of droplet size distribution as a result of condenstional growth and /or coagulation was investigated using $(NH_4)_2SO_4$ solution droplet in the submicrometer size range. Also, the air oxidation of SO_2 in submicrometer aerosol droplet in the presence of NH_3 and/or $MnSO_4$ was monitored by using the same technique as well as ion chromatographic methods. The salient points in the results are summarised below.

V.1 Behaviour of $(NH_4)_2SO_4$ solution aerosols:

1. At 98% R.H. and 25° C, it was not possible to obtain persistent aerosols from pure distilled water by the method of air blast atomisation. Hence it was necessary to stabilize it towards evaporation by introducing an inorganic solute. A salt that did not interfere with the oxidation was chosen.

2. The aerosol droplet size depended on the molar concentration of the master solution in a way consistent with heterogeneous condensation onto an inorganic solution droplet.

3. Droplet size increased with relative humidity in the reactor with a sudden jump after the deliquiscent point of $(NH_4)_2SO_4$.

4. The droplet size distribution and number concentration variation with aerosol residence time in the tube is consistent with a theoretical prediction of Brownian monodisperse and polydisperse coagulation operating sequentially.

5. Loss of droplets in the tube bends of the reactor is significant and likely to affect some of the results obtained at residence times above 1.1 minutes.

V.2 SO_2 oxidation - monitoring by means of light scattering

1. In the SO_2 air oxidation system, there is a positive correlation between droplet size and contact time. The effect of coagulation was negligible.

2. The correlation between droplet size and the partial pressure of SO_2 is positive but very low in the absence of NH_3 or Mn^{2+} but high in the presence of NH_3.

3. Correlation between droplet size and the partial pressure of NH_3 is positive. It is high up to 10 vpm of NH_3 and very low above this; for SO_2 partial pressure of 1.0 and 50vpm.

4. At high gas phase concentration of the reacting gases (p_{SO_2} = 50 and $p_{NH_3} > 10$ vpm) and high humidity, a solid adduct, $SO_2.NH_3$ was formed to a substantial degree and hence the amount of each that was available to participate in droplet phase oxidation was substantially reduced.

5. Catalysed (Mn^{2+}) oxidation in the presence of NH_3 shows negative correlation between droplet size and the partial pressure of NH_3.

V.3 Monitoring by means of chemical analysis

1. The annular denuder coated with gum tragacanth - PbO_2 slurry was highly efficient in removing from the aerosol stream SO_2 at concentrations up to 50vpm.

2. The electrostatic precipitator is not an efficient method for sampling aerosol droplets for chemical analysis at the aerosol flow rate of 4 $dm^3\ min^{-1}$. On the other hand, filtration using the Millipore VMWP membrane filter or scrubbing with two impingers in series are very efficient methods of sample collection.

3. Reaction rate dependence on SO_2 partial pressure was very weak at values between 1 and 100 vpm in an unbuffered system.

4. Reaction rate was very rapid initially but tailed off to an asymptotic limit after about thirteen minutes in the condition of the experiments.

5. Reaction rate was much higher in the presence than in the absence of NH_3. The correlation between reaction rate and the partial pressure of NH_3 was positive and high. However, in the Mn^{2+} catalysed system a negative correlation was found to exist between them.

6. The S(IV) species most likely to form a complex with Mn^{2+} in the initiation step of the catalysed system is HSO_3^-.

7. A zero order rate mechanism with respect to SO_2 was indicated for partial pressures of SO_2 1 - 50 vpm. However, a confirmation of this was not obtained.

8. The pseudo-first order rate constants with respect to SO_2 are hydrogen ion dependent.

9. The overall pseudo first order rate constant is within one order of magnitude of the values obtained by most other workers (Table II.13)

V.4 Recommendations and suggestions for further work

1. Experience in the use of the equipment has revealed certain areas where modifications are likely to result in improved accuracy. The most important is the flow reactor design which results into a significant loss of droplets at the tube bends. The use of a single tube as the reactor and aerosol flow-rate to vary residence time will eliminate the limitations of the bends and improve the quality of the results obtained.

2. It will be necessary to carry out a more detailed study of the SO_2-NH_3-Mn^{2+}-O_2-H_2O oxidation system to cover partial pressures of the reacting gases ranging from those of the ambient unpolluted atmosphere (for the NH_3, according to Georgii, 1970 is 1.75×10^{-9} - 2.63×10^{-9}atmospheres) to the concentration in a typical stack plume.

Prominence should be given to ion chromatography as a means of quantifying sulphate.

3. A detailed study should be carried out on the operation of the diffusion denuder with the aim of optimising it to handle high SO_2 concentrations and to eliminate droplet scavenging.

4. It will be informative to study the oxidation at a range of relative humidity between 20% and supersaturation to deduce the effect of the rate of condensation on oxidation rate.

5. Studies should be carried out to develop the light scattering method of aerosol analysis to measure in situ both the droplet size and number concentration simultaneously.

6. Since a stack plume contains concentrations of CO_2 much higher than the ambient, it will be valuable to study the effect of CO_2 concentrations on SO_2 oxidation.

7. It will be useful to investigate the use of ammoniated water droplets in flue gas desulphurisation since the $(NH_4)_2SO_4$ produced could be of use in agricultrue.

REFERENCES

ABBAS, R. and TANNER, R.L. (1981): Atmos. Environ. 15, 3, 377-281

ABEL, E. (1951): Monatshefte fur Chemie 82, 815

ADAMS, D.F., FARWELL, S.O., PACK, M.R. & ROBINSON, E. (1981): J. Air Pollut Control Assoc. 31, 1083

ADAMOWICZ, R.F. & Hill, F.B. (1977): BNL 22576, Brookhaven National Laboratory

ADEWUYI, Y. G. & CARMICHAEL, G.R. (1982): Atmos. Environ. 16, 4, 719

ALKEZWEENY, A.J. (1978): J. Appl. Met. 17, 609

ALKEZWEENY, A.J. & POWWEL, D.C. (1977): Atmos. Environ. 11, 179

ALTSHULLER, A.P. (1976): J. Air Polut. Control Assoc. 26, 318

ANDERSON, T. (1967): Tellus 21, 685

APCA: 'Directory and Resource Book' special Anniversary Edition pp180-1 1981-82

ARROWSMITH, A., HEDLEY, A.B. & BEER, J.M. (1973): Nature Phys. Sci. 244, 104

ATKIN, D.H.F. & GARLAND, J.A. (1974): W.M.O. Special Environment Report 3, 579-594

AVOL, E.L., JONES, M.P., BAILEY, B.M., CHANG, N.N., KLEINMAN, M.T. LINN,W.S., BELL, K.A. & HACKNEY, J.D. (1979): Am. Rev. Resp. Dis. 120, 319

BACKSTROM, H. (1934): Z. Physik. Chem. B25, 99

BARNES, R. & STOCK, C.R. (1949): Analyt. Chem. 29, 18

BARRIE, L.A. & GEORGII, H.W. (1976): Atmos. Environ. 10, 743

BASSETT, H. & PARKER, W. (1951): J. Chem. Soc. 47, 540

BASSETT, M. & SEINFELD, J.H. (1983): Atmos Environ. 17, 11, 2237

BAYVEL, L.P., EISENKLAM, P. & JONES, A.R. (1982): ICLASS - '82 The 2nd International Conference on Liquid Atomisation and Spray System June 20 - 22, 1982, Madison, Winsconsin, USA

BAYVEL, L.P. & JONES, A.R.: 'Electromagnetic Scattering and its Applications', Applied Science Publishers, London, 1981

BEILKE, S. & GRAVENHORST, G. (1978): Atmos. Environ. 12, 231

BEILKE, S., LAMB, D. & MULLER, J. (1975): Atmos Environ. 9, 1083

BEILKE, S., LAMB, D. & MULLER, J. (1979): Atmos. Environ. 13,1083

BENARIE, M., NONAT, A., & MENARD, T. (1973): Atmos. Environ. 7, 403

BHUMRALKAR, C.M., MANCUSO, R.L., WOLF, D.E., THUILLIER, R.H., NITZ, K.C. & JOHNSON, W.B.: 'Adaptation and Application of a long-term air pollution Model ENAMAP-1 to Eastern North America,' Final Report Project 7760, SRI, International Menlo Park, CA. Prepared by USEPA Research Triangle Park, NC Contract No. EPA/68-02-2959, 1980

BIRD, R.B., STEWART, W.E., LIGHTFOOT, E.N.:Transport Phenomena, Wiley, N.Y. 1960

BOTTGER,A., EHHALT, D.H. & GRAVENHORST, G. (1981):NASA Technical Memorandum, NASA TM-76652

BOUDART, M.:'The Kinetics of Chemical Processes' pp246 Prentice-Hall, N.J. 1968

BRIGGS, G.A.: 'Plume Rise', AEC Critical Review Series TID 25075. U.S. Atomic Energy Commission, 1969

BRIMBLECOMBE, P. & SPEDDING, D.J. (1974): Atmos Environ. 8, 937

BROOKHAVEN NATIONAL LABORATORY: The atmospheric Diagnostics Program at Brookhaven National Laboratory:- Fourth Status Report, June 1972. Contract No. AT(30-1)-16 with the USAEC. BNL Associated Universities Inc., Upton, NY.

BUFALINI, H. (1971): Environ. Sci., Technol. 5, 685

BUNDIASKY, S. (1981): Environ Sci., Technol. 15, 2,135

CADLE, R.D. (1975): J. Geophys. Res. 80, 1650

CADLE, R.D. (1980): Rev. Geophys. Space Phys. 18, 746

CAINS, P.W. (1975): PhD Thesis, University of London

CAINS, P.W. & CARABINE, M.D. (1978): J.Chem. Soc. Farad. Trans. II, 11, 2689

CALVERT, J.G., BOTTONMEIM, J.W., SU, F. & STRAUSZ, O.P.(1978): Atmos. Environ. 12, 197

CALVERT, J.G. & MOHNEN, V. (1983): National Academy of Science Report 'Acid Deposition, Atmospheric Processes in Eastern North America, Appendix A' ppl55-201. National Academic Press Washington D.C.

CARABINE, M.D., MADDOCK, J.E.L. & MOORE, E.A.P. (1971): Nature Phys. Sci. 231, 18

CARABINE, M.D. & MADDOCK, J.E.L. (1975): Atmos. Environ. 10, 735

CARABINE, M.D. & MOORE, A.P. (1973): Farad. Symp. Chem. Soc. 7,

CARLSON, R.M., ROSSEL, R.A. & VALLEJOS, W. (1967): Analyt. Chem. 39, 6, 688

CARMICHAEL, G.R. & PETERS, L.K. (1979): Atmos. Environ. 13, 1507

CASTLEMAN, A.W., MUUKELWITZ, H.R. & MANOWITZ, B. (1974): TELLUS 26, 222

CHAMBERLAIN, A.C. (1960): Int. J. Air. Pollut. 3, 63

CHAMBERLAIN, A.C. (1966): Proc. Royal Soc. (London) A290, 236

CHANG, S.G. & NOVAKOV, T. (1979): NASA - No. 79 - 10644

CHANG, S.G., TOOSI, R. & NOVAKOV, T. (1981): Atmos. Environ. 15, 1287

CHARLSON, R.J., COVERT, D.S., LARSON, T.V. & WAGGONER, A.P. (1978): Atmos. Environ. 12, 39

CHARLSON, R.J., VANDERPOL, A.H., COVERT, D.S., WAGGONER, A.P. & AHLQUIST, N.C. (1974): Atmos. Environ 8, 1257

CHENG, R.Y. CORN, M. & FROHLIGER, J.O. (1971): Atmos. Environ. 5, 987

CISNIEGA-ROJAS, M.G. (1983):PhD Thesis, London University

CLARK, A.I., MCINTRYE, A.E., LESTER, J.N. & PERRY,R.(1984): Environmental Monitoring & Assessment 4, 205

CLARK, R.H. (1979):'A model for short and medium range dispersion of radionuclides released to the atmosphere,'NRPB-R91, National Radiological Protection Board, Harwell, UK. pp74

CLARKE, A.G. & RADOJEVIC, M. (1983):Atmos. Environ. 17, 3, 617

CLARKE, A.G. & WILLIAMS, P.T. (1983): Atmos. Environ. 17, 3 607

COFFIN, D.L. & STOKINGER, H.Z.: 'Air Pollution' (edited by Stern, A.C.) 3rd edition, pp445-546; N.Y. Acad. Press, 1974

CONSIDINE, B.M. 'Energy Technology Handbook,' pp3.22 McGraw Hill, NY, 1977

COOPER, D.W., BYERS, R.L. & DAVIS, J.W. (1973): Environ. Sci. Technol, 7, 142

COTTON, F.A. & WILKINSON, G.:'Advanced Inorganic Chemistry - a comprehensive text' pp846-9 4th Edition, Wiley, Chichester, 1980

COX, R.A.(1974): J. Photochem. 3, 291

COUGHANOWR, D.R. & KRAUSE, F.E. (1965): Ind. Engng. Chem. Fundam. 4, 61

C.R.C:'Diffusion of Gases into Air,' Handbook of Chemistry and Physics (edited by Weast, R.C. and Astle, M.J.) 61st edition (1980-81), F62. CRC Press Inc. Florida

C.R.C.:'Solubility of Inorganic Compounds.' Handbook of Chemistry and Physics (edited by Weast, R.C. and Astle, M.J.) 61st edition (1980-81), B73-166. CRC Press Inc. Florida

C.R.C.:'Solubility Product of Inorganic Compounds.' Handbook of

Chemistry and Physics (edited by Weast, R.C. and Astle, M.J.) 61st edition (1980-81), B242. CRC Press Inc. Florida

CRUMP, J.G., FLAGAN, R.C. & SEINFELD, J.H. (1983): Aerosol Sci. Technol. 2, 301

CRUMP, J.G., FLAGAN, R.C. & SEINFIELD, J.H. (1983b): Atmos. Environ. 17, 7, 1277

CULLIS, C.F. & HIRSCHLER, M.M. (1980): Atmos. Environ 14, 1263

CUNNINGHAM, P.T., HOLT, B.D., HUBBLE, B.R., JOHNSON, S.A., SIEGAL, S., WILSON, W.I., CAASSO, F.A. & FURRIS, L. (1975): Annual Report, Report No. ANL-75-51, Chemical Engineering Division, Environmental Chemistry, Argonne National Laboratory

DANKWERTS, P.V. (1968): Chem. Engng Sci. 23, 1045

DASGUPTA, P.K., de CESARE, K.B. & BRUMMER, M. (1982): Atmos Environ 16, 5, 917

DAUBENDIECK, R.L. & CALVERT, J.G.(1975): Envir. Lett. 8, 103

DAUTREBAND, L., HIGHMAN, B., ALFORD, W.C. & WEAVER, F.L. (1948): Arch. Int. Pharmocodyn et de Therapie 76, 247

DAVIDSON, J.A. & COLLINS, E.A.(1972): J. Colloid Interface Sci. 40, 437

DAVIES, C.N. (1945): Proc. Phys. Soc.57, 259

DAVIES, C.N.:'Evaporation of Airborne droplets,' in Fundamentals of Aerosol Science (edited by D.T. Shaw), Wiley, N.Y., 1978

DAVIES, R.A., HAGOPIAN, K.E. & SYKES, A.G. (1969): J chem. Soc. (A) 623

DAVIES, T.D. (1983):Atmos Environ 17, 4, 497

DAWSON, G.A.(1977): J. Geophys. Res. 82, 3125

DELMAS, R.J., BANDET, J. & SERVANT, J. (1978): Tellus, 30, 158

DELMAS, R.J., BANDET, J., SERVANT, J. & BAZARD, Y.(1980): J. Geophys. Res. 85, 4468

DENNIS, W.L.:'The Physical Chemistry of Aerosols - A General Discussion of the Faraday Society, 1960' pp78-85. Aberdeen University Press, 1961

DERJAGUIN, B.V., BAKANOV, S.P. & KURGHIN, I.S.:'The Physical Chemistry of Aerosols - A General Discussion of the Faraday Society, 1960 pp96-99. Aberdeen University Press, 1961

DOBBINS, R.A.:Atmospheric Motion and Air Pollution, pp223-226. John Wiley and Sons N.Y. 1979

DUNNING, W.J. (1960):'The growth of hygroscropic drops in a humd air stream.' in The General Physical Chemistry of Aerosols - A general discussion of the Faraday Society. pp9-19

DURHAM, J.L. WILSON, W.E. & BAILEY, E.B. (1978): Atmos. Environ. 12, 883

EASTER, R.C. & HOBBS, P.V.(1974): J. Atmos. Sci. 31, 1589

EGGLETON, A.E.J.(1969): Atmos. Environ. 3, 3, 355

EGGLETON, A.E.J. & ATKINS, D.H. (1972): Atomic Energy Research Establishment, Report No. R6983

EGGLETON. A.E.J.& COX, R.A. (1978): Atmos. Environ. 12, 227

EISNER, H.S., QUINCE, B.W. & SLACK, C.:'The Physical Chemistry of Aerosols - A General Discussion of the Faraday Society, 1960' pp86-95. Aberdeen University Press, 1961

ENDLICH, R.M., BHUMRALKER, C.M., BRODZINSKY, R., NITZ, K. CONTREL, B. & MAYEHOFFER, P.(1982):'ENAMAP - A Long-term Air Pollution Model' Paper No. 82 - 10.3, Presented at the 25th APCA Annual Meeting and Exhibition New Orleans

ENGER, L. & HOGSTROM, U. (1979): Atmos. Environ. 13, 797

EPA: METHOD 5, Federal Register Vol 42, No. 160 August 1977

EPA: METHOD 6, Federal Register Vol 42, No. 160 August 1977

ERICKSSON, E. (1960): Tellus 12, 63

ERICKSSON, E. (1963): J. Geophys. Res. 68, 4001

ESPENSHEID, W.F., KERKER, M. & MATIJOVIC, E. (1964): J. Phys. Chem. 68, 11, 3093

FEREK, R.J., LAZRUN, A.L., HAAGENSON, P.L. & WINCHESTER, J.W. (1983): Environ. Sci. Technol. 17, 6, 315

FERM,M.(1979):Atmos. Environ. 13, 1385

FIRKET, J. (1936): J. Trans. Farad.. Soc. 32, 1192

FISH, (1971):Enviro. Lett. 2, 13

FOWLER, D. (1978):Atmos. Environ. 12, 369

FRANK, S.N. & BARD, A.J.(1974): J. Phys. Chem. 81, 1484

FREIBERG, J.E. (1974):Atmos. Environ. 8, 661

FREIBERG, J.E. (1975): Atmos Environ. 9, 661

FREIBERG, J.E. (1976):Atmos. Environ. 10, 121

FREIBERG, J.E. (1978):Atmos. Environ. 12, 339

FREIBERG, J.E. & SCHWARTZ (1981):Atmos. Environ. 15, 7, 1129

FRIEDLANDER, S.K. (1970): J. Aerosol Sci. 1, 295

FRIEND, J.P. (1972): Technical Comment, Science 175, 1278

FRIEND, J.P.:'The Global Sulphur Cylcle' in Chemistry of the Lower

Atmosphere (edited by Rasool, S.I.) ppl77-201. Plenum Press London, 1973

FUCHS, N.A.(1934): Z. Phys. Chim., 171, 34, 199

FUCHS, N.A.:'Evaporation and droplet growth in gaseous media'. Pergamon Press Oxford, 1959

FUCHS, N.A. 'Aerosol Impactors (A Review)' in Fundamentals of Aerosol Science (D.T. Shaw, editor). Wiley Inter. Science, N.Y. 1978

FULLER, E.C. & CRIST, R.H. (1941): J. Am. Chem. Soc. 63, 1644

FUZZI, S. (1978):Atmos. Environ. 12, 1439

GALLOWAY, J.N. & LIKENS, G.E. (1978): Tellus 30, 71

GARLAND, J.A. (1977):Proc. Roy. Soc. London A354, 245

GARLAND, J.A. (1978): Atmos. Environ. 12, 349

GEORGII, H.W. (1970): J. Geophys. Res. 75, 2365

GIFFORD, F.A. (1982):Atmos, Environ. 16, 3, 505

GILLANI, N.W., HUSAR, R.B., HUSAR, J.D., PATTERSON, D.E. & WILSON, W.E. (1978):Atmos Environ. 12, 589

GJERDE, D.T. & FRITZ, J.S. (1979): J. Chromatogr. 176, 199

GLADNEY, E.S., ZOLLER, W.H., JONES, A.G. & GORDON, G.E.(1974): Environ. Sci. Technol. 8, 6, 551

GMELIN(1963):Handuch Schwefel, Teil B-Lieferung 3

GMUR, N.F., EVANS, L.S. & CUNNINGHAM, E.A. (1983): Atmos. Environ. 17, 4, 715

GOKHALE, N. & GOOLD, J. (1969): J. geophys. Res. 74, 5374

GORMLY, P. & KENNEDY, M. (1949): Proc. R. Lr. Acad. 52A, 163

GRANAT, L. & JOHANSSON, C. (1983): Atmos. Environ. 17, 1, 191

GREEN, H.L. & LANE, W.R.:'Particle Clouds: Dust, Smokes and Mists.' pp3-58; E. & F.N. SPON Ltd, London, 1957

HALES, J.M. (1972): Atmos. Environ. 6, 9, 635

HALES, J.M. (1978):Atmos. Environ. 12, 389

HALPARINE, J. & TAUB, H. (1952): J. Am. Chem. Soc. 74, 375

HAMILTON, P.M., VAREY, R.H. & MILLAN, M.M. (1978):Atmos. Environ. 12, 127

HANSEN, L.D., RICHTER, B.E., ROLLINGS, D.K., LAMB, J.D. & EATOUGH, D.J. (1979):Analyt. Chem. 51, 6, 633

HARKER, A.E. (1975): J. Geophys. Res. 80, 3399

HARRISON, H.T., LARSON, T.V. & HOBBS, P.V. (1974): I.E.E.E. Annals No. 75 (H4004-123-1) ppl-7

HAULET, R., ZETTWOOG, P. & SABROUX, J.C. (1977): Nature, 268, 715

HAYON, E., TREININ, A. & WILF, J. (1972): J. Am. Chem. Soc. 94, 47

HEALY, T.V.(1974):Atmos. Environ. 8, 81

HEALY, T.V., McKAY, H.A.C., PILBEAM, A. & SCARGILL, D. (1970): J. Geophys. Res. 75, 2317

HEGG, D.A. & HOBBS, P.V. (1978): Atmos. Environ. 12, 241

HEGG, D.A. & HOBBS, P.V. (1980): Atmos. Environ. 14, 99

HEGG, D.A. & HOBBS, P.V. (1981): Atmos. Environ. 15, 9, 1597

HELLER, W. & WALLACH, M.L.(1963): J. Phys. Chem. 67, 565

HELLER, W. & WALLACH, M.L. (1964): J. Phys. Chem. 68, 931

HICKEY, H.R., HENDRICKSON, E.R.J. (1965): J. Air Pollut. Control Assoc. 15, 409

HIDY, G.M. & BROCK, J.R. (1965): J. Coll. Sci. 20, 6, 477

HILBIG (1966):Optic 23, 313

HIMMELBLAU, D.M. (1964): Chem. Rev. 64, 527

HINDS, W.C.: 'Aerosol Technology'. Wiley-Interscience, N.Y. 1982

HINZE, J.O. & MILBORN. H. (1950): J. Appl. Mech. 17, 145

HITCHCOCK, D.R. (1976): J. Air. Pollut. Control Assoc. 26, 210

HITCHCOCK, D.R. & BLACK, M.S. (1984): Atmos. Environ. 18, 1, 1

HOATHER, R.C. & GOODEVE , C.F. (1934): Trans. Farad. Soc. 30, 1149

HOGSTROM, U. (1973): Ambio 2, 37

HOLSER, W.T. & KAPLAN, I.R. (1966): Chem. Geol. 1, 93

HOLT. B.D., KUMAR, R. & CUNNINGHAM, P.T. (1981): Atmos. Environ. 15, 557

HUYGEN, C. (1963): Anal. Chim. Acta. 28,, 349

IBUSUKI, T. & BARNES, H.M. (1984): Atmos. Environ. 18, 1, 145

JOHNSON, W.B. (1983): J. Air Pollut. Control Assoc. 33, 6, 563

JOHNSTONE, H.F. & COUGHANOWR, D.R. (1958): Ind. Engng Chem.

JOHNSTONE, H.F. & LEPLA, P.W. (1934): J. Amer. Chem. Soc. 56, 2, 2233

JOHNSTONE, H.F. & MOLL, A.J. (1960): Ind. Engng. Chem. 52, 861

JONES, H.C., LACASSE, N., LIGETTI, W.S. & WEATHERFOR, F. (1977): EPA Report 600/7-77-12 NTIS

JUDEIKIS, H.S. & SIEGEL, S. (1973): Atmos. Environ. 7, 619

JUDEIKIS, H.S. & STEWART, T.S. (1978): Atmos. Environ. 12, 1633

JUNGE, C.E. (1953): Tellus 5, 1

JUNGE, C.E. (1956): Tellus 8, 127

JUNGE, C.E. (1960): J. Geophys. Res. 65, 227

JUNGE, C.E.:'Air Chemistry and Radioactivity ', Acad. Press, N.Y. 1963

JUNGE, C.E. & RYAN, T.G. (1958): Quart. J. Roy. Meteorol. Soc. 84, 46

KALLEND, A.S. (1972): RD/L/N125/72 Central Electricity Research

Laboratory, C.E.G.B., Leatherhead, England

KAPLAN, D.J., HIMMELBLAU, D.M. & KANOAKA, C. (1981a):Atmos. Environ. 15, 5, 763

KAPLAN, D.J., HIMMELBLAU, D.M. & KANOAKA, C. (1981b): Environ. Sci. Technol. 15, 5, 558

KARAKER, D.G. (1963): J. Phys. Chem. 67, 871

KELLOG, W.W., CADLE, R.D., ALLEN, E.R., LAZRUS, A.L. & MARTEL, J.A. (1972): Science 175, 587

KERKER, M.M.:'The Scattering of Ligh and Other Electromagnetic Radiation.' pp354- Acad. Press, N.Y. 1969

KIRSCH, A.A. & STECHKINA, I.B.:'The Theory of Aerosol Filteration with Fibrous Filters,' in Fundementals of Aerosol Science edited by D.T. Shaw. Wiley-Intersicence N.Y. 1978

KLEINMAN, L.I. (1984): Atmos. Environ., 18, 7, 1453

KOIDE, M. & GOLDBERG, E.D. (1971): J. Geophys. Res. 76, 6589

KOUSAKA, Y., OKUYAMA, K., SUMI, K. & YOSHIDA, T. (1978): Aerosol Sci. 9, 489

KUKLA, G.J. & KUKLA, H.J. (1974): Science 183, 709

LARSEN, P.S. & SORENSEN, S.K. (1984): Atmos. Environ. 18, 1963

LARSON, T.V., HORICKE, N.R. & HARRISON, H. (1978): Atmos. Environ. 12, 1597

LEE, R.E., PATERSON, R.H. & WAGMAN, J.(1968):Envir. Sci. Technol. 2, 288

LEIGHTON, P.A.:'Photochemistry and Air Pollution.' Acad. Press, N.Y., 1961

LENHARD, U. GEORJII, H.W. (1980): Pure Appl. Geophys. 118, 5, 1145

LENHARD, U. & GRAVENHORST, G. (1980): Tellus 32, 48

LEVY, A., DREWES, R.R. & HALES, J.M. (1976):SO_2 oxidation in plumes: A Review of Assessment of Relevant Mechanistic and Rate Studies. Final Report to EPA. EPA. 450/3-76-022

LIBERTI, A., BROCCO, D. & POSSANZINI, M. (1978): Atmos. Environ. 12, 225

LINEK, V. & MAYRHOFEROVA, J. (1970):Chem. Engng Sci. 25, 787

LINZON, S.M. (1971): J. Air Pollut. Control Assoc. 21, 81

LISS, P.S (1971): Nature 233, 327

LISS, P.S. & SLATER, P.G. (1974): Nature 247, 181

LLOYD, R.M. (1967): Science 156, 1228

LOGAN, J.A., PRATHER, M.J., WOFSY, S.C. & McELROY, M.B. (1981): J. Geophys. Res. 86, 7210

LOOMIS, :'Solubilities of Gases in Water' in Int. Crit. Tables 3, pp255-61. McGraw Hill, N.Y. 1928

LUNAK, S. & VEPREK-SISKA, J. (1976): Coll. Szech., Chem. Commun. 41, 3495

LURIA, M., OLSZYNA, K.J. & MEAGHER, J.F. (1982): Atmos. Environ. 16, 183

LURIA, M., OLSZYNA, K.J. & MEAGHER, J.F.(1983): J. Air Pollut. Control Assoc. 33, 5, 483

MacDONALD, G.A.:'Volcano' pp45, Prentice Hall, N.J. 1972

MADDOCK, J.E.L. :'A Light Scattering Study of Growth of H_2SO_4 Particles PhD Thesis, London University, 1974

MAREK, M., SCHONGUT, J. & GRACKO, P. (1976): Chemicke Inzenyrstvi, K11, 129

MARTIN, L.R. (1983): 'Acid Precipitation: SO_2, NO, NO_2 Oxidation Mechanism' (edited by J.G. Calvert) Ann Arbor Science Publishers Michigan

MARTIN, L.R. & DAMSHEN, D.E. (1981):Atmos. Environ. 15, 9, 1615

MARTIN, L.R., DAMSCHEN, D.E. & JUDAIKIS, H.S. (1981): EPA Report No. 600/7-81-085, Research Triangle Park NC

MASON, B.J.:'The Physics of Clouds'. pp Clarendon Press Oxford, 1957

MATTESON, M.J. & OLIVERS, M.J. (1978): Am. Ind. Hyg. Assoc. J. 39, 783

MATTESON, M.J. & STOBER, W. (1967): J. Coll. Int. Sci. 23, 203

MATTESON, M.J., STOBER, W. & LUTHER, H. (1969):I. & E.C. Fund. 8, 677

McCLENNY, W.A., GAILEY, P.C., BRAMAN, R.S. & SHELLEY (1982): Analyt. Chem. 54, 365

McDONALD, J.E. (1953): J. Meteorol. 10, 68

McKAY, H.A.C. (1969): Chemistry & Industry, Aug. 1969, 1162

McKAY, H.A.C. (1971): Atmos. Environ. 5, 7

McLAREN, E., YENCHA, A.J. & KUSHNIR, J.M. (1974): Tellus, 26, 291

MEADLEY, C.K. (1971):Quart. J. Mech. & Applied Math. 24, 43

MEAGHER, J.F. & LURIA, M. (1982): Atmos. Environ. 16, 183

MEDICI, M.:'The Natural Gass Industry' p128 BUTTERWORTHS, London, 1974

MESZAROS, E., MOORE, O.J. & LODGE, P.J. (1977):Atmos. Environ. 11, 345

MESZAROS, E., VARHELYI, G. & HASZPRA, L. (1978): Atmos. Environ. 12, 2273

MIDDLETON, P., KIANG, C.S. & MOHNEN, V.A. (1980): Atmos. Environ. 14, 463

MIE, G. (1908): Ann. Physik 25, 1377

MILLER, J.M. & de PENA, R. (1972): J. Geophys. Res. 30, 5905

MILLER, R.L.:'Liquid Chromatography Application System for Ion Chromatography.' LC-235. Perkin Elma, April, 1982

MIYAMOTO, S. & KAYA, T. (1930): Bull. Chem. Soc. Japan 5, 123

MOLLER, D. (1984a): Atmos. Environ. 18, 1, 19

MOLLER, D. (1984b): Atmos. Environ. 18, 1, 29

MOORE, A.P.: A light scattering study of the Kinetic Size Distribution Changes of Aerosols. PhD Thesis. London University, 1974

MORGAN, O.M. & MAASS, O. (1931): Can. J. Res. 5, 162

NEWMAN, L. (1981): Atmos. Environ. 15, 2231

NICKLESS, G. (Editor):'Inorganic Sulphur Chemistry.' Elsevier Publishing Company, Amsterdam, 1968

NICOL, D.J., SHAW, M.K. & LEDWARD, D.A. (1970): Appl. Microbiol. 19, 937

NOVAKOV, T., CHANG, S.G. & HARKER, A.B. (1974): Science 186, 259

O.E.C.D. (1977): The O.E.C.D. programme on long-range transport of air pollutants. Measurements and findings. OECD, Paris

OKUYAMA, K., KOUSAKA, Y. & ODACHI, M. (1980): J. Aerosol Sci. 11, 11

OTTER, B. (1978): Atmos. Environ. 12, 455

PASQUILL, F. (1961): The Meteoriol. Mag., 90, 1063, 33

PASQUILL, F. :'Atmospheric Diffusion'. John Wiley & Sons, N.Y. 1974 2nd Edition

PATE, J.B., AMMONS, B.E., SWANSON, G.A. & LODGE, J.P. (1965): Analyt. Chem. 37, 942

PATE, J.B., LODGE, J.P. & WARTBURG, A.F. (1962): Analyt. Chem. 34, 1660

PENKETT, S.A. (1972): Nature Phys. Sci. 240, 105

PENKETT, S.A., JONES, B.M.R., BRICE, K.A. & EGGLETON, A.E.J. (1979): Atmos. Environ. 13, 123

PENKETT, S.A., JONES, B.M.R. & EGGLETON, A.E.J (1979): Atmos. Environ. 13, 139

PERHAC, R.M. (1978):Atmos. Environ. 12, 641

PERRY, R.A., ATKINS, R. & PITTS, J.N. (1976): J. Phys, Chem. 64, 3237

PETERSON, T.W. & SEINFELD, J.H. (1979):A.I.Ch.E. Journal 25, 5, 831

PETERSON, T.W. & SEINFELD, J.H.: 'Advances in Environmental Science and Technology,' Vol 10, ppl25-180, (Edited by Pitts, J.N. & Metcalf, R.L.) John Wiley & Sons 1980

PICH, J., FRIEDLANDER, S.K. & LAI, F.S. (1970): J. Aerosol Sci. 1, 115

POHL, C.A., JOHNSON, E.L. (1980): J. Chromatogr. Sci. 18, 442

POLYCHRONAKIS, S. (1978): PhD Thesis, University of London

POSSANZINI, M., FEBO, A., & LIBERTI, A. (1983): Atmos. Environ. 17, 2605

POSTMA, A.K.: US AEC Smposium Series No 22, pp247-59 United States Atomic Energy Commission, Oak Ridge, Tennessee, 1970

PRUPPACHER, H.R. & BEARD, K.V. (1970): Quart. J. Roy. Met. Soc. 96, 247

PUESCHEL, R.F. & VAN VALIN, C.C. (1978): Atmos. Environ. 12, 307

RALL, D.P. (1974): Environ. Health Persp. 8, 97

ROBERTS, T.M. (1984): Atmos. Environ. 18, 629

ROBINSON, R.A. & STOKES, R.H.: 'Electolytic Solutions.' Butterworths, London, 1965

ROBINSON, E. & R.C. ROBBINS. (1968): SRI Final Report, Project PR-6755 Menlo Park CA

ROBINSON, E. & ROBBINS, R.C. (1970): J. Air Pollut. Control Assoc. 20, 303

ROHDE, H. (1978): Atmos. Environ 12, 671

SAWICKI, J.E., MULIK, J.D. & WITTGENSTEIN, E.:'Ion Chromatographic Analysis of Environmental Pollutants. Ann Arbor (USA). Ann Arbor Publication, 1977

SCARINGELLI, F.P., SALTZMAN, B.E. & FREY, S.A. (1967): Analyt. Chem. 39 14,1709

SCEP:'Man's Impact on the Global Environment. MIT Press, Cambridge Mass., 1970

SCHLEGEL, H.C. (1974): Tellus 26, 11

SCHROETER, L.C. (1963):J. Pharm. Sci. 52, 559

SCORER, R.S.: 'Environmental Aerodynamics'. p363 Ellis Horwood Publishers, Chichester, 1978

SCOTT, W.D.: PhD Thesis, University of Washington, 1964

SCOTT, W.D. (1978):Atmos. Environ. 12, 917

SCOTT, W.D. & HOBBS, P.V.(1967): J. Atmos. Sci., 24, 54

SCOTT, W.D., LAMB, D. & DUFFY, D. (1969): J. Atmos. Sci. 26, 726

SEMB, A. (1978): Atmos. Environ. 12, 455

SHANNON, J.D.: 'The Advanced Statistical Trajectory Regional Air Pollution Model' in Proceedings of the 4th Symposium on Turbulence, Diffusion & Air Pollution. pp376-80. American Meteorological Society, Boston, 1980

SHEPHARD, D., EPSTEIN, J., BETHEL, R., KIRKPATRICK, M., NADEL, J.A. &

BOUSHEY, H.A. (1982): Am. Rev. Resp. Dis. 125, 151

SHEPHARD, D., NADEL, J.A. & BOUSHEY, H.A. (1981a): Am. Rev. Resp. Dis. 124, 252

SHEPHARD, J.G.(1974): Atmos. Environ. 8, 69

SHEPPARD, D., SAISHO, A., NADEL, J.A. & BOUSHEY, H.A. (1981): Am. Rev. Resp. Dis. 123, 486

SILLEN, L.G. (1964): 'Stability Constants of Metal-ion Conmplexes - Inorganic Ligands.' 2nd edition, Chem. Soc. (London), Special Publication No.17

SINCLAIR, D., COUNTESS, R.J. & HOOPES, G.S. (1974): Atmos. Environ. 8, 1111

SLINN, W.G.N., HASSE, L., HICKS, B.B., HOGAN, A.W., LAL, D., LISS, P.S. MUNICH, K.O., SEHMEL, G.A. & VITTORI, O. (1978): Atmos. Environ. 12, 2055

SMALL, H., STEVENS, T.S. & BAUMAN, W.C. (1975): Analyt. Chem. 47, 11, 1801

SMITH, B.M., WAGMAN, J. & FISH, B.R. (1969): Environ. Sci. Technol. 3, 558

SMOLUCHOWSKI, (1916): Phys. Z. 17, 557

SONDERLUND, R. (1977): Ambio 6, 118-122

SPICER, C.W., GEMMA, J.L., JOSEPH, D.W. & LEVY, A. (1975): ACS Symposium Series 17 - Removal of Trace Contaminants Air Symposium 1974. pp157-173

SPURNEY, K.R., LODGE, J.P., FRANK, E.R. & SHEESLEY, D.C. (1969): Environ. Sci. Technol. 3,, 5, 453

STEELE, R.L., GERTLER, A.W., KATZ, U., LAMB, D.& MILLER, D.F. (1981): Atmos. Environ. 15, 2341

STEVENS, R.K., DZUBAY, T.G., RUSSWURM, G. & RICKEL, D. (1978): Atmos. Environ. 12, 55

STEVENSON, A.F., HELLER, W. & WALLACH, M.L. (1961): J. Chem. Phys. 34, 1789

STEWART, D.A. & LIN, M.K. (1981):Atmos. Environ. 15, 2377

STOIBER, R.E. & JENSEN, A. (1973): Science 182, 577

STROM, L. (1972): Atmos. Environ 6, 133

STUHL, F. (1973): J. Chem. Phys. 59, 535

SUCK, S.H. (1979): J. Aerosol Sci. 10, 581

SZE, N.D. & KO, M.K.W. (1979): Nature, 280, 308

SZE, N.D. & KO, M.K.W. (1980): Atmos. Environ. 14, 1223

TADMOR, J. & GUR, Y. (1969): Atmos. Environ. 3, 688

TANNER, R.L., ABBAS, R. & LEPORE, J. (1980): BNL REPORT 2677R. Brookhaven National Laboratory

TARTARELLI, R., DAVINI, P., MORALLI, F. & CORSI, P. (1978): Atmos. Environ. 12, 289

TAYLOR, D.D. & FLAGAN, R.C. (181): ACS Symposium Series No. 167. Atmospheric Aerosol: Source/Air quality Relationships

TELMAN, R.C., VLIET, E.B., PIERCE, W.M. & DOUGHERTY, R.H. (1919): J. Am. Chem. Soc. 41, 304

THOMAS, J.W. (1958): J. Air Pollut. Control Assoc. 8, 32

TOMASI, C., GUZZI, R. & VITTORI, O. (1975): J. Atmos. Sci. 32, 1580

TOPP, M.N. & EISENKLAM, P. (1972): Ultrasonics 10, 127

TORRES, A.L., MAROULIS, P.J., GOLDBERG, A.B. & BANDY, A.R. (1979): J. Geophys. Res. 84, C12

TRINDADE, H.A., PFEIFFER, W.C. & LONDRES, H. (1981): Environ. Sci. Technol. 15, 1, 84

TU, K.W. & KANAPILY, G.M. (1978): Atmos. Environ. 12, 1628

TWOMEY, S. (1976): J. Atmos. Sci. 33, 1073

TWOMEY, S. :'Atmospheric aerosols', Elsevier, N.Y., 1977

URONE, P., LUTSEP, H., NOYES, C.M. & PARCHER, J.F. (1968): Environ. Sci. Technol. 2, 611

VAN BREEMAN, N., BURROUGH, P.A.,VELTHOST, E.J., VAN DOBBEN, H.F., DE WIT, T., RIDDER, T.B. & REIJNDERS, H.F.R. (1982): Nature 299, 548

VAN DER HEUVEL, P.P. & MASON, B.J. (1963): Quart. J. Roy. Meteor. Soc. 89, 271

VOHRA, K.G., NAIR, P.V.N (1970): J. Aerosol Sci., 1, 127

VOHRA, K.G., SUBBARAMU, M.C. & MURALEEDHARAN, T.S. (1984): Atmos. Environ. 18, 8, 1653

WAGMAN, D.D., EVANS, W.H., PARKER, V.B., HALLOW, I., BAILEY, S.M., & SCHUMM, R.H. (1968): NBS Technical Note 270-3 National Bureau of Standards, US Dept. of Commerce, Washington D.C. 20230

WAGNER, P.E.:'Aerosol Microphysics II' (Edited by Marlow, W.H.) ppl29-178. Springer-Verlag Heidelberg, N.Y., 1982

WALKENHORST, W. & DAUTREBAND, L. (1964): Staub 24, 505

WANG, J.C. & HIMMELBLAU, D.M. (1964): AIChE Journal 21, 402

WARNECK, P. (1974): Tellus 26, 39

WEISS, R.E., WAGGONER, A.P., CHARLSON, R.J. & ALQUIST, N.C. (1977): Science 195, 979

WEST, P.W. & G.C. GAEKE (1956): Analyt. Chem. 28, 12m 1816

WHELPDALE, D.M. (1978): Atmos. Environ. 12, 661

WHELPDALE, D.M. & SHAW, R.W. (1974): Tellus 26, 196

WHITE, P.A.F., SMITH, S.E.: 'High Efficiency Air Filtration' pp66-85 Butterworths, London 1964

WHYTLAW-GRAY, R. (1935): J. Chem. Soc. 268, 80

WILLISON, M.J. & CLARKE, A.G. (1984): Analyt. Chem. 56, 1039

WILSON, B.J.:'The Physical Chemistry of Aerosols - A General Discussion of the Faraday Society'. pp20-38. Aberdeen University Press, Scotland, 1960

WILSON, C.T.R. (1900): Phil. Trans. A.193, 265

WILSON, W.E. (1978): Atmos. Environ. 12, 537

WINTER, E.R.S. & BRISCOE, H.U.A. (1951): J. Am. Chem. Soc. 73, 375

YAGI, S. & INOUE, H. (1962): Chem. Engng Sci. 17, 411

YUE, G.K., MOHNEN, V.A. & KIANG, C.S. (1976): Wat. Air Soil Pollut. 6, 277

ZEBEL, G.:'Coagulation of Aerosols' in Aerosol Science (Edited by Davies, C.N.) pp31-57 Acad. Press, London, 1977

ANDREAE, M.O. (1980): Limnology and Oceanogr. 25, 1054

BARRON, C.H. & O'HERN, H.A. (1966): Chem. Engng. Sci. 21, 397

BENGTSSON, S. & BJERLE, I. (1975): Chem. Engng. Sci. 30, 1429

BERTOLACINI, R.J. & BARNEY, J.E. (1957): Analyt. Chem. 29, 281

BOLIN, B., CHARLSON, R.J. (1976): Ambio 5, 47

BROSSET, C., ANDREASSON, K. & FERM, M. (1975): Atmos Environ. 9, 631

CLARKE, A.G. & RADOJEVIC, M. (1984): Atmos. Environ. 18, 12

GRANAT, L. (1975): Final Report on Nordforsk Research Project, University of Stockholm, Stockholm, Sweden

GRANAT, L., RODHE, H. & HALLBERG, R.O. (1976): Ecological Bull. 22, 89

HALLBERG, R.O. (1976): SCOPE Report No. 7, Ecol. Bull. (Stockholm) 22, 89

HOFFMAN, M.R. & BOYCE, S.D.: 'Catalytic autoxidation of aqueous SO_2 in Relationship to Atmospheric Chemistry' in Trace Atmospheric Consituents edited by Schwartz, S.E. Wiley-Interscience N.Y., 1983

HUNTZICKER, J.J., HOFFMAN, R.S. & LING, C.S. (1978): Atmos. Environ. 12, 83

MAROULIS, P.J.: PhD Dissertation, Drexel University PA, 1979

MAROULIS, P.J., TERRES, A.L., GOLDBERG, A.B. & BANDY, A.R. (1980): J. Geophys. Res. 85, C12, 7345

MOLLER, D. (1980): Atmos. Environ. 14, 1067

PETIT, C., LEDOUX, M. & TAINITE, M. (1977): Atmos. Environ. 11, 11, 1123

RASMUSSEN, R.A. (1974): Tellus, 26, 254

SAWICKI, J.E. & BARRON, C.H. (1973): Chem. Engng. J. 5, 153

THOMOS, L.C. & CHAMBERLEIN, G.C. (Ed):'Colorimetric Chemical Analytical Methods' John Wiley & Sons, London, 8th Edition, 1974

Appendix A

Some Thermodynamic Properties used in the study

1. Air

   Kinematic Viscosity of air at 20°C and 1 atmosphere

   $0.152\ cm^2\ s^{-1}$

   Diffusion coefficient of oxygen in air at 0° C

   $0.178\ cm^3\ s^{-1}$ (CRC, 1983)

   Diffusion coefficient of oxygen in water at 20° C

   $2.3 \times 10^{-5}\ cm^2\ s^{-1}$ (Himmelblau, 1964)

   Henry's Law constant for oxygen

   $1.27 \times 10^{-3}\ M\ atm^{-1}$ (Loomis, 1928)

2. Water

   Ionic product of water at 25° C

   $1.008 \times 10^{-14}\ M^2$ (Wagman et al, 1968)

   Diffusion coefficient of water vapour in air at 8° C

   $0.239\ cm^2\ s^{-1}$ (CRC, 1983)

3. Ammonia

   Solubility in cold water

   89.9 g per 100 cm^3 (CRC, 1983)

   Diffusion coefficient in dilute aqueous solution at 20° C

   $1.76 \times 10^{-5}\ cm^2 s^{-1}$ (Arnold, 1930)

   Diffusion coefficient in air at 25° C and 1 atmosphere

   $0.28\ cm^2\ s^{-1}$ (International Crit. Table, 1928)

   Henry's Law constant at 25° C

   57 M atmosphere^{-1} (Scott and Hobbs, 1967)

   Equilibrium constant at 25° C

   1.774×10^{-5} M (Robinson and Stokes, 1959)

4. Sulphur dioxide

   Solubility in cold water

   22.8 g per 100 cm^3 (CRC, 1983)

   Diffusion coefficient in dilute aqueous solution at 20° C

   $1.8 \times 10^{-5}\ cm^2 s^{-1}$ (Himmelblau, 1964)

Diffusion coefficient in air

$0.004832 \frac{T^{1.75}}{P}$ cm^2s^{-1} or

0.132 cm^2s^{-1} at 20° C (Fish, 1971)

Henry's Law constant at 25° C

1.24 M atm^{-1} (Gmelin, 1963)

First ionisation constant at 25° C

0.0174 M(Sillen, 1974)

Second ionisation constant at 25° C

6.24×10^{-8} M (Sillen, 1974)

5. Manganese hydroxide

Solubility product at 18° C

4×10^{-14} M^2 (CRC 1981)

6. Lead sulphate

Solubility product at 18° C

1.06×10^{-8} (CRC 1981)

Appendix B

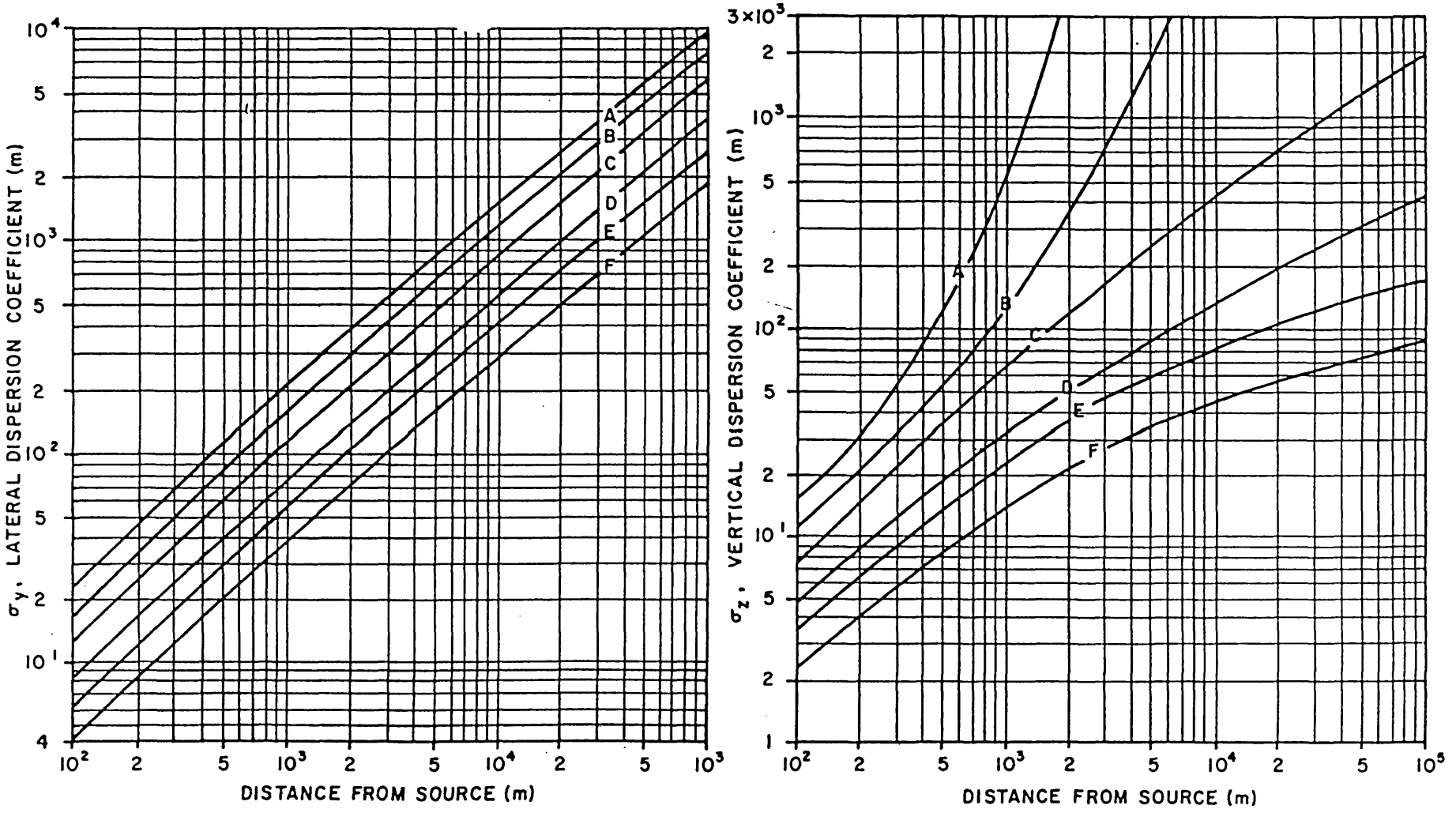
Plume Dispersion Parameters

(a) Pasquill Dispersion Classes (Pasquill, 1974)

Insolation/Cloud Cover		Surface wind speed ($m\ s^{-1}$) 2.0	2 to 3	3- 5	5- 6	6
Day	Strong Insolation (Solar elevation 60°	A	A-B	B	C	C
	Moderate Insolation	A-B	B	B-C	C-D	D
	Slight Insolation (Solar Elevation 15°-35°)	B	C	C	D	D
Day or Night	Overcast	D	D	D	D	D
	Thin overcast (0.5 cloud cover)		E	D	D	D
Night	Thin overcast (0.4 cloud cover)	G	F	E	D	D

(b) Power Law Constants for the calculation of the Dispersion Coefficients given by the equations (Tadmor et al. 1969)

Stability class	σ_y		σ_z (0.5-5 km)		σ_z (5-50 km)	
	α ($km^{(1-p)}$)	p	β ($km^{(1-q)}$)	q	β ($km^{(1-q)}$)	q
A	0.3658	0.9031	2.5×10^{-4}	2.1250	-	-
B	0.2751	0.9031	1.9×10^{-3}	1.6021	-	-
C	0.2089	0.9031	0.20	0.8543	0.5742	0.7160
D	0.1474	0.9031	0.30	0.6532	0.9605	0.5409
E	0.1046	0.9031	0.40	0.6021	2.1250	0.3979
F	0.0722	0.9031	0.20	0.6020	2.1820	0.3310
G	-	-	-	-	-	-



(a) Lateral Dispersion

(b) Vertical Dispersion

Appendix B:-The Pasquill-Gifford dispersion coefficients versus downwind distance for various dispersion classes.(From R.A.Dobbins,1979.)

Appendix C

Inversion of droplet size to sulphate concentration

Since droplet sulphate concentration data based on ion chromatographic analysis are available only for the runs 6, 7 and 9, a strategy was developed for obtaining them for other runs from the droplet size data. One method of doing this is the solution of the equation which combines the Kelvin curvature effect (for droplets below 0.1 μm diameter) and Raoult's solution effect.

$$H = \left(1 + \frac{6imM_w}{M\rho\pi d^3}\right)^{-1} \exp\left(\frac{4\gamma M_w}{\rho RTd}\right)$$

where m is the mass of $(NH_4)_2SO_4$ in a droplet of equilibrium diameter d; M and M_w are the molar masses of $(NH_4)_2SO_4$ and water respectively, γ and ρ are the surface tension and density respectively of water at temperature, T; i is the vant Hoff's factor and R is the gas constant; and H is the relative humidity. The limitation of this method of converting droplet size to sulphate concentration lies in the uncertainty in the values of the density and surface tension of droplets of unknown molar concentration. This method was therefore not used in calculating the sulphate concentrations of the droplets.

The technique adopted was a straight-forward calibration between the droplet sizes in the general case and those in runs 6, 7 and 9 whose sulphate concentrations were determined by ion chromatography. The justification of this technique is based on the high positive correlation between droplet volume and the sulphate loading of the aerosols in these runs as shown in Table C1. Correlation coefficient and test of significance are highest in run7. So the droplet sizes obtained at each residence time in run 7 are compared with corresponding ones in the rest of the runs (except 6 and 9) to obtain their sulphate loadings. The regression coefficient was not used in calculating the sulphate loading. This was as a result of the nature of the oxidation of SO_2; a regression line obtained from data across the entire residence time would produce a regression coefficient too low to account for the initial rate of sulphate production and too high to represent SO_2 oxidation rate at high residence times. The sulphate loadings are listed in Tables C2, C3 and C4.

C1 Correlation between droplet volume and the sulphate loading of the aerosol

Run	6		7		9	
Contact Time (min)	Droplet volume $x10^{14}$ (cm^3)	$[SO_4^{2-}]$ $x10^9$(moles dm^{-3} aerosol)	Droplet volume $x10^{14}$ (cm^3)	$[SO_4^{2-}]$ $x10^9$(moles dm^{-3} aerosol)	Droplet volume $x10^{14}$ (cm^3)	$[SO_4^{2-}]$ $x10^9$(moles dm^{-3} aerosol)
0.65	0.371	1.73	0.485	1.82	0.0796	1.70
1.1	0.478	1.86	0.506	1.94	0.310	1.92
5.1	0.558	2.39	0.779	3.05	0.471	2.53
9.1	1.19	3.47	1.68	4.14	0.889	3.43
13.2	3.80	3.47	10.6	4.17	1.22	3.72
17.2	4.65	3.55	11.6	4.24	2.81	3.72
21.2	6.82	3.62	12.0	4.68	3.48	3.83
25.2	11.0	3.66	24.8	4.79	11.6	3.94
Correlation coefficient	0.719		0.760		0.620	
Test of significance	2.53		2.86		1.94	
Regression constant	$2.40x10^{-9}$		$2.79x10^{-9}$		$2.69x10^{-9}$	
Regression coefficient	$1.57x10^4$		$1.04x10^4$		$1.43x10^4$	

Table C2 Aerosol sulphate loading in uncatalysed SO_2 oxidation in the absence of NH_3

Residence Time (min)	Sulphate loading (moles dm^{-3} aerosols x 10^9) Run 1	Run 2	Run 3	Run 4
0.65	3.93	1.37	4.33	0.53
1.1	1.23	0.886	14.24	1.40
5.1	1.19	2.93	8.71	1.12
9.1	1.44	1.11	7.35	0.77
13.2	1.26	1.96	8.79	0.605
17.2	0.603	0.497	3.63	0.267
21.2	0.479	0.917	2.90	2.39
25.2	0.971	0.477	3.17	0.271

Table C3 Aerosol sulphate loading in uncatalysed system in the presence of NH_3

Res. Time (min)	Sulphate loading (moles dm^{-3} aerosols x 10^9) Run 5	Run 8	Run 10	Run 11	Run 12	Run 13	Run 14
0.65	0.441	1.41	53.5	29.1	20.2	13.2	16.9
1.1	1.80	6.27	1.88	15.7	16.4	15.9	4.63
5.1	2.00	1.67	13.1	32.3	20.5	28.2	15.4
9.1	1.91	1.07	2.67	55.5	27.5	11.1	10.1
13.2	2.32	2.36	49.5	132.3	16.2	53.6	4.37
17.2	8.28	0.651	59.8	58.6	11.2	54.6	25.8
21.2	6.30	0.781	82.6	31.8	27.5	15.3	29.3
25.2	9.07	3.93	14.3	25.3	20.8	16.4	18.5

Table C4 Aerosol sulphate loading in Mn^{2+}-catalysed system

Res. Time	Sulphate Loading (moles dm^{-3} aerosol x 10^9)							
(min)	Run 15	Run 16	Run 17	Run 18	Run 19	Run 20	Run 21	Run 22
0.65	4.66	5.11	2.13	1.42	2.34	7.91	5.20	4.25
1.1	1.30	2.99	3.39	0.906	2.79	14.1	8.63	1.27
5.1	2.02	6.76	7.05	1.13	5.30	22.1	17.7	1.77
9.1	3.17	2.94	12.4	1.26	2.16	22.6	14.0	2.02
13.2	1.07	9.39	3.93	1.39	14.77	7.27	11.1	0.66
17.2	3.39	4.58	1.47	13.2	4.89	13.8	68.8	0.339
21.2	1.14	4.12	3.87	1.96	1.06	12.3	4.42	0.277
25.2	2.10	2.79	8.98	5.14	1.35	14.5	17.5	0.477

Appendix D

Reaction Kinetics of the Aerosol System

The kinetics of the oxidation of SO_2 in droplets in a tubular reactor were evaluated in terms of a plug flow reactor (Boudart, 68). The scheme is shown in Fig D.

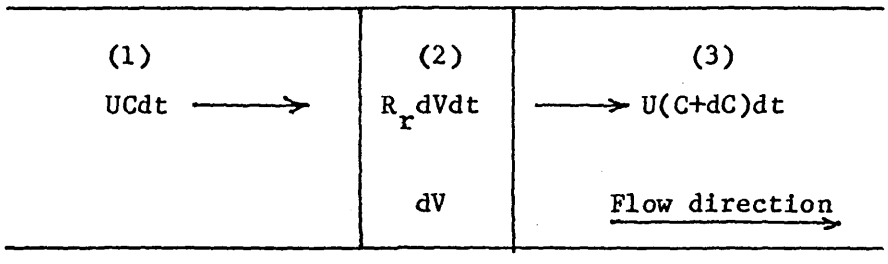


Fig. D. Processes occuring in a plug flow reactor

1 = moles of product entering the volume element dV in time dt;

2 = moles of product produced by reaction in time dt; and

3 = moles of product leaving the volume element in time dt.

U = the volume flow-rate of the feed aerosol in $dm^3 min^{-1}$, typically, 4 dm^3 min in this study.

C = molar concentration of product

R_r = reaction rate

At steady state, the molar balance of the product in the volume element is obtained by equating the rate of exit, (3) to the sum of the rates of entry into, (1) and formation in (2) the volume element of the products. Thus

$$U(C + dC)dt = UCdt + R_r dVdt \qquad D1$$

from which

$$\frac{dC}{R_r} = \frac{dV}{U} \qquad D2$$

This is integrated under the boundary condition that at V = 0, C = 0; $V = V_R$, $C = \chi$.

Equation D2 becomes

$$\int_0^{\chi} \frac{dC}{R_r} = \frac{1}{U} \int_0^{V_R} dV \qquad D3$$

$$\frac{V_R}{U} = \int_0^{\chi} \frac{dC}{R_r} \qquad D4$$

where V_R = reactor volume and

$R_r = k[S(IV)]^n$ for a simple case (Scott and Hobbs, 1967)

n = reaction order and k = rate constant

$$[S(IV)] = [S(IV)]_i - C$$

the subscript i stands for initial S(IV) concentrations. Equation D.4 becomes

$$\tau = \int_0^{\chi} \frac{dC}{k([S(IV)]_i - C)^n} \qquad D5$$

where $\tau = \frac{V_R}{U}$ = contact time

For S(IV) = gas phase concentration of SO_2 in moles dm^{-3} of aerosols,

$$[S(IV)] = p_{SO_2}/RT \qquad D6$$

For S(IV) = droplet phase concentration of SO_3^{2-} (moles dm^{-3} aerosols)

$$[S(IV)] = p_{SO_2} H_c K_1 K_2 \phi / [H^+]^2 \text{ or } \frac{p_{SO_2} H_c K_1 K_2 \phi}{[H^+]^2} \qquad D7$$

where R = 0.0821; T = ambient temperature and ϕ is the liquid water mass concentration of the aerosols.

Putting n = 0, $\frac{1}{2}$, 1 and 2 into equation D5, the folowing rate equations are obtained if $[S(IV)]_i$ is substituted with a, and C with x:

n = 0;

$$k\tau = \chi \qquad D8$$

n = $\frac{1}{2}$;

$$k\tau = 2\{a^{\frac{1}{2}} - (a - x)^{\frac{1}{2}}\} \qquad D9$$

$$n = 1;$$

$$k\tau = \ln \frac{a}{a - x} \qquad D.10$$

$$n = 2;$$

$$k\tau = x/(a - x) \qquad D.11$$

A plot of the right hand side of equations D8 - D11 against the corresponding values of τ for each of runs 6, 7 and 9 gave the graphs in Fig D1 to D4. Except in the case of run 9 where a definite zero order relation is indicated, it is not easy to tell from the shapes of the graphs the order of the reactions.

The numerical values of the orders of the oxidation in runs 6, 7 and 9 were obtained from the rate constants and sulphite ion concentrations.

$$n = \frac{\ln \text{Rate}/k}{\ln[S(IV)]_i} \qquad D.12$$

where $S(IV)_i$ is the initial concentration of S(IV) in the aerosols.

The reaction rates used for the calculation were obtained from the linear portion of Fig. IV.17 to IV.19

Zero order and pseudo-first order rate constants were determined for the runs listed in Tables C2, C3 and C4 by plotting the right hand side of equations D8 and D10 respectively against residence time and considering the linear portions of the graphs (Table D). In some of the runs, the rate constant calculation was based on the sulphite concentration calculated from equation D7. In runs 1, 3, 8, 15, 16 and 21 the gas phase concentrations of SO_2 computed from equation D.6 were used in calculating the rate constant.

Oxidation Time constant in % min^{-1}:

The rection was also expressed in % min^{-1} or % hr^{-1}, calculated from the equation for a first order reaction.

R_r = rate of oxidation = $\frac{-d[SO_2]}{dt} = k[SO_2]$

Hence at any time, the fraction rate of conversion

$$= -\frac{R_r}{[SO_2]} = -\frac{k[SO_2]}{[SO_2]}$$

The oxidation time constant in % min^{-1} is simply

$$\frac{-k[SO_2]}{[SO_2]} \times 100$$

$$= 100\ k\%\ min^{-1}$$

Characteristic time of oxidation:

This is obtained by integrating the rate equation. For the first order rate equation

$$\frac{d[SO_2]}{dt} = k[SO_2]$$

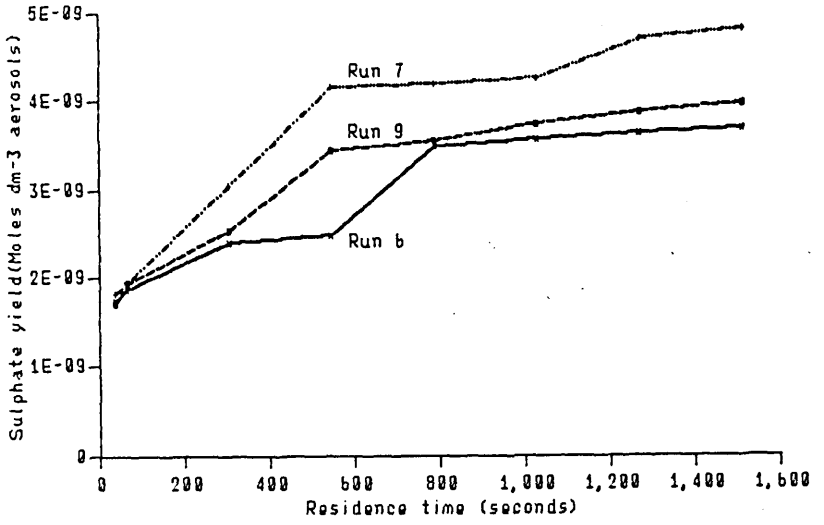
From which

$$\frac{[SO_2]}{[SO_2]} = e^{-kt}$$

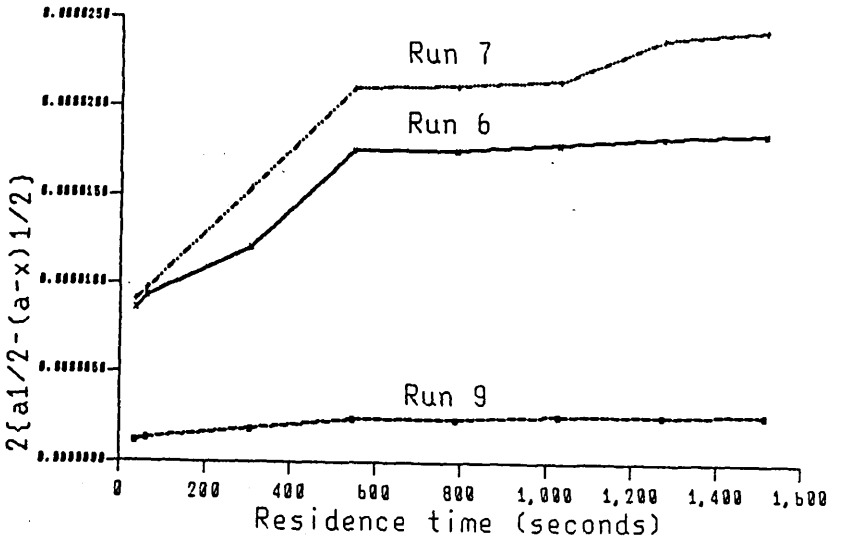
$\tau = k^{-1}$ (min) = characteristic time
where τ is the time after which SO_2 decays to 63% of its original value. Also

$$\tau = \frac{100}{\%\ min^{-1}}$$

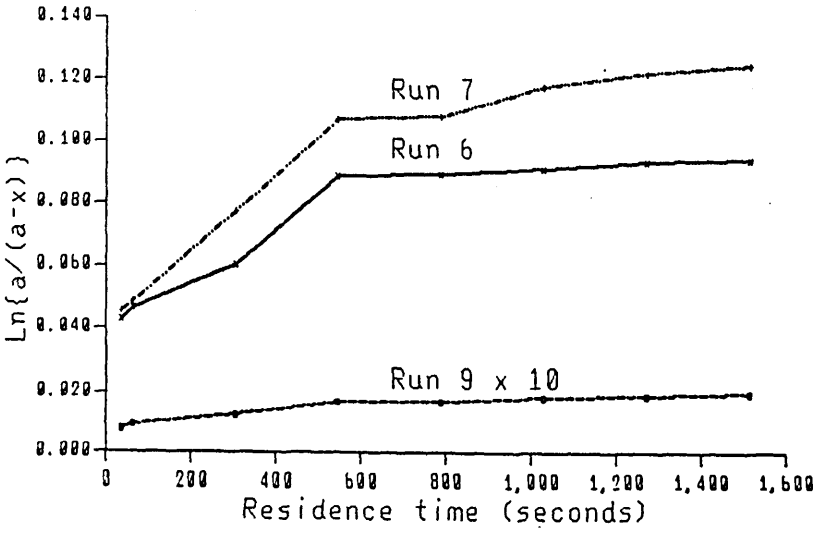
Appendix D1:-Zero order rate mechanism



Appendix D2:-Half-order rate mechanism



Appendix D3:-First order rate mechanism



Appendix D4:-Second order rate mechanism

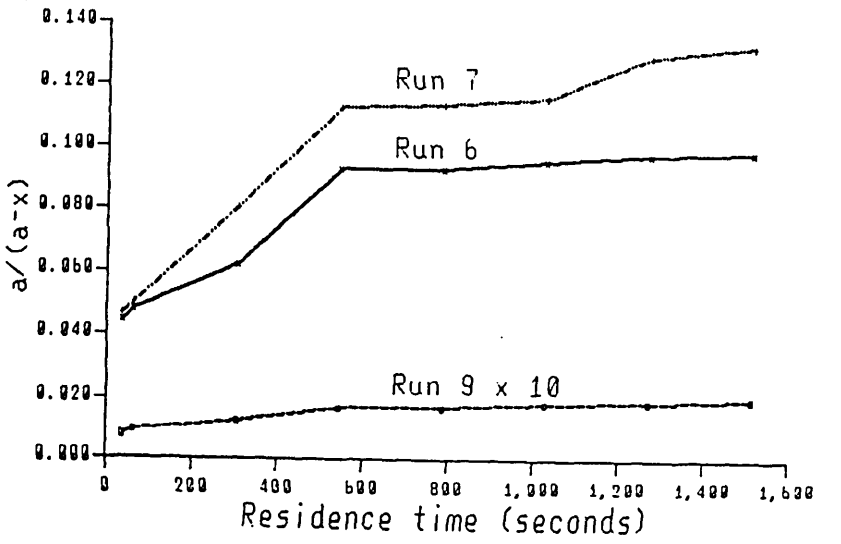


Table D Zero and Pseudo-First Order Rate Constants

Runs	p_{SO_2} (vpm)	p_{NH_3} (vpm)	pH	Mn^{2-} Catalyst	Rate Constants: Zero Order (mol $dm^{-3}s^{-1}$)	Rate Constants: Pseudo-first order (s^{-1})
1	1.0	0.0	2.7		1.40×10^{-13}	3.55×10^{-6}
15		0.0	2.7	1mM	1.91×10^{-13}	9.35×10^{-8}
5		0.5	6.1		1.01×10^{-6}	6.54×10^{-4}
6		1.0	6.3		1.29×10^{-6}	4.04×10^{-4}
7		2.0	6.4		2.14×10^{-6}	2.95×10^{-4}
17		0.5	6.1	1mM	5.48×10^{-12}	1.62×10^{-4}
18		1.0	6.3	1mM	4.10×10^{-7}	9.89×10^{-5}
19		2.0	6.4	1mM	2.40×10^{-7}	1.00×10^{-3}
2	10.0	0.0	2.6		1.33×10^{-12}	3.27×10^{-6}
3	50.0	0.0	2.6		4.92×10^{-12}	2.41×10^{-6}
8		0.1	5.0		8.92×10^{-13}	4.37×10^{-7}
9		1.0	5.5		1.59×10^{-6}	3.70×10^{-4}
11		10.0	6.0		3.09×10^{-5}	1.27×10^{-3}
12		25.0	6.1		1.66×10^{-6}	1.41×10^{-5}
13		50.0	6.3		3.32×10^{-5}	1.44×10^{-4}
16		0.0	2.6	1mM	4.82×10^{-12}	2.36×10^{-6}
20		0.1	5.0	1mM	2.58×10^{-11}	1.27×10^{-5}
21		1.0	5.5	1mM	6.86×10^{-12}	3.37×10^{-6}
22		10.0	6.0	1mM	1.55×10^{-12}	7.59×10^{-7}

Appendix E

```
      PROGRAM POLYN(DATA,OUTPUT,TAPE1=DATA,TAPE6=OUTPUT)
C          THIS PROGRAM CALCULATES THE HYDROGEN ION CONCENTRATION OF AN
C          AQUEOUS DROPLET SUSPENDED IN AN ATMOSPHERE OF SULFUR DIOXIDE
C          ,AMMONIA AND CARBON DIOXIDE OF KNOWN PARTIAL PRESSURES.IT IS
C          THE SOLUTION OF THE THIRD ORDER POLYNOMIAL OBTAINED FROM THE
C          ELECTRO_NEUTRALITY EQUATION BASED ON THE HENRY'S LAW AND THE
C          EQUILIBRIUM CONSTANTS OF THESE GASES.
      INTEGER T,I,IFAIL,N,NN,NOF
      REAL RE(6),XZ(6),YZ(6),TOL,ZZ,XO2AAF,PI,CHYD,SPBH,
     1TITLE(7),KA,HENCA,K1S,K2S,HENCS,KW,K1C,K2C,HENCC
      DATA PI/0.1E0/
      DATA KA/1.774E-05/,HENCA/57.0/,K1S/1.74E-02/,K2S/6.24E-08/,
     1HENCS/1.24/,KW/1.008E-14/,K1C/4.45E-07/,K2C/4.68E-11/,
     1HENCC/3.4E-02/
      TOL=XO2AAF(PI)
      PRINT*,'PROGRAM RESULTS'
      REWIND  1
      READ(1,*)N,PSO,PNH,PCO,CFAT
      WRITE(6,1004)PSO,PNH,PCO,CFAT
      NN=N-1
      A=1.0+(KA*HENCA*PNH/KW)
      B=-2.0*CFAT
      CS=K1S*PSO*HENCS
      CC=K1C*PCO*HENCC
      C=-(KW+CS+CC)
      DS=2.0*K2S*K1S*HENCS*PSO
      DC=2.0*K2C*K1C*HENCC*PCO
      D=-(DS+DC)
      RE(1)=A
      RE(2)=B
      RE(3)=C
      RE(4)=D
      IFAIL=0
      DO    500   I=1,N
            XZ(I)=0.
            YZ(I)=0.
  500 CONTINUE
      CALL CO2AEF(RE,N,XZ,YZ,TOL,IFAIL)
      DO  100 J=1,NN
      IF(ABS(YZ(J)).LT.TOL.AND.XZ(J).GT.0.0)CHYD=XZ(J)
  100 CONTINUE
      SPBH=-ALOG10(CHYD)
      WRITE(6,1030)CHYD,SPBH
 1004 FORMAT(/* PSO...*,E13.6, *PNH...*,E13.6, *PCO...*,E13.6, *CFAT...
     1*,E13.6)
 1030 FORMAT(/* CHYD...*,E13.6,5X,*SPBH...*,F5.3)
      END
```